UNIVERSITY OF SOUTHAMPTON

Mathematical models of wound formation, disease progression and treatment pathways of Buruli ulcer disease

by

Fatumah Atuhaire

ORCiD:0000-0002-2768-9472

A thesis submitted in partial fulfilment for the degree of Doctor of Philosophy

in the

Faculty of Social Sciences

School of Mathematical Sciences

February 6, 2024

UNIVERSITY OF SOUTHAMPTON

ABSTRACT

FACULTY OF SOCIAL SCIENCES
SCHOOL OF MATHEMATICAL SCIENCES

Doctor of Philosophy

by Fatumah Atuhaire
ORCiD:0000-0002-2768-9472

Buruli ulcer (BU) is a skin-related neglected tropical disease caused by infection with *Mycobacterium ulcerans* (*M. ulcerans*). Our research elucidates the evolution of BU skin lesions, early detection and treatment of the BU-infected population. First, we formulate a mathematical model that describes the formation of an ulcer, including the space-time dynamics of *M. ulcerans* bacteria, mycolactone toxin, endothelial and stromal skin cell densities. The skin cell death processes causing the large ulcers in BU are ischaemia and direct cytotoxicity. Our results show that cell death occurs when either direct cytotoxicity, ischaemia, or both are present, and we also illustrate the speed of wound enlargement. Second, we develop an epidemiological model for the incidence, progression and treatment of BU. Our model shows the trend that populations in different compartments can take after being infected with BU. In our model results, an increase in the transfer rates between categories of infection leads to a decrease in the proportion of the population infected. Additionally, increasing the rate of transitioning to treatment decreases the proportion of cases that progress to ulcerative categories. Third, we investigate the cost-effectiveness of introducing a rapid diagnostic test (RDT) for testing BU from a healthcare provider perspective in Ghana. We develop a decision tree model and compare the RDT with the polymerase chain reaction test (PCR). The main result was the incremental cost-effectiveness ratio (ICER) of $-\$272.73$ per disability-adjusted life year (DALY) averted from using an RDT compared to a PCR. In the probabilistic sensitivity analysis, most ICER pairs spread out in the southeast quadrant, where the RDT was less costly and yielded fewer DALY. Finally, we develop an agent-based model to explore the effects of introducing community health volunteers (CHV) in referring BU patients for treatment. We compare the effect of either self-referral (SR) independently or both SR and CHV in the early diagnosis and treatment of BU. Our results show that using CHV in active case finding leads to an increase in the detection of BU in early categories, spearheading the early start of treatment and hence reducing disability.

Keywords: Buruli ulcer; *Mycobacterium ulcerans*; mycolactone; ischaemia; direct cytotoxicity; endothelial cells; cost-effectiveness analysis, rapid diagnostic test, community health volunteers, agent-based model.

Contents

List of Figures

List of Tables

Listings

Research Thesis: Declaration of Authorship

Print name: **Fatumah Atuhaire**

Title of thesis: **Mathematical models of wound formation, disease progression and treatment pathways of Buruli ulcer disease**

I declare that this thesis and the work presented in it are my own and has been generated by me as the result of my own original research.

I confirm that:

1. This work was done wholly or mainly while in candidature for a research degree at the University of Southampton;
2. Where any part of this thesis has previously been submitted for a degree or any other qualification at this University or any other institution, this has been clearly state;
3. Where I have consulted the published work of others, this is always clearly attributed;
4. Where I have quoted from the work of others, the source is always given. With the exception of such quotations, this thesis is entirely my own work;
5. I have acknowledged all main sources of help;
6. Where the thesis is based on work done by myself jointly with others, I have made clear exactly what was done by others and what I have contributed myself;
7. Parts of this work have been published as conference proceedings.

   Atuhaire. F, Currie. C. S. M, Hoyle. R.B. (2023). Modelling the potential impact of community health volunteers in the diagnosis and treatment of Buruli ulcer disease, Proceedings of the 2023 Winter Simulation Conference.

Signed:

Date: February 6, 2024

Acknowledgements

First, I thank God for his guidance and grace in finishing this thesis. "*For You are great, and do wondrous things; You alone are God,*" Psalms 86 : 10.

Second, I am profoundly grateful to my supervisors, Professor Rebecca Hoyle and Professor Christine Currie, for their invaluable guidance, encouragement and insightful comments throughout this thesis's research process and writing. Thank you for always going the extra mile to read and offer feedback on several revisions of every word I have written. Thank you for being supportive emotionally.

I am grateful to Professor Rachel Simmonds (University of Surrey) for the research discussions, constructive recommendations, feedback and revisions on chapter 3 of this thesis.

This thesis is only complete with your help and support through it all. What a privilege to have had you as my supervisors! Thank you!

I am grateful to my friends from AIMS, particularly Buri Gershom and Grace Mwakyoma, for your support and friendship over the years. A big thank you to my PhD colleagues specifically Patricia Ndugga, Mohammed Alammar, Eunice Mueni and Tristan Madeleine. Thank you for listening to me when the dots were not connecting. Your presence made PhD work enjoyable and less lonely.

My friends at the Grace Hub Fellowship, Southampton with whom we study the bible together every Thursday evening. Thank you for the good memories!

I am deeply thankful to my family in Uganda for their unwavering emotional support, prayers and love. It was always a pleasure to share beautiful moments every time I came home.

Lastly, I acknowledge funding from the University of Southampton under the centrally awarded Vice-Chancellors Scholarships, without which I would have been unable to conduct this study. The additional funds from the University of Southampton under the COVID-19 funding extension scheme were instrumental in assisting me in carrying out my research during the pandemic.

Ad maiorem dei gloriam

Nomenclature

BU	Buruli ulcers
M. ulcerans	*Mycobacterium ulcerans*
RDT	Rapid diagnostic test
PCR	Polymerase chain reaction
CHV	Community health volunteers
WHO	World Health Organisation
ECM	Extra cellular matrix
ODEs	Ordinary differential equations
PDEs	Partial differential equations
R_0	Basic reproduction number
SIR	Susceptible infected and recovered
DT	Direct cytotoxicity
CEA	Cost effectiveness analysis
ICER	Incremental cost effectiveness ratio
DALYs	Disability adjusted life years
ABM	Agent based models

Chapter 1

Introduction

1.1 What is Buruli ulcer?

Buruli ulcer (BU) is a neglected tropical disease caused by infection with a bacteria called *Mycobacterium ulcerans (M. ulcerans)* (WHO, 2018). It is a chronic, debilitating disease that affects the skin and soft tissue (Asiedu et al., 2000). BU is the third most common mycobacterial disease after tuberculosis and leprosy and has been reported in 33 countries globally. The most prevalent cases have been reported from west and central Africa, Australia, and Japan (Yotsu et al., 2015). It is also highly probable that cases are under-reported since many countries that are likely to have cases do not report to WHO. Figure 1.1 shows annual reported BU cases from 2010 to 2021.

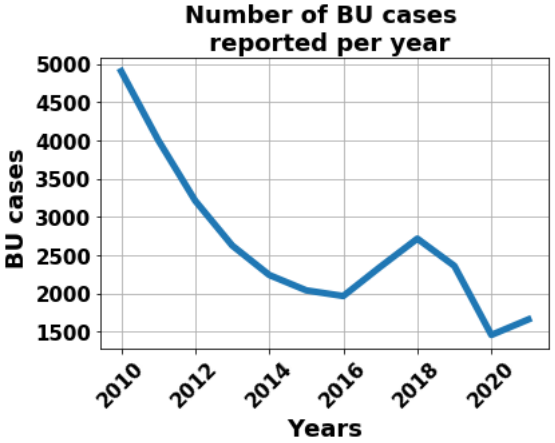

FIGURE 1.1: A plot showing reported BU cases globally from 2010 to 2021. The data was obtained from the WHO website (WHO, 2022).

BU may affect people of all ages, but the highest number of cases occur in children aged between 5 and 15 in West Africa (Van der Werf et al., 1989; Debacker et al., 2004). It manifests as a painless itchy nodule, a plaque, or an oedematous lesion which eventually

ulcerates within weeks with undermined edges (WHO, 2018). BU does not kill but if not treated early can lead to functional limitation, permanent disability and social stigmatization (Stienstra et al., 2002; Ellen et al., 2003; Johnson et al., 2005). According to WHO, early diagnosis and treatment with antibiotics before ulceration are the quickest remedies for the disease.

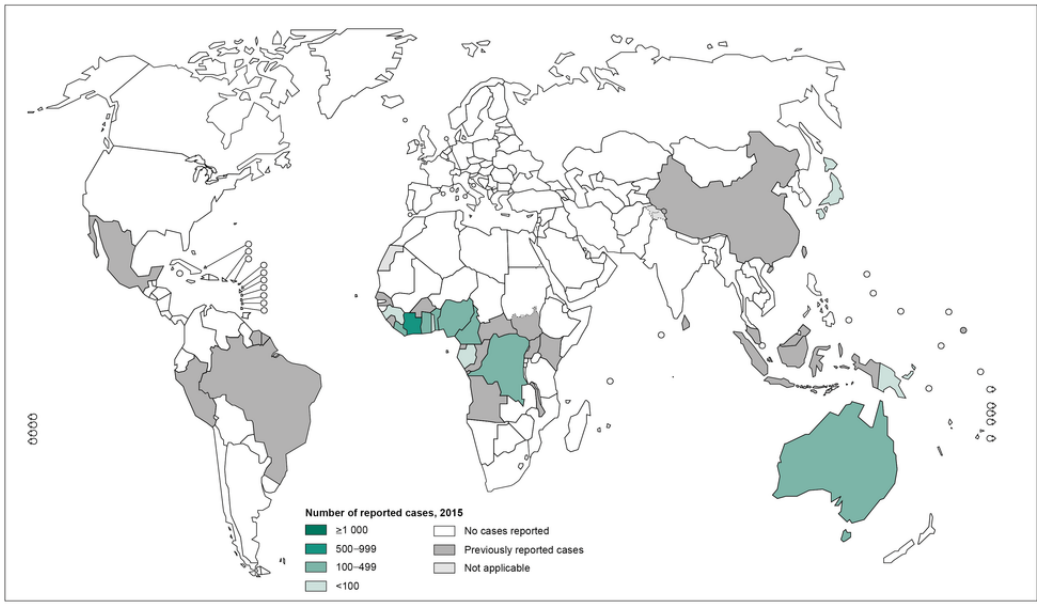

FIGURE 1.2: World map showing the geographical distribution of reported BU cases. Image source: (WHO, 2018).

1.1.1 *Mycobacterium ulcerans*

To understand the dynamics of BU transmission and spread, an understanding of the reservoirs of *M.ulcerans* is key. *M.ulcerans* is an environmental pathogen which could explain why BU has been associated with places near slow-flowing water bodies, wetlands, human-associated activities like dam construction, deforestation, farming and agriculture (Barker, 1972; Portaels, 1989, 1995; Walsh et al., 2008; Bratschi et al., 2014; Maman et al., 2018). Person-to-person transmissions of *M.ulcerans* are extremely rare (Merritt et al., 2010; O'Brien et al., 2017).

The path of its transmission in humans is still an enigma, however, there have been two hypotheses as to how BU is transmitted. One is that it is spread by the bite of an aquatic bug and the other is that it is introduced into the body when the skin is injured through interaction with an aquatic environment (Dhungel et al., 2021; Singh et al., 2018).

M.ulcerans is a slow growing mycobacterium that grows best at a low temperature of $(29 - 33°C)$ and a low atmospheric oxygen concentration of 2.5% (Van der Werf et al., 1999; George et al., 2000). This growth temperature of the *mycobacterium* is significant in limiting the infection to the cutaneous tissue where the bacteria is likely to encounter

favourable growth temperatures (Merritt et al., 2010). *M. ulcerans* secretes a lipid toxin known as mycolactone (George et al., 1999). The incubation period between infection of *M. ulcerans* and clinical manifestation of BU is $1-8$ months (Trubiano et al., 2013).

1.1.2 Mycolactone toxin

The pathological features observed in BU are best explained by the presence of mycolactone (George et al., 1999; Stinear et al., 2004). Some of the effects of mycolactone on the skin are described below.

In vitro studies have revealed that cells respond to mycolactone depending on the cell type and stage of activation of the cell (Hong et al., 2008). When L929 fibroblasts were exposed to mycolactone, the resultant effect was cell detachment, cell round-off and arrest leading to cell death after $48-72$ hours (Hong et al., 2008).

Mycolactone fosters cell death apoptosis and tissue necrosis
In a study conducted by (George et al., 2000), mycolactone was injected into a guinea pig's skin. After 8 days, destruction of lipid and fat cells and oedema were observed in the area. In a study by (Dobos et al., 2001), exposure of an adipose cell to mycolactone induced apoptosis and necrosis. In addition, mycolactone was shown to promote coagulation necrosis (cell death caused by ischaemia) of subcutaneous tissue surrounding areas of bacterial colonization (Sarfo et al., 2016).

Mycolactone leads to fibrin deposition
Fibrin is one of the main components of blood clots. Ogbechi et al. (2015) found fibrin deposits in necrotic areas of BU lesions, whereas no fibrin deposits were observed in normal healthy skin. Furthermore, mycolactone caused the depletion of Thrombomodulin (TM), a protein that binds thrombin, regulates clot formation and is a cofactor in the activation of protein C (Carter et al., 2013).

Mycolactone plays a key role in the immunosuppression and painlessness of BU lesions causing patients to delay seeking treatment (En et al., 2008).

1.1.3 Manifestation of BU

The *M.ulcerans* infection is followed by the non-ulcerative form of the disease which appears as a nodule, papule, plaque or oedematous form (Yotsu et al., 2015).

Lesions can occur on any part of the body but most observed cases are on the extremities. WHO categorised the disease based on the size and severity of the lesions as (WHO et al., 2012):

1. Category I, which appears as a single small lesion (32%),

2. Category II, which appears in non-ulcerative and ulcerative plaque and oedematous forms (35%).

3. Category III, which involves disseminated and mixed forms. Here ulcers spread out to the bones (osteomyelitis) and to the joints (33%).

Figure 1.3 is an illustration of the manifestations of BU disease.

FIGURE 1.3: Manifestation of BU disease. The pre-ulceration forms are represented as (A)-nodule, (B)-papule (C)- plaque. The ulcerative form is represented in (D): notice the presence of oedema. The illustrated cases (A), (C) and (D) were obtained from the WHO website (WHO, 2018). Case (B) was obtained from (Adu and Ampadu, 2015).

1.1.4 Diagnosis and treatment

Early laboratory diagnosis of BU is a crucial step to avoid misdiagnosis and antibiotic misuse (Sakyi et al., 2016). Some of the main methods used for laboratory confirmation include: microscopy for detecting bacteria, culture to isolate viable organisms, polymerase chain reaction (PCR) for detecting pathogen-specific DNA and histopathology (Sakyi et al., 2016). WHO recommends at least two laboratory tests to confirm the disease.

The standard diagnostic method for detection for BU in most endemic countries is PCR which is 100% accurate and is specific to *M.ulcerans* (Phillips et al., 2005). Microscopy and culture have a low sensitivity while histopathology is rarely available in endemic areas (Frimpong et al., 2019). Although PCR has been the recommended diagnostic tool, it is expensive, performed in laboratories with sophisticated set-ups and unavailable to most endemic places which are mainly rural areas (Stinear et al., 1999; Ablordey et al., 2012).

There has been a need for a field-friendly and rapid diagnostic tool (RDT) that would bring diagnosis nearer to patients. This would lead to timely reception of results hence quickening the start of treatment (Frimpong et al., 2019).

A molecular diagnostic tool called *M.ulcerans* recombinase polymerase amplification (Mu-RPA) has been proposed as an alternative to PCR. It yields readily readable results within a short period (Ablordey et al., 2012). Mu-RPA has been applied in diagnosing tuberculosis and proved effective (Boyle et al., 2014). For simplicity of terminologies in this thesis, we will refer to the Mu-RPA as RDT. RDT has the following advantages:

i. RDT offers molecular diagnosis in fieldwork and at the point of care.

ii. RDT is more rapid offering readable results in < 20 minutes compared to PCR (2 hours).

iii. RDT is simpler to run: for example does not require sophisticated set-up compared to PCR.

There is a need to assess the effectiveness of RDT and the impact of its usage on BU patients.

Treatment of BU

The main treatment of BU before 2004 was surgical excision (Dega et al., 2002). This was seen as effective but had been associated with high rates of recurrence, long hospital stays and high treatment costs (Asiedu, Kingsley and Etuaful, Samuel, 1998; Kanga et al., 2003). After several clinical studies, WHO recommended antimicrobial therapy which included a combination of rifampicin and clarithomycin given orally for 8 weeks

as the first line treatment (WHO et al., 2004). In some cases, surgery is still sometimes preferred in Australia (O'Brien et al., 2019).

With early diagnosis, antimicrobial treatment administered daily for 56 days is effective to sterilise the infection site of the disease in the majority of the cases (80%). However, due to the painless nature of the disease, people tend to seek treatment when the ulcers are already advanced. In these advanced stages, treatment will require antibiotics, surgery, skin-grafting accompanied with careful wound management and physiotherapy, and even after intervention patients heal with some form of deformity (WHO, 2018).

There have been attempts to develop vaccines against *M.ulcerans* including strategies to inhibit the effect of mycolactone. However, these developments have not yielded much success so far (Watanabe et al., 2015). One of the research priorities recommended by WHO is to focus on evaluation of shorter treatment for limited lesions (Pluschke and Röltgen, 2019).

Community health volunteers (CHV)

Inclusion of health interventions for example, community involvements and training health workers have been ways to educate and encourage early diagnosis and treatment. Introducing CHV in referring BU cases was instrumental in improving the number of BU cases reported (Vouking et al., 2013; Barogui et al., 2014; Vouking et al., 2014).

1.2 Thesis motivation

The need to demystify mechanisms behind wound growth and healing times in BU coupled with the economic burden of BU treatment on impoverished endemic regions are some of the motivations of this research (Kpeli and Yeboah-Manu, 2019). In addition to the functional limitations that proceed with prolonged hospital stays which are evident among BU survivors.

In the quest to understand BU disease, Ogbechi et al. (2018) explains the molecular mechanisms driving skin cell death: for example, understanding how mycolactone stimulates programmed cell death (apoptosis) and how chronic exposure to stress leads to pathways which have been shown to drive *M. ulcerans* induced apoptosis. Ogbechi et al. (2015) suggested that the cytotoxicity of mycolactone on the cell (the direct effect) and mycolactone-dependent loss of coagulant control (the indirect effect) are the two possible mechanisms that may contribute to tissue necrosis in BU.

These two mechanisms may collaborate to produce the cell death observed in BU. What is not known is the contribution of each mechanism to cell death. This thesis aims to investigate the mycolactone-dependent processes leading to cell death to elucidate the pathogenesis of BU, what drives cell death, and to provide insights into controlling or managing BU disease.

In addition, there is still an urgent need to curb the number of cases that are diagnosed in late stages (WHO, 2018). The painless nature of the disease causes people to report late leading to chronic deep wounds that take a long period to heal. This work investigates interventions that could be adopted to encourage early reporting and provide insights which cannot easily be obtained otherwise by biological sciences or experimental studies alone. The introduction of a RDT and community health volunteers (CHV) are two interventions that this thesis analyses.

Mathematical and computational models represent a useful tool in BU disease modelling in literature (Aidoo and Osei, 2007; Bonyah et al., 2014a,c,b; Nyabadza and Bonyah, 2015; Garchitorena et al., 2015; Assan et al., 2017) and provide some new mechanistic insights. This thesis uses a differential equation model, compartmental model, decision tree model and an agent-based model, to produce novel solutions and recommendations for understanding BU disease.

The first mathematical model of this thesis describes Buruli ulcer lesion formation as initiated by skin cell death processes. This model is motivated by the unresolved question regarding the relative contribution of ischaemia and direct toxicity mechanisms in cell death. Specifically, the model investigates the main mechanism by which cells die and the speed of wound enlargement and demonstrates the growth of *M.ulcerans* and mycolactone in the skin.

The second model investigates the disease progression and treatment pathway of BU in the population of endemic areas in Ghana. This model aims to elaborate on the possible outcomes of populations as they transition from one disease state to another without any intervention. This model accounts for the infected population the same way WHO classified them in categories depending on severity (WHO, 2018). This compartmental model is unique in describing BU transmission in a way that has not been done by previous models for example (Assan et al., 2017; Bonyah et al., 2014c; Nyabadza and Bonyah, 2015; Bonyah et al., 2014b). Specifically, our model takes into consideration, the disease progression and treatment pathway of BU in the population in a way that exactly mimics the nature of the disease.

The third model accounts for the economic evaluation of the introduction of a RDT. It investigates the costs and effects, cost-effectiveness analysis of the RDT compared to the currently used PCR diagnostic test for BU. This model is motivated by studies (Frimpong et al., 2019) who developed a new diagnostic tool with the potential for quick diagnosis of BU at the point of care providing timely results to health workers. There is a need to investigate its availability, affordability and sustainability given the limited resources in most endemic countries. In this thesis, a decision-analytical model and probabilistic sensitivity analysis are used to estimate the relative cost effectiveness of PCR and RDT in the most endemic areas in Ghana. Results from this study can serve as a key element to inform decision makers in public health policy.

The fourth model investigates the role of CHV in referring BU patients for diagnosis and treatment while still in early stages. This model compares the path of BU patients with self-referral alone and with both self-referral and CHV. Specifically, this work uses an agent-based model which is well known for capturing the complex interactions between individuals and the environment (Macal, 2016; Macal and North, 2005). The goal of the third and fourth models is to increase BU disease case detection rates in the early stages and to the extent possible, to improve diagnosis and treatment rates.

This thesis is based upon a critical analysis of the available literature, aiming to understand BU disease. The research results in this work could be tested experimentally and consequently, elucidate on some controversial findings, encourage future avenues of research and contribute towards early diagnosis, treatment, prevention of severe BU cases.

1.3 Research objectives

The main objective of this work was to develop mathematical models which describe and advise on the dynamics of Buruli ulcer disease taking into consideration skin-cell death mechanisms, BU disease progression and treatment pathway, cost-effectiveness of diagnostic tests and the role of CHV in referring BU patients in early stages. The specific objectives for each chapter are:

1. (i) To develop a mathematical model to describe the dynamics of ulcer formation including mycolactone diffusion, *M.ulcerans* growth, decrease in cell densities and increase in fibrin deposition in the skin as time evolves.
   (ii) To investigate the processes within the model that lead to cell death caused by mycolactone diffusion in the skin.
   (iii) To investigate how the ulcers progress when ischaemia or direct toxicity pathways are restrained.

2. (i) To develop an epidemiological model for the incidence, progression and treatment of BU.
   (ii) To briefly describe the aetiology and epidemiology of Buruli ulcers as a neglected tropical disease, and explore possible interventions for managing late-category cases.

3. (i) To evaluate the cost-effectiveness of diagnosing BU with the proposed RDT compared to the traditional PCR in Ghana.
   (ii) To calculate the extent of disability caused by delayed treatment of BU using disability-adjusted life years (DALY).

4. (i) To examine the impact of introducing CHV in referring BU patients for diagnosis and treatment in the early categories of BU disease.

(ii) To use an agent-based model to analyse individual interactions between BU patients and CHV.

1.4 Significance of this study

This work is important in the future direction of the control and management of BU in several ways:

It gives insights into the processes that lead to wound development as observed in BU. This will help in the direction and current progress on BU treatment options such as surgery.

The mathematical framework described in this thesis contributes to the bank of knowledge for research and experimental analysis related to mathematical modelling for BU.

The results of this work could aid decision-making on resource allocation of health facilities. For example on the implementation of cost-friendly diagnostic tools for BU in Ghana.

This work contributes to the existing literature on neglected tropical diseases. It creates a platform for further work on such diseases.

1.5 Thesis overview

In Chapter 2, we review some previous studies done in modelling BU. The review highlights a mathematical model for tissue invasion observed in BU, BU transmission models, and selected models for CEA and ABM for the spread of diseases (for example Malaria).

Chapter 3 presents a mathematical model that uses a system of coupled partial differential equations to understand ulcer formation of BU lesions. Basic properties of the model including parameter estimation are described, followed by numerical simulations and sensitivity analysis of the model behaviour.

Chapter 4 presents a compartmental transmission model that was built based on an SIT (susceptible, infected and treated) model to describe the pathway of BU patients in different stages of the disease. Numerical simulation results are presented and discussed.

Chapter 5, extends the compartmental model by incorporating the use of a RDT as a health intervention. A decision tree model is constructed for BU and two diagnostic approaches are compared. A cost-effectiveness analysis (CEA) of using a RDT compared to a PCR for BU diagnosis in a rural health centre setting in Ghana is conducted. Probabilistic sensitivity analysis is performed and the results are discussed.

Chapter 6 looks at the potential impact of CHV in the early diagnosis of BU disease. An ABM is built to take into account the interaction of BU patients and CHV. Numerical simulation results are presented and discussed.

Chapter 7 presents concluding remarks and highlights future extensions of this study.

Chapter 2

Review of models of BU

Mathematical and epidemiology models have been used to transform research on diseases. These models have been previously used to offer insights on controlling and managing diseases (Hollingsworth, 2009). They have been employed hand in hand with experimental studies to assist policy-makers in deciding which preventive and treatment measures to implement.

The spectrum of mathematical models can vary from ordinary differential equations to agent-based models (ABM), stochastic simulations composed of millions of individuals (Riley, 2007). This variation depends on the type of disease modelled, spatial structure, demographic arrangement, treatment procedures, what the study questions are and the quantity and level of detail of data available (Grassly and Fraser, 2008).

Understanding the progression of BU is vital in the fight to prevent severe cases. Mathematical models offer an avenue to understand the transmission, control, management, and treatment of BU. We explore the dynamics of the BU disease extending and modifying existing models to produce plausible mathematical models motivated by available new research.

In this chapter, we review previous modelling work on BU and other related diseases and pointed out critical results on particular selected models. We review models for tissue invasion in section 2.1, models for the spread of BU in section 2.2, models for cost effectiveness analysis (CEA) in section 2.3 and ABM in section 2.4 respectively.

2.1 Modelling of tissue invasion in BU

Nyarko et al. (2017) developed a mathematical model that uses reaction-diffusion equations to describe the macroscopic effect of mycolactone diffusion on cell density (c), extracellular matrix (ECM) density (ν), and *M.ulcerans* bacterial population (m). The model focuses on making predictions about tissue degradation caused by mycolactone.

The model was formulated based on assumptions that *M. ulcerans* feeds on lipids from the necrotic cell for further growth. In addition, *M.ulcerans*, cells and the ECM compete for tissue space. Furthermore, the production of mycolactone depends on *M.ulcerans* density, and the body responds against the toxin. They also assumed that ECM interaction with mycolactone causes ECM degradation. When ECM fibres get in direct contact with mycolactone, they are degraded and later re-create and re-construct themselves. Their immediate neighbourhood influenced cell movement, which was modelled by haptotaxis and chemotactic responses of cells.

These assumptions led to a system of PDEs as indicated in Equations (2.1) -(2.4) with corresponding boundary and initial conditions. The system was non-dimensionalised and numerical simulations were obtained. A finite-difference method was used to discretize the system.

$$\frac{\partial m}{\partial t} = D_m \nabla m + \gamma \zeta(b) - \lambda_m m, \tag{2.1}$$

$$\frac{\partial b}{\partial t} = \nabla(D_b \nabla b) - \nabla(\chi(c) b \nabla c) + \lambda_b b\left(1 - a_{12}\frac{c}{K_c} - a_{13}\frac{\nu}{K_\nu} - \frac{b}{K_b}\right), \tag{2.2}$$

$$\frac{\partial \nu}{\partial t} = -\delta_\nu m \nu + \lambda_\nu \nu\left(1 - a_{32}\frac{c}{K_c} a_{31} - \frac{b}{K_b} - \frac{\nu}{K_\nu}\right), \tag{2.3}$$

$$\begin{aligned}\frac{\partial c}{\partial t} = {} & \nabla(D_c \nabla c) - \nabla(\rho(\nu) c \nabla c) - \nabla(\psi(c,m) c \nabla m) - \delta_c c m + \\ & \lambda_c c\left(1 - a_{21}\frac{b}{K_b} - a_{23}\frac{\nu}{K_\nu} - \frac{c}{K_c}\right).\end{aligned} \tag{2.4}$$

Parameter	**Description**
$\psi(c, m)$	Function for the influence of chemotactic response
$\rho(\nu)$	Function for the influence of haptotactic response
δ_ν	Degradation rate of ECM fibers
δ_c	Degradation rate of the cell
$\zeta(b)$	Production rate of mycolactone
γ_m	Production rate of *M.ulcerans*
$\chi(c)$	Chemotactic response of the bacteria
λ_b	Birth rate of *M.ulcerans*
λ_m	Decay rate of of *M.ulcerans*
λ_c	Production rate of c
λ_ν	Production rate of ECM fibers
D_m	Diffusion coefficient of mycolactone
D_b	Diffusion coefficient of bacteria
D_c	Diffusion coefficient of the cell
K_b	Carrying capacity of *M.ulcerans*
K_c	Carrying capacity of the cell
K_ν	Carrying capacity of ECM fibers
a_{12}	Competitive effect of c on b
a_{13}	Competitive effect of ν on b
a_{21}	Competitive effect of b on c
a_{23}	Competitive effect of ν on c
a_{31}	Competitive effect of b on ν
a_{32}	Competitive effect of c on ν

TABLE 2.1: Description of parameters used in (Nyarko et al., 2017)'s model.

Their model results suggested that mycolactone degrades ECM, decreasing cell density and creating space for the migration of *M.ulcerans*. This concept indicated that mycolactone diffuses further into the tissue space than *M.ulcerans* as time evolves, was said to explain the difficulty in measuring excision margins during surgery. Their results confirm the toxicity of mycolactone to cells and its degrading effect on ECM.

However, the model included a decay term that accounts for the body's response against the toxin. This phenomenon indicated that the body's immune system fights mycolactone, which contradicts mycolactone's immunosuppressive nature (Goto et al., 2006). In addition, most parameters lacked references or explanations for the choice of particular values.

The main difference between our model in chapter 3 and (Nyarko et al., 2017)'s is the inclusion of ischaemia as a possible pathway of skin cell death. Our model focuses on the effect of mycolactone on skin cells and analyses how the two suggested pathways

(ischaemia and direct toxicity of mycolactone) lead to cell death, which (Nyarko et al., 2017)'s does not consider.

Nyarko et al. (2017) considered chemotaxis and haptotaxis processes in their model. Chemotaxis involves cell movement in response to a chemorepellent or chemoattractant, and haptotaxis, involves cells migration directionally along adhesive substrates like the ECM (Stock and Baker, 2009; Carter, 1967; Rikitake and Takai, 2011).

The authors also incorporated the dynamics of ECM fibre concentration and degradation into their model. By contrast, we focus on the inclusion of ischaemia as a possible pathway of skin cell death using insights obtained by discussion with experts. Our model focuses on the effect of mycolactone on skin cells, and explores the contribution of ischaemia in leading to cell death, thereby paving the way for advancements in this field.

Their model grouped all skin cells as of the same type. However, research has elucidated how mycolactone affects different cell types and different cells are sensitive to different amounts of mycolcatone. For example, mycolactone influences the production of immune cells, primary T-cells (Phillips et al., 2009), endothelial cells (Ogbechi et al., 2015), and dendritic cells (Coutanceau et al., 2007). In this context, our model considered the effect of mycolactone on endothelial cells and categorised all the other cells as stromal cells.

Nevertheless, the results obtained from this paper illuminate some critical points on the role of *M.ulcerans* and mycolactone in tissue invasion in BU disease. We will extend these concepts and apply them to our model in chapter 3.

2.2 Mathematical models for BU

In this section, we explore some epidemiological models that have analysed the interaction of humans and the environment and how *M.ulcerans* infections lead to BU.

Aidoo and Osei (2007) proposed a SIR model for the transmission of BU incorporating the role played by water bugs and levels of arsenic in the environment. The authors considered the fact that arsenic-containing environments have been linked to the prevalence of *M. ulcerans* infection (Duker et al., 2004). This model is one of the earliest mathematical models for BU describing the interrelations between humans, vectors and arsenic-polluted water. The model equations were as follows:

$$\begin{aligned} \frac{dx}{dt} &= maby(1-x) - rx, \\ \frac{dy}{dt} &= a_1 x(1-y) - y(\mu - \alpha). \end{aligned} \tag{2.5}$$

Parameter	Description
x	Proportion of humans infected by *M. ulcerans*
y	Proportion of water bugs infected by *M. ulcerans*
r	Death rate of humans
a	Bite frequency
b	
a_1	Rate of ingestion of *M. ulcerans* by water bugs
m	Number of water bugs per human
α	Relative arsenic concentration in water
μ	Death rate of water bugs

TABLE 2.2: Description of variables and parameters used in (Aidoo and Osei, 2007)'s model.

The higher the rate of ingestion of *M.ulcerans* by water bugs, the higher the rate of its infectiousness. Their model described BU as a micro-parasitic disease in which host-parasite interaction occurred within isolated environments. In their assumptions, humans who contracted BU become immune to further attack. This assumption is incorrect since being infected with BU does not infer immunity as there have been cases of relapse and reinfection (Eddyani et al., 2015). They established the model equations describing the proportion of humans infected by *M. ulcerans* and the proportion of water bugs.

Results from the model concluded that higher arsenic concentration in water caused BU to thrive in the environment. Hence arsenic concentration is likely to influence the transmission of BU. Aidoo and Osei (2007) suggested preventive measures for controlling BU, like wearing protective garments while working outdoors and non-exposure to arsenic environments.

Their model incorporated a key feature of associating arsenic environments with *M. ulcerans* prevalence which has been previously studied (Duker et al., 2004). The model focused on a few aspects of BU spread ignoring key features of BU.

Bonyah et al. (2014b) proposed a compartmental SIR model for transmission of *M. ulcerans* to humans. The authors assumed that an infectious water bug bite in an aquatic environment causes an infection in susceptible humans.

When susceptible water bugs feed on infected fish, they get infected. Furthermore, susceptible fish get infected when they prey on infected water bugs. A set of non-linear ordinary differential equations stated in Equations (2.6)- (2.13) describes the human, fish and water bug interactions populations

$$\frac{dS_H}{dt} = \theta R_H + \mu_H N_H - S_H\left(\beta_H \frac{I_V}{N_H} - \mu_H\right), \tag{2.6}$$

$$\frac{dI_H}{dt} = \beta_H \frac{S_H I_V}{N_H} - I_H(\mu_H + \gamma), \tag{2.7}$$

$$\frac{dR_H}{dt} = \gamma I_H - (\mu_H + \theta) R_H, \tag{2.8}$$

$$\frac{dS_V}{dt} = \mu_V(N_V - S_V) - \beta_V S_V\left(\frac{I_F}{N_V} - \eta_V \frac{U}{K}\right), \tag{2.9}$$

$$\frac{dI_V}{dt} = \beta_V S_V\left(\frac{I_F}{N_V} - \eta_V \frac{U}{K}\right) - \mu_V I_V, \tag{2.10}$$

$$\frac{dS_F}{dt} = \mu_F(N_F - S_F) - \beta_F\left(\frac{S_F I_V}{N_F} - \eta_F \frac{S_F U}{K}\right), \tag{2.11}$$

$$\frac{dI_F}{dt} = \beta_F\left(\frac{S_F I_V}{N_F} - \eta_F \frac{S_F U}{K}\right) - \mu_F I_F, \tag{2.12}$$

$$\frac{dU}{dt} = \sigma_F I_F - \mu_E U, . \tag{2.13}$$

where S_H, S_V and S_F represent the susceptible human population, susceptible water bugs and susceptible fish, respectively. The terms I_H, I_V, I_F and R_H are the infected human population, infected water bugs, infected fish and recovered human population, respectively. U represents the density of *M.ulcerans*.

Parameters β_H, β_V and β_F represent the effective contact rates between the vector and susceptible humans, the fish and susceptible vectors, the susceptible fish and *M.ulcerans* respectively. Parameters μ_H, μ_V and μ_F represent the natural mortality rates of humans, vectors and fish, respectively. Parameters σ_F and σ_V represent the rate of shedding of *M.ulcerans* into the environment by fish or by water bugs, respectively. μ_E is the rate which *M.ulcerans* is cleared from the environment. (Bonyah et al., 2014b) explained the remaining parameters in detail.

They introduced controls on interventions like insecticide ($u_1(t)$), mass education ($u_2(t)$) and treatment ($u_3(t)$). These controls focused on decreasing the exposure of susceptible humans to infected water bugs, curbing the infection of water bugs and fishes, and reducing the infection between the water bugs and the environment. The optimal control strategy was applied, where one strategy was activated while the remaining two were set to zero for a period of 100 days.

In their numerical simulation results, a combination of controls $u_1(t)$, $u_2(t)$ and $u_3(t)$ was capable of helping reduce the number of infected humans, water bugs, small fishes and *M.ulcerans* in the environment and reducing the number of BU infections.

The principal concept with (Bonyah et al., 2014b)'s model is the use of optimal control theory to mitigate BU, an approach that had not been applied explicitly for BU before.

Nyabadza and Bonyah (2015) extended the work of Bonyah et al. (2014b) by adding a term $\sigma_V I_V$ to the environment compartment U in Equation (2.13). This term represented the shedding of *M. ulcerans* into the environment by water bugs.

According to the sensitivity analysis results, parameters like the removal rate of *M.ulcerans* from the environment μ_E, the shedding rate of *M.ulcerans* in the environment by water bugs σ_V, and by fish σ_F greatly influenced the prevalence of BU in humans. For example, the prevalence of human infections increased by 6% after an increase in σ_F by 0.01. When the population of infected fish that shed bacteria into the environment increases, this leads to the growth of *M.ulcerans*.

After fitting the incidence data of BU cases in Ghana to the model, the resultant projections for the next 5 years showed a slight decrease in cases that remained constant after 1 year. In other words, if there is no implementation of policies to curb the cases, BU cases will remain constant. Their model concluded that BU's management depends on environmental management.

The fundamental observation from work by (Bonyah et al., 2014b) and (Nyabadza and Bonyah, 2015) is the inclusion of interactions among fish, water bugs and human populations in the transmission model. These interactions coincide with the suggested transmission mode where aquatic insects are possible natural reservoirs for *M.ulcerans*.

The models focused on intervention strategies, for example, mass education and treatment which concur with the Information, Education and Communication (IEC) (Clift, 1998) strategy. This strategy could contribute to the control of BU.

Bonyah et al. (2014a) developed a mathematical model for BU with saturated treatment. The saturated treatment function modelled the lack of sufficient treatment facilities amidst an increasing number of infected individuals. This model differs from that of Bonyah et al. (2014b) by adding a treatment compartment and incorporating two modes of transmission.

The two modes of BU transmission were either through direct contact with *M.ulcerans* in the environment or through biting by water bugs. This work aimed to model the potential influence of challenges linked with the treatment and management of BU. For example, limited resources, delays in accessing treatment and inadequate medical facilities affect the treatment of ulcers. The model analysis involved determining the steady states and the basic reproduction number of BU (R_0).

Results from their numerical simulations suggested that environmental management, such as the elimination of *M.ulcerans* from the environment and reducing the shedding of water bugs, influenced the eradication of BU. Their results suggested the inclusion of concepts like social interventions for possible extensions of the model.

Studies by Bonyah et al. (2014b,a) described the spread of BU with the inclusion of environmental dynamics and control strategies. They present a good starting point capturing a broader phenomena related to BU in Africa.

Bonyah et al. (2014c) developed an age-structured SIR model for BU in Ghana. The authors assumed that *M.ulcerans* was introduced into the water reservoirs by a disturbed environment. They grouped the human population into three compartments; age and population varied over time in each group.

These considerations led to a coupled system of hyperbolic PDEs for the population and an ODE for *M.ulcerans* transmission. The fixed point theory was applied to prove the existence and uniqueness of the solutions to the PDE system. Furthermore, the solution to the PDE was calculated using the method of characteristics and R_0 was determined.

Their simulation results showed a peak spread period of *M. ulcerans*, which reduced over time. Bonyah et al. (2014c) concluded that the spread of *M. ulcerans* was influenced by human behaviour and the recovery rate of untreated BU depended on a person's immunity. Bonyah et al. (2014c) recommended consideration of treatment control strategies in an age-structured Buruli ulcer model for improved understanding of BU.

One significant feature of the work of Bonyah et al. (2014c) was the inclusion of age as an independent variable. In many tropical and subtropical countries, children below 15 years are at a higher risk of contracting BU (Debacker et al., 2006; Jacobsen and Padgett, 2010; WHO et al., 2012; Maman, Issaka and Tchacondo, Tchadjobo and Kere, Abiba Banla and Piten, Ebekalisai and Beissner, Marcus and Kobara, Yiragnima and Kossi, Komlan and Badziklou, Kossi and Wiedemann, Franz Xaver and Amekuse, Komi and others, 2018).

Studies by Garchitorena et al. (2015) explored the relative contribution of two modes of transmission of BU to humans in Akonolinga district, Cameroon. The authors considered two suggested possible hypotheses: environmental or water bug transmission. They used a SEITR compartmental model to illustrate the cycle of BU accounting for the two transmission routes. In the model, a statistical model linked the presence of *M.ulcerans* with BU incidence. When the contribution of the two routes was quantified, it was observed that the environmental transmission route described the temporal and spatial patterns in the selected endemic areas better than the water bug transmission route. Although research on the mode of transmission is still inconclusive, this work highlights a key aspect in understanding the pathway in the spread of BU to humans.

Assan et al. (2017) proposed a deterministic model for BU transmission in fluctuating environments. It included seasonal environmental variations which caused the disease transmission pathways and *M. ulcerans* to also change periodically. In the model, they established conditions for disease extinction and persistence. The time-averaged reproduction number $[R_0]$ was compared with the original basic reproduction number R_0.

In the numerical simulations, R_0 was found to be slightly less than $[R_0]$. This implied inaccuracies in the number of infections predicted by $[R_0]$. Assan et al. (2017) recommended the inclusion of climatic and environmental changes in building realistic mathematical models.

Other mathematical models of BU include "Mathematical modelling and stability analysis of Buruli ulcers in possum mammals" by (Chu et al., 2021), among others. This paper is the one describing the situation in Australia.

Previous modelling has focused on the disease dynamics and natural history alongside methods for prevention of BU in West Africa. We are instead more focused on its treatment, aiming to evaluate the impact of faster detection of BU on the population.

Nevertheless, concepts from studies in (Aidoo and Osei, 2007; Bonyah et al., 2014a,c,b; Nyabadza and Bonyah, 2015; Garchitorena et al., 2015; Assan et al., 2017; Chu et al., 2021) inspired our modelling work in chapter 4. These models act as an initial step towards understanding BU, showing ways various authors have modelled BU.

2.3 Models for cost effectiveness analysis

In this section we review some of the studies related to costs for BU treatment and cost effectiveness analysis (CEA) models that inspired our work in chapter 5. Whilst knowledge about the aetiology of BU has progressed, there is still need to investigate the economic burden of BU so as to influence health care expenditure (Ackumey et al., 2011).

2.3.1 Economic burden related to BU treatment

The studies in Drummond and Butler (2004), Pak et al. (2012),Amoakoh and Aikins (2013) and Chukwu et al. (2017) evaluated the overall costs of diagnosis and treatment of BU in Australia, Ghana, and Nigeria, respectively.

Drummond and Butler (2004) assessed costs of diagnosis, treatment and lost income of BU patients in Australia. Pak et al. (2012) estimated the treatment cost of *M.ulcerans* infection in the antibiotic era managed at Barwon health centre in Victoria, Australia, from 1998 and 2006. They compared it with costs in the pre-antibiotic era in the neighbouring region from $1991 - 1998$.

Amoakoh and Aikins (2013) estimated the household economic costs and the related intangible costs suffered by BU patients in Obom, Ga South, Ghana. Chukwu et al. (2017) assessed the costs of BU care to patients from the start of illness, diagnosis and to the end of treatment. The study was conducted among patients with BU in four states in Nigeria between July and September 2015.

These models in highlight the costs BU patients incur in order to attain recovery. This information is crucial in estimating costs for BU diagnosis and treatment in our CEA studies.

2.3.2 Cost effectiveness analysis

In this subsection, we review selected CEA studies for diseases like malaria, typhoid and others, in different countries. Of particular interest in this section are models that performed CEA for a similar set of interventions to those we consider in chapter 5 specifically the evaluation of rapid diagnostic tests (RDTs) and can therefore provide a framework that we can build on.

Shillcutt et al. (2008) performed a CEA of a RDT, presumptive treatment and field-standard microscopy in various settings in sub-Saharan Africa where malaria is endemic.

In their model, they developed a decision tree that allows suspected malaria patients to present to a health facility. The population proceed through diagnosis and treatment as determined by the prevalence of malaria among patients, the patient's age, sensitivity and specificity of each unit diagnostic method.

At each decision tree node, the probability, cost and health outcome in terms of DALY are determined. There after, the increment cost and effect of substituting one diagnostic strategy for another are calculated. The authors performed a probabilistic sensitivity analysis using Monte-Carlo simulations with $10,000$ generations of cost and health outcomes from the uncertainty ranges for the input parameters.

Their results showed that the RDT was cost-effective compared to presumptive treatment. Policy-makers can be at least 95% confident of these findings when the prevalence levels of malaria are below 62% and 50% confident when malaria prevalence levels are below 81%. More over, RDTs had a 50% chance of being cost-saving when malaria prevalence levels are below 58%. When compared to microscopy, RDTs were more than 85% likely to be cost-effective across all prevalence levels.

Their study elucidates the importance of introducing RDT for malaria diagnosis in sub-Saharan Africa. Their results paint a picture of RDT's expected accuracy under real-life conditions.

(Hansen et al., 2015) undertook a CEA of a RDT for malaria diagnosis. They compared the RDT with a diagnosis with microscopy and diagnosis by symptoms alone. The CEA of malaria diagnosis was conducted from a health facility and society perspective in regions in Afghanistan with different transmission levels. The authors substituted RDT with either clinical diagnosis or microscopy in the model and calculated the incremental CEA at each substitution.

A decision tree model was built with intervention arms in the three malaria diagnoses for the low and moderate transmission regions.

In the model, they established costs, effects and probabilities at each decision tree node. The effects considered were proper treatment of suspected malaria. Costs included; health sector cost per service, including the cost of RDT, cost of treatment per service, out-of-pocket expenditure, and consultation fee, among others. They conducted a probabilistic sensitivity analysis to deal with uncertainty in parameter estimation.

The key results from their probabilistic analyses indicated that RDTs were more effective than clinical diagnosis in the low transmission setting. For example, the proportion of appropriately treated patients was 65.2% for RDT compared to presumptive diagnosis, which was 12.5%. The societal cost for each patient who used a RDT was US$13.2 and US$1.8 for presumptive diagnosis. This led to an additional cost of US$4.5 for every appropriately treated patient.

The cost-effectiveness acceptability curves showed that the diagnosis with the RDT had a high probability of being cost-effective in the low, moderate and high settings. The RDT's cost-effectiveness remained even when the decision maker was willing to pay less for each appropriately treated patient.

Their results indicated that the introduction of RDT was cost-effective in both the low and moderate malaria transmission settings. They concluded that RDT intervention provided value for money regarding the accurate, appropriate treatment of febrile patients in each setting.

Saito et al. (2018) conducted a study that evaluated the cost-effectiveness of employing a RDT in diagnosing typhoid fever in a remote area in Cambodia. They constructed a decision tree analytical model where the RDT and clinical diagnosis were compared with a hypothetical 1000 children at each arm.

Costs included costs of diagnosis, treatment, and effects, including the number of correctly diagnosed cases and treatment successes.

For each 1000 children, the RDT detected 38.45 true-positives while clinical diagnosis detected 32.59. Moreover, there were 3.61 more treatment successes for the RDT than clinical diagnosis. On calculating the ICER, the incremental cost of the RDT compared to clinical diagnosis was estimated at $5700.

A cost-effectiveness plane illustrated the results of the probabilistic sensitivity analysis. Most of the cost-effect pairs lay in the northeast quadrant, indicating that using RDT resulted in many treatment successes but proved more costly than clinical diagnosis.

Their results found that the RDT was more effective but costly compared to the baseline scenario's clinical diagnosis.

Momoh et al. (2021) formulated a model for BU transmission that incorporated three intervention strategies. These strategies included spraying with insecticides, education on the use of protective equipment and treatment of infected humans. The authors first developed a SEIT compartmental model that involved interactions between humans and water bugs in the environment leading to a system of non-linear differential equations. The model analysis calculated equilibrium points, the basic reproductive number, global stability and bifurcation analysis.

The authors focused on minimizing the number of exposed humans, infected humans and the water bug population while keeping the cost of control strategies at a minimal level.

When the cost-effectiveness analysis was performed, their results indicated that a combination of health education on the use of protective wear, treatment of infected humans and insecticides was the most effective control strategy.

A vital feature of this model is the inclusion of CEA in intervention strategies. The authors calculated the ICER with related costs and infections averted affiliated with each intervention. However, their CEA was basic, excluding critical methodologies like the ICER plane and sensitivity analysis of cost and effect parameters. Furthermore, the authors considered just one cost and effect parameter, with no decision tree model.

The studies reviewed gave us helpful information on the model formulation of the CEA work. The CEA for RDT were for different diseases since, to our knowledge, no specific CEA of RDT on BU diagnosis has been previously conducted.

The methods and hypotheses used in Shillcutt et al. (2008), Hansen et al. (2015), and Saito et al. (2018) provide a framework for the analysis in chapter 5 that intends to examine the cost-effectiveness of introducing a RDT for diagnosis and treatment of BU.

2.4 Review of previous Agent based models

In the past, ABMs have been a valuable tool for studying disease transmission dynamics. ABMs allow the analysis of diseases for heterogeneous populations considering factors like movement patterns, sex, age, and spatial and temporal changes in the model design which are difficult to incorporate into compartmental models (Kong et al., 2016).

ABMs are a type of computational simulation tool composed of agents that can interact with each other and within their environment governed by a set of pre-defined rules. ABMs are powerful for their ability to incorporate stochasticity, individuality and spatial variation in the model formulation (Hackl and Dubernet, 2019).

A population-based behaviour emerges from interactions among different agents in space and time. In general, agent-based modelling is characterised by its bottom-up structure, a micro-scale perspective, discrete-event considerations and non-intuitiveness (Macal and North, 2005; Macal, 2016; Smith et al., 2018).

Research in biological sciences that used ABMs include applications in cell behaviour and interaction (Alber et al., 2003), modelling the spread of cancer (Preziosi, 2003), prey and predator populations (Taylor et al., 2007), modelling the interactions of cells of the adaptive immune system (Folcik et al., 2007).

Hence, we developed our model in chapter chapter 6 based on worked examples in *NetLogo* (Tisue and Wilensky, 1999), the epiDEM model (Epidemiology: Understanding Disease Dynamics and Emergence through Modelling) (Yang and Wilensky, 2011), on HIV model (Wilensky, 1997) and a malaria model (Smith et al., 2018).

The ABM we discuss in this thesis has taken inspiration from a combination of ideas from the following studies.

Modu et al. (2020) used an ABM to model and analyse malaria transmission for heterogeneous populations. They employed a hybrid methodology that incorporates a mathematical model and an ABM. In the mathematical model, they described the spread of malaria based on mosquito and human populations. These descriptions were presented in the form of a compartmental transmission model.

The authors described humans, mosquitoes, pathogens, and environmental agents in the ABM. They employed climatic data from three malaria-prevalent cities of Benin (Nigeria), Tripura (India) and Limpopo (South Africa). The two models were validated against data on reported malaria cases in the three cities.

The model illustrated the relationship between reported malaria cases and the mean temperature. Simulations were done using *VenSim* Eberlein and Peterson (1992) and *NetLogo* (Tisue and Wilensky, 1999) for the mathematical modelling and ABM, respectively. In the *NetLogo* simulation, the authors created the environment and set up the agent procedure.

They compared the mathematical model and the ABM results with reported malaria case data. Their results showed that the ABM was robust in predicting the season of malaria and possible fluctuations.

The model discussed by Modu et al. (2020) acted as a sample model for building our model. For example, the details and algorithms used gave us a flow of what to include in our ABM.

Yang and Wilensky (2011) developed a simulation tool called *epiDEM*, which modelled the spread of an infectious disease in a closed population based on the Kermack-McKendrick model. Agents represented individuals interacting with each other in the environment according to pre-set rules. An individual had 5% probability of being initialized as infected. This model allowed users to engage in modelling epidemics in a natural and individualistic manner.

Individuals were allowed to wander around randomly. A susceptible person can be infected when interacting with an infected person within the same vicinity.

Each agent had direct neighbours and surroundings on all eight neighbouring grid squares. There is a chance for an infected person to recover after reaching the estimated recovery time. An individual's recovery time was drawn out of a Gaussian distribution with a mean of the average recovery time. The user sets the total population, the probability of being infected, and the mean of the average recovery time.

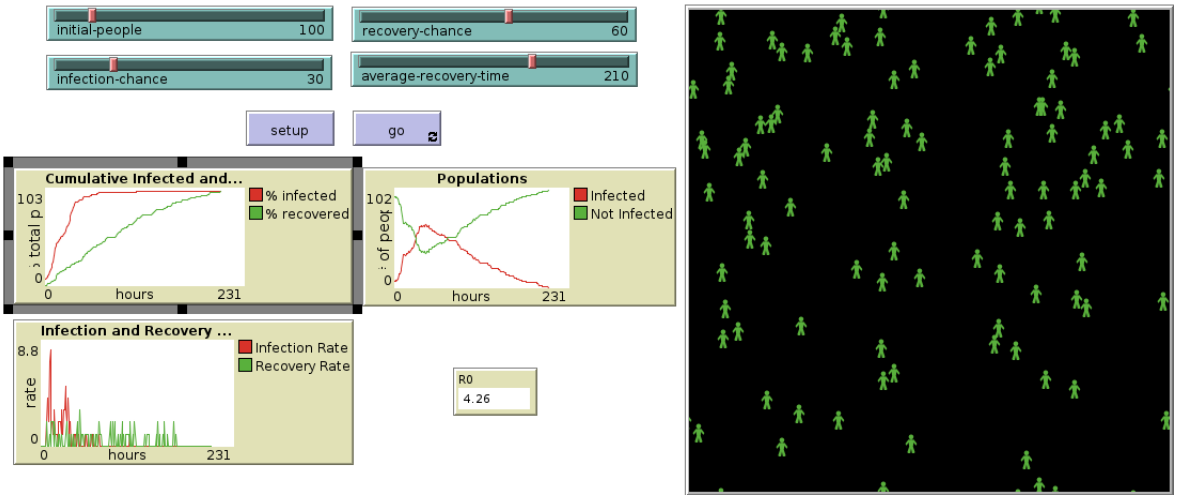

FIGURE 2.1: A screen shot showing the interactive NetLogo interface for the *epiDEM* simulation model. We observe sliders for the user, R_0 values, the percentage of the infected, recovered populations, infected and recovered rates.

Figure 2.1 illustrates how the infection and recovery rates vary over time. In these graphs, the user observed the rate of change of the cumulative infected and recovered in the population. In the Figure interface, the user keeps track of the changes in R_0 and the recovered population per tick.

Different colours represent an individual's state of health. The colours white, red and green represented the susceptible, infected, and recovered populations, respectively.

The set-up and go sliders allow the user to initiate the population and run the simulation. Other sliders like the initial people, infection chance, recovery chance, and average recovery time allow the user to set parameter values.

The *epiDEM* is a basic simulation tool that can be improved. Some of the key questions that could be explored in the model were as follows:

What would be the effect of increasing the initial susceptible population to the rate of disease spread? How do parameters like recovery chance, average recovery time and the rate of infection influence the spread of the disease? What influences the shape of the

cumulative infected and recovered graphs? How do parameters like the recovery chance influence the shape of the graphs? What impact would assuming a population with births, human mobility, and death imply on the model?

Our model in chapter 6 will focus on human movements and interactions between BU patients and community health volunteers (CHV). We employ the same analogy for the modelling and ideas from (Yang and Wilensky, 2011)'s *epiDEM* tool in work in chapter 6.

2.5 Summary

In Chapter 2, we have discussed a variety of models used to model BU and other diseases. In section 2.1, we reviewed a model on tissue invasion in BU. In section 2.2, we reviewed examples of previous models of BU transmission incorporating control strategies. In section 2.3, we discussed models on cost-effectiveness. In section 2.4, we reviewed ABM.

In this thesis, modifications, questions to answer and observations from the existing models are mentioned below:

- In the previous models, no account is given of the role or contribution of ischaemia in influencing cell death observed in BU. An inclusion of ischaemia in modelling cell death processes of BU will elucidate the pattern behind wound development.
- In the BU transmission dynamics, the specific categories of the infected population as defined by WHO are not given much attention in the previous compartmental models. If all the categories of the infected population and the compartments of the treated population were considered, the model would give realistic dynamics on the disease progression and treatment pathway. This feature would enable evaluation of different ways of promoting early diagnosis and treatment of BU.
- The aforementioned models of BU transmission need to put into consideration the role and impact of the introduction of a RDT through CEA. There have been models evaluating the economic burden of BU treatment, but none have considered the possible costs and effects of an RDT so far. In addition to incorporating the effects of seeking treatment late in terms of disability, for example, DALYs. The question is whether the RDT is cost-effective, feasible and possible to implement.
- An ABM provides a new possible approach to modelling BU disease by considering interactions between CHV and BU patients. Population heterogeneity is a characteristic of human lifestyles. Using an agent-based computer simulation model incorporates an element of individual variation that could be closer to reality.

Chapter 3

Modelling the formation of skin ulcers observed in Buruli ulcer disease

One of the clinical presentations of Buruli ulcer (BU) disease are deep wounds with undermined edges on the skin (WHO et al., 2012). The pathological features observed in BU are best explained by an exotoxin produced by *Mycobacterium ulcerans* called mycolactone (George et al., 1999; Stinear et al., 2004). It is well established that exposure of cells to mycolactone is cytotoxic and leads to their death (George et al., 2000; Sarfo et al., 2016). This is due to its inference with normal cellular function, by disrupting protein transport into the endoplasmic reticulum (Hall et al., 2014) leading to activation of apoptotic pathways (Bieri et al., 2017; Ogbechi et al., 2018). Mycolactone has been shown to bind directly to Sec61α, the major subunit of the Sec61 protein conducting channel (Baron et al., 2016; Gérard et al., 2020) and inhibit its functions (McKenna et al., 2016, 2017).

Other mechanisms may also feed into the coagulative necrosis that is commonly seen in BU skin tissue by histopathology. This pattern of necrosis is usually associated with ischaemia, where the tissue architecture is maintained despite the death of the constituent cells. In line with this, fibrin (the end product of the coagulation cascade) is widespread in BU lesions, both as blood clots in capillaries and larger veins and deposited within tissue (Connor et al., 1966; Ogbechi et al., 2015; Hsieh et al., 2022). Fibrin formation can block the transportation of blood to the tissue, cutting off the oxygen supply to cells and explaining the coagulative necrosis seen.

Hence, two mechanisms may elucidate the process of cell death observed in BU disease (Figure 3.1). Here we categorise them as direct cytotoxicity and ischeamia which are explained in section 3.1.

The work flow of the chapter is as follows: in section 3.1, we explain what cell death processes for BU are. In section 3.2, we construct a model for ulcer formation of BU lesions obtaining a system of coupled partial differential equations. We non dimensionalise the equations, initial and boundary conditions. We estimate the model parameters, variables and their corresponding sources. In section 3.3, we carry out numerical simulations, find the speed of the wound formation in section 3.4 and perform a sensitivity analysis of key parameters in section 3.5. We conclude the chapter in section 3.6.

3.1 Direct and indirect mechanisms of mycolactone-dependent cell death

Cell death due to direct cytotoxicity: Certain single amino acid substitutions of Sec61α render those cells resistant to mycolactone-induced cell death (Baron et al., 2016; Ogbechi et al., 2018; Zong et al., 2019; Gérard et al., 2020). Hence, the direct cytotoxicity due to mycolactone is dependent on its action at the protein conducting channel. The underlying mechanism involves the cytosolic build-up of mislocalised proteins, due to disruption of protein transport into the endoplasmic reticulum (Hall et al., 2014). This leads to activation of cellular stress pathways, ultimately leading to activation of caspase pathways involved in apoptosis (Hall et al., 2014; Ogbechi et al., 2018).

Cell death due to ischaemia: While the formation of fibrin in BU lesions is well-established, the molecular mechanism driving it is less well understood. Recently it was shown that mycolactone reduces the ability of endothelial cells to anticoagulate blood by reducing the expression of a protein called thrombomodulin (TM) (Ogbechi et al., 2015). One of the roles of TM is to accelerate the formation of the anticoagulant, activated protein C (Esmon et al., 1982; Esmon, 1995) on the surface of endothelial cells that line all blood vessels and form the capillaries. Hence it was proposed that depletion of TM (which happens within 24 hours) initiates the loss of coagulant control hence causing fibrin deposition (Ogbechi et al., 2015). The depletion of TM depended on mycolactone's action at Sec61, hence a wider endothelial dysfunction may likely also be induced.

In this chapter, we propose a mathematical model that analyses the formation of BU lesions. We consider the dynamics of *M. ulcerans* growth, mycolactone production, and the potential contribution of direct cytotoxicity versus ischaemia mechanisms. It is possible that the direct and indirect effects of mycolactone collaborate leading to the apoptosis and necrosis observed in BU lesions. Our study was conducted to investigate these mycolactone-dependant mechanisms in order to unravel the pathogenesis of BU, what drives cell death, and to provide insights on managing BU disease.

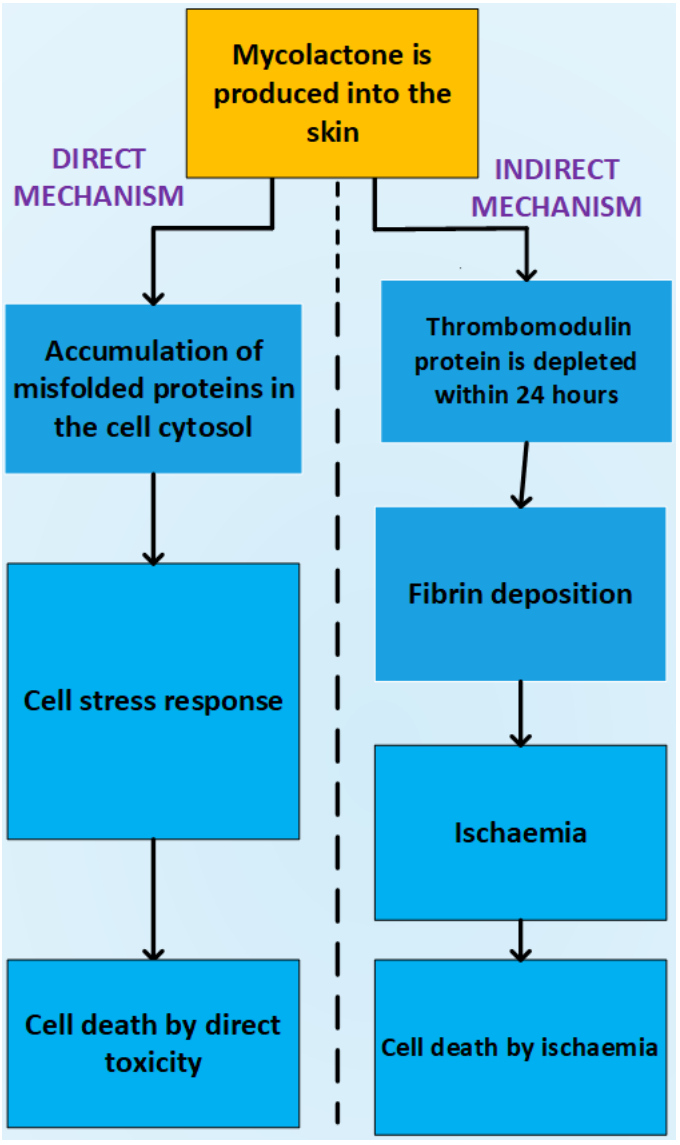

FIGURE 3.1: A flow chart illustrating the direct and indirect mechanisms of mycolactone-dependent cell death processes in the skin exposed to mycolactone. Steps for each mechanism were extracted from studies by (Ogbechi et al., 2015).

The skin tissue is made up of various cell types and the effect of mycolactone on these cells has been studied (Sarfo et al., 2016). Endothelial cells line the blood vessels and form capillaries. They regulate blood clotting (Van Hinsbergh, 2012) within blood vessels in the absence of tissue damage and are highly sensitive to as little as 2 ng ml^{-1} of mycolactone (Ogbechi et al., 2015). Mycolactone disrupts the normal function of endothelial cells by inhibiting its anticoagulant functions.

To simplify our model, we have classified all other cells found within skin as “stromal cells". Stromal cells are sensitive to mycolactone at a concentration of 125 ng ml^{-1} but do not play a direct role in blood coagulation control. An illustration of the structured

spatial arrangement of endothelial and stromal cells in the skin is illustrated in Figure 3.2.

3.2 Model formulation

We formulate a model that describes how the skin ulcer forms with time. We assume the skin is made up of two types of cells: the endothelial and stromal cells with densities $n_e(x,t)$ and $n_s(x,t)$ respectively, where $x \in \mathbb{R}^2$ is a spatial coordinate in the plane of the skin and $t \geq 0$ is time. Both types of cell are sensitive to mycolactone, but endothelial cells have a higher sensitivity than stromal cells (Hall et al., 2014; Ogbechi et al., 2015). We denote as $u(x,t)$ and $m(x,t)$ the density of bacteria and the local mycolactone concentration respectively. When the local concentration of mycolactone, $m(x,t)$, exceeds a certain threshold, skin cells die because of direct cytotoxicity of mycolactone and this process takes 4 days. The stromal cell toxicity threshold (c_s) is greater than that of the endothelial cells (c_e). Endothelial cells also die 1 day after mycolactone reaches c_e through ischaemia (lack of oxygen). Nearby stromal cells also die through ischaemia. Mycolactone causes TM depletion from endothelial cells in culture within 1 day. This would cause rapid formation of fibrin and cell death due to absence of oxygen supply. The precise rate at which these latter events take place in tissue or in culture are not known, hence we have estimated that the whole process of ischaemic cell death takes 24 hours.

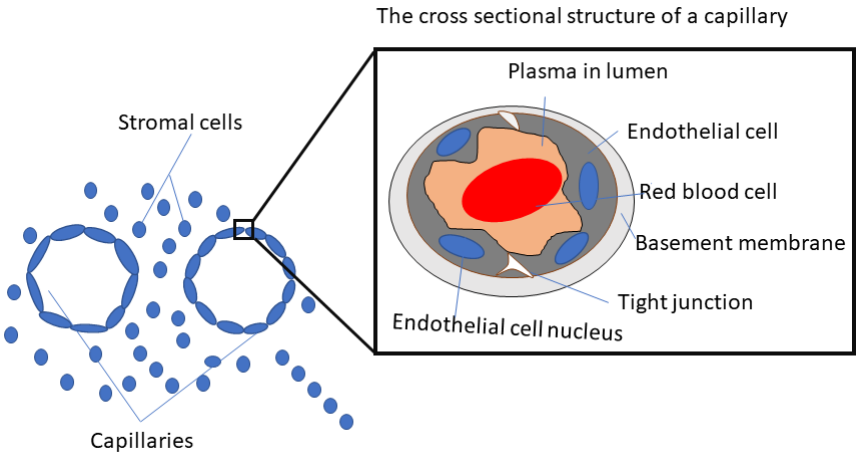

FIGURE 3.2: Illustration of capillaries, endothelial and stromal cells in the skin. Endothelial cells form the capillaries in a layer one cell thick. The capillaries lie in the skin, and outside them are all the other skin cells which we call stromal cells in this work.

3.2.1 Model assumptions and equations

We make the following assumptions:

1. **Skin cell distribution**: In this model, we make the simplifying approximation that on the scale of a BU wound we can treat the distribution of skin cells as spatially mixed with a uniform 9 : 1 ratio of the number of stromal cells to endothelial cells in a healthy skin. We also assume that when cells die, no new cells grow within the time of ulceration. This is because the presence of mycolactone inhibits the cell cycle (George et al., 2000) and its effects are irreversible (Hall et al., 2014; Zong et al., 2019).

2. **Skin cell death**: Direct contact of mycolactone with skin cells leads to cell death. This skin cell death is proportional to the skin cell density if mycolactone concentration, m, is above threshold and zero otherwise:
$$\frac{\partial n_i}{\partial t} = -d_i n_i H(m - c_i),$$
where i are the two cell types e and s and $H(m-c_i)$ is the Heaviside step function that takes the value 0 for $m \leq c_i$ and 1 for $m > c_i$ as follows:
$$H(m - c_i) = \begin{cases} 0 & \text{if } m \leq c_i; \\ 1 & \text{if } m > c_i. \end{cases}$$

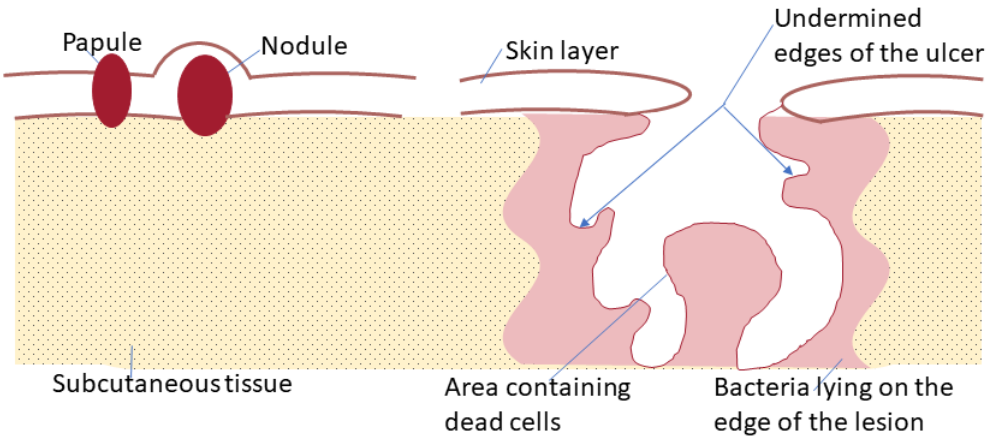

FIGURE 3.3: Illustration of categories of BU disease in the skin. This Figure is a cross section view of a papule, nodule and an ulcer that has penetrated deep into the subcutaneous tissue. We observe undermined edges of the ulcer in the skin which is a key characteristic of BU lesions. Image reproduced from (Van der Werf et al., 1999).

3. **Cell death by ischaemia:** When mycolactone is above the endothelial cell toxicity threshold c_e, fibrin accumulates in the capillaries causing cells to die. This is represented as:
$$\frac{\partial n_i}{\partial t} = -d_k H(m - c_e) n_i,$$
where d_k is the rate of cell death caused by ischaemia. The appearance of skin cell death is illustrated in Figure 3.3.

4. **Diffusion**: According to Fick's second law of diffusion, the flux of a substance is proportional to the concentration gradient of the substance. We use this law

to predict how diffusion causes the concentration to change with time. This is calculated as

$$\frac{\partial \omega}{\partial t} = D\nabla^2\omega,$$

where ω is a representation of the diffusing substances which are the bacterial cell density, $u(x,t)$, and the mycolactone concentration, $m(x,t)$. D is a representation of diffusion coefficients which are D_u and D_m respectively. We shall model diffusion for all the equations in this work in this same way.

5. **Bacterial cell growth** is proportional to bacterial cell density:

$$\frac{\partial u}{\partial t} = \lambda_u u,$$

where λ_u is the constant net birth rate. We also include a density-dependent death rate with parameter, K_u, which controls the bacterial population from growing exponentially in time indefinitely.

$$\frac{\partial u}{\partial t} = \lambda_u u - K_u u^2,$$

where $K_u u^2$ is the term representing bacterial death. The quadratic form indicates that the death rate is higher when the bacterial density is higher for example owing to competition for resources.

6. **Bacterial cell movement** is modelled as a diffusion process:

$$\frac{\partial u}{\partial t} = D_u\nabla^2 u,$$

with a bacteria diffusion coefficient D_u.

7. **Mycolactone** is produced by bacterial cells at rate λ_m. We assume that the toxin diffuses away from the colonisation area with diffusion coefficient D_m

$$\frac{\partial m}{\partial t} = \lambda_m u + D_m\nabla^2 m,$$

and decays at a rate K_m

$$\frac{\partial m}{\partial t} = \lambda_m u - K_m m \ + D_m\nabla^2 m.$$

8. Skin cell densities are initially uniform and non-zero: $n_e(x,0) = n_{e0}$, $n_s(x,0) = n_{s0}$ and mycolactone concentration is initially zero, $m(x,0) = 0$. We introduce an initial colony of bacteria $u(x,0) = u_0$.

The resultant equations from the assumptions represent the dynamics of bacterial cells, mycolactone, endothelial cells and stromal cells for this system respectively.

$$\frac{\partial u}{\partial t} = \lambda_u u + D_u\nabla^2 u - K_u u^2, \tag{3.1}$$

$$\frac{\partial m}{\partial t} = \lambda_m u + D_m\nabla^2 m - K_m m, \tag{3.2}$$

$$\frac{\partial n_e}{\partial t} = -\big(d_e + d_k\big)n_e H(m - c_e), \tag{3.3}$$

$$\frac{\partial n_s}{\partial t} = -d_s n_s H(m - c_s) - d_k n_s H(m - c_e). \tag{3.4}$$

3.2.2 Model variables and parameters

The variables and parameters used in the equations are listed in Table 3.1.

Variable	Description
$n_e(x,t)$	Endothelial cell density
$n_s(x,t)$	Stromal cell density
$u(x,t)$	Bacterial cell density
$m(x,t)$	Mycolactone concentration
x	Spatial variable (Distance)
t	Time
Parameter	**Description**
d_e	Death rate by direct cytotoxicity for endothelial cells
c_e	Threshold value of mycolactone for cytotoxicity in endothelial cells
d_k	Death rate by ischaemia for all cells
d_s	Death rate by direct cytotoxicity for stromal cells
c_s	Threshold value of mycolactone for cytotoxicity in stromal cells
λ_u	Constant net birth rate by which bacteria are produced
D_u	Diffusion coefficient of bacteria
K_u	Constant for density-dependent bacterial death rate
λ_m	Constant rate at which mycolactone is produced by bacterial cells
D_m	Diffusion coefficient of mycolactone
K_m	Degradation rate for mycolactone
L	Typical length scale of ulceration
σ	Standard deviation of the initial Gaussian distribution of bacteria
μ	Mean value of the initial Gaussian distribution of bacteria

TABLE 3.1: Description of variables and parameters used in the model.

3.2.3 Non-dimensionalization of equations, boundary and initial conditions

The basic principle of non-dimensionalization is to rewrite the system of equations in non-dimensional variables so as to simplify the effects of physical scale. We express the equations in dimensionless variables by scaling as follows:
Let

$$u = U_0\tilde{u}, \quad m = M_0\tilde{m}, \quad n_e = A\tilde{n_e}, \quad n_s = B\tilde{n_s}, \quad t = T_0\tilde{t}, \quad x = X_0\tilde{x}. \tag{3.5}$$

We transform the derivatives

$$\frac{\partial}{\partial t} = \frac{\partial \tilde{t}}{\partial t}\frac{\partial}{\partial \tilde{t}} = \frac{1}{T_0}\frac{\partial}{\partial \tilde{t}}, \tag{3.6}$$

$$\frac{\partial}{\partial x} = \frac{\partial \tilde{x}}{\partial x}\frac{\partial}{\partial \tilde{x}} = \frac{1}{X_0}\frac{\partial}{\partial \tilde{x}}, \tag{3.7}$$

We substitute Equations (3.5), (3.6) and (3.7) into Equations (3.1) to (3.4) and we obtain;

$$\frac{\partial \tilde{u}}{\partial \tilde{t}} = \lambda_u T_0 \tilde{u} + \frac{D_u T_0}{X_0^2}\frac{\partial^2 \tilde{u}}{\partial \tilde{x}^2} - K_u T_0 U_0 \tilde{u}^2, \tag{3.8}$$

$$\frac{\partial \tilde{m}}{\partial \tilde{t}} = \lambda_m \frac{T_0 U_0}{M_0}\tilde{u} + \frac{D_m T_0}{X_0^2}\frac{\partial^2 \tilde{m}}{\partial \tilde{x}^2} - K_m T_0 \tilde{m}, \tag{3.9}$$

$$\frac{\partial \tilde{n_e}}{\partial \tilde{t}} = -T_0(d_e + d_k)\tilde{n_e} H\Big(\tilde{m} - \frac{c_e}{M_0}\Big), \tag{3.10}$$

$$\frac{\partial \tilde{n_s}}{\partial \tilde{t}} = -T_0 \tilde{n_s}\Big[d_s H\Big(\tilde{m} - \frac{c_s}{M_0}\Big) + d_k H\Big(\tilde{m} - \frac{c_e}{M_0}\Big)\Big]. \tag{3.11}$$

Now we choose scalings to make the equations as simple as possible. We did this by equating the coefficients of variables in Equations (3.8) - (3.11), to 1 as follows:

$$\lambda_u T_0 = 1, \quad T_0 = \frac{1}{\lambda_u}, \tag{3.12}$$

$$\frac{D_u T_0}{X_0^2} = 1, \quad X_0 = \sqrt{\frac{D_u}{\lambda_u}}, \tag{3.13}$$

$$K_u T_0 U_0 = 1, \quad U_0 = \frac{\lambda_u}{K_u}, \tag{3.14}$$

$$\frac{\lambda_m T_0 U_0}{M_0} = 1, \quad M_0 = \frac{\lambda_m}{K_u}, \tag{3.15}$$

We now have values for T_0, X_0, U_0, M_0. The diffusion coefficient in Equation (3.9) simplifies to

$$\frac{D_m T_0}{X_0^2} = \frac{D_m T_0}{D_u T_0} = \frac{D_m}{D_u}.$$

We group parameters D_m and D_u such that

$$\frac{D_m}{D_u} = \alpha, \tag{3.16}$$

Similarly, we substitute for $T_0 = \frac{1}{\lambda_u}$ in $K_m T_0$ to obtain;

$$K_m T_0 = \frac{K_m}{\lambda_u}$$

We group parameters K_m and λ_u such that

$$\frac{K_m}{\lambda_u} = \beta. \tag{3.17}$$

We let

$$\frac{c_e}{M_0} = \tilde{c_e}, \quad \frac{c_s}{M_0} = \tilde{c_s}, \quad \delta_e = \frac{d_e}{\lambda_u}, \quad \delta_s = \frac{d_s}{\lambda_u} \quad \text{and} \quad \delta_k = \frac{d_k}{\lambda_u}. \tag{3.18}$$

We substitute T_0, X_0, U_0, M_0 and α, β, $\tilde{c_e}$, $\tilde{c_s}$, δ_e, δ_s, δ_k into Equations (3.8) - (3.11) and drop the tildes for simplicity of notation. This rescaling gives Equations (3.19) to

(3.22).

$$\frac{\partial u}{\partial t} = u + \nabla^2 u - u^2, \tag{3.19}$$

$$\frac{\partial m}{\partial t} = u + \alpha \nabla^2 m - \beta m, \tag{3.20}$$

$$\frac{\partial n_e}{\partial t} = -\big(\delta_e + \delta_k\big) n_e H(m - c_e), \tag{3.21}$$

$$\frac{\partial n_s}{\partial t} = -\delta_s n_s H(m - c_s) - \delta_k n_s H(m - c_e). \tag{3.22}$$

which are the non-dimensionalized versions of Equations (3.1), (3.2), (3.3) and (3.4).

Non-dimensionalized boundary conditions

We assume that the wound propagates into healthy skin where there are no bacteria or mycolactone. On an infinite domain of healthy skin the boundary conditions for u and m would be $u(t,x) \to 0$ as $x \to \pm\infty$ and $m(t,x) \to 0$ as $x \to \pm\infty$. We will approximate these on a finite domain $[0, \tilde{L}]$ by

$$u(t,0) = u(t,\tilde{L}) = 0, \quad m(t,0) = m(t,\tilde{L}) = 0, \qquad \forall \quad t \geq 0. \tag{3.23}$$

Non-dimensionalized initial conditions

We make the transformations for t, x, u, m, n_e and n_s and drop the tildes as before. Initial conditions for the equations in the non-dimensionalized form now become:

$$\begin{aligned} u(0,x) = u_0(x), \quad m(0,x) = 0, \\ n_e(0,x) = n_{e0}, \quad n_s(0,x) = n_{s0}. \end{aligned} \tag{3.24}$$

The endothelial cell density in the healthy skin was estimated to be 1.0×10^{-3} g.cm^{-3} and the density of stromal cells was estimated as 9 times the density of endothelial cells ($9n_e$) (Schugart et al., 2008). The total density of cells in healthy skin now becomes

$$n_e + n_s = 9.0 \times 10^{-3} + 1.0 \times 10^{-3} = 1.0 \times 10^{-2} \text{g.cm}^{-3}.$$

Then

$$\tilde{n_{e0}} = \frac{n_{e0}}{A} = \frac{1.0 \times 10^{-3}}{1.0 \times 10^{-2}} = 0.1, \quad \tilde{n_{s0}} = \frac{n_{s0}}{A} = \frac{9.0 \times 10^{-3}}{1.0 \times 10^{-2}} = 0.9,$$

where we choose A to be the total density of skin cells in the healthy skin tissue. Then the non-dimensionalized values for the initial conditions are as follows;

$$n_e(0,x) = 1.0 \times 10^{-1}, \quad n_s(0,x) = 9.0 \times 10^{-1},$$

where again we have dropped the tildes for convenience. And $u_0(x)$ was defined as;

$$u_0(x) = \epsilon \exp^{-\frac{(x-\mu)^2}{2\sigma^2}} \tag{3.25}$$

where $\epsilon = 1.0 \times 10^{-6}$, $\mu = 1$ and $\sigma = \frac{L}{2}$.

We now proceed to estimate the values of variables and parameters used in the model.

3.2.4 Model parameters, values and source used

Some parameter values have been obtained from experimental data available in literature. Other parameters are still difficult to specify accurately so we have estimated them based on similar observations cited in previous studies. Reasons for choosing particular parameter values include:

(i) Bacteria are produced by binary fission and the doubling time of *M. ulcerans* was estimated as 2 days (Cadapan et al., 2001; Zingue et al., 2018b). The rate of increase of the bacterial population with time is proportional to the number of bacteria at any moment in time:

$$\frac{du}{dt} = \lambda_u u.$$

We re-arrange, separate variables and integrate both sides to obtain

$$u = u_0 e^{\lambda_u t}.$$

For u to be doubled, $\frac{u}{u_0}$ must be equal to 2, hence;

$$\frac{u}{u_0} = 2 = e^{\lambda_u t_1} \quad \text{where } t_1 \text{ is the time period for doubling.}$$

Taking the natural log (ln) on both sides, we obtain;

$$\lambda_u = \frac{\ln 2}{t_1}, \quad t_1 = 2 \text{ days} = 2 \times 24 \times 60 \times 60 \text{ seconds},$$
$$\lambda_u = \frac{\ln 2}{48 \times 60 \times 60},$$
$$\lambda_u = 4.011 \times 10^{-6} \text{s}^{-1}. \tag{3.26}$$

(ii) The toxin production rate of mycolactone (λ_m): We estimated this based on experimental studies on mycolactone production by (Cadapan et al., 2001). From Equation (3.2), neglecting diffusion and degradation rate:

$$\frac{dm}{dt} = \lambda_m u.$$

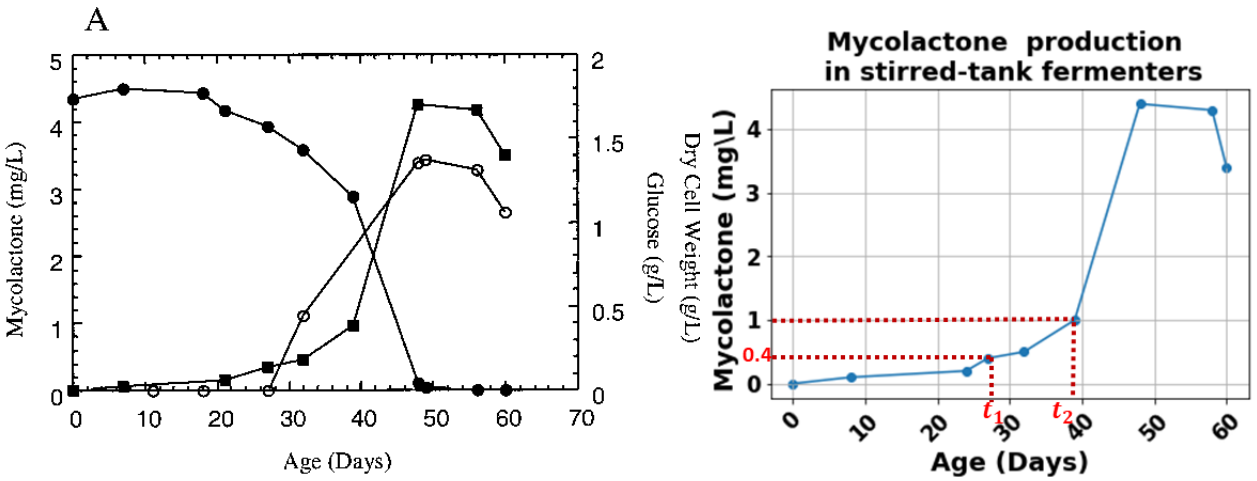

FIGURE 3.4: Illustration of mycolactone production as in Figure 5A of (Cadapan et al., 2001) (left). Illustration of mycolactone production plotted using data estimated from Figure 5A of (Cadapan et al., 2001)(right). We focused on day 27 (t_1) and day 39 (t_2) with corresponding mycolactone concentrations of 0.4 mgL^{-1} and 1.0 mgL^{-1} respectively.

We focused on the beginning of the growth phase of Figure 5A from (Cadapan et al., 2001)'s work to estimate λ_m. We let m_1 and m_2 be mycolactone concentrations at day 27 (t_1) and day 39 (t_2) respectively. We estimate the values for m_1 and m_2 to be 0.4 mgL^{-1} and 1.0 mgL^{-1} from Figure 5A. We estimate the value for u to be approximately between 10^{-2} and 0.5 gL^{-1}. We have

$$\frac{dm}{dt} \approx \frac{m_2 - m_1}{t_2 - t_1} \approx \lambda_m u,$$
$$\lambda_m \approx \frac{1}{u}\frac{m_2 - m_1}{t_2 - t_1}.$$
$$\lambda_m \approx \frac{1}{0.5} \times \frac{0.001 - 0.0004}{(39-27)\times 86400}\text{gL}^{-1}\ \text{s}^{-1}, \quad \approx \frac{1}{10^{-2}} \times \frac{0.001 - 0.0004}{(39-27)\times 86400}\text{gL}^{-1}\ \text{s}^{-1},$$
$$\lambda_m = 1.157 \times 10^{-9}\text{s}^{-1}, \quad \lambda_m = 5.787 \times 10^{-8}\text{s}^{-1}. \tag{3.27}$$

The values obtained in Equation (3.27) give us an idea on the order of magnitude estimate that we can adopt for λ_m. Hence we choose

$$\lambda_m = 1.0 \times 10^{-8} s^{-1}. \tag{3.28}$$

(iii) We estimate that endothelial cells die 1 day after mycolactone reaches the threshold c_e. Assuming that 90% of the cells die to ischaemia in a day, there would be $100\% - 90\% = 10\%$ remaining alive. Applying the concept of half life, the rate of decrease of skin cell density with time is proportional to the skin cell density at any moment in time:

$$\frac{dn_e}{dt} = -d_k n_e.$$

We re-arrange, separate variables and integrate both sides to obtain

$$n_e = n_{e0}e^{-d_k t}$$

For n_e to have decreased to 10% of its initial value, $\frac{n_e}{n_{e0}}$ must be equal to $\frac{1}{10}$, and we have;

$$\frac{1}{10} = e^{-d_k \tau} \quad \text{where } \tau \text{ is the time period for decay.}$$

Taking the natural log (ln) on both sides, we obtain;

$$\begin{aligned} d_k &= \frac{\ln 10}{\tau} \\ d_k &= \frac{\ln 10}{24 \times 60 \times 60} = \frac{\ln 10}{86400} \\ d_k &= 2.665 \times 10^{-5} \text{s}^{-1} \end{aligned} \tag{3.29}$$

(iv) The rate constants d_e, d_s and d_k (death by direct toxicity for endothelial, stromal cells and ischaemia respectively) are inversely proportional to the time for cell death. The time for cell death by direct toxicity is 4 days compared to 1 day for death by ischaemia hence

$$\begin{aligned} d_e = d_s &= \frac{1}{4} d_k \\ &= \frac{1}{4} \times 2.665 \times 10^{-5} \\ &= 6.6625 \times 10^{-6} \text{s}^{-1} \end{aligned}$$

(v) The diffusion coefficient of a diffusible chemical is in the range $10^{-9} - 10^{-6}$ cm^2 s^{-1} (Sherratt and Murray, 1990; Chaplain et al., 1995). In this work, we made specific choices for the diffusion coefficients to model the behaviour accurately. For mycolactone, we opted for a diffusion coefficient of 1.0×10^{-9} cm^2 s^{-1}. This selection reflects the passive diffusion of mycolactone across cell membranes and its uptake into ER membranes, as indicated by (Aydin et al., 2019).

Similarly, we set the diffusion coefficient for bacteria at 5.0×10^{-8} cm^2 s^{-1}, a value derived from the research conducted by (Kim, 1996).

The choice of $D_m = 1.0 \times 10^{-9}$ cm^2 s^{-1} for mycolactone is informed by its established passive diffusion mechanism through cell membranes and uptake into ER membranes. We let this value be lower than D_u.

When mycolactone diffuses more slowly than the bacteria, it suggests that mycolactone diffusion will not be a major contributor to the dynamics of wound formation.

In Section 3.5 of our work, we explored the effects stemming from altering the ratio of mycolactone's diffusion coefficient to that of bacteria on the densities of skin cells. This exploration enabled us to uncover valuable insights into how different diffusion coefficients can influence the fall in skin cell densities.

(vi) According to studies by (Hall et al., 2014; Ogbechi et al., 2015, 2018), the stromal cell toxicity threshold is 125 ng/ml which is equivalent to 1.25×10^{-7} g.ml^{-1} and the endothelial cell toxicity threshold is 4 ng/ml which is equivalent to 4×10^{-9} g.ml^{-1}.

(vii) We find the value of K_m using experimental work by (Marsollier et al., 2007) which suggests that

$$\frac{m_{\text{eqm}}}{u_{\text{eqm}}} = 2.0 \times 10^{-4}, \tag{3.30}$$

where u_{eqm} and m_{eqm} are the equilibrium values for bacterial density and mycolactone concentration in the spatially uniform case respectively. To evaluate K_m, we set the right hand side of Equation (3.2) and the spatial derivatives to zero, giving

$$K_m = \frac{u_{\text{eqm}}}{m_{\text{eqm}}}\lambda_m,$$

and substituting from Equation (3.30) and Equation (3.28), we obtain:

$$K_m = \frac{1.0 \times 10^{-8} s^{-1}}{2.0 \times 10^{-4}\text{gml}^{-1}} = 5.0 \times 10^{-5}\text{s}^{-1}\ \text{gml}^{-1}.$$

(viii) Similarly, we estimate the value of K_u by first calculating the equilibrium bacterial density for a given equilibrium mycolactone concentration from Equation (3.30). We choose $m_{\text{eqm}} = 1.5 \times 10^{-7}\text{gml}^{-1}$ which is a value slightly above the sensitivity thresholds for the two cell types. This will enable us to observe the ulcer formation. Thus

$$u_{\text{eqm}} = \frac{1.5 \times 10^{-7}}{2.0 \times 10^{-4}} = 7.5 \times 10^{-4}\text{gml}^{-1}, \tag{3.31}$$

Then setting $u = u_{\text{eqm}}$ in Equation (3.1) gives

$$K_u = \frac{\lambda_u}{u_{\text{eqm}}} = \frac{4.011 \times 10^{-6}\text{s}^{-1}}{7.5 \times 10^{-4}\text{gml}^{-1}},$$
$$K_u = 5.348 \times 10^{-3}\text{s}^{-1}\ \text{g}^{-1}\ \text{ml}^{-1},$$

where λ_u is the value in Equation (3.1) and u_{eqm} was estimated in (3.31).

We choose $m_{\text{eqm}} = 6.0 \times 10^{-9}\text{gml}^{-1}$ which is a value slightly above the endothelial sensitivity threshold. This will enable us to observe the ulcer formation. Thus

$$u_{\text{eqm}} = \frac{6.0 \times 10^{-9}}{2.0 \times 10^{-4}} = 3.0 \times 10^{-5}\text{gml}^{-1}, \tag{3.32}$$

Then setting $u = u_{\text{eqm}}$ in Equation (3.1) gives

$$K_u = \frac{\lambda_u}{u_{\text{eqm}}} = \frac{4.011 \times 10^{-6}\text{s}^{-1}}{3.0 \times 10^{-5}\text{gml}^{-1}},$$
$$K_u = 1.337 \times 10^{-1}\text{s}^{-1}\ \text{g}^{-1}\ \text{ml}^{-1},$$

where λ_u is the value in Equation (3.26) and u_{eqm} was estimated in (3.32). We have two K_u values where each value corresponds to an equilibrium value.

(ix) According to WHO et al. (2012), the length of the wound lesion in the ulceration stage (WHO category three can extend to $>$ 15 cm). We consider only wounds up to 15 cm terminating the simulation when the wound reaches at 15 cm , the domain

(representing the skin into which the wound is growing) is chosen as larger than this so as to track wound growth. We select 30 cm as the domain size which is large enough to prevent boundary effects and allow the boundary conditions Equation. (3.23) to be applied.

Notation	Dimensional value	Source
λ_u	4.011×10^{-6} s^{-1}	Estimated in (i)
λ_m	1.0×10^{-8} s^{-1}	Estimated in (ii)
d_k	$2.665 \times 10^{-5} s^{-1}$	Estimated in (iii)
d_s	6.6656×10^{-6} s^{-1}	Estimated in (iv)
d_e	6.6656×10^{-6} s^{-1}	Estimated in (iv)
D_m	1.0×10^{-9} cm ^{2} s^{-1}	Estimated in (v)
K_u	5.348×10^{-3} s^{-1} g.ml	Estimated in (viii)
K_u	1.337×10^{-1} s^{-1} g.ml	Estimated in (viii)
K_m	5.0×10^{-5} s^{-1}	Estimated in (vii)
c_e	4.0×10^{-9} g.ml^{-1}	(Ogbechi et al., 2015)
c_s	1.25×10^{-7} g.ml^{-1}	(Hall et al., 2014; Ogbechi et al., 2015, 2018)
D_u	5×10^{-8} cm ^{2} s^{-1}	(Kim, 1996)
L	30 cm	Estimated in (ix)

TABLE 3.2: Parameter values used in the model

The non-dimensional parameter values were calculated as follows:

- The non-dimensional parameters, α and β were obtained by substituting values of D_m, D_u, K_m and λ_u in Equations (3.16) and (3.17).

$$\alpha = \frac{D_m}{D_u} = \frac{1.0 \times 10^{-9}}{5 \times 10^{-8}} = 2.0 \times 10^{-2},$$
$$\beta = \frac{K_m}{\lambda_u} = \frac{5.0 \times 10^{-5}}{4.011 \times 10^{-6}} = 12.46.$$

- Values for δ_e and δ_s were obtained by substituting values of d_e, d_s and d_k in Equation (3.18).

$$\delta_e = \frac{d_e}{\lambda_u} = \frac{6.662 \times 10^{-6}}{4.011 \times 10^{-6}} = 1.662, \quad \delta_s = \frac{d_s}{\lambda_u} = \frac{6.662 \times 10^{-6}}{4.011 \times 10^{-6}} = 1.662,$$
$$\delta_k = \frac{d_k}{\lambda_u} = \frac{2.665 \times 10^{-5}}{4.011 \times 10^{-6}} = 6.637.$$

- The non-dimensional value of L is

$$L = \frac{30}{X_0}, \quad \text{where} \quad X_0 = \sqrt{\frac{D_u}{\lambda_u}},$$
$$X_0 = \sqrt{\frac{5 \times 10^{-8}\text{cm}^{\ 2}\ \text{s}^{-1}}{4.011 \times 10^{-6}\text{s}^{-1}}} = 0.1116\text{cm}, \quad L = \frac{30\text{cm}}{0.111\text{cm}} = 268.697.$$

The non-dimensional values are indicated in Table 3.3.

Notation	Description	Value
α	Ratio of the mycolactone to bacterial diffusion coefficients	2.0×10^{-2}
β	Ratio of the mycolactone decay rate to the bacterial growth rate	12.46
δ_e	Ratio of death rate (endothelial cell) to birth rate by which bacteria is produced	1.662
δ_s	Ratio of death rate (stromal cell) to birth rate by which bacteria is produced	1.662
δ_k	Ratio of death rate by ischaemia to constant net birth rate by which bacteria are produced	6.637
L	Length of the wound	268.697

TABLE 3.3: Non-dimensional parameters used in the model.

3.3 Numerical simulations

Equations (3.19), (3.20), (3.21) and (3.22) with corresponding initial and boundary conditions were solved numerically using finite differences and the "odeint" package in Python 3.6. This function solves a system of ODEs using LSODA from the FORTRAN library odepack. It solves the initial value problem for stiff and non-stiff systems for first order ODEs. It continuously monitors data so as to decide on which method to use (Jones et al., 2014).

For Equations (3.19) and (3.20), we first replaced the second order derivative by the central finite difference approximation. The algebraic equation obtained was then solved using the Python scipy "odeint" function. We approximated the second derivative in the spatial dimension as

$$\frac{\partial^2 u}{\partial x^2} \approx \frac{u(x+h) - 2u(x) + u(x-h)}{h^2}$$

at each node. This leads to a set of coupled ODEs that we then solve as a system of ODEs where $h = l/(N-1)$. N is the number of points in the discretization, and l is the length of the domain. We choose our domain length l to be the typical length scale of ulceration, L in order to capture the early stages of ulcer development.

3.3.1 Evolution of bacterial population and mycolactone concentration

After solving the system of equations in (3.19)- (3.22), we plot the solutions for bacterial (3.19) and mycolactone concentrations (3.20). The equations were solved in a non-dimensional form and plotted in a dimensional form.

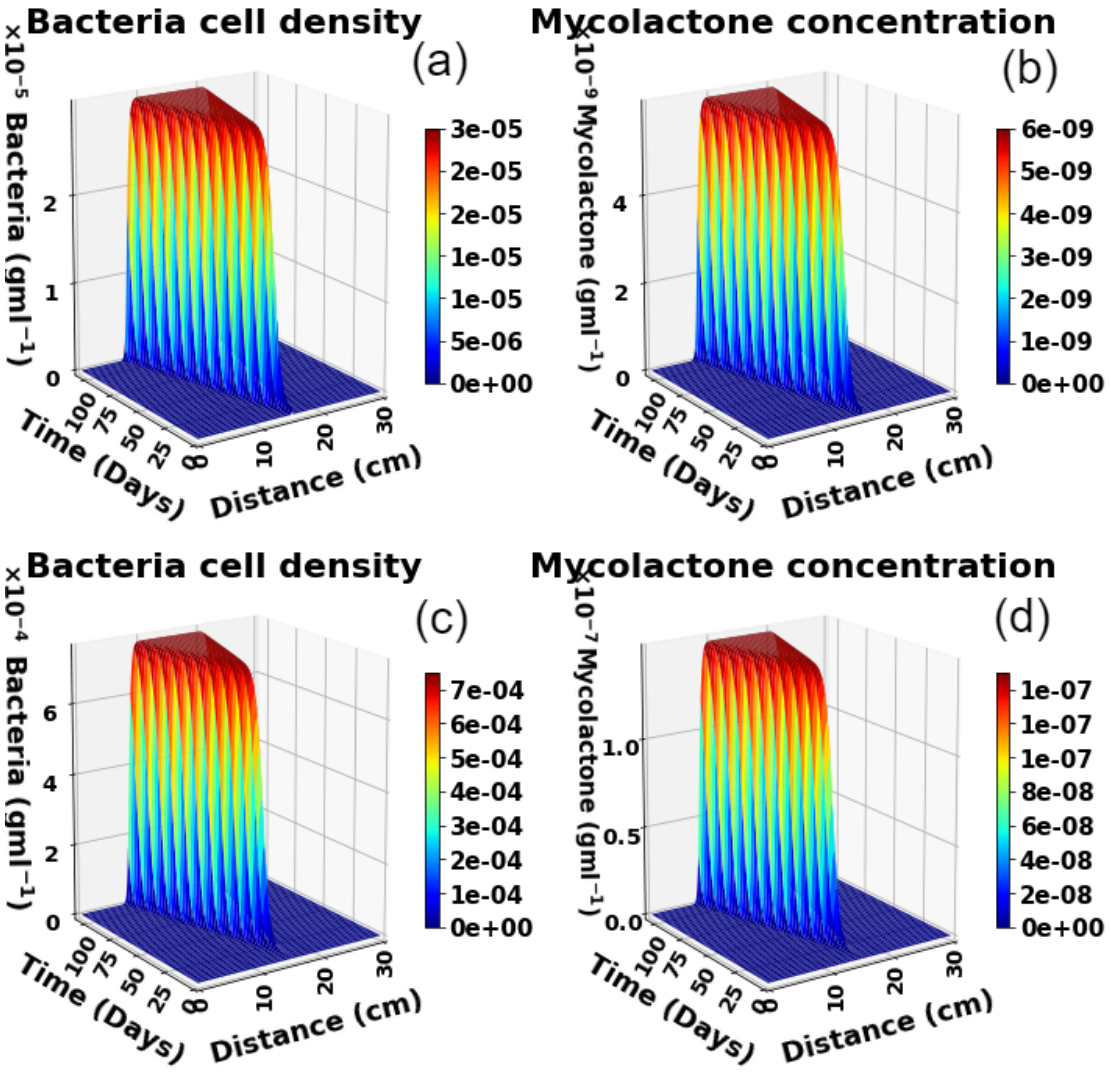

FIGURE 3.5: Evolution of bacteria population and production of mycolactone in a given skin region over a period of 144 days from an initial Gaussian infection profile. In (a) and (b), the maximum bacterial population density at 3.0×10^{-5} g.cm^{-3} produces mycolactone density of 6.0×10^{-9} g.cm^{-3}. In (c) and (d), the maximum bacterial population density at 7.0×10^{-4} g.cm^{-3} produces mycolactone density of 1.4×10^{-7} g.cm^{-3}.

In Figure 3.5 of u and m with a Gaussian initial infection, we start with an initial small amount of *M. ulcerans* bacteria which multiplies logarithmically. As time passes, bacterial cells continue to double in amount every few days until it reaches a plateau. Here the solution does not vary with change in time. We stop the simulation before the bacteria reaches the edges of the wound.

Where *M. ulcerans* bacteria grow, they produce mycolactone toxin which also accumulates in the same pattern as the bacteria. By setting the values of K_u as described in (viii), we set mycolactone concentrations m_{eqm} as 6×10^{-9} gml^{-1} and 1.5×10^{-7} gml^{-1}

as the values of mycolactone when it has reached its plateau or stationary phase. These values are slightly above the cell toxicity thresholds of the endothelial and stromal cells. Mycolactone increases in the centre of the lesion and later diffuses across the lesion with increase in time.

Spread of the lesion using a travelling wave solution

The equation for the bacterial population (Equation (3.1)) is similar to the Fisher KPP equation (De Rijk et al., 2016). The Fisher KPP is used to describe the propagation of biological populations in space. It combines the diffusion term with a logistic growth term, expressed as:

$$\frac{\partial u}{\partial t} = D\frac{\partial^2 u}{\partial t^2} + ru(1-u),$$

where D is the diffusion coefficient, r is the intrinsic growth rate of the population and $u(x,t)$ represents the population density at position x and time t.

The analytical solution for the Fisher-KPP equation in the form of a travelling wave is given as

$$u(x,t) = \frac{1}{1+\exp\left(\frac{x-ct}{\sqrt{4Dr}}\right)},$$

where c is the wave speed, determined by the balance between the growth and diffusion terms and $\sqrt{(4Dr)}$ is a diffusion-related term that influences the width of the wave.

We solved the bacteria population (Equation (3.19)) analytically and showed that there exists a physically realistic solution when the wave speed c ≥ 2. We used the travelling wave solution to understand the spread of ulcers over the skin.

This solution represents a propagating front where the population density increases from 0 to 3.0×10^{-5} as the wave advances in space as illustrated in Figure 3.6. The logistic growth term ensures that the population saturates at $u = 3.0 \times 10^{-5}$ as it reaches a stable equilibrium.

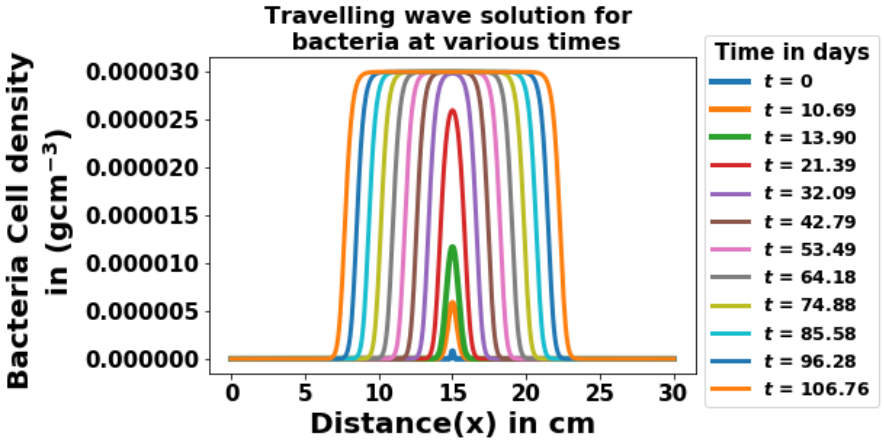

FIGURE 3.6: Travelling wave solution of the bacterial population. The initial condition is 0 everywhere except near $x = 15$ where the initial condition is a Gaussian curve of mean and variance 1 and $L/2$ respectively.

In Figure 3.6, there exist two travelling waves, both starting near $x = 15$ cm, one going to the right and another to the left. This solution approaches the equilibrium for the bacterial population equilibrium at 3.0×10^{-5} gml^{-1}. With the travelling wave solution we can observe how the lesion spreads out on the entire domain at different times.

3.3.2 Death of skin cells in response to mycolactone

We illustrate the solutions to Equations (3.21) and (3.22) by plotting n_e and n_s respectively.

Cell death when both ischaemia and direct toxicity are switched on

Figure 3.7 shows cell death when ischaemia and direct cytotoxicity is switched on. Mycolactone equilibrium values (m_{eqm}) are set to 6×10^{-9} gml^{-1} or 1.5×10^{-7} gml^{-1} respectively.

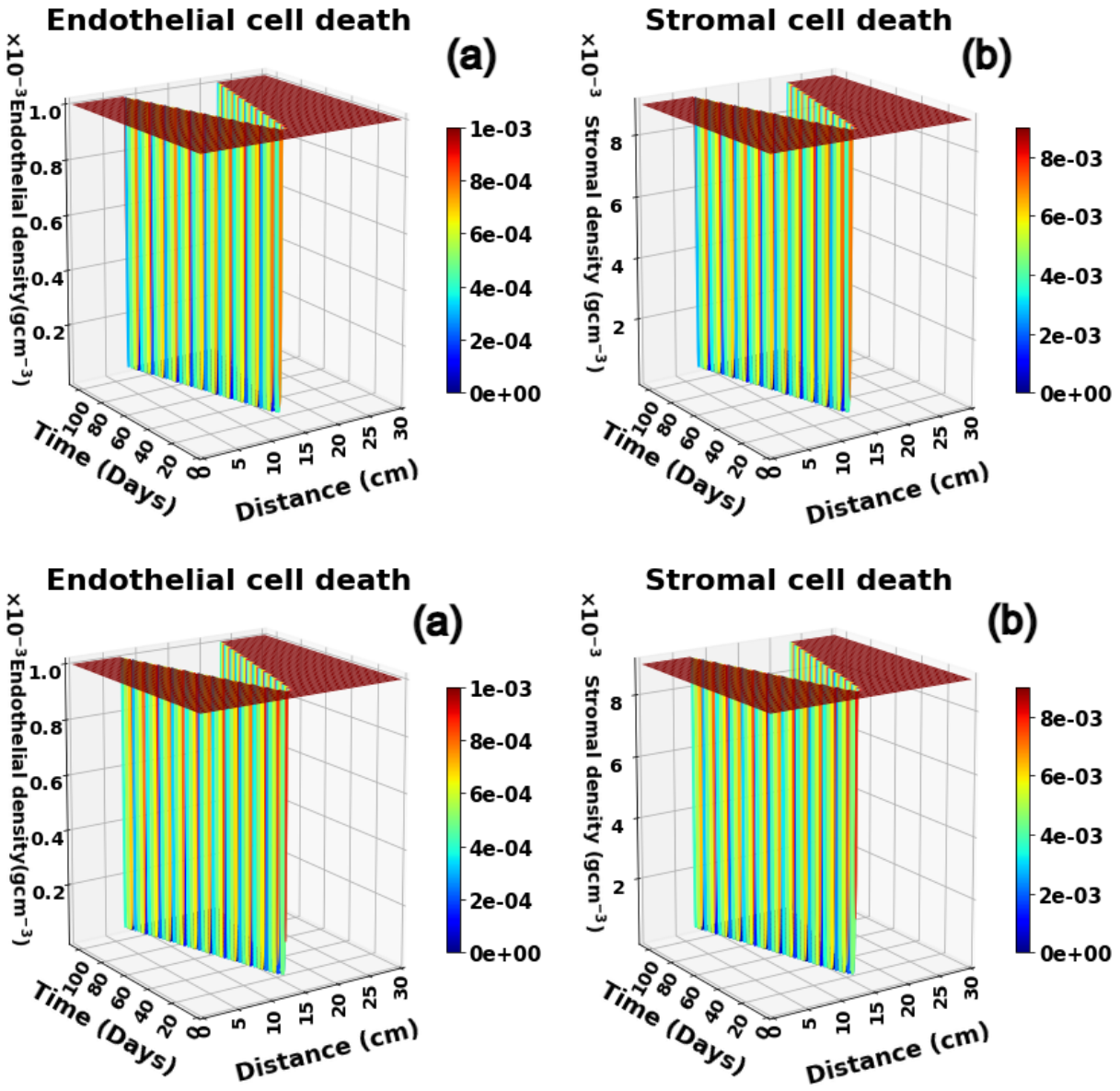

FIGURE 3.7: **Cell death when both ischaemia and direct cytotoxicity are switched on**. In the first row, $m_{\text{eqm}} = 6 \times 10^{-9}$ gml^{-1} such that $c_s > m_{\text{eqm}} > c_e$, and in the second row, $m_{\text{eqm}} = 1.5 \times 10^{-7}$ gml^{-1} such that $m_{\text{eqm}} > c_s$. In (a), we illustrate how endothelial cells respond to the presence of mycolactone and, (b), the stromal cell response to the presence of mycolactone.

In Figure 3.7, we observed a significant and rapid reduction in skin cell densities. The regions of healthy skin observed at the left and right edges are because mycolactone is not above the cell threshold in those regions.

Cell death by direct cytotoxicity only

In this subsection, we aim at capturing the individual effect of direct cytotoxicity on cell death. In other words, we switch on cell death by direct cytotoxicity and switch off cell death by ischaemia. This means that the equations for cell death in (3.21) and (3.22) will now become:

$$\frac{\partial n_e}{\partial t} = -\delta_e n_e H(m - c_e), \tag{3.33}$$

$$\frac{\partial n_s}{\partial t} = -\delta_s n_s H(m - c_s) \tag{3.34}$$

Substitutions for the parameter values and initial conditions are made. Equation (3.33) and (3.34) are solved using Python scipy "odeint" function to obtain Figure 3.8.

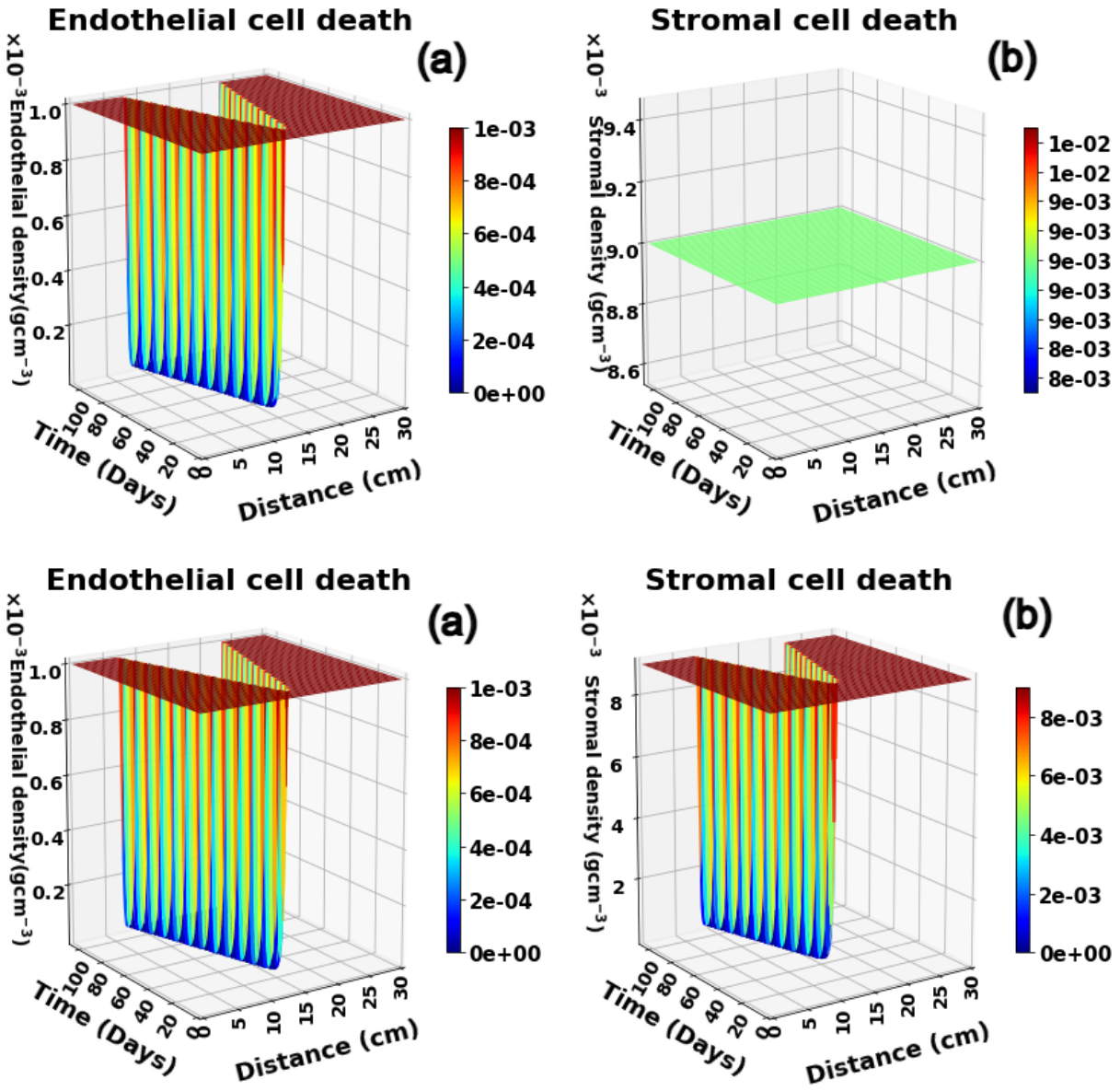

FIGURE 3.8: **Cell death by direct cytotoxicity:** In the first row, $m_{\text{eqm}} = 6 \times 10^{-9}$ gml^{-1}, such that $c_s > m_{\text{eqm}} > c_e$. In the second row, $m_{\text{eqm}} = 1.5 \times 10^{-7}$ gml^{-1}, such that $m_{\text{eqm}} > c_s > c_e$. In (a), we illustrate how endothelial cells respond to the presence of mycolactone and (b), stromal cell response to the presence of mycolactone.

In the first row of Figure 3.8, no stromal cell death happening because the mycolactone there is below the toxicity threshold for stromal cells that is ($m_{\text{eqm}} < c_s$).

In the second row of Figure 3.8, we observe a fall in endothelial and stromal cell density due to the presence of mycolactone. The regions of healthy skin observed at the left and right edges in Figure 3.8 are because mycolactone is not above the threshold in those regions.

Cell death by ischaemia only

In this case, we switch on cell death by ischaemia and switch off cell death by direct cytotoxicity. Equations for cell death in (3.21) and (3.22) will now become:

$$\frac{\partial n_e}{\partial t} = -\delta_k n_e H(m - c_e), \tag{3.35}$$

$$\frac{\partial n_s}{\partial t} = -\delta_k n_s H(m - c_e). \tag{3.36}$$

Substitutions for parameter values and initial conditions are made. Equations (3.35) and (3.36) are solved using Python scipy "odeint" function to obtain Figure 3.9.

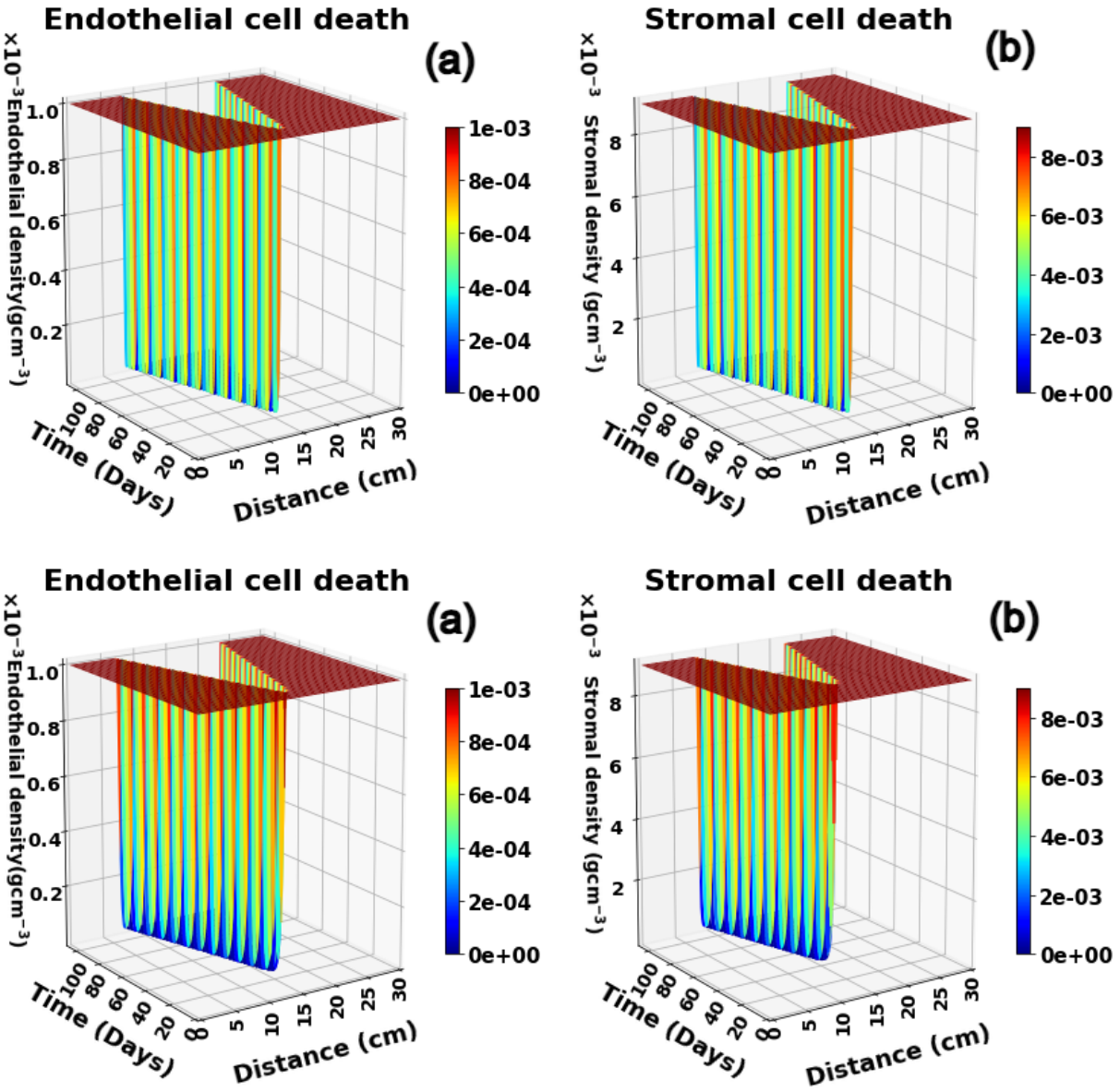

FIGURE 3.9: **Cell death by ischaemia:** In the first row, $m_{\text{eqm}} = 6 \times 10^{-9}$ gml^{-1}, such that $c_s > m_{\text{eqm}} > c_e$. In the second row, $m_{\text{eqm}} = 1.5 \times 10^{-7}$ gml^{-1}, such that $m_{\text{eqm}} > c_s > c_e$. In (a), we illustrate how endothelial cells respond to the presence of mycolactone and (b), stromal cell response to the presence of mycolactone.

In Figure 3.9, we observed a significant and rapid reduction in skin cell densities. The regions of healthy skin observed at the left, and right edges are because mycolactone is not above the cell threshold in those regions. The variation in cell density in the spatial region is because mycolactone values are increasing until they exceed the toxicity threshold across a given part of the domain. This variation shows how the wound gradually develops.

Comparison between cell death by ischaemia and cell death by direct cytotoxicity for endothelial cells

To establish the distinction or difference between cell death by both direct cytotoxicity (Figure 3.8), cell death by both ischaemia (Figure 3.9), cell death by both direct cytotoxicity and ischaemia (Figure 3.7), we visualise the comparison as indicated in Figure 3.10.

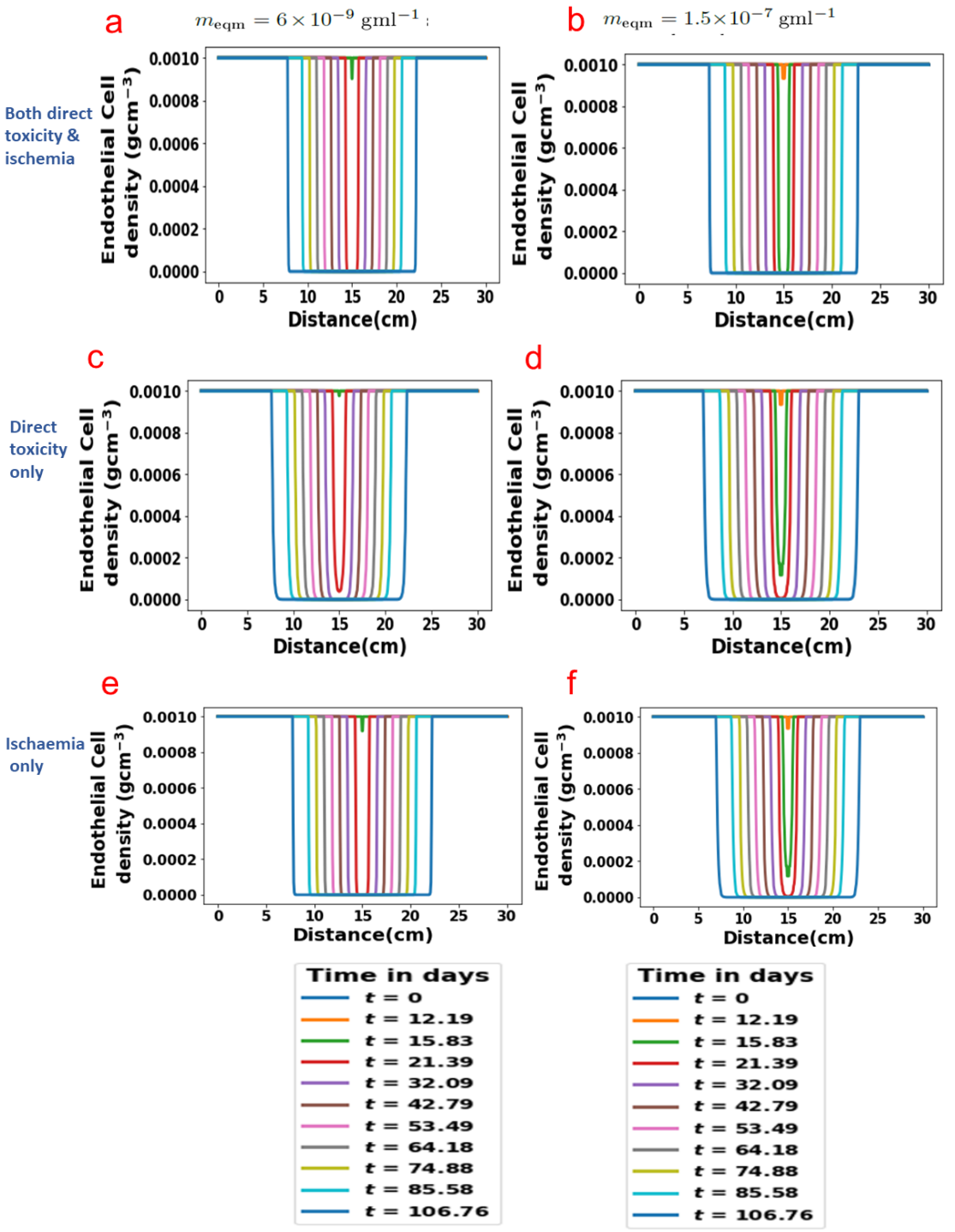

FIGURE 3.10: In the left column, $m_{eqm} = 6.0 \times 10^{-9}$ gml^{-1} and in the right column, $m_{eqm} = 1.5 \times 10^{-7}$ gml^{-1}. This plot illustrates the variation in the endothelial cell density after the exposure to mycolactone at chosen time points.

In the comparisons of the three scenarios, our focus was on the time when cell density drops in the plots. The earliest drop in endothelial cell density for the three cases in

Figure 3.10 happens at $t = 12.19$ days. This happens when m_{eqm} was set to 1.5×10^{-7} gml^{-1} and both ischaemia and direct cytotoxicity operate at the same time.

When the m_{eqm} was set to 6×10^{-9} gml^{-1}, the earliest drop in endothelial cell density for the three cases in Figure 3.10 happens at $t = 15.83$ days when both ischaemia and direct cytotoxicity operate at the same time.

From our simulation outcomes, cell death happened earliest when the mycolactone equilibrium value was set to 1.5×10^{-7} gml^{-1} and both direct cytotoxicity and ischaemia operate at the same time. And latest when the mycolactone equilibrium value was set to 6.0×10^{-9} gml^{-1} and with direct cytotoxicity only.

The reason for earlier cell death for $m_{\text{eqm}} = 1.5 \times 10^{-7}$ is that mycolactone surpasses the toxicity threshold more quickly compared to when $m_{\text{eqm}} = 6 \times 10^{-9}$ gml^{-1}.

The key feature to observe in our results is how changes in mycolactone values relative to skin cell toxicity thresholds can influence the process of cell death observed in BU. These results affirm what is already known on how high amounts of mycolactone combined with the type of skin cell speed up cell death.

3.4 Speed of the wound lesion

In Figure 3.11, we capture the edge of the wound at each time point and plot it against time. At the point where mycolactone is greater than the threshold, there is a sudden fall in the cell density and there the wound starts at the centre extending out in both directions. We observe the distance of the wound edges from the edge of the domain reducing with increase in days. The speed of the wound is obtained by evaluating the slope of the curve.

$$\text{Wound Speed} = \text{Slope}\left[\frac{\text{Change in distance}}{\text{Change in time}}\right] \tag{3.37}$$

Equation 3.37 represents the ratio of how far the wound's edge has moved to the amount of time it took for that movement to occur. It provides a basic representation of the rate at which the wound is spreading over time.

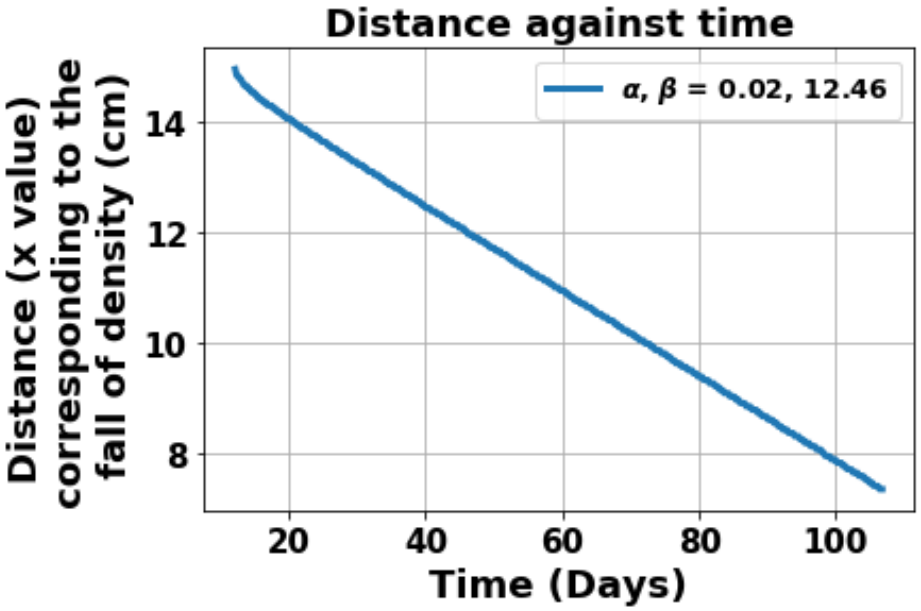

FIGURE 3.11: **Illustration of wound movement against time:** We pick up the left side of wound expansion from the centre ($x = 15$ cm). We monitor how the wound extends from the centre outwards. Our interest is when the cell density drops. We note the positions in the simulation when the cell density drops and obtain the corresponding distance (x value). We plot this distance versus the time with α and β as $(2.0 \times 10^{-2}, 12.46)$ respectively. The slope of the curve is -0.07787.

The other parameter values used in the speed plots were obtained from Table 3.2.

Figure 3.11 represents the movement of the front of the wound as the density of the skin cells decreases. The slope of this curve represents the wound speed: how fast the wound is forming and the cell density is decreasing.

We set the number of time points in the simulation to 100 days to capture the wound's formative phase, excluding boundary effects.

3.5 The effect of different α and β combinations on the skin cell densities

In this work, some of the parameters were estimated implying potential disparities between true and experimental values. We now investigate the dependence of model outputs on parameter values. In this model, the most significant parameters are α and β. α is the ratio of the diffusion coefficient of mycolactone (D_m) to that of bacteria (D_u) and β is the ratio of the degradation rate of mycolactone (K_m) to the bacteria growth rate (λ_u).

We analyse the effects of chosen parameters on the state variables. Specifically, we chose to focus on the parameter combinations that remain after scaling model equations and

also because we are interested in parameters that influence the growth of the BU wound lesions.

We assign a range of values to α and β and observe how these values influence the speed at which the wounds develop. We run the simulation at a discretization of N= 500. With N= 500 we obtained an accurate numerical solution without the code running for long.

We run the simulation for several α and β combinations. At every α and β, we illustrate the position at which the cell density decreases. We obtain the slope of the curve for the speed. We set the number of time points in the simulation to 100 days and use the same time points to calculate the speed.

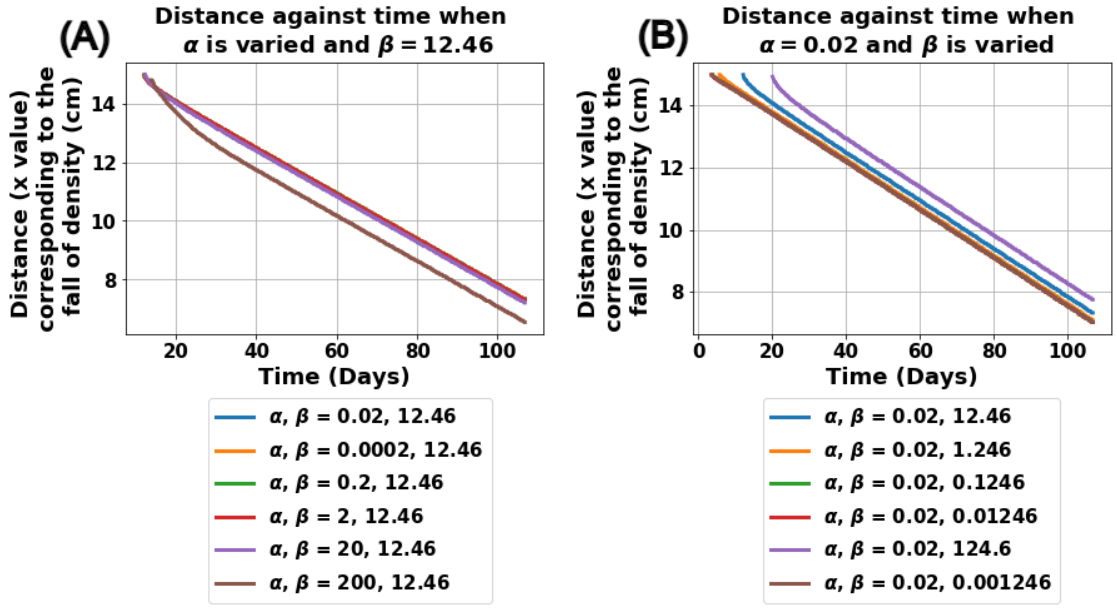

FIGURE 3.12: Illustration of wound movement against time at selected α and β values.

Slopes for Figure 3.12A

α	β	Slope (cm/day)
0.0002	12.46	−0.07787
2	12.46	−0.07805
20	12.46	−0.07847
200	12.46	−0.08141

Slopes for Figure 3.12B

α	β	Slope (cm/day)
0.02	0.1246	−0.07691
0.02	1.246	−0.07716
0.02	12.46	−0.07786
0.02	124.6	−0.07870

In Figure 3.12 (A), we vary α and keep β constant. And in Figure 3.12 (B), we vary β and keep α constant. The slopes of selected α and β combinations in Tables 3.5 show the rate of change of wound spread over time. We observe the combination $(\alpha, \beta) = (200, 12.46)$ has the most negative slope corresponding to the fastest wound growth speed and the combination $(\alpha, \beta) = (0.02, 1.246)$ has the least negative slope (corresponding to the slowest wound growth).

When β, the ratio of the degradation rate of mycolactone (K_m) to the bacteria growth rate (λ_u) was increased, mycolactone decays faster than the rate of bacteria growth. This is because mycolactone equilibrium becomes very small which delays the initiation of the wound. For example in Figure 3.12 (B), when $\beta = 124.6$, the first instance of the wound was observed at approximately $t = 20$ compared to when $\beta = 0.001246$, the wound spreads out earlier at approximately $t = 4$. We observe the wound expanding at a slow pace gradually spreading linearly over the domain in days for $\beta < 124.60$.

The wound speed is not greatly influenced by the β parameter. In other words, β parameter doesn't have a significant impact on the rate of wound growth but instead determines when the wound initiates or starts.

When the value of α is 200, we observe a significant increase in the speed at which wounds enlarge. This implies that a higher value of the mycolactone diffusion coefficient relative to that of the bacteria has a positive effect on the speed at which wounds enlarge. This means when mycolactone diffuses faster than bacteria, BU lesions expand fast.

In other words, if mycolactone does not diffuse faster than the bacteria, it will be stack where the bacteria are. This means the wound never goes beyond where the bacteria are. But if mycolactone diffuses faster, it can expand out ahead of where the bacteria are and the wound can extend out ahead where of the bacteria are as well.

At the combination $(\alpha, \beta) = (200, 12.46)$, we observe the fastest movement of the edge of the wound. The wound breaks out quickly and expands at a fast pace. This means to mitigate the rate of wound enlargement in BU, we ought to decrease the ratio of the diffusion coefficient of mycolactone (D_m) to that of bacteria (D_u) and also increase the ratio of the degradation rate of mycolactone (K_m) to the bacteria growth rate (λ_u).

3.6 Conclusion

In Chapter 3, we have formulated a mathematical model that describes Buruli ulcer lesion formation. Using a set of assumptions, we established model equations, defined variables, parameters and their corresponding initial and boundary conditions. We solved the equations numerically, illustrated the numerical results for bacterial growth, mycolactone concentration and skin cell density and showed how the lesions spread using a travelling wave solution.

Our results confirm the role mycolactone plays in the enlargement of BU lesions. These results coincide with the very earliest observations of BU that led to the proposal of a diffusible lipid toxin (Connor et al., 1966). The simulation plots show an exponential increase in *M. ulcerans* bacteria leading to increases in mycolactone over time. This pattern is in agreement with the pathology of Buruli ulcers. The simulation results also illustrate mycolactone's varying effect on different cell types.

Our model presents the progress of skin cell death processes as affected by the presence of mycolactone. We switched the two cell death mechanisms on and off and analysed the model's behaviour. We presented results for cell death by ischaemia alone, cell death by direct toxicity alone and cell death by both ischaemia and direct cytotoxicity. The simulation results reflect that combining the two mechanisms leads to quicker skin cell death than individual mechanisms. When analysed independently, skin cell death through ischaemia was more rapid than through direct cytotoxicity.

Analysis of the impact of key parameters on the speed of wound growth led to the following conclusions. The ratio of the diffusion coefficient of mycolactone (D_m) to that of bacteria (D_u) more strongly influenced the speed at which the BU lesions enlarge compared to the ratio of the degradation rate of mycolactone (K_m) to the bacteria growth rate (λ_u). The sensitivity analysis results indicate rapid wound enlargement when mycolactone diffuses faster than *M. ulcerans* bacteria.

One of the model's limitations was the lack of sufficient data for parameter estimations. We recommend data collection on parameters like the production rate of mycolactone (λ_m), the degradation rate of mycolactone (K_m) and the density-dependent bacterial death rate (K_u). This will help in improving the estimated parameter values.

To simplify our model, we assumed that *M. ulcerans* density and mycolactone concentration would ultimately reach a level of equilibrium. This feature, however, may not be the case in natural infections. In natural human infections, the growth of *M. ulcerans* and the production of mycolactone goes on infinitely and may not reach equilibrium unless individuals start treatment.

Some estimated parameter values match what was found experimentally but not in humans. For example, estimation of the production rate of mycolactone and the doubling rate of *M. ulcerans* parameters were based on an artificial system where bacteria could grow where nutrients are (Cadapan et al., 2001).

In the future, with the availability of more information, we could explore how changing these parameters to match what happens in people influences the model. For example, a longer doubling time for *M. ulcerans* in tissue corresponds to a lower growth rate λ_u. In addition, increasing the diffusion rate of mycolactone over that of the bacteria would be in keeping with these observations. These changes might improve the model further, making it more in keeping with what is seen in tissue.

The model discussed in this work contributes to understanding skin cell death processes in Buruli ulcer formation. The ability to switch the mechanisms on and off may not be possible in reality, so this model can aid in understanding how the two mechanisms collaborate to influence cell death.

Since there are still gaps in what is known about the disease, understanding how the lesions observed in BU spread out over time may be instrumental in guiding clinicians

and researchers to make predictions about skin tissue degradation caused by *M. ulcerans*. This knowledge is important in assessing wounds' resection margins, which is key in BU treatment. Consequently, our results could be important in making informed decisions on surgical excision during surgery.

Chapter 4

Modelling the disease progression and treatment pathway of Buruli ulcer in Ghana

4.1 Introduction

A crucial step towards understanding Buruli ulcer disease is to identify the pattern from infection to treatment and finally recovery. Once an individual is infected, it takes a period of $0-6$ months to manifest symptoms and these can worsen over several weeks.

Various mathematical models have been used to investigate BU disease transmission. Some of these are in the form of compartmental models (Bonyah et al., 2014c; Aidoo and Osei, 2007; Bonyah et al., 2014a; Nyabadza and Bonyah, 2015; Garchitorena et al., 2015; Assan et al., 2017; Bonyah et al., 2014b).

The key question for most of these models has been to establish how the disease spreads from the environment to humans. This involves characterising human and host populations in compartments. A distinction between these models and our model is that we divide the infected population into compartments according to the classification of BU severity defined by WHO (WHO, 2018). Rather than taking the infected population as one whole, our model takes into consideration the three classification categories that define the infection transitions from the incubation period to ulcer formation in BU disease.

The rationale behind the modelling work in this chapter is

(i) To develop an epidemiological model for the incidence, progression and treatment of BU.

(ii) To build a compartmental model that will be used to predict the proportions of BU infected population in early and late categories.

(iii) To establish and specify the contribution of key parameters in influencing BU disease progression.

(iv) To use our model findings and provide insight on which control program to implement for the prevention of BU late category cases.

We develop a SIT (susceptible, infected and treated) compartmental transmission model to explore the pathway of BU patients from infection to treatment. We calibrate a flexible model that portrays the pattern BU patients go through when no additional case-finding intervention is applied.

The model consists of the total population residing in compartments and moving between them over a given period. This movement of the population between compartments is represented by a system of ordinary differential equations. These equations describe the flow in and out of all compartments as a function of time.

A quick guide to the model assumptions and equations are in Section 4.2 and model analysis is presented in Section 4.3. Parameter estimation is found in Section 4.4, the numerical simulation results and sensitivity analysis are presented in Section 4.5. We conclude the chapter in Section 4.6.

4.2 Model formulation

Suppose the disease is such that the total human population can be grouped into three distinct classes. We vary each class as a function of time, t: the susceptible, $S(t)$, who at risk of catching the disease; the infected, $I(t)$, who have contracted the disease, and the treated, $T(t)$, who are undergoing treatment. $S(t)$, $I(t)$ and $T(t)$ represent fractions of the total population ($N(t)$). The total human population, $N(t)$ is denoted by

$$N(t) = S(t) + I(t) + T(t) \quad \text{and} \quad \frac{dN}{dt} = 0.$$

The infected and treated population are further divided into four and three categories respectively.

In formulating the model, we make assumptions of which some of them are supported by evidence and are well accepted in literature on BU, while others are made for the sake of simplicity or due to the absence of complete information.

The following assumptions are made:

- We assume a constant human population ignoring births, deaths and immigration over the modelling time. An individual exits the susceptible compartment by becoming infected. This assumption is often made in epidemiological models when focusing on short-term dynamics or specific outbreaks.

- The human population can be infected with *Mycobacteruim ulcerans* through being randomly bitten by an infectious aquatic insect or contact with infected water.
- We assume that if an individual adheres to treatment prescribed and proper wound care, treatment is 100% successful. This assumption is based on the effectiveness of the prescribed treatment when perfectly adhered to, although real-world adherence rates is likely to lower and impact the outcomes.
- These assumptions were made for the simplicity of the model.
  - The model does not consider the dynamics of the aquatic insect population.
  - Individuals cannot be infected while undergoing treatment.
- These assumptions were made specific to BU and were supported by Wynne et al. (2018)'s work on BU reinfection.
  - Individuals do not develop any immunity to BU infection and can be reinfected as soon as treatment is completed.
  - An individual's previous infection does not affect their susceptibility to another infection.

Model variables and parameters

The variables and parameters stated in the equations are described in Tables 4.1 and 4.2 respectively. It is important to note that S, I_a, I_b, I_c, I_d, T_b, T_c and T_d are proportions of the population rather than absolute numbers.

Variable	Description
S	Susceptible population
I	Infected population
I_a	Infected population in incubation period of the infection
I_b	Infected population with a nodule or a plaque or oedema
I_c	Infected population with wound ulcers
I_d	Infected population with wounds spread to the bone
T	Population in treatment
T_b	Population in treatment for nodule or a plaque or oedema
T_c	Population in treatment for wound ulcers
T_d	Population in treatment for wound ulcers extending to the bone
t	Time

TABLE 4.1: Description of variables used in the BU model.

Parameter	Description
β	The rate of infecting the population with BU
δ_a	Transfer rate from the incubation period to when signs of BU manifest
δ_b	Transfer rate of a nodule/plaque/oedema to a wound ulcer
δ_c	Transfer rate of a wound ulcer to the bones/joint
γ_b	Rate at which a BU patient with a nodule/papule/oedema starts treatment
γ_c	Rate at which a BU patient with a wound ulcer starts treatment
γ_d	Rate at which a BU patient with a wound ulcer extending to the bones starts treatment
λ_b	Rate at which a BU patient recovers with no disability following treatment for a nodule/paque/oedema
λ_c	Rate at which a treated BU patient recovers with minor disability following treatment for an ulcer
λ_d	Rate at which a treated BU patient recovers with major disability following treatment for an ulcer that has extended to the bone

TABLE 4.2: Description of parameters used in the BU model.

Susceptible population

Susceptible population become infected with BU and leave the compartment at a rate given by β. Individuals return to the susceptible population after being treated with antibiotics at a rate (λ_b), antibiotics plus minor surgeries (λ_c) and antibiotics plus major surgeries (λ_d). For the rest of this chapter, we omit t dependence in $N(t)$, $S(t)$, $I(t)$, $T(t)$ and write N, S, I, T for simplicity.

$$\frac{dS}{dt} = \lambda_b T_b + \lambda_c T_c + \lambda_d T_d - \beta S. \tag{4.1}$$

where T_b, T_c and T_d are populations in treatment for nodule or a plaque or oedema, wound ulcers and wound ulcers extending to the bone respectively.

Infected population

We group the infected population into four categories. We let

- The infected population in the incubation period (the period between *M.ulcerans* infection and when symptoms of BU first appear) be I_a.
- The infected population that manifests BU disease in clinical forms of a nodule, papule or plaque and oedema be I_b.

- The infected population that manifests BU disease as a wound ulcer be I_c.
- The infected population where the wound ulcers have extended to the bones be I_d.

These populations are represented as I_a, I_b, I_c, I_d in Figure 4.1. Transfer rates δ_a, δ_b, δ_c describe the movement of the infected population from compartments I_a to I_b, I_b to I_c and I_c to I_d respectively.

Parameters γ_b, γ_c, γ_d describe the rate at which the infected population start treatment hence moving from compartments I_b to T_b, I_c to T_c and I_d to T_d respectively. Populations in compartment I_a do not start treatment since they are unaware of having BU and symptoms are not yet evident.

$$\begin{aligned}
\frac{dI_a}{dt} &= \beta S - \delta_a I_a, \\
\frac{dI_b}{dt} &= \delta_a I_a - I_b\big(\delta_b + \gamma_b\big), \\
\frac{dI_c}{dt} &= \delta_b I_b - I_c\big(\delta_c + \gamma_c\big), \\
\frac{dI_d}{dt} &= \delta_c I_c - I_d \gamma_d.
\end{aligned} \tag{4.2}$$

The infected population is now equivalent to

$$I = I_a + I_b + I_c + I_d. \tag{4.3}$$

Treated population

BU patients undergoing treatment are assumed to be in compartments T_b, T_c and T_d.

$$\begin{aligned}
\frac{dT_b}{dt} &= \gamma_b I_b - \lambda_b T_b, \\
\frac{dT_c}{dt} &= \gamma_c I_c - \lambda_c T_c, \\
\frac{dT_d}{dt} &= \gamma_d I_d - \lambda_d T_d.
\end{aligned} \tag{4.4}$$

The total population undergoing treatment is now equivalent to

$$T = T_b + T_c + T_d. \tag{4.5}$$

The progress of the individuals within susceptible, infected and treated compartments is represented in Figure 4.1.

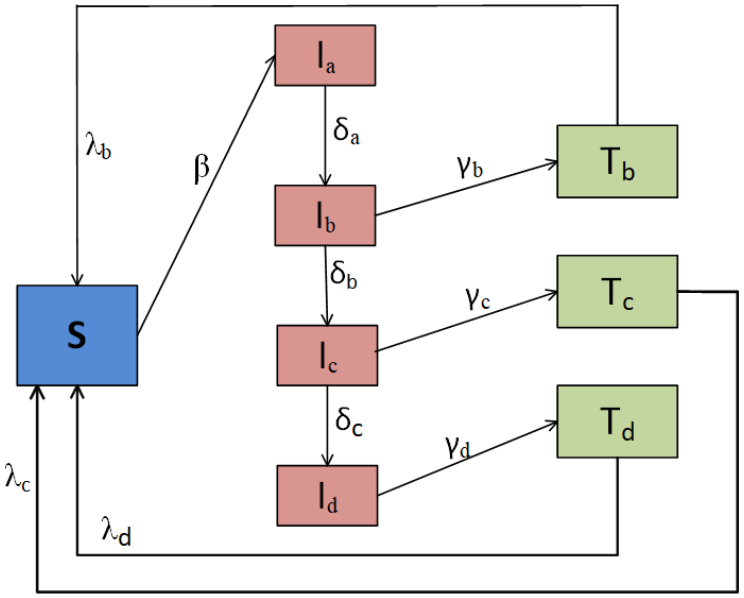

FIGURE 4.1: Schematic representation of the susceptible, infected and treated populations.

It is important to note that S, I_a, I_b, I_c, I_d, T, T_b, T_c and T_d are proportions of the population rather than absolute numbers. Now, the equations become:

$$\begin{aligned}
\frac{dS}{dt} &= \lambda_b T_b + \lambda_c T_c + \lambda_d T_d - \beta S, \\
\frac{dI_a}{dt} &= \beta S - \delta_a I_a, \\
\frac{dI_b}{dt} &= \delta_a I_a - \big(\delta_b + \gamma_b\big) I_b, \\
\frac{dI_c}{dt} &= \delta_b I_b - \big(\delta_c + \gamma_c\big) I_c, \\
\frac{dI_d}{dt} &= \delta_c I_c - \gamma_d I_d, \\
\frac{dT_b}{dt} &= \gamma_b I_b - \lambda_b T_b, \\
\frac{dT_c}{dt} &= \gamma_c I_c - \lambda_c T_c, \\
\frac{dT_d}{dt} &= \gamma_d I_d - \lambda_d T_d.
\end{aligned} \tag{4.6}$$

4.2.1 Initial conditions

We are interested in non-negative solutions of S, I and T. In the susceptible, we assumed that the disease is initialized at $S(0) = S_0 > 0$. We assume that initially the whole population is in the state Susceptible, and hence $S_0 = 1$.

We start with 0 infected people since BU is not transmitted from person to person. Hence we let $I_a(0) = I_{a0} = 0$, $I_b(0) = I_{b0} = 0$, $I_c(0) = I_{c0} = 0$ and $I_d(0) = I_{d0} = 0$. There

is no treatment at time 0 hence we set the treated, $T(0) = 0$. Then $T_b(0) = T_{b0} = 0$, $T_c(0) = T_{c0} = 0$ and $T_d(0) = T_{d0} = 0$.

4.3 Model analysis

4.3.1 Positivity of solutions

We aim at making sure all the solutions to the SIT populations are non-negative and remain non negative for all $t > 0$. We prove that using the following lemma.

Lemma 4.1. *Given non-negative initial conditions;* $S_0 \geq 0$, $I_{a0} \geq 0$, $I_{b0} \geq 0$, $I_{c0} \geq 0$, $I_{d0} \geq 0$, $T_{b0} \geq 0$, $T_{c0} \geq 0$ *and* $T_{d0} \geq 0$, *the solutions for the system of equations in* (4.6) *remain non-negative* $\forall t > 0$.

Proof. Let $\tilde{t} = \sup\{t > 0 : S_0 \geq 0,\ I_{a0} \geq 0,\ I_{b0} \geq 0,\ I_{c0} \geq 0,\ I_{d0} \geq 0,\ T_{b0} \geq 0\}$ where $\tilde{t} \in [0, t]$.

Thus, $\tilde{t} \geq 0$. For S; ignoring other terms in Equation (4.1), focusing on the term with S, we rewrite the susceptible equation and integrate to obtain

$$\frac{dS}{d\tilde{t}} = -\beta S, \quad S(\tilde{t}) = S(0)\exp(-\beta\tilde{t}) \geq 0.$$

For I; ignoring other terms in Equations (4.2) and focusing on the terms with I_a, I_b, I_c and I_d, we rewrite the infected equations and integrate to obtain

$$\begin{aligned}
\frac{dI_a}{d\tilde{t}} &= -\delta_a I_a, && I_a(\tilde{t}) \geq I_a(0)\exp\big(-\delta_a\tilde{t}\big) \geq 0,\\
\frac{dI_b}{d\tilde{t}} &= -\big(\delta_b + \gamma_b\big)I_b, && I_b(\tilde{t}) \geq I_b(0)\exp\big(-(\delta_b + \gamma_b)\tilde{t}\big) \geq 0,\\
\frac{dI_c}{d\tilde{t}} &= -\big(\delta_c + \gamma_c\big)I_c, && I_c(\tilde{t}) \geq I_c(0)\exp\big(-(\delta_c + \gamma_c)\tilde{t}\big) \geq 0,\\
\frac{dI_d}{d\tilde{t}} &= -\gamma_d I_d, && I_d(\tilde{t}) \geq I_d(0)\exp(-\gamma_d\tilde{t}) \geq 0.
\end{aligned}$$

For T; ignoring other terms in Equations (4.4) and focusing on the terms with T_b, T_c and T_d, we rewrite the treated equations and integrate to obtain

$$\begin{aligned}
\frac{dT_b}{d\tilde{t}} &= -\lambda_b T_b, \quad T_b(\tilde{t}) \geq T_b(0)\exp(-\lambda_b\tilde{t}) \geq 0,\\
\frac{dT_c}{d\tilde{t}} &= -\lambda_c T_c, \quad T_c(\tilde{t}) \geq T_c(0)\exp(-\lambda_c\tilde{t}) \geq 0,\\
\frac{dT_d}{d\tilde{t}} &= -\lambda_d T_d, \quad T_d(\tilde{t}) \geq T_d(0)\exp(-\lambda_d\tilde{t}) \geq 0.
\end{aligned}$$

All variables are positive for non-negative initial conditions. We deduce all solutions are non-negative. □

4.4 Parameter estimates

The parameters were estimated based on the assumptions about the disease and previous literature available. In the estimation of transfer rates, we shall use weeks as our time step.

(I) **Transfer rate from S to $\mathbf{I}_a$**

To estimate the transfer rate from S to I_a, we calculated the proportion of people (labelled as P_g in Table 4.3) that are infected compared to the total population per year from 2010 to 2020. To calculate that proportion, we use the number of BU cases recorded per year (K_g) divided by the total population of Ghana for that year (M_g). The values obtained are in a range of 1.0×10^{-5} and 1.0×10^{-6} per year as shown in Table 4.3.

Picking parameters suitable for overall population would give $\beta = 1.0 \times 10^{-5}$ per year which is approximately $1.0 \times 10^{-5}/52 = 1.923 \times 10^{-7}$ week^{-1}. This assumes each infection lasts less than a year and people only get infected once a year at most.

Year	**New reported cases (K_g)**	**Population of Ghana (M_g)**	**Proportion of infected to the total Ghana population ($P_g = \frac{K_g}{M_g}$)**
2010	1048	$24,658,823$	4.2500×10^{-5}
2011	971	$25,261,000$	3.8438×10^{-5}
2012	632	$25,867,000$	2.4432×10^{-5}
2013	550	$26,479,000$	2.0771×10^{-5}
2014	443	$27,092,000$	1.6351×10^{-5}
2015	275	$27,849,205$	9.8746×10^{-5}
2016	371	$28,481,945$	1.3025×10^{-5}
2017	538	$29,121,465$	1.8474×10^{-5}
2018	630	$29,767,102$	2.1164×10^{-5}
2019	296	$30,417,856$	9.7311×10^{-6}
2020	127	$31,072,940$	4.0871×10^{-6}

TABLE 4.3: Ghana population 2010 to 2020 (Source: (Service et al., 2020)) and number of new reported cases of BU in Ghana per year. Source: World Health Organisation fact file 2019 retrieved from (WHO, 2019).

(II) **Transfer rates within I**

Without diagnosis and treatment, individuals progress between compartments I_a, I_b, I_c and I_d. This evolution within compartments can take between 3 weeks and 1 year where the mean incubation period of BU is between $2-3$ months (Zingue et al., 2018a). During the incubation period, BU patients are not aware they have the disease. In this work, we assumed an incubation period of 3 months roughly 13 weeks, resulting in a transition rate of $\frac{1}{13} = 0.0769$ week^{-1}.

Within weeks, BU lesions rapidly increase in diameter and depth, resulting in oedematous plaques with ill-defined borders. The time it takes for the lesions to

ulcerate (I_b to I_c) is 4 weeks, equivalent to a rate of 0.25 week^{-1} (WHO, 2018; Portaels et al., 2001). We also estimate that it takes 6 weeks for an ulcer to extend to the joints and bone (from I_c to I_d), equivalent to a rate of 0.166 week^{-1}.

The estimated values of δ_a, δ_b and δ_c become 0.0769 week^{-1}, 0.25 week^{-1} and 0.166 week^{-1} respectively.

(III) **Transfer rates from I to T**

A patient moves out of compartment I by starting treatment. Early BU diagnosis will lead to early treatment and late diagnosis will lead to delayed treatment. We estimate γ_b, γ_c and γ_d by considering how long it takes an infected individual to start treatment.

Ackumey et al. (2012) suggests that individuals should start medical treatment within 1 month, equivalent to 4 weeks, after observing BU symptoms on the skin, it is important to note that this assumption is unlikely to hold true in practice. However, we make this simplifying assumption due to a lack of available data and for simplicity. We will discuss the limitations of this assumption later. Hence, we consider the average time that individuals with BU take to start treatment, denoted as γ, as 4 weeks, equivalent to a rate of 0.25 week^{-1}. We assume equal values for γ across different categories, such that $\gamma_b = \gamma_c = \gamma_d = 0.25$ week^{-1}.

(IV) **Transfer rates from T to S**

According to (Agbenorku et al., 2012), treatment for a BU patient is antibiotics, excision, skin grafting, release of contracture or a combination of more than one of these treatments. These treatment options depend on the severity of the ulcer at the time of seeking medical treatment. Transfer rates from T to S were estimated by considering the duration of treatment.

Individuals with BU in pre-ulceration (WHO category 1) are treated with antibiotics for 8 weeks and this has been proved to be effective. We take the healing time for category 1 ulcers (λ_b) as 8 weeks equivalent to $\lambda_b = \frac{1}{8} = 0.125$ week $^{-1}$.

BU patients who start treatment when the ulcers are deep (WHO category 2) have a median healing time of 30 weeks (95% CI $26 - 34$ weeks) (Nienhuis et al., 2010). Hence we will take the $\lambda_c = \frac{1}{30} = 0.033$ week $^{-1}$. We shall consider the healing time for WHO category 3 BU lesions as 52 weeks from that we estimated $\lambda_d = \frac{1}{52} = 0.0192$ week $^{-1}$.

The parameters values used in the equations are defined in Table 4.4.

Parameter	**Value (week $^{-1}$)**	**Source**
β	1.923×10^{-7}	Estimated in (I)
δ_a	0.0769	Estimated in (II)
δ_b	0.25	Estimated in (II)
δ_c	0.166	Estimated in (II)
γ_b	0.25	Estimated in (III)
γ_c	0.25	Estimated in (III)
γ_d	0.25	Estimated in (III)
λ_b	0.125	Estimated in (IV)
λ_c	0.033	Estimated in (IV)
λ_d	0.0192	Estimated in (IV)

TABLE 4.4: Values of parameters used in the BU model for simulations and sensitivity analysis.

4.5 Numerical simulations

In this section, we discuss numerical results of the system and perform a sensitivity analysis for the model. We substitute for the parameter values and the initial conditions into Equations (4.6) and integrate numerically using *odeint* solver in *scipy-python* (Jones et al., 2014). We used weeks as the time step for the simulation because the transfer rates within compartments were measured in weeks.

4.5.1 Plots for S, I and T

We illustrated the results for the system of equations obtained in Equation (4.6) in Figure 4.2.

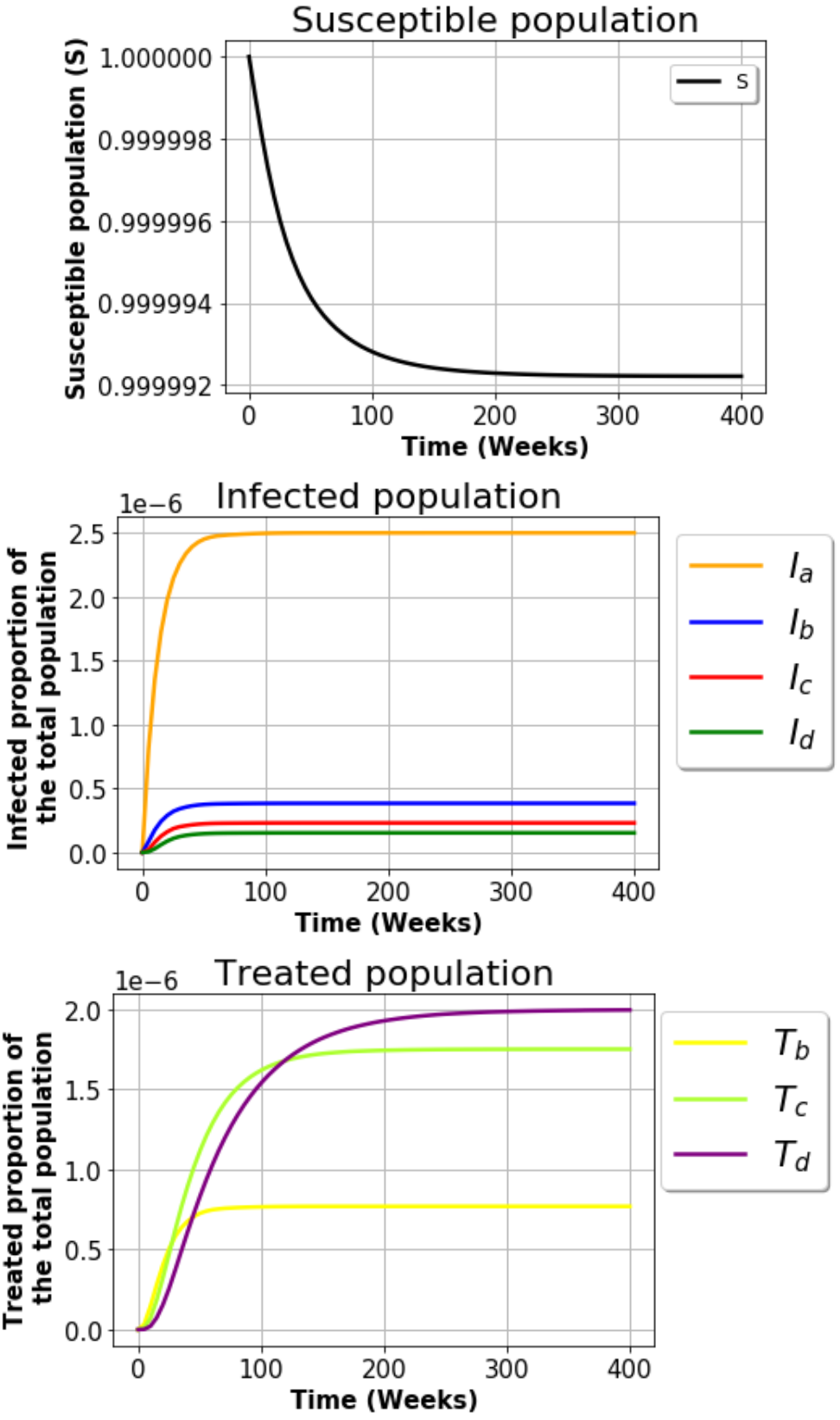

FIGURE 4.2: Plots showing susceptible, infected and treated populations obtained from the model numerical solutions using parameter values in Table 4.2.

Figure 4.2 represents the susceptible, infected and treated populations. The susceptible population decreases slowly over time as the infected population in the incubation period increases. Infected populations move from one infected compartment to another when they stay infected for long periods.

The pattern of the populations in the model is dependent on the model parameter values chosen. For parameters chosen, the susceptible and infected populations reach a steady state after about 250 and 100 weeks respectively. The treated population (T_c and T_d) reaches a steady state after about 100 weeks while T_b reaches a steady state after about 200 weeks.

When S, I and T populations reach a steady state, we analyse the final prevalence rate there since the solution is stable.

4.5.2 Estimating the prevalence of BU in selected endemic countries in West Africa

Prevalence of BU tells us the extent of BU in a population in a particular period. It is the proportion of the population who have BU. Prevalence of BU is represented as

$$= \frac{\text{Number of individuals infected with BU in the population at a particular time}}{\text{Total Population}}, \tag{4.7}$$

where the number of individuals infected with BU in the population at a particular time. In the model, this is equivalent to the total infected population (I) in addition to the population in treatment (T). The total population of Ghana is represented as 1 since the analysis is conducted using proportions. The rate of BU infection (β) for the most endemic countries in West Africa is calculated based on available data regarding the number of reported BU cases per year (WHO, 2018). We calculated for Ivory Coast, Benin and Democratic Republic of Congo (DRC) as indicated in Table 4.5, Table 4.6 and Table 4.7 respectively. We substitute β in our model and run the simulation. We make projections on the possible trend of BU prevalence using our model.

Year	**New reported cases (K_i)**	**Population of Ivory Coast (M_i)**	**Proportion of newly infected to the total Ivory Coast population ($P_i = \frac{K_i}{M_i}$)**
2010	2533	$20,532,944$	1.2336×10^{-4}
2011	1659	$21,028,652$	7.8892×10^{-5}
2012	1386	$21,547,188$	6.4323×10^{-5}
2013	1039	$22,087,506$	4.7040×10^{-5}
2014	827	$22,647,672$	3.6515×10^{-5}
2015	549	$23,226,148$	2.3637×10^{-5}
2016	376	$23,822,726$	1.5783×10^{-5}
2017	344	$24,437,475$	1.4076×10^{-5}
2018	261	$25,069,226$	1.0411×10^{-5}
2019	251	$25,719,554$	9.7591×10^{-6}
2020	231	$26,378,275$	8.7572×10^{-6}

TABLE 4.5: Ivory Coast population 2010 to 2020 (Source: (UN, 2022c)) and number of new reported cases of BU in Ivory Coast per year. Source: World Health Organisation fact file 2019 retrieved from (WHO, 2019). The rate of infection (β) for Ivory Coast per year is 8.041×10^{-7} week $^{-1}$ which was obtained by taking the average of values in column P_i, divided by 52 weeks.

Year	**New reported cases (K_b)**	**Population of Benin (M_b)**	**Proportion of newly infected to the total Benin population ($P_b = \frac{K_b}{M_b}$)**
2010	572	9,199,254	6.2178×10^{-5}
2011	492	9,460,829	5.2003×10^{-5}
2012	365	9,729,254	3.7515×10^{-5}
2013	378	10,004,594	3.7782×10^{-5}
2014	330	10,286,839	3.2079×10^{-5}
2015	311	10,575,962	2.9406×10^{-5}
2016	312	10,872,072	2.8697×10^{-5}
2017	267	11,175,192	2.3892×10^{-5}
2018	219	11,485,035	1.9068×10^{-5}
2019	240	11,801,151	2.0336×10^{-5}
2020	197	12,123,198	1.6249×10^{-5}

TABLE 4.6: Benin population 2010 to 2020 (Source: (UN, 2022a)) and number of new reported cases of BU in Benin per year. Source: World Health Organisation fact file 2019 retrieved from (WHO, 2019). The rate of infection (β) for Benin per year is 6.2797×10^{-7} week^{-1} which was obtained by taking the average of values in column P_b, divided by 52 weeks.

Year	**New reported cases (K)**	**Population of DRC (M)**	**Proportion of newly infected to the total DRC population ($P_d = \frac{K_d}{M_d}$)**
2010	136	64,563,853	2.1064×10^{-6}
2011	209	66,755,151	3.0859×10^{-6}
2012	284	69,020,749	4.1147×10^{-6}
2013	214	71,358,804	2.9989×10^{-6}
2014	192	73,767,445	2.6027×10^{-6}
2015	234	76,244,532	3.0690×10^{-6}
2016	175	78,789,130	2.2211×10^{-6}
2017	120	81,398,765	1.4742×10^{-6}
2018	99	84,068,092	1.1776×10^{-6}
2019	41	86,790,568	4.7240×10^{-7}
2020	334	89,561,404	3.7292×10^{-6}

TABLE 4.7: DRC population 2010 to 2020 (Source: (UN, 2022b)) and number of new reported cases of BU in DRC per year. Source: World Health Organisation fact file 2019 retrieved from (WHO, 2019). The rate of infection (β) for DRC per year is 3.0099×10^{-8} week^{-1} which was obtained by taking the average of values in column P_d, divided by 52 weeks.

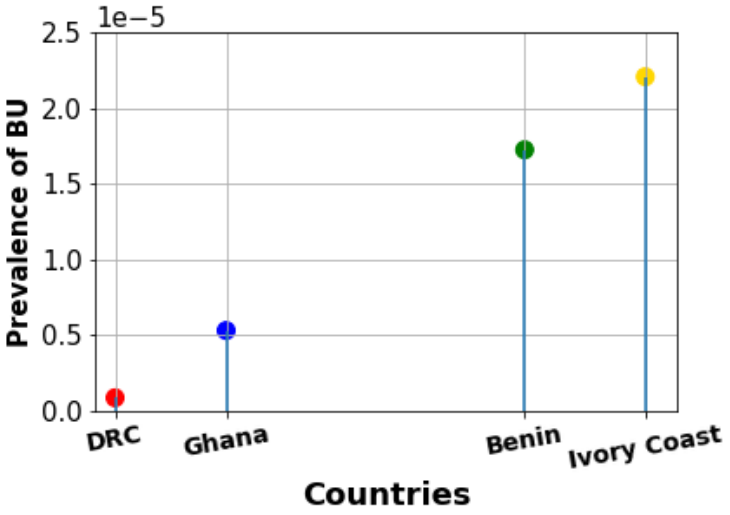

FIGURE 4.3: The modelled prevalence of BU for DRC, Ghana, Benin and Ivory Coast calculated using the corresponding β values as $\left(3.0099 \times 10^{-8}\ \text{week}^{-1},\ 1.923 \times 10^{-7}\ \text{week}^{-1},\ 6.2797 \times 10^{-7}\ \text{week}^{-1},\ 8.041 \times 10^{-7}\ \text{week}^{-1}\ \right)$ respectively. The prevalence rates plotted were extracted at the steady state time $t = 300$ weeks.

Model results in Figure 4.3, show that countries with high rates of infection, β had high prevalence of BU. The results indicate that an increase in β leads to an increase in BU prevalence where as reduction in β reduces BU prevalence. Our model confirms the trend to expect when the rate of infection is increased.

4.5.3 Sensitivity analysis: effect of varying the transfer rates within I (δ) on the infected population

In this subsection, we explore the impact of uncertainty in estimating the parameter value (δ). We evaluate how δ influences the number of infected individuals at a specific time. Our approach involves selecting key parameters and examining the effects of increasing their values on the infected population.

We check the proportions of people in each compartment at a steady state. Thereafter, we analyse how these proportions change when the transfer rates within I (δ) are varied. These proportions are then compared to available data on the percentages of BU patients in different infected and treatment states.

We analyse how adjustments in the parameters; δ_a, δ_b and δ_c influence the model results. With the exception of β (explained on Page 72), the values for all the other parameters used in the simulation were taken from Table 4.4.

Our primary objective is to investigate the effect of picking up BU patients early and how that can improve prevalence rates.

In a study conducted by (Amofah et al., 2002), it was found that of individuals suspected to have BU, 66.3% exhibited active lesions, corresponding to a prevalence of 20.7 per 100,000. In our model, the infected population with active lesions is represented by the sum of I_b, I_c, and I_d. This relationship is expressed as;

$$I_b + I_c + I_d + T_b + T_c + T_d = \frac{20.7}{100000}, \tag{4.8}$$

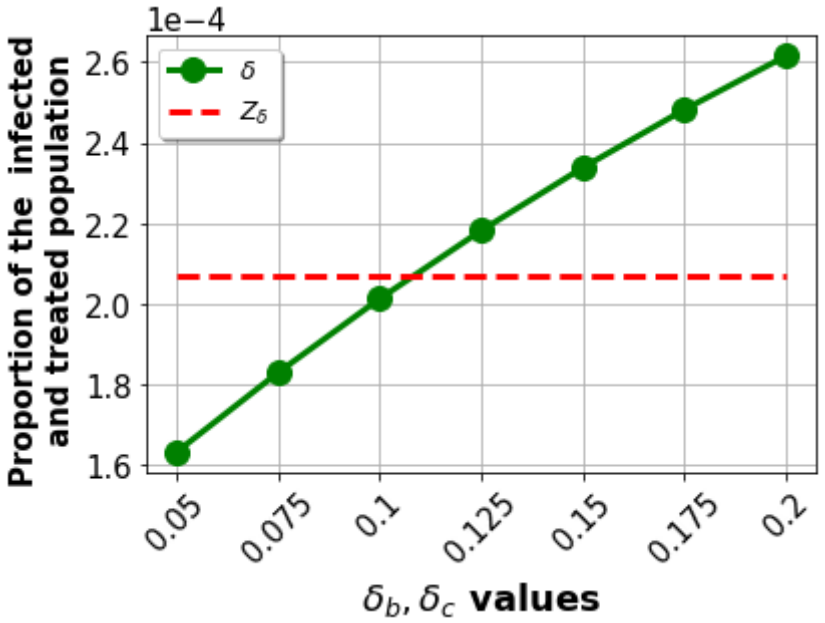

FIGURE 4.4: The green line illustrates the proportion of the infected BU population at the steady state when parameters $\delta_a = 0.0769$, and $\delta_b = \delta_c$ are assigned values $[0.05, 0.075, 0.1, 0.125, 0.15, 0.175, 0.2]$. The red line ($Z_\delta$) is the ratio calculated in Equation (4.8).

For this plot, β was increased from 10^{-5} to 10^{-7}, calculated prevalence as $I_b+I_c+I_d+T_b+T_c+T_d$ and the range of δ_b and δ_c values changed to $[0.05, 0.075, 0.1, 0.125, 0.15, 0.175, 0.2]$.

The step size between the δ_b and δ_c values indicated in Figure 4.4 was set to 0.025.

In the initial model run to produce Figure 4.2, WHO data was utilized for β at face value. However, upon running the model to calculate prevalence, a β value of 10^{-7} resulted in prevalence values several orders of magnitude lower than those reported in (Amofah et al., 2002).

The decision was then made to calibrate the model by adjusting the β value to align with the prevalence reported in (Amofah et al., 2002). This calibration ensured that the model produces prevalence figures consistent with a more reliable study, addressing potential discrepancies arising from under-reporting and the considerable variation evident in Tables 4.3-4.6.

In Figure 4.4, the green line representing the prevalence $I_b + I_c + I_d + T_b + T_c + T_d$ intersects with Z_δ when $\delta_b = \delta_c \approx 0.1125$.

To obtain the prevalence of 20.7 per $100,000$ using our model then the value of β must be increased to 10^{-5}, δ_b and δ_c must be ≈ 0.1125.

In the future, more recent data on BU incidence will be helpful in this estimation.

4.5.4 Model experimentation

We establish the influence of parameters on the number of infected individuals at a particular time. We choose key parameters and investigate how increasing their values affects the infected population.

In subsubsection 4.5.4.1 and subsubsection 4.5.4.2, we check the proportions of people in each compartment at a steady state. Thereafter, we analyse how these proportions change when the rate of starting treatment (γ) or transfer rates within I (δ) are varied. We compare these proportions with the available data on the percentages of BU patients in different infected and treatment states.

4.5.4.1 Effect of varying the rate of starting treatment (γ) on the infected population

We ascertain the extent to which changes in the value for γ influence the model output. We let $\gamma_b = \gamma_c = \gamma_d$ and assign them a range of values. Thereafter, we observe how the proportion of the infected BU population in the ulcerative category changes as these values increase. This is illustrated in Figure 4.5.

In studies by (WHO, 2018), 70% of the BU patients who reported to hospital had lesions in the ulcerative category. This implies that;

$$\frac{\gamma_c I_c + \gamma_d I_d}{\gamma_b I_b + \gamma_c I_c + \gamma_d I_d} = \frac{70}{100}. \tag{4.9}$$

We fit data on the proportion of people in the infected stage to obtain Figure 4.5.

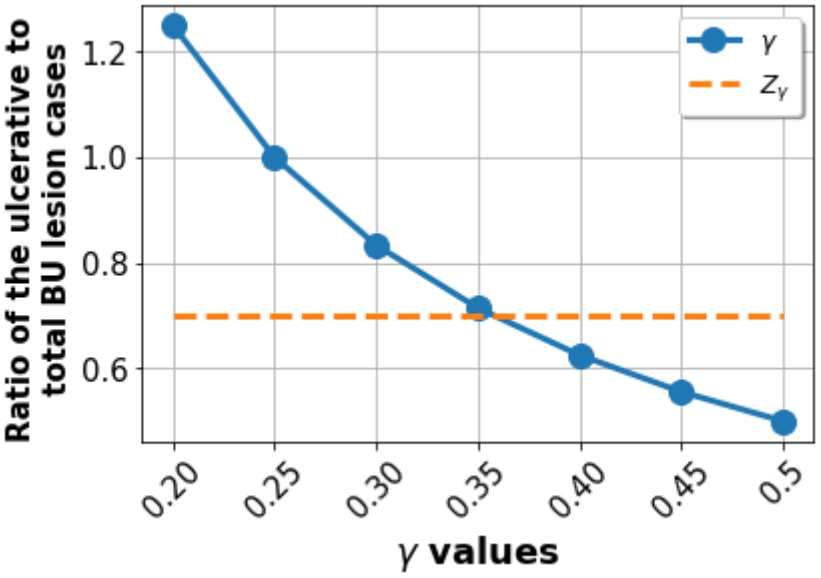

FIGURE 4.5: The blue line illustrates the change in the proportion of the infected BU population in the ulcerative category at the steady state when parameters $\gamma_b = \gamma_c = \gamma_d$ are assigned values $[0.20, 0.25, 0.30, 0.35, 0.40, 0.45, 0.5]$. The orange line (Z_γ) is the ratio calculated in Equation (4.9).

Figure 4.5 depicts the ratio of ulcerative BU lesion cases to total BU cases for different γ values. Increasing the values of γ means that people seek treatment quicker hence reducing the proportion of cases that progress to ulcerative categories. To have more people picked up in early category of BU, we increase the value of γ which reduces the ratio (Z_γ).

In Figure 4.5, the blue line representing the ratio $I_b : I_c + I_d$ intersects with Z_γ when when $\gamma \approx 0.35$. The blue line is an interpolation, based on a set of point values.

To obtain a ratio of $70 : 100$ ulcerative BU lesion cases to total BU cases using our model then the value of γ must be ≈ 0.35.

Effect of using the rate of starting treatment $(\gamma = 0.35)$ on the model

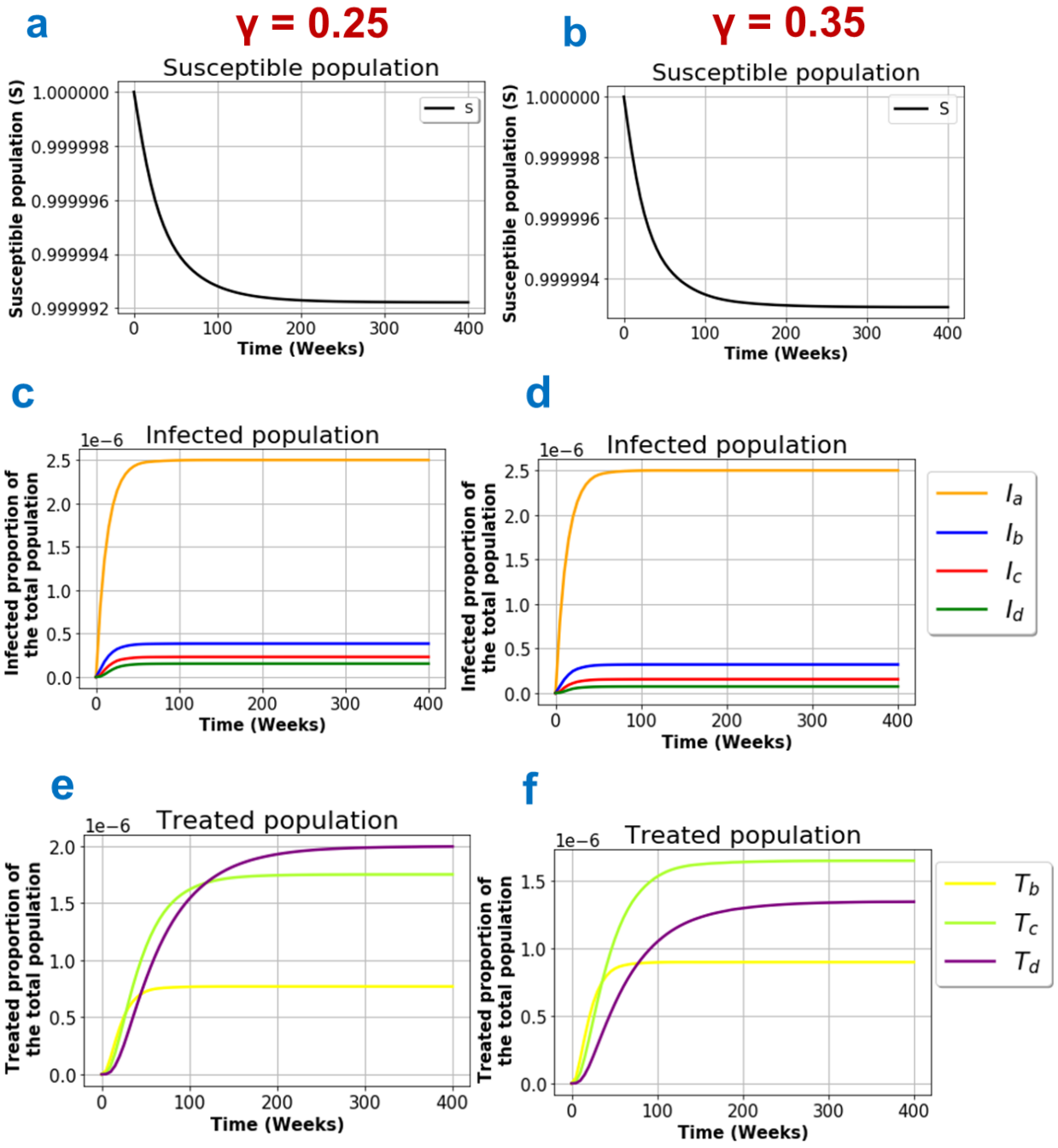

FIGURE 4.6: Plots showing susceptible, infected and treated populations obtained from the model numerical solutions using parameter values in Table 4.2 and $\gamma = 0.11$.

Figure 4.6 is a comparison of simulations when $\gamma = 0.25$ and when it is $\gamma = 0.35$. We observe a decrease in the proportion of T_d cases from 2.0×10^{-6} to $\approx 1.4 \times 10^{-6}$ when γ was increased from 0.25 to 0.35. From these results, we can deduce that when the rate of starting treatment is increased, the proportion of the population in treatment for wound ulcers extending to the bone (T_d) decreases.

4.5.4.2 Effect of varying the rate of starting treatment (γ_b) on the infected population

We analyse the effect of varying the rate of starting treatment (γ_b) on the infected population.

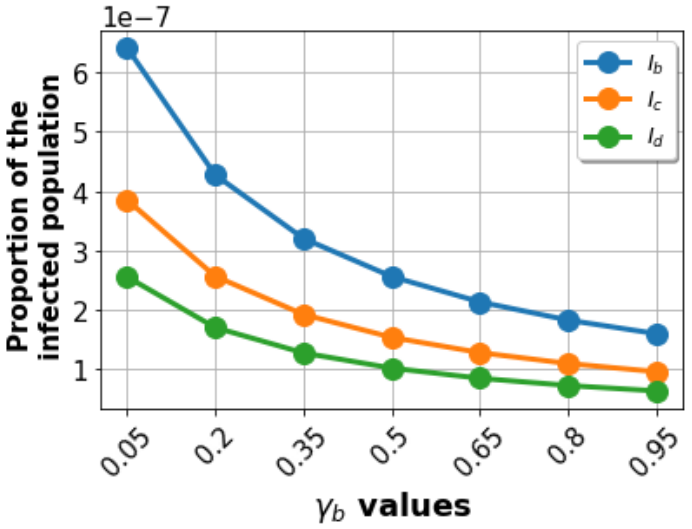

FIGURE 4.7: This plot illustrates the change in the proportion of the infected BU population at the steady state when γ_b is assigned values $[0.05, 0.2, 0.35, 0.5, 0.65, 0.8, 0.95]$ while parameters (γ_c, γ_d) remain constant.

In Figure 4.7, an increase in the rate of seeking treatment in early stages (γ_b) leads to reduction in the infected population. We observe a rapid decrease in number of infected people (I_d) in the late category compared to other categories.

4.6 Conclusion

In this chapter, we have presented a deterministic model that describes the disease progression and treatment pathway of BU in the population of the most endemic areas in Ghana. We aimed at analysing BU progression in a way that mimics the nature of the disease. The model was formulated and parameters for the model simulations were estimated. The steady state solution of the model was determined. Numerical results on the behaviour of the model were illustrated.

Model results showed us the trend that populations in different compartments can take. We calculated the rate of infection for Ghana, DRC, Benin and Ivory Coast using data from (WHO, 2019). We used our model to predict the prevalence of BU in those countries. Our results showed that DRC has the lowest prevalence of 10^{-6} and Ivory Coast has the highest of approximately 10^{-5}. To control the number of people getting infected, it is paramount to establish what influences the rate of infection (β). However, this maybe difficult to analyse due to the uncertainty on the accurate mode of transmission of BU.

We performed a sensitivity analysis on the δ parameters of the model. We assigned the transfer rates within the infected population (δ) to a range of values and observed how this influenced the proportion of infected population. Results from our model showed that as δ increases, the proportion of infected population also increases as observed in Figure 4.4. This means people spend more time in the infected compartment before starting treatment.

We analysed the effect the rate of starting treatment γ has on the infected population. We compared this output with the data about the proportion of infected population in Ghana. From our results, a high γ leads to a decrease in the proportion of infected population. Also when γ_b was increased, we observed a significant decrease in the number of BU patients in the late category compared to other categories.

One limitation of our model is the assumption of uniform transfer rates from infection to treatment across all BU categories. This simplification was necessary due to limited data and literature on this parameter. The values used in the model were derived from the work of Ackumey et al. (2012), suggesting that individuals should begin medical treatment within four weeks of observing BU symptoms on the skin. It is essential to distinguish between seeking and starting treatment, as the latter involves various steps such as diagnosis, waiting times, and resource accessibility, which can vary based on infection severity and healthcare system capacity. Category I patients may exhibit lower treatment-seeking rates; however, if they seek treatment, they require only antibiotics, enabling a relatively prompt start. In contrast, Category III patients, necessitating surgery and hospital admission, might face delays due to the limited availability of operating theatre facilities. Figure 4.7 illustrates the significant impact of altering the transfer rate (γ_b) on the proportion of the infected population. To enhance model accuracy and relevance to real-world scenarios, we recommend comprehensive data collection on the rate of treatment initiation (γ).

Another noteworthy limitation of our model is the assumption made during sensitivity analysis, where we set the transfer rates $\delta_b = \delta_c$. It is essential to acknowledge that these parameters are intrinsic properties of the disease and reflect the natural course of BU if left untreated. Consequently, in practice, they cannot be modified.

In order to mitigate BU, we have to focus on creating avenues that encourage starting treatment before the ulceration. In this way, BU patients take antibiotics for 8 weeks and can recover without functional disabilities. From our model results this can be achieved by increasing the transfer rate γ_b. We suggest the following ways of increasing this rate as:

- Making it easy and accessible for people to test for BU whenever they suspect any symptoms. In this case adopting the rapid diagnostic test (RDT) for point of care testing would be a remedy.

- Working with community health volunteers (CHV) for active case finding of BU patients. Introduction of CHV can be instrumental in fast tracking infected BU population while in early categories.

Going forth, suppose we introduce the RDT in the compartmental model for example between compartments I_b and I_c in Figure 4.1. How affordable would it be for policy makers to implement? Specifically, what are the corresponding costs and effects of implementing a RDT as a control strategy? In chapter 5, we will perform a comprehensive study on this.

Suppose we allow CHV to spot the BU-infected population and refer them for treatment. How will introducing CHV in active case finding influence the early diagnosis and treatment? This phenomenon implies that the infected can start treatment through self-referral and CHV. In chapter 6, we investigate this using an agent-based model.

We recognise the fact that this model has limitations which include, lack of adequate clinical data for model validation. For example the specific number of infected population in each I compartment would be instrumental in making projections on BU infections. There was also limited information on parameter values. Parameters like transfer rates within the infected population and the rate of starting treatment could be influenced by individual behaviour hence difficult to estimate.

Chapter 5

Cost-effectiveness analysis of rapid diagnostic test compared to polymerase chain reaction in the diagnosis and treatment of Buruli ulcer in four endemic districts in Ghana

5.1 Introduction

One of the research priorities of WHO on BU is the development of rapid diagnostic tests (RDT) for accurate diagnosis of BU at the primary health care level (WHO et al., 2018), (WHO et al., 2022). The most used standard laboratory method to confirm BU is the polymerase chain reaction test (PCR). Although PCR has been a recommended diagnostic tool, it is expensive. It is performed in laboratories with sophisticated set-ups and not readily available to most endemic places, mainly rural areas (Stinear et al., 1999; Ablordey et al., 2012).

The model in this chapter is motivated by (Frimpong et al., 2019)'s work, which developed a RDT with the potential for quick diagnosis of BU at the point of care, providing timely results to health workers, in addition to being simpler to run and cost-friendly for endemic countries.

We investigate the affordability of the RDT given the limited resources in most endemic countries. To implement this, we shall conduct a cost-effectiveness analysis (CEA) of

using the RDT for BU diagnosis in rural Ghana from a healthcare provider perspective. The comparator is the PCR which is the current recommended clinical diagnostic test.

The model considers patients with suspected BU who attend a health clinic for diagnosis and treatment. Unlike the SIT model in chapter 4, this model uses a slightly modified version of the WHO categories as defined in chapter 1, page 3. Patients with suspected BU are either in category I (non-ulcerative lesions) or category II (ulcerative lesions). These are equivalent to states I_b and I_c of the SIT model.

This chapter proceeds as follows; in section 5.2, we describe the model starting with assumptions, construct a decision tree model in section 5.3 and in section 5.4, we establish corresponding probabilities. We then calculate the costs and effects at each decision tree node in section 5.5 and section 5.6. After that, we estimate the effects using DALY and calculate the incremental cost-effectiveness in section 5.6. Finally, we perform the probabilistic sensitivity analysis to cater for the uncertainty in parameter estimation in section 5.8 and conclude the chapter in section 5.9.

5.2 Model description

We developed a decision tree model for BU where we compared two diagnostic approaches: the RDT and PCR based on previous models for malaria (Shillcutt et al., 2008; Hansen et al., 2015, 2017) and typhoid fever (Saito et al., 2018). Ghana was selected because it is a high-burden country for BU and also owing to the existence of data to inform model parametrisation. An example of BU cases for the four endemic districts of Amansie West, Asante Akim, Afigya Sekyere and Ga is illustrated in Table 5.1.

Endemic area	**Prevalence per** $100,000$	**Cases**	**Total Population**
Amansie West	150.8	474	$162,848$
Asante Akim	131.5	265	$312,556$
Afigya Sekyere	107.1	149	$116,322$
Ga	87.7	$1,113$	$1,104,885$

TABLE 5.1: Population in the four endemic districts in Ghana showing the highest prevalence of BU (Amofah et al., 2002; Service et al., 2020).

5.2.1 Model assumptions

We make the following assumptions when designing the model

- No individual has been treated with antibiotics before visiting the health centre.
- An individual is assumed to have one disease and no co-infection.
- Healthcare workers adhere to test results and treatment procedures.

- There is 100% availability of antibiotics.
- A time horizon of 52 weeks as the estimated average treatment time of a BU patient with severe lesions (WHO et al., 2012).
- Individuals with category three BU (equivalent to state I_d in the SIT model) will not need a diagnostic test. The symptoms can be accurately identified with clinical diagnosis and treated immediately; hence we did not include that category in the decision tree (van der Werf, 2018).

5.3 Decision analysis

We constructed a decision tree to illustrate intervention arms for each diagnostic tool with pathways leading to treatment. Patients are diagnosed by either having BU or not, as determined by their reference diagnosis using RDT and PCR. After the diagnostic test result, a decision is made on which treatment to administer. We assume that when the diagnostic test result is positive, antibiotics are prescribed as first-line treatment for 8 weeks or antibiotics plus surgery if the patient is in a late category of BU (Asiedu et al., 2000). When the test is negative, we prescribe no medication.

Each decision tree branch had a probability, effect, cost of diagnosis and treatment assigned to it. These parameters were estimated based on previous studies, and others were estimated using the available data.

The expected costs and effects for the two tests (PCR and RDT) were then computed by 'rolling back' the decision tree displayed in Figure 5.1 along the branches. Thus, the incremental cost per additional DALY of the alternative option could be compared.

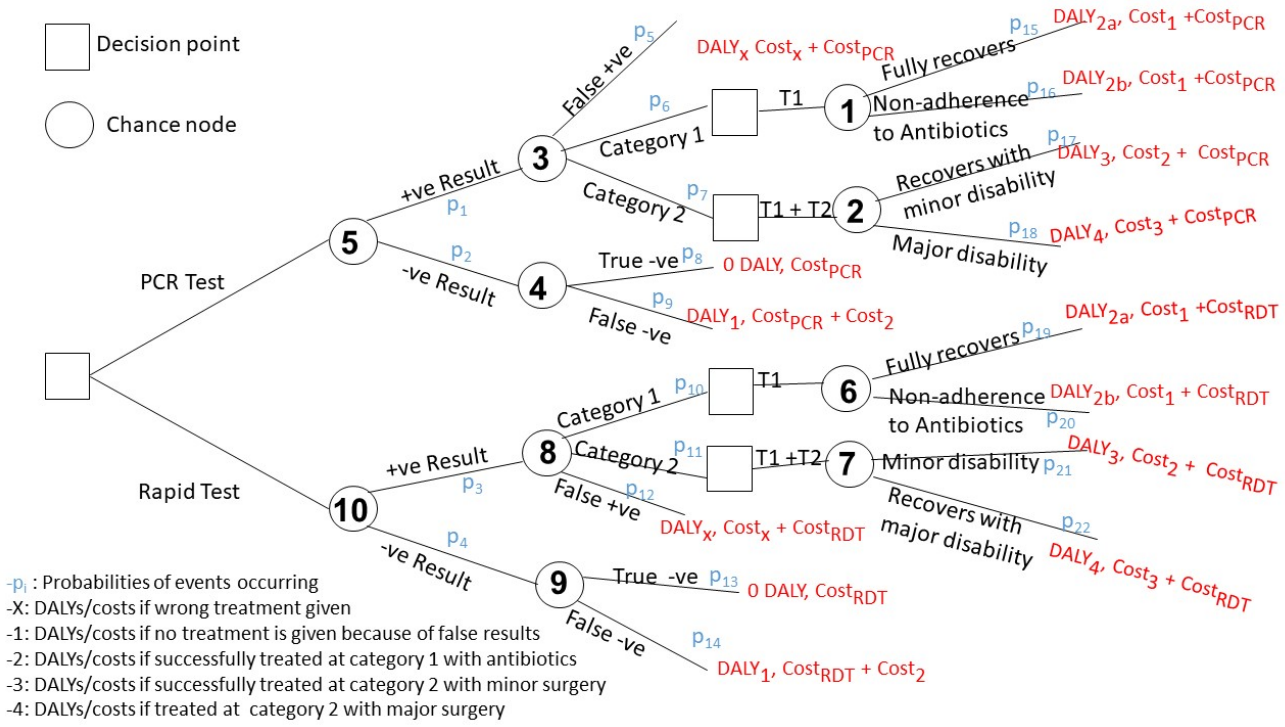

FIGURE 5.1: Decision tree model for the population that come for BU diagnosis and treatment. At every decision tree branch, the corresponding probability (p_i), cost and DALY are illustrated. T_1 and T_2 represent antibiotic treatment and surgery respectively.

5.4 Estimation of probabilities

We test a proportion of the population with any form of BU symptoms like nodules, plaques, oedema and skin lesions. We let α_1 and α_2 be the proportion of the population who have BU at category 1 and category 2 at the time of testing respectively. Hence $1-(\alpha_1+\alpha_2)$ will be the proportion of the population who do not have BU. Without treatment, the nodule or oedema will ulcerate within $4-6$ weeks (Bolz et al., 2016). Hence we can estimate the threshold time (period taken to move from category 1 to category 2) in the range of $4-6$ weeks.

In a national study survey in Ghana carried out by Amofah et al. (2002), of the $6,332$ people suspected to have BU, $5,619$ of them had BU at different categories. 48.5% of the lesions were in the ulcerative category and 12.5% in the pre-ulcerative category.

From this data, we let the values of α_1 and α_2 be 12.5% and 48.5%, respectively. We assume that the sensitivity and specificity of the PCR and RDT are the same for both categories.

- Let σ_p be the specificity of the PCR test evaluated as

$$\text{probability}\left[\text{negative PCR test}\middle|\text{negative for BU}\right]$$

which we estimated as 100% (95% Confidence Interval (CI) $69 - 100$) (Phillips et al., 2005).

- Let σ_r be the specificity of the RDT evaluated as the

$$\text{probability}\big[\text{negative RDT}\big|\text{negative for BU}\big]$$

which we estimated as 100% (95% C1 $84 - 100$) (Frimpong et al., 2019).

- Let ω_p be the sensitivity of the PCR test evaluated as

$$\text{probability}\big[\text{positive PCR test}\big|\text{positive for BU}\big]$$

which has been estimated as 98% (95% CI $91 - 100$)(Phillips et al., 2005).

- Let ω_r be the sensitivity of the RDT evaluated as

$$\text{probability}\big[\text{positive RDT}\big|\text{positive for BU}\big]$$

which has been estimated as 88% (95% CI $77 - 95$) (Frimpong et al., 2019).

- Let β_p be the probability that PCR test results come back within a threshold time. The turnaround time between transportation of samples and availability of PCR results is approximately 2 weeks (Bretzel et al., 2011). Results from the PCR return in weeks, so we choose the probability that the disease has not progressed by the time the tests come back to be approximately 40%.

- Let β_r be the probability that the RDT results come back within a threshold time. Test results have a runtime of 15 minutes, so we set β_r to be 100% (Frimpong et al., 2019).

We calculate the probabilities using values for σ_p, σ_r, ω_p and ω_r in (a) to (l).

(a) Probability that a test done using a PCR is positive (p_1) and the probability that a test done using a PCR is negative (p_2) .

$p_1 = \text{probability[test positive with PCR]}$ and $p_2 = \text{probability[test negative with PCR]}$

$$\begin{aligned} p_1 &= \omega_p(\alpha_1 + \alpha_2) + (1 - \sigma_p)(1 - \alpha_1 - \alpha_2) \text{ and } p_2 = 1 - p_1, \\ p_1 &= 0.98(0.125 + 0.485) + (1 - 1)(1 - 0.125 - 0.485), \\ p_1 &= 0.5978, \quad p_2 = 0.4022. \end{aligned} \tag{5.1}$$

(b) Probability that a test done using a RDT is positive (p_3) and the probability that a test done using a RDT is negative (p_4) .

$p_3 = \text{probability[test positive with RDT]}$ and $p_4 = \text{probability[test negative with RDT]}$

$$\begin{aligned} p_3 &= \omega_r(\alpha_1 + \alpha_2) + (1 - \sigma_r)(1 - \alpha_1 - \alpha_2) \text{ and } p_4 = 1 - p_3, \\ p_3 &= 0.88(0.125 + 0.485) + (1 - 1)(1 - 0.125 - 0.485), \\ p_3 &= 0.5368, \quad p_4 = 0.4632. \end{aligned} \tag{5.2}$$

(c) Probabilities on node 3 are defined as $p_5 + p_6 + p_7 = 1$. The probability that the positive result obtained using a PCR is false (p_5), which is equivalent to probability [false positive result with PCR].

$$\begin{aligned} p_5 &= \text{probability [negative for BU}\big|\text{test positive with PCR]}, \\ &= \frac{\text{probability}\big[\text{test positive with PCR}\big|\text{negative for BU}\big]\text{probability(negative for BU)}}{\text{probability (test positive with PCR test)}}, \\ &= \frac{(1-\sigma_p)(1-\alpha_1-\alpha_2)}{p_1} = \frac{(1-1)(1-0.125-0.485)}{0.5978}, \\ &= 0.000. \end{aligned} \tag{5.3}$$

(d) The probability that the positive result obtained using a PCR is BU (a) in pre-ulcerative categories (p_6) or (b) in ulcerative categories (p_7). Probabilities p_6 and p_7 are the positive predictive values. We evaluate them as:

$p_6 = \text{probability}\big[\text{category 1 positive PCR \& not progressed}\big|\text{test positive with PCR}\big]$.

p_7 = probability [category 2 with PCR **or** category 1 with PCR and progressed | test positive with PCR], $p_6 + p_7 = 1 - p_5$. Assume the same sensitivity for category 1 and category 2 for BU patients.

$$\begin{aligned} p_6 &= \frac{\omega_p \alpha_1 \beta_p}{p_1} = \frac{(0.98 \times 0.125 \times 0.4)}{0.5978} = 0.0819, \\ p_7 &= 1 - p_5 - p_6 = 0.9181 \end{aligned}$$

(e) The probability that the negative result was obtained using a PCR: (a) is true (p_8) or (b) is false (p_9). Probability (p_8) is also the negative predictive value. We estimate probabilities p_8 and p_9 as,

$$\begin{aligned} p_8 &= \text{probability}\big[\text{negative for BU}\big|\text{test negative with PCR}\big], \\ &= \frac{\sigma_p(1-\alpha_1-\alpha_2)}{p_2} = \frac{1(1-0.125-0.485)}{0.4022} = 0.9696, \qquad (5.4) \\ p_9 &= 1 - p_8 = 0.0304. \qquad (5.5) \end{aligned}$$

(f) Probabilities on node 8 are defined as $p_{10} + p_{11} + p_{12} = 1$. The probability that the positive result obtained using a RDT has BU: (a) in pre-ulcerative categories (p_{10}) or (b) in ulcerative categories (p_{11}). We estimate the probabilities p_{10} and p_{11} as follows:

$p_{10} = \text{probability}\big[\text{category 1 with RDT and not progressed }\big|\text{test negative with RDT}\big]$

$$\begin{aligned} p_{10} &= \frac{\omega_r \alpha_1 \beta_r}{p_3} = \frac{0.88 \times 0.125 \times 1}{0.5368} = 0.204918, \qquad (5.6) \\ p_{11} &= \frac{\omega_r \alpha_2}{p_3} = \frac{0.88 \times 0.485}{0.5368} = 0.7950. \qquad (5.7) \end{aligned}$$

(g) We estimate the probability that the positive result obtained using a RDT is false (p_{12}) as

$$\begin{aligned} p_{12} &= \text{probability}\left[\text{negative for BU}\middle|\text{test positive with RDT}\right], \\ &= \frac{\text{probability}\left[\text{test positive with RDT}\middle|\text{negative for BU}\right]\text{probability(negative for BU)}}{\text{Probability (Test positive the RDT)}}, \\ &= \frac{(1-\sigma_r)(1-\alpha_1-\alpha_2)}{p_3} = \frac{(1-1)(1-0.125-0.485)}{0.5368}, \\ &= 0.0000. \end{aligned} \tag{5.8}$$

(h) Probability that the negative result obtained using a RDT is; (a) true (p_{13}) and (b) false (p_{14}). Probability (p_{13}) is also the negative predictive value. Probabilities p_{13} and p_{14} are calculated as follows:

$$\begin{aligned} p_{13} &= \text{probability}\left[\text{negative for BU}\middle|\text{negative with RDT}\right], \\ &= \frac{\sigma_r(1-\alpha_1-\alpha_2)}{p_4} = \frac{1(1-0.125-0.485)}{0.4632}, \end{aligned} \tag{5.9}$$

$$p_{13} = 0.8419689, \tag{5.10}$$

$$p_{14} = 1 - p_{13} = 0.1580311. \tag{5.11}$$

(i) The probability that a BU patient diagnosed using a PCR or RDT is treated with antibiotics and fully recovers is p_{15} and p_{19}, respectively. We estimate p_{15} and p_{19} relating to the rate of treatment completion from values found in the literature, namely; 84.4% (Collinson et al., 2020) and 46% (Klis et al., 2014). Taking the average of 84.4% and 46% we obtain 65.2%.

(j) The probability that a BU patient diagnosed using a PCR or RDT does not adhere to treatment leading to delayed full recovery is p_{16} and p_{20}, respectively. Using p_{15} and p_{19} we obtain p_{16} and p_{20} as 34.8% using the decision tree in Figure 5.1.

(k) Probability that a BU patient diagnosed using a PCR or RDT is treated with antibiotics, and surgery recovers with minor disability (p_{17} and p_{21}). The combination of antibiotics and surgery was highly effective up to 80% (Cowan et al., 2015). Hence we estimate p_{17} and p_{21} as 80%.

(l) Probability that a BU patient diagnosed using a PCR or RDT is treated with antibiotics, and surgery recovers with major disability (p_{18} and p_{22}). Using p_{17} and p_{21} we obtain p_{18} and p_{22} as 20% using the decision tree in Figure 5.1.

Prob	**Parameter**	**Value**	**Source**
p_1	Probability that a test done using a PCR is positive	0.5978	Estimated in (a)
p_2	Probability that a test done using a PCR is negative	0.4022	Estimated in (a)
p_3	Probability that a test done using a RDT is positive	0.5368	Estimated in (b)
p_4	Probability that a test done using a RDT is negative	0.4632	Estimated in (b)
p_5	Probability that the positive result obtained using a PCR is false	0.0000	Estimated in (c)
p_6	Probability that the positive result obtained using a PCR has BU in pre-ulcerative categories	0.0819	Estimated in (d)
p_7	Probability that the positive result obtained using a PCR has BU in ulcerative categories	0.9181	Estimated in (d)
p_8	Probability that the negative result obtained using a PCR is true	0.9696	Estimated in (e)
p_9	Probability that the negative result obtained using a PCR is false	0.0304	Estimated in (e)
p_{10}	Probability that the positive result obtained using a RDT has BU in pre-ulcerative categories	0.2049	Estimated in (f)
p_{11}	Probability that the positive result obtained using a RDT has BU in ulcerative categories	0.7940	Estimated in (f)
p_{12}	Probability that the positive result obtained using a RDT is false	0.0000	Estimated in (g)
p_{13}	Probability that the negative result obtained using a RDT is true	0.8419	Estimated in (h)
p_{14}	Probability that the negative result obtained using a RDT is false	0.1580	Estimated in (h)
p_{15}	Probability that a BU patient diagnosed using a PCR and is treated with antibiotics fully recovers	0.6520	Estimated in (i)

TABLE 5.2: Sensitivity and specificity of diagnostic tests, probability estimates of treatment success of BU disease.

Prob	**Parameter**	**Value**	**Source**
p_{16}	Probability that a BU patient diagnosed using a PCR does not adhere to treatment leading to delayed full recovery	0.3480	Estimated in (j)
p_{17}	Probability that a BU patient diagnosed using a PCR is treated with antibiotics and surgery recovers with minor disability	0.8000	Estimated in (k)
p_{18}	Probability that a BU patient diagnosed using a PCR is treated with antibiotics and surgery recovers with major disability	0.2000	Estimated in (l)
p_{19}	Probability that a BU patient diagnosed using a RDT and is treated with antibiotics fully recovers	0.6520	Estimated in (i)
p_{20}	Probability that a BU patient diagnosed using a RDT does not adhere to treatment leading to delayed full recovery	0.3480	Estimated in (j)
p_{21}	Probability that a BU patient diagnosed using a RDT is treated with antibiotics and surgery recovers with minor disability	0.8000	Estimated in (k)
p_{22}	Probability that a BU patient diagnosed using a RDT is treated with antibiotics and surgery recovers with major disability	0.2000	Estimated in (l)

TABLE 5.3: Sensitivity and specificity of diagnostic tests, probability estimates of treatment success of BU disease.

5.5 Estimation of costs

This section estimates the costs in decision tree 5.1. These costs include the cost of RDT, the cost of PCR, the cost of first-line treatment, and the cost of minor and major surgery.

Considering the limited information available on costs, such as the cost of RDT and surgery, we made estimations based on the best available scenarios and data. Despite the inherent uncertainty, potential variations in cost estimates for minor surgery and RDT are unlikely to have a significant impact on the overall outcome of the decision tree calculations. Therefore, even if the estimates for these costs are under-estimations or over-estimations, the ultimate decision tree outcomes remain unaffected.

We assume all the costs incurred during this period are due to BU. From a health system perspective, we shall estimate these costs. We shall work with direct costs only, which include costs for diagnosis and treatment. We convert all costs to 2019 United States

dollars (USD) based on the US Bureau of Statistics from CPI Inflation Calculator (UBLS, 2020).

(I) Cost of the RDT (Cost_{RDT}): To estimate the price of the Buruli ulcer (BU) RDT, we relied on the cost of a Malaria RDT as reported in (Ezennia et al., 2017). Since there is no available information regarding the specific cost of an RDT for BU, we used the cost of the Malaria RDT as a proxy. Malaria is currently one of the leading infectious diseases in this context, with an RDT available.

The average cost of a Malaria RDT kit was US$0.15 (US$0.13−US$0.17) in 2017, equivalent to US$0.16 (US$0.14−US$0.18) in 2019. According to (Bath et al., 2020), the average retail price of a Malaria RDT in sub-Saharan Africa was US$0.33 in 2019. The global fund price list in 2022 is US$0.45 (US$0.25−US$0.65) which is equivalent to US$0.4 (US$0.22−US$0.58) in 2019 (website, 2022a,b). We take the unit costs of the RDT of US$0.16, US$0.33 and US$0.4 to obtain the average unit cost of the RDT as US$0.29.

(II) Cost of PCR (Cost_{PCR}): A PCR requires health personnel to administer it, which takes approximately 1 hour of staff time. The unit cost per sample, including staff time, has been estimated as US$11.24 in 2011 (Yeboah-Manu et al., 2011), equivalent to US$12.77 in 2019 for Ghana. We take $12.77 as the cost of one PCR. Training and fixed costs associated with a PCR have not been included.

(III) First line treatment cost (Cost_1): This includes the cost of antibiotics per dose taken for 8 weeks. 150 mg of rifampin cost between US$0.59 − 1.01 (year 2020) (checker, 2020) and 125 mg of clarithromycin cost US$2.72 (year 2020) (NHIS, 2020). Using the (UBLS, 2020) converter, 150 mg of rifampin cost lies in the range of US$0.57 − 0.98 (year 2019) and 125 mg of clarithromycin cost US$2.64 (year 2019). In Ghana, the price of 1 box of antibiotics (12 doses) was US$5.10 (Expatistan, 2020).

(IV) Cost of false positive (Cost_x): We calculate the cost when the wrong treatment is given. This is equivalent to first-line treatment administered to an individual, which we estimated as US$5.10 in (III).

(V) Unit cost of surgery: These include the costs incurred by the health facility for performing surgery on BU patients. The costs will be different for minor and major surgery. It includes the unit price of surgery multiplied by the number of surgeries done.

In Ghana, the average cost of treating BU per patient was US $966.85, US$706.08 and US$658.74 in 1994, 1995 and 1996 respectively (Asiedu, Kingsley and Etuaful, Samuel, 1998). We convert these costs to USD 2019, and an average is taken, which becomes US$1,307.01. Amofah et al. (2002) estimated the cost of surgery as US$780 (year 2002) which is equivalent to US$1,108.61 (year 2019). We use

costs US$1,307.01 and US$1,108.61 to calculate the average cost of surgery as US$1,207.81 (year 2019) (Agbenorku et al., 2012; Asiedu, Kingsley and Etuaful, Samuel, 1998; Amofah et al., 2002).

In the estimation of the cost of surgery, we relied on the average cost calculated from previous data in the literature. However, we acknowledge that the exact number of surgeries performed to derive this cost was unknown. To streamline the estimation process, we assigned the unit cost of surgery as equivalent to the previously calculated average cost.

(VI) Minor surgery ($Cost_2$): According to (WHO et al., 2012), two surgeries for minor surgery include surgical excision and skin grafting. The cost of this surgery will be twice the unit cost of surgery which is US$2,415.62.

(VII) Major surgery ($Cost_3$): WHO recommends three surgeries for major surgery which include surgical excision, skin grafting and contracture (WHO et al., 2012). The cost of this surgery will be thrice the unit cost of surgery which is US$3,623.3.

Cost parameter	**Value (US$)**	**Source**
Cost of RDT ($Cost_{RDT}$)		
Unit cost per RDT kit	0.29	Estimated in (I)
Cost of PCR ($Cost_{PCR}$)		
Unit cost per PCR	12.77	Estimated in (II)
First line treatment cost		
Cost of Antibiotics per dose	0.425	Estimated in (III)
Total cost for first line treatment ($Cost_1$)	5.10	Estimated in (III)
Secondary treatment cost		
Unit cost per surgery	1,207.80	Estimated in (V)
Minor surgery ($Cost_2$)	2,415.62	Estimated in (VI)
Major surgery ($Cost_3$)	3,623.43	Estimated in (VII)

TABLE 5.4: Cost parameters for the diagnostic tests and treatment.

5.6 Estimation of effects

We measure the effects of the diagnostic tests using disability-adjusted life years (DALY). For each branch of the decision tree, we estimate the expected number of DALY lost by an individual who follows that branch. As a result, a high number of DALY lost suggests a worse outcome. DALY depends on the period of hospitalisation and the extent of disability caused by the illness (disability weight-DW). We use the decision tree to calculate the expected effects of the different interventions.

We calculate DALY as the sum of the years of life lost (YLL) due to premature death in a population and the years lost due to disability (YLD) for people with BU (WHO, 2013). The YLL correspond to the number of deaths multiplied by the standard life expectancy at the age at which death occurs (L). Since BU does not lead to death, L= 0 hence YLL= 0. YLD is determined by DW and the average duration a person lives with a disability until death (T_d). We include a detailed description of DALY in the literature review in Chapter 2, Section 2.2 of the thesis.

$$\text{YLD} = \text{DW} \times T_d \tag{5.12}$$

T_d is equivalent to life expectancy at birth for Ghana, which is 64 years (Bank, 2022) minus the average age at which a person gets infected with BU, which is 20 years (WHO, 2018). Hence T_d = 64 years - 20 years = 44 years.

No specific DW is attributed to BU categories, so we estimate them using the best-related situations with unique DW. DW values lie in the $[0, 1]$ range where 0 represents perfect health, and 1 represents death (GBoDC, 2017). We substitute in Equation (5.12) to obtain the values for DALY as below.

DALY_1: We calculate DALY when a test shows negative, yet a person has BU. This means the individual does not receive BU treatment, and the disease progresses to the next categories. We relate this situation to DW for untreated burns of the second degree (< 20%), which is 0.156 (WHO et al., 2008). So YLD= $44 \times 0.156 = 6.864$.

DALY_{2a}: We calculate DALY if a person is successfully treated at category 1 with antibiotics. An individual was treated and healed successfully, so take YLD = 0.000.

DALY_{2b}: We calculate DALY if a person has not adhered to antibiotic treatment. The disease progresses to a wound; hence, we relate this situation to DW for open wounds, which is 0.108 (WHO et al., 2008). On calculating, we have YLD = $44 \times 0.108 = 4.752$.

DALY_3: We calculate DALY when a BU patient has recovered with a minor disability. We relate this situation to DW for treated burns of the second degree (< 20%) which is 0.158 (WHO et al., 2008). So YLD = $44 \times 0.158 = 6.952$.

DALY_4: We calculate DALYs when a BU patient has recovered with a major disability. We relate this situation to DW for treated burns of the third degree (> 20% and 60%) which is 0.469 (WHO et al., 2008). Major disability is between minor disability and before amputation. Hence we get YLD = $44 \times 0.469 = 20.636$.

DALY_x: We calculate DALY when wrong treatment is given. Individuals will be given BU treatment, yet they do not have the disease. This can lead to antibiotic

resistance. There was no estimated DW for this condition in the global burden of diseases. Hence we assume a DW of 0.000, leading to YLD = 0.000.

5.7 Incremental cost effectiveness ratio

The incremental cost-effectiveness ratio (ICER) of replacing PCR with RDT will be obtained by calculating the total expected costs between RDT and PCR and dividing by the difference in the total expected effects between the RDT and PCR at each node of the decision tree. ICER represents the extra cost incurred to gain an extra health outcome. This is represented as follows:

$$\text{ICER} = \frac{\text{Cost}_{\text{RDT}} - \text{Cost}_{\text{PCR}}}{\text{Effect}_{\text{RDT}} - \text{Effect}_{\text{PCR}}}. \tag{5.13}$$

We graphically represent the differences in costs and effects using a cost-effectiveness acceptability plane (CEAP). We divide the CEAP into four quadrants which we interpret as follows (Jamison et al., 2006) :

North-east: interventions generate more effective health outcomes but more expensive than comparator.

North-west: interventions generate less effective health outcomes but more expensive than comparator.

South-east: interventions generate more effective health outcomes and less costly than comparator.

South-west: interventions generate less effective health outcomes and less costly than comparator.

We calculate the ICER and establish which quadrant the value lies in, and that will guide us on which diagnostic test to adopt. To obtain the ICER in the decision tree, we first calculate the expected effects and costs for the RDT and PCR at each node as illustrated in Figure 5.2.

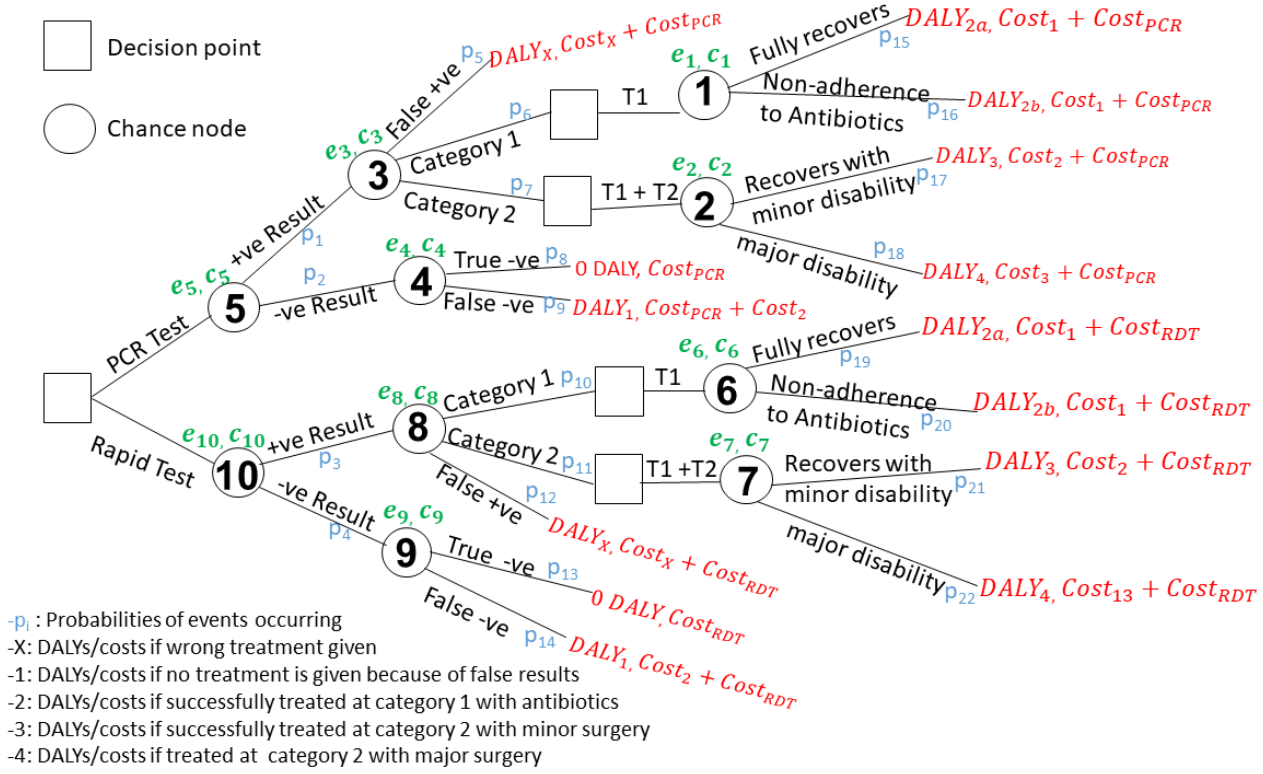

FIGURE 5.2: Decision tree model indicating the expected costs and effects at each node used in calculation of the ICER.

The terms e_1, e_2, e_3, e_4, e_5 and c_1, c_2, c_3, c_4, c_5 represent the expected effects and costs for the PCR at nodes, 1, 2, 3, 4, 5 as represented in the decision tree respectively. The terms e_6, e_7, e_8, e_9, e_{10} and c_6, c_7, c_8, c_9, c_{10} represent the expected effects and costs for the RDT at nodes, 6, 7, 8, 9, 10 in the decision tree respectively. Note: We dropped the dollar sign for costs during the calculations for ease of notation.

$$
\begin{aligned}
e_1 &= p_{15}\text{DALY}_{2a} + p_{16}\text{DALY}_{2b}, & c_1 &= p_{15}(\text{Cost}_1 + \text{Cost}_{\text{PCR}}) + p_{16}(\text{Cost}_1 + \text{Cost}_{\text{PCR}}),\\
e_2 &= p_{17}\text{DALY}_3 + p_{18}\text{DALY}_4, & c_2 &= p_{17}(\text{Cost}_2 + \text{Cost}_{\text{PCR}}) + p_{18}(\text{Cost}_2 + \text{Cost}_{\text{PCR}}),\\
e_3 &= p_5\text{DALY}_x + p_6e_1 + p_7e_2, & c_3 &= p_5(\text{Cost}_x + \text{Cost}_{\text{PCR}}) + p_6c_1 + p_7c_2,\\
e_4 &= p_9\text{DALY}_1, & c_4 &= \text{Cost}_{\text{PCR}} + p_9\text{Cost}_2,\\
e_5 &= p_1e_3 + p_2e_4, & c_5 &= p_1c_3 + p_2c_4,\\
e_6 &= p_{19}\text{DALY}_{2a} + p_{20}\text{DALY}_{2b}, & c_6 &= (p_{19} + p_{20})(\text{Cost}_1 + \text{Cost}_{\text{RDT}}),\\
e_7 &= p_{21}\text{DALY}_3 + p_{22}\text{DALY}_4, & c_7 &= (p_{21} + p_{22})(\text{Cost}_2 + \text{Cost}_{\text{RDT}}),\\
e_8 &= p_{12}\text{DALY}_x + p_{11}e_7 + p_{10}e_6, & c_8 &= p_{12}(\text{Cost}_x + \text{Cost}_{\text{RDT}}) + p_{11}c_7 + p_{10}c_6,\\
e_9 &= p_{14}\text{DALY}_1, & c_9 &= p_{13}(\text{Cost}_{\text{RDT}}) + p_{14}(\text{Cost}_2 + \text{Cost}_{\text{RDT}}),\\
e_{10} &= p_3e_8 + p_4e_9, & c_{10} &= p_3c_8 + p_4c_9.
\end{aligned}
$$

$$\begin{aligned} \text{ICER} &= \frac{c_{10} - c_5}{-(e_{10} - e_5)} = \frac{1311.760 - 1500.752}{-(4.782 - 5.475)} \\ &= -\$272.734 \text{ per DALY averted.} \end{aligned} \tag{5.14}$$

As discussed in Section 5.6, we estimate the expected DALYs incurred by an individual following a particular branch of the tree; therefore, we reverse the sign of our effects e_5 and e_{10} in the calculation of the ICER so that a positive denominator in the ICER calculation suggests that individuals who test with RDT have a better outcome than those who are tested via a PCR.

Negative effects mean individuals who test with a RDT have fewer years living with a disability than those who test with a PCR. When evaluating the ICER in Equation (5.14), we adjusted negative to positive effects to capture the fact that low DALYs generate more effective health outcomes.

An ICER of -272.734 was obtained to have one additional DALY averted. We include a detailed calculation in the Appendix A. The incremental costs are negative and incremental effects are positive, indicating the ICER lies in the southeast quadrant; hence, the RDT is less costly and leads to fewer DALY incurred. In our model, negative effects mean individuals who test with a RDT have fewer years (4.782) living with a disability than those who test with a PCR (5.475). On the other hand, negative costs mean individuals who test with a RDT pay less (US$1311.76) compared to those who test with a PCR (US$1500.752).

5.8 Probabilistic sensitivity analysis

We perform the probabilistic sensitivity analysis (PSA) to cater for the uncertainty that arises from an estimation of parameters. We use the PSA to determine the sensitivity of the ICER to changes in relevant parameter values. In the PSA, we will sample parameters from a probability distribution that best describes the parameter instead of adopting its median or mean (Briggs et al., 2006).

We used a uniform probability distribution for all the parameters. This distribution is a suitable choice, allowing us to assign corresponding minimum and maximum values for each parameter. In cases where the information on the range interval is unavailable, we estimate the minimum and maximum values by $\pm K$, where K is 10% of the parameter value.

To establish the minimum and maximum values, we made the following assumptions:

(i) Probabilities of occurrences in the decision tree: We centre the uniform distribution for these parameters on the estimated values, A_i. For σ_p, σ_r, ω_p, ω_r, β_p and β_r, we use confidence interval ranges as the minimum and maximum values. K values for α_1 and α_2 are 0.0125 and 0.0485 respectively. Table 5.5 indicates these ranges .

(ii) Costs in the decision tree: We take the minimum and maximum values for the unit cost per RDT kit as $[0.16, 0.58]$ estimated from (Ezennia et al., 2017; Bath et al., 2020; website, 2022a,b). The unit cost per PCR kit, we take the minimum and maximum values as $[11.4929, 14.047]$ since $K = 1.277$. For first line treatment, we take the minimum and maximum values as $[0.57, 5.1]$ estimated from (checker, 2020; NHIS, 2020; Expatistan, 2020; UBLS, 2020). The unit cost per surgery lies between $[1108.6, 1307.01]$ (Agbenorku et al., 2012; Asiedu, Kingsley and Etuaful, Samuel, 1998; Amofah et al., 2002). We double this range for minor surgery leading to $[2217.22, 2614.02]$. We triple this range for major surgery leading to $[3325.83, 3921.03]$. This is because minor surgery and major surgery requires 2 and 3 surgeries respectively. Table 5.6 indicates these ranges.

(iii) DALYs in the decision tree: We estimate the the minimum and maximum value to lie in the range of DALY$\pm K$. K values for each DALY are indicated in Table 5.7. For DALYs equivalent to 0, we estimate the minimum and maximum values as $[0, 0.5]$.

Parameter	**Value (US$)**	**K-value**	**Probability distribution**
Specificity of PCR (σ_p)	1.0	-	Uniform (0.69,1.0)
Specificity of RDT (σ_r)	1.0	-	Uniform (0.84,1.0)
Sensitivity of PCR (ω_p)	0.98	-	Uniform (0.91,1.0)
Sensitivity of RDT (ω_r)	0.88	-	Uniform (0.77,0.95)
Probability that PCR results come back within threshold time (β_p)	0.40	-	Uniform (0.30,0.90)
Probability that the RDT results come back within threshold time (β_r)	1.0	-	Uniform (0.90,1.0)
Proportion of the population who have BU at category 1 at the time of testing (α_1)	0.125	0.0125	Uniform (0.1125,0.1375)
Proportion of the population who have BU at category 2 at the time of testing (α_2)	0.485	0.0485	Uniform (0.4365,0.5335)

TABLE 5.5: Probability estimates of diagnosis and treatment of BU disease used in the PSA. Uniform distribution: the first value represents the minimum, and the second is the maximum. K is 10% of the parameter value. In **(i)**, we explain the assumptions of these estimates.

Parameter	**Value (US$)**	**K-value**	**Probability distribution**
Unit cost per RDT kit (Cost_{RDT})	0.16	-	Uniform (0.16,0.58)
Unit cost per PCR test (Cost_{PCR})	12.77	1.277	Uniform (12.77,13.27)
Cost for first line treatment (Cost_1)	5.10	-	Uniform (0.57,5.10)
Cost for false positive (Cost_x)	5.10	-	Uniform (0.57,5.10)
Minor surgery (Cost_2)	1704.18	-	Uniform (2217.22,2614.02)
Major surgery (Cost_2)	2556.27	-	Uniform (2556.27,3578.9)

TABLE 5.6: Probability distributions for the cost parameters used in the PSA. Uniform distribution: the first value represents the minimum, and the second is the maximum. K is 10% of the parameter value. In **(ii)**, we explain assumptions on these estimates.

Parameter	**Value (US$)**	**K-value**	**Probability distribution**
DALY_1	6.864	0.6864	Uniform (6.1776,7.5504)
DALY_{2a}	0.00	-	Uniform (0.00,0.5)
DALY_{2b}	4.752	0.4252	Uniform (4.2768,5.2272)
DALY_3	6.952	0.6452	Uniform (6.2568,7.6472)
DALY_4	20.636	2.0136	Uniform (18.5724,22.6996)
DALY_x	0.00	-	Uniform (0.00,0.5)

TABLE 5.7: Probability distributions for the DALYs used in the PSA. Uniform distribution: the first value represents the minimum, and the second is the maximum. K is 10% of the parameter value. In **(iii)**, we explain the assumptions of these estimates.

The variables were randomly sampled from the uniform probability distribution $10,000$ times. Each time, the variables took on a new value which resulted in $10,000$ specific results compared to no sampling, which will give 1 fixed value for each variable and will give us one set of results. Figure 5.3 represents the PSA results in an incremental cost-effectiveness plane.

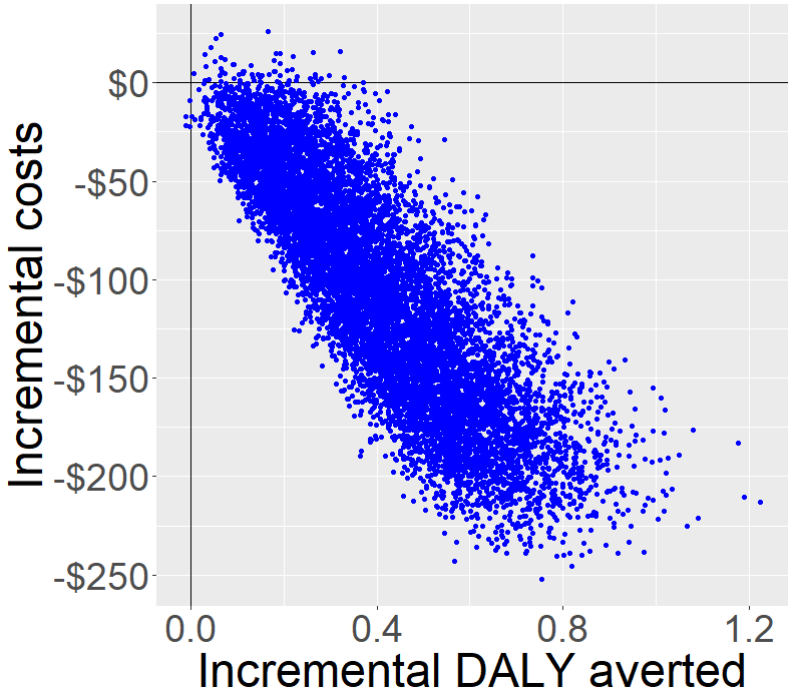

FIGURE 5.3: Incremental cost-effectiveness plane from PSA for cost per DALY averted by choosing RDT over PCR showing 10,000 sampled cost effectiveness pairs. Each point illustrates the cost and effect of one iteration where the value of each variable was chosen randomly from within the uniform probability distribution.

In Figure 5.3, the x-axis measures the incremental number of DALYs averted when RDT replaces PCR, and the y-axis measures incremental costs when RDT replaces PCR. Costs considered include the unit cost of the diagnostic tests and cost of treatment; effects considered were the number of DALYs averted.

In Figure 5.3, two quadrants of the cost-effectiveness plane are represented in this graph. To decide which test is most cost-effective, we check which quadrant contains the highest number of ICER pairs. In Figure 5.3, almost all cost-effect pairs lie in the southeast quadrant, showing the RDT as less costly and more effective than the PCR. The incremental costs are negative, indicating that the costs of using RDT and treatment are always lower than PCR. Incremental effects are positive, which suggests that using the RDT leads to low DALYs hence few years spent with a disability. This means that if RDT led to increased health outcomes (less DALYs), then RDT would be a feasible intervention.

Overall, certain assumptions were made in our model formulation, such as anticipating that the future cost of a diagnostic test for BU would be comparable to the current cost of a Malaria RDT. Additionally, we assumed that the costs of minor and major surgeries would be twice and thrice the unit cost, respectively, introducing a level of uncertainty around these estimates.

Despite the inherent uncertainty in cost estimates, the decision to opt for the RDT over PCR remains favourable. The PSA demonstrates that the majority of points fall in the southeast quadrant. Moreover, the BU RDT exhibits high sensitivity, a fact supported by (Frimpong et al., 2019) which suggests that even if the surgery costs are overestimated, the RDT would need to be significantly more expensive than the malaria RDT to alter the decision.

Considering these factors, the overall effectiveness of the RDT is robust, as evidenced by the PSA results where almost all points lie in the southeast quadrant, indicating a positive outcome.

5.9 Conclusion

In this chapter, we presented a comprehensive analysis of the costs and effects of the two diagnostic tests as an intervention to encourage early diagnosis and treatment of BU disease. A decision analysis model evaluated the probabilities, costs and effects of adopting a RDT and a PCR. The economic evaluation was from the healthcare provider's perspective using data from Ghana.

Our main result was the ICER of $-\$272.7342$ per additional DALY averted from using a RDT compared to a PCR. To test the robustness of the ICER results, we performed a probabilistic sensitivity analysis around the parameter values used in our model. The PSA resulted in a cost-effectiveness plane, which tells us the quadrant with the highest number of cost-effect pairs. Results of the PSA showed the majority of the ICER pairs spread out in the southeast quadrant, where the RDT is less costly and yields fewer DALYs.

There have been several limitations in this study, which include the following:

Most importantly, there is a lack of detailed aggregate data on costs and effects: for example, there were no disability weights on Buruli ulcers. We derived most of the cost estimates from trial experiments in a particular region which may not represent the exact situation when applied to a different region, Ghana. Some data was outdated, yet BU disease research has evolved over time.

In this study, we assumed that people start treatment after receiving test results. However, in most endemic African countries, BU can be correctly identified with clinical diagnosis. Most often, the health care practitioners base their decision on administering treatment for the suspected BU patients. This means introducing a RDT could be vital in reducing long waiting periods for the PCR results and avoiding unnecessary treatment rather than preventing BU patients from getting to advanced stages.

We recommend continued careful evaluation of the RDT before implementation. Success with the RDT in diseases like Malaria could mean that it may be adopted for BU in most endemic areas.

There is a need for studies on specific health states; for example, updating the disability weights for BU would be essential for DALY calculations. An update on parameters like standard treatment costs would be instrumental in calculating the ICER. The availability of better data will improve the model's accuracy.

In this study, we considered one measure of effect, namely the DALY. We recommend the inclusion of more effects like quality-adjusted life years, correctly diagnosed BU cases, and treatment successes in a specific treatment period. Extending the model to capture prevalence rates, for example, could investigate how the rapid diagnostic test would perform in an area of low prevalence versus in high prevalence.

According to WHO, a recommended diagnostic tool should be affordable, sensitive, specific, user friendly, robust, equipment free and deliverable to the end user (ASSURED) (Mabey et al., 2004). Our research elucidates how affordable the suggested RDT for testing BU is, which is part of the ASSURED criteria.

With the ease and affordability that comes with testing using a RDT, it will encourage health practitioners to prioritize following the appropriate procedure of testing first before treatment as recommended by WHO.

Chapter 6

Modelling the potential impact of community health volunteers in the diagnosis and treatment of Buruli ulcer

6.1 Introduction

One of the consequences of late diagnosis and treatment of BU is recovering with severe disability and facing social stigma (Stienstra et al., 2002; Shina, 2011). This challenge may be mitigated by implementing public health strategies that lead to early detection of BU.

6.1.1 Community health volunteers and their roles

Community health volunteers (CHV) is a generic term for lay people who work outside the formal health environment to assist local communities in accessing health facilities. They may be semi-literate or illiterate but are often trained for particular tasks they are to perform (Perry et al., 2014).

Roles of CHV include promoting healthy behaviours among populations, assisting in conducting outreach and advocating for the community's health needs (Cherrington et al., 2010).

The following selected studies cite evidence of the effectiveness of CHV in improving the health of populations.

In Davis et al. (2013)'s work, an evaluation of CHV involvement in a population of 1.1 million in rural Mozambique demonstrated a one-third decrease in the prevalence of child under-nutrition.

According to Hall (2011), the possibility of exclusive breastfeeding was 5.6 times higher in a community exposed to CHV compared to a group that was not. In addition, CHV proved instrumental in identifying malnourished children in such communities and guided mothers on positive nutrition (Wollinka et al., 1997).

According to WHO, of the 313 tasks identified for HIV/AIDS management and control, 115 can be performed by CHV (Organization et al., 2008). Studies by (Apondi et al., 2007; Behforouz et al., 2004; Wouters et al., 2009) found that the employment of CHV in Uganda, Haiti and South Africa improved antiretroviral adherence and treatment success.

The introduction of women's groups practising participatory learning and action led to a 37% decrease in maternal mortality in India, Nepal, Bangladesh and Malawi (Prost et al., 2013).

CHV were influential in delivering malaria-related services, for example, the distribution of insecticide-treated mosquito bed nets, community education, delivery of rapid diagnostic tests, malaria prevention and diagnosis. Studies have indicated that CHV can accurately read malaria test results, guide treatments and follow up using those test outcomes (Counihan et al., 2012).

The ability of CHV to perform these tasks highlights their relevance, which is of particular relevance to our model.

6.1.2 Role of CHV in BU disease

In some parts of West Africa, introducing CHV in referring BU cases was instrumental in improving the number of BU cases reported (Vouking et al., 2013; Barogui et al., 2014; Vouking et al., 2014).

Using CHV in active case finding led to a 70% increase of detected category 1 BU cases in a high endemic district in Ghana (Abass et al., 2015).

In another study by (Vouking et al., 2014) in the Ngoantet region, Cameroon, CHV referred 95% of BU cases, and 91.5% of those suspected cases were confirmed by health personnel. In addition, (Barogui et al., 2014) indicated the existence of an essential link of CHV in the management of BU in Benin.

Vouking et al. (2013) reviewed 17 studies on the impact of CHV on BU in sub-Saharan Africa. The impact focused on BU cases referred, confirmed, and identified. This review concluded that implementing CHV programmes may have a considerable impact on the control of BU.

The model we present in this chapter was inspired by (Vouking et al., 2014; Abass et al., 2015; Vouking et al., 2013)'s work, where CHV were proposed and introduced as an intervention to curb late category BU cases.

6.1.3 Agent based models

This research aims to develop an agent-based model (ABM) that incorporates the interaction of BU patients with CHV in improving detection rates and reducing the time between detection and starting treatment.

ABMs are computational simulation tools composed of agents interacting with each other and within their environment governed by a set of pre-defined rules. They are powerful for their ability to incorporate stochasticity, individuality and spatial variation in the model formulation (Hackl and Dubernet, 2019).

This work uses human movements to model the diagnosis and treatment of BU since BU does not have person-to-person transmissions. The bottom-up approach of ABMs allows representation of each individual in the system, giving them rules that govern their interactions (Macal, 2016).

A population-based behaviour emerges from interactions among different agents in space and time. In general, agent-based modelling is characterised by its bottom-up structure, a micro-scale perspective and discrete-event considerations (Macal and North, 2005; Macal, 2016; Smith et al., 2018).

The emphasis on modelling the heterogeneity of agents across a population and the emergence of an autonomous organization are two of the distinguishing features of agent-based simulation compared to other simulation techniques such as discrete-event simulation, and system dynamics (Macal and North, 2005).

The stochasticity of ABMs permits variation due to randomness and thus more accurately mimics the transmission of BU.

Hence, we developed our model based on worked examples in NetLogo (Wilensky, 1999), for example, the epiDEM (Epidemiology: Understanding Disease Dynamics and Emergence through Modelling) (Yang and Wilensky, 2011). Studies done by (Wilensky, 1997; Yang and Wilensky, 2011) were instrumental in the initial steps of the ABM. We adapted and extended concepts from the introductory sample models in their NetLogo simulation work.

This chapter is arranged as follows: Section 6.2 discusses the theoretical background of the model. In Section 6.3, we describe elements of the model, for example, agents, their environment and their relationships. In Section 6.4, we describe the model's processes and schedule specifying the order they are executed in. Section 6.5, explains the model's design concepts, including explaining how the concepts characterising the model were

implemented. In Section 6.6, we describe the initialisation, input data and sub-models. We explain the NetLogo simulation methodology in Section 6.7. Section 6.8 presents the numerical simulations of the model. The conclusion is included in Section 6.9.

6.2 Model description

The model description follows the ODD (Overview, Design concepts, Details) protocol for describing ABM (Grimm et al., 2006) updated in (Grimm et al., 2020). We customised the elements of our model such that it adheres to the guidelines stated by (Grimm et al., 2006, 2020). The model was implemented in a software platform called NetLogo (v.6.2.2) (Wilensky, 1999) which is freely available.

The purpose of the model is to explore the effects of the introduction of CHV in referring BU patients for treatment. In particular, it is designed to help us understand and predict how interactions between BU patients and CHV can influence early diagnosis and treatment of BU.

Precisely, we will:

(i) illustrate the individual interactions of BU patients with CHV;

(ii) observe BU disease progressions within the infected and treated population over a period of 400 weeks;

(iii) compare and contrast the effect of either self-referral (SR) independently or both SR and CHV in the early diagnosis and treatment of BU.

In this model, we assume that

- CHV do not contract BU while referring BU patients,
- a fixed population size, in this case, a closed population with no birth, migration or death,
- direct contact of susceptible individuals with the environmental habitat of *M. ulcerans* bacteria leads to a BU infection,
- CHV are 100% effective in diagnosing infected BU patients,
- if an individual adheres to treatment prescribed and proper wound care, treatment is 100% successful in removing the BU infection; although people in categories 2 and 3 will heal with some form of disability.

6.3 Entities, state variables and scales

In this section, we describe the structure of the model in terms of entities, state variables and scales.

6.3.1 Agents

The model contains two types of agents: (a) people in the general population and (b) CHV. We classify the general population as susceptible (S), infected (I), treated (T) and recovered (R). The I, T and R populations are each grouped into 3 categories.

Agent Description	**Colour**
Susceptible population	Blue
Infected population in incubation period of the infection and category one of BU	Red
Infected population in category two of BU	Green
Infected population in category three of BU	Yellow
Population on antibiotic treatment	Brown
Population on antibiotic treatment and minor surgery	Magenta
Population on antibiotic treatment and major surgery	Orange
Population who recovered with no disability	Cyan
Population who recovered with minor disability	Pink
Population who recovered with major disability	Gray
CHV	White

TABLE 6.1: Description of Agents-population and CHV.

We represent the population as mobile individuals with state variables for their location and status.

Note: In this chapter, we will use hospitalTwo to mean people in treatment with antibiotics and minor surgery, hospitalThree to mean people in treatment with antibiotics and major surgery.

6.3.2 Spatial and temporal scales

Spatial scale:

We represent the area occupied by the total population using a 17×17 grid of square cells. The environment represents the spatial distribution of agents in an area.

The model is two-dimensional, representing space as a collection of discrete units called patches. An agent's location is defined by which spatial unit it is in. This model uses a discrete square grid for spatial variables but allows agent locations to use continuous space. If an individual and a CHV occupy the same patch, they are considered to be in the same place and in contact with each other.

Temporal scale:

One time step represents one week, and simulations run for 400 weeks. We set the simulation to 400 weeks to match the time used in the compartmental model when it reached equilibrium. In other words, it should allow time for observations to reach an equilibrium.

6.3.3 Description of state variables

Variable name	Type	**Description**
susceptible?	Boolean	True if the person is in state susceptible, otherwise False
infection-length	Real	The current length of time since initial infection spent by an individual with BU who is either incubating or in category 1.
infection-lengthTwo	Real	The current length of time an individual has spent in category two
infected?	Boolean	True if the person is in state incubation period or state infected in category 1, otherwise False
infectedTwo?	Boolean	True if the person is in state infectedTwo, otherwise False
infectedThree?	Boolean	True if the person is in state infectedThree, otherwise False?
hospitaltwo?	Boolean	True if the infected person is in state antibiotic and minor surgery treatment, otherwise False
hospitalthree?	Boolean	True if the infected person is in state antibiotic and major surgery treatment, otherwise False
antibiotics?	Boolean	True if the infected BU patient is in state antibiotic, otherwise False
antibiotic-time	Real	The current length of time an infected BU patient has spent on antibiotics treatment
hospital-time-two	Real	The current length of time an infected BU patient has spent on antibiotic and minor surgery treatment.
hospital-time-three	Real	The current length of time an infected BU patient has spent on antibiotic and major surgery treatment.
noDisability?	Boolean	True if a person is in state no disability, otherwise False
minorDisability?	Boolean	True if a person is in state minor disability, otherwise False
majorDisability?	Boolean	True if a person is in state major disability, otherwise False

TABLE 6.2: Description of the agent population and their state variables.

Table 6.2 describes state variables for each agent. Agents move between states depending on infection length, their interactions with CHV, how soon they commence treatment and recovery times.

There are two categories of states: states relating to disability and states relating to disease progression. A person starts the simulation with no disability, for example noDisability? set to be true but may develop a minor or major disability following illness with BU. At this point either minorDisability? or majorDisability? is set to be true. If a person contracts BU again, their disability status will remain the same or worsen and will not improve. A person can cycle through any of the disease states regardless of their disability status.

6.3.3.1 Model parameter values

We describe model parameters used in the model and their units.

(A) **BU-symptoms: the incubation period;** the elapsed time from initial infection until the development of symptoms. This period takes between $2-3$ months; for this model, we use 3 months, equivalent to 13 weeks (Zingue et al., 2018a).

(B) **Threshold-timeone: the duration in category 1;** the elapsed time from development of symptoms until transition to category 2. The average threshold-timeone was estimated to take approximately $4-6$ weeks (WHO, 2018). We draw this value from a random-exponential distribution around the average threshold-timeone.

(C) **Threshold-time:** the elapsed time from initial infection until the transition to category 2. Threshold-time is therefore equal to BU-symptoms plus Threshold-timeone.

(D) **Threshold-timeTwo: the duration in category 2;** the elapsed time from category 2 until the transition to category 3. The average threshold-timetwo was estimated to take approximately 4 weeks (WHO, 2018; Portaels et al., 2001). We draw this value from a random-exponential distribution around the average threshold-timetwo.

(E) **SR probabilities:** SR probabilities are the probabilities that individuals with BU in categories 1, 2 and 3 will self-refer for treatment, respectively. WHO (2018) showed that 70% of all BU cases were diagnosed after ulceration. To mimic this, we let the SR probabilities for BU patients in categories 1, 2 and 3 be 10%, 20% and 70%, respectively.

(F) **Recovery-timeone:** the elapsed time for an individual who has been on antibiotic treatment until full recovery. The average recovery time one for treatment was estimated to take approximately 8 weeks. We draw this value from a random-exponential distribution around the average recovery time one.

(G) **Recovery-time-two:** the elapsed time for an individual who has been on antibiotic treatment and minor surgeries until full recovery. The average recovery-time-two for treatment was estimated to take approximately 30 weeks. We draw this

value from a random-exponential distribution around the average recovery-time-two.

(H) **Recovery-time-three:** the elapsed time for an individual who has been on antibiotic treatment and major surgeries until full recovery. This treatment was estimated to take an average of 52 weeks. We draw this value from a random-exponential distribution around the average recovery-time-three.

Name	Baseline value	Probability distribution	Source
BU-symptoms	13.0 weeks	-	Estimated in (A)
Threshold-timeone	6.0 weeks	Exponential	Estimated in (B)
Threshold-timeTwo	4.0 weeks	Exponential	Estimated in (D)
Self-refer-prob-category1	10%	-	Estimated in (E)
Self-refer-prob-category2	20%	-	Estimated in (E)
Self-refer-prob-category3	70%	-	Estimated in (E)
Recovery-timeone	8 weeks	Exponential	Estimated in (F)
Recovery-timetwo	30 weeks	Exponential	Estimated in (G)
Recovery-timethree	52 weeks	Exponential	Estimated in (H)

TABLE 6.3: State constants used in the model. Population initialization parameters used in the model.

6.3.3.2 Model variables

We describe variables used in the model.

(i) **Infection-length:** This is the period an individual has been infected with category one BU. Proceeding to the next category depends on how long they stay infected.

(ii) **Infection-lengthTwo:** This is the period an individual has been infected with category two BU.

(iii) **Antibiotic-time:** The time until recovery of an individual who is administered antibiotics only.

(iv) **Hospital-time-two:** The time until recovery of an individual who is administered antibiotic and minor surgery treatment.

(v) **Hospital-time-three:** The time until recovery of an individual who is administered antibiotic and major surgery treatment.

6.4 Process, overview and scheduling

In this section, we present an brief overview of elements executed by the model and the order in which they are executed. We represented the processes and schedule using a flow chart in Figure 6.1 and the pseudo-code 1.

6.4.1 Processes:

We develop the model and the following processes are executed at each time step in the same predetermined order. These processes are: infect-start, infect-two, infect-three, self-referral, meet-chvs, recover, move-time-on and move. The population update their state variables every time step over the whole simulation and change their status.

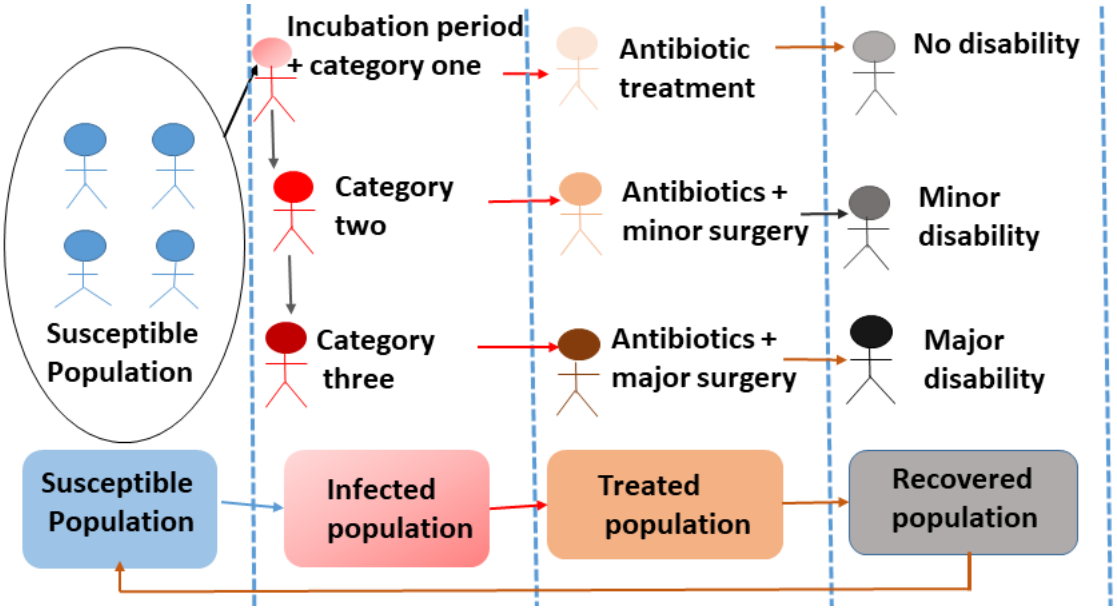

FIGURE 6.1: Illustration of different states of the model to simulate the progress of BU in a population. Parameters for transition within states are explained in detail in 6.3.3.1.

6.4.2 Schedule:

The flow chart presents an outline of the sequence processes and the schedule of interactions between the different agents at each time step. We define each process by the following.

First, the time counter is updated at each time step. Then, the unit values of chosen input parameters and the infection history are updated.

Next, we let agents move randomly across space. If they are uninfected and move into the patch representing initial infection, they become infected and move to category 1. If

they are already infected and enter the same patch as a CHV agent, the CHV will refer them to treatment. The infected BU can also start treatment through self-referral.

Infected individuals proceed to commence treatment and can recover with either no disability or different forms of disability. Some processes are only activated under particular conditions; for example, the possibility of infection only starts after a human interacts with the *M. ulcerans* habitat.

The final action executed at each time step is an update of model outputs. The graphical interface outputs are re-drawn, and updated population information are written to an output file.

A detailed description of each of these processes and schedule is in subsection 6.6.3.

Algorithm 1 SUMMARY OF WORK FLOW OF THE TOTAL POPULATION PROCEDURES

procedure POPULATION AND CHV PROCEDURES
Let initial susceptible population be h **and** assign colour blue
Let the CHV population be k **and** assign colour white
Let m be a circle centred at the origin with a **radius of** 3 filled with square grids **and** assign colour gray to m.
Initialise agents in terms of their **spatial positions** in the environment
Let h **and** k populations **move randomly**
Infected:
    if any of h people go through m **then**
        set infected? **true**
        assign colour red
    end if
Infectedtwo:
    if infection length exceeds threshold time **then**
        set infectedtwo? **true**
        assign colour green
    end if
Infectedthree:
    if infection-length-two exceeds threshold time two **then**
        set infectedthree? **true**
        assign colour yellow
    end if
Self referral:
    if infection-length exceeds BU-symptoms **then**
        if infected **and** probability of self referral in category 1 > random float value **then**
            set antibiotics? **true**
            assign colour brown
        end if
        if infectedtwo **and** probability of self referral in category 2 > random float value **then**
            set hospitaltwo? **true**
            assign colour magenta
        end if
        if infectedthree **and** probability of self referral in category 3 > random float value **then**
            set hospitalthree? **true**
            assign colour orange
        end if
    end if
end procedure

Algorithm 2 SUMMARY OF WORK FLOW OF CHV PROCEDURES

38: ***Meet chv***:
39: **if** infected **and** meet chvs **then**
40: **set** antibiotics? **true**
41: **assign** colour brown
42: **end if**
43: **if** infectedtwo **and** meet chvs **then**
44: **set** hospitaltwo? **true**
45: **assign** colour magenta
46: **end if**
47: **if** infectedthree **and** meet chvs **then**
48: **set** hospitalthree? **true**
49: **assign** colour orange
50: **end if**
51: ***Recover***:
52: **if** antibiotics **and** antibiotic-time exceeds recovery-timeone **then**
53: **set** noDisability? **true**
54: **assign** colour cyan
55: **set** susceptible? **true**
56: **set** infected? **false**
57: **end if**
58: **if** hospitaltwo **and** hospital-time-two exceeds recovery-timetwo **then**
59: **set** minorDisability? **true**
60: **assign** colour pink
61: **set** susceptible? **true**
62: **set** infectedtwo? **false**
63: **end if**
64: **if** hospitallthree **and** hospital-time-three exceeds recovery-timethree **then**
65: **set** majorDisability? **true**
66: **assign** colour gray
67: **set** susceptible? **true**
68: **set** infectedthree? **false**
69: **end if**
70: ***Update iterations***:
71: **if** (infected? **or** infectedtwo? **or** infectedthree?) **then**
72: infection-length ← infection-length +1
73: **end if**
74: **if** infectedtwo **then**
75: infection-lengthtwo ← infection-lengthtwo +1
76: **end if**
77: **if** antibiotics **then**
78: antibiotic-time ← antibiotic-time +1
79: **end if**

Algorithm 3 SUMMARY OF WORK FLOW OF CHV PROCEDURES

if hospitalltwo **then**
    hospital-time-two ← hospital-time-two +1
end if
if hospitallthree **then**
    hospital-time-three ← hospital-time-three +1
end if

To maintain brevity in the pseudocode for the main algorithm, we selected the "infectedTwo" state to serve as a representative for other states, providing a detailed account of all the procedures.

Algorithm 4 SUMMARY OF WORK FLOW OF THE INFECTEDTWO PROCEDURES

Infectedtwo:
if infection length exceeds threshold time **then**
    set infectedtwo? **true**
    set infected? **false**
    set infection-lengthTwo= 0 ▷ Reset elapsed time in BU state 2
    set thresholdtimeTwo=random(exponential(4)) ▷ Sample time to transition to BU state 3 for this agent
    assign colour green
end if

6.5 Design concepts

In this section, we use the design concepts of the ODD protocol (Grimm et al., 2006, 2020) to describe key characteristics of model. We focused on concepts that apply to our model. The elements of the design concepts that characterise our model are basic principle, interaction, stochasticity and observation.

6.5.1 Basic principle

The basic principle of this model is to illustrate how interactions between CHV and BU patients influence treatment referral. The aim of the model is to estimate the reduction in the number of people with a disability as a result of using CHVs. Understanding this principle can be critical for developing policies to address BU treatment issues such as the delayed start of BU treatment.

6.5.2 Interaction

The model assumes direct interaction between BU patients and CHV. The CHV interactions occur when CHVs meet infected people in the population. In self-referral (SR), BU patients seek treatment without the involvement of CHV.

When the CHV occupies the same grid square as a BU patient, we observe both agents as being on the same patch. This implies that both agents interacted, leading to the referral of an infected BU individual.

6.5.3 Stochasticity

There are three key elements of stochasticity used in initializing the model and during the simulation. Due to this stochasticity, each model run produces different results. These include:

(a) the probability of self-referral.

(b) randomness on how populations move between the grid squares.

(c) the time spent in each infection category. Threshold time and the agent's time to recovery which influence disease progression periods were drawn from an exponential distribution for each infected person.

Here, by making the threshold and recovery times random, a patient's outcome is also stochastic.

6.5.4 Observation

The graphical output on the NetLogo interface shows the parameters that can be adjusted. In every run of the model, data is collected on the number of agents who are susceptible, infected, treated and recovered at each time step. Summary statistics of the model output are saved at every time step.

6.5.5 Emergence, adaptation, learning, prediction, sensing and collectives

Emergence, adaptation, learning, prediction, sensing and collectives were not represented in this model.

6.6 Details

6.6.1 Initialization

We set the initial population in the simulation to 1000, representing the entire area's population. This value was chosen to provide a sufficient sample size while allowing a suitable simulation period.

The CHV-to-population ratio is 100 : 1000, meaning there is 1 CHV for every 10 individuals. In the model's initial state, at $t = 0$ in a single simulation run, we use the parameters listed in Table 6.3.3.1 on page 106.

To initialize the agents within the environment in terms of their spatial positions, we employ the method [random-xcor random-ycor] during the simulation.

6.6.2 Input data

The model does not use input data to represent time-varying processes.

6.6.3 Submodels

We detail how the processes represented in Section 6.4 are simulated. These are represented as procedures and reporters in NetLogo. The corresponding parameters of the model are explained in subsubsection 6.3.3.1.

6.6.3.1 Clock

To keep track of the time in the model. The time is determined as the modulus of ticks. In this model, we represent time in weeks.

6.6.3.2 Move

Agents continuously move forward one step at a time and turns through a random angle between 0° and 360°. NetLogo implements this using procedures `(fd 1)` and `(rt random-float 360)`, respectively.

The step size used in the simulation tells us how an agent moves in each time step of the simulation. This parameter determines how fast agents move in the simulation and in this model, we set the step size to 1 and the initial domain size on which agents move is (17×17) grids.

In Section 6.8.3, we investigate the impact of altering both the domain size and step size on the movement and interactions of agents in the simulation.

The movement and interactions of agents in the simulation is influenced by the balance between the domain size and the step size. For example by setting an appropriate stepping distance relative to the domain size, we can control the scale and pace of the simulation, ensuring that the agents' movements and interactions align with the dynamics of BU.

6.6.3.3 Infection

Infection is in terms of infect-start, infect-two and infect-three procedures.

Infect-start: When the population interact with the habitat of *M. ulcerans*, an uninfected individual has a chance of contracting BU. The habitat of *M. ulcerans* is represented as a circle centred at the origin with a radius of 3 filled with square grids.

Infect-two: When the infection length exceeds the threshold time, infected agents transition to a category two infection.

Infect-three: When the infection-lengthTwo exceeds the threshold timeTwo, agents with category two BU infection transition to a category three infection.

6.6.3.4 Treatment

Access to treatment can be either through SR or by meeting CHV, who refer infected individuals to treatment.

Self-referral: After being infected for a period called BU-symptoms, there is a probability that agents with:

- Category one BU infection will start antibiotic treatment only.
- Category two BU infection will get antibiotic treatment and minor surgery.
- Category three BU infection will get antibiotic treatment and major surgery.

Once in treatment, agents are no longer counted as infected, and their infection length(s) are reset to zero. Once an agent has received treatment, they can become infected again. However, their colour is now different from their initial colour (blue as indicated in Figure 6.1) at the the start of the simulation. The change in color is because their disability stage may change following treatment and can only worsen following a subsequent infection.

Meet-chvs: When infected people meet CHV, they are picked up and start treatment. This can be antibiotic treatment and minor or major surgery, depending on what category of BU infection they were at when they met the CHV.

6.6.3.5 Recovery

A person in treatment will recover after reaching their recovery time. Each individual's recovery time is sampled from an exponential distribution with a mean of the average recovery time set by the user as indicated in Table 6.3.3.1.

If antibiotic-time exceeds the recovery timeone, hospital-time-two exceeds the recovery timetwo, or hospital-time-three exceeds the recovery timethree, BU patients recover with no disability, minor disability or major disability, respectively. Otherwise, the patient continues on treatment for one more week and keeps the same disability state as they had prior to this BU infection.

At the end of each time step, all global variables are updated. The counts and percentage of susceptible, infected, treated and recovered agents are all calculated.

6.6.3.6 Update global variables

Considers the progress pattern of the population each week and updates the agent locations and states.

6.7 NetLogo Simulation

We created the NetLogo environment, and the set-up is presented in Figure 6.2. It has three key components. First is the main environment, where all agents are spatially distributed to mimic the arrangement of the human population. Secondly, frames for plotting the simulation outputs as agents interact in the environment. Four plot frames represent the susceptible, infected, treated and recovered populations plotted against time. Lastly are buttons and sliders, which are used in interacting with the agents through the calibration of model parameters and start or run.

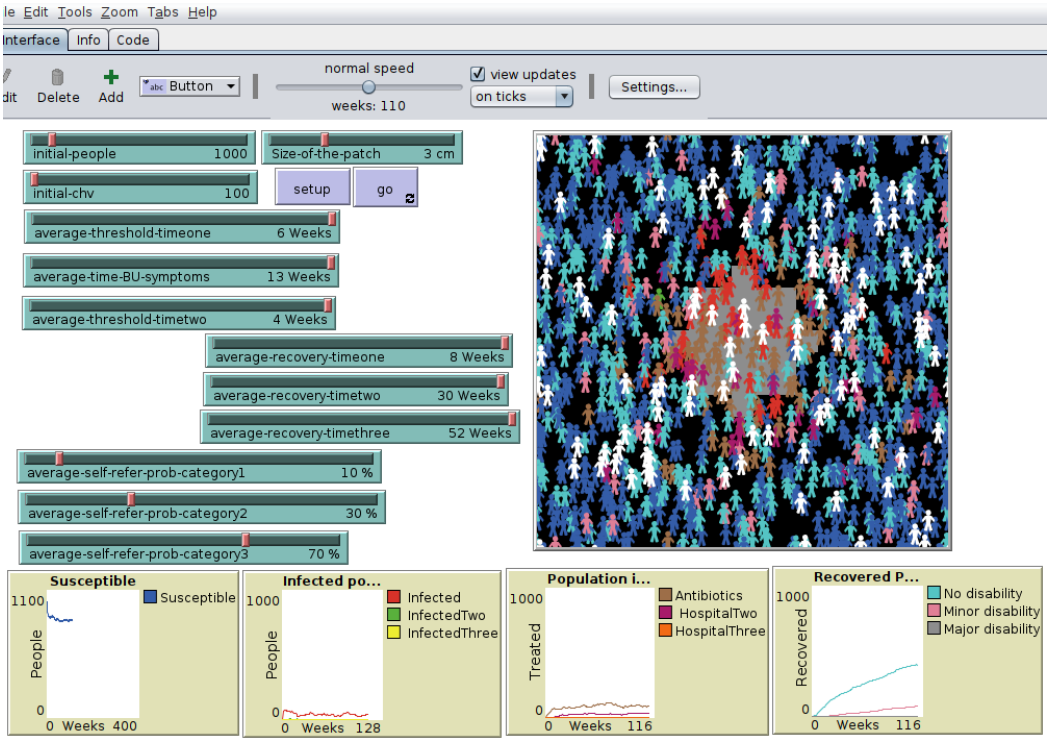

FIGURE 6.2: A screen-shot showing the interface of the ABM using NetLogo. The interface includes sliders where global variables are varied, the set-up and go buttons which start and execute the instructions from the user. These plots illustrate the data generated by the model.

6.8 Model Experimentation and Results

We test the model with different scenarios and observe how these changes affect or influence the model outputs. We make changes to key parameters and observe the resultant effects on the model. The parameters considered are: the initial population, number of CHV; and the patch size representing the probability of a *M. ulcerans* infection. We compare the output for each of these scenarios with the base case scenario (SR1 and SR1CHV1). In Appendix B, we represent individual plots of the trends for each scenario in subsections 6.8, illustrating the mean, maximum and minimum values of 10 model runs.

Figure 6.4, Figure 6.5 and Figure 6.7, present time series plots showing people who are currently susceptible (a), infected in category one (b), infected in category two (c), and infected in category three (d); on antibiotics (e), receiving minor hospital treatment (f), and major hospital treatment (g); and with no disability (h), minor disability (i) and major disability (j). Note that these categories are not mutually exclusive, since infected people may also be receiving treatment and plots (h) to (j) include people who are currently susceptible, infected and/or undergoing treatment.

In subsections 6.8.1, 6.8.2 and 6.8.3, we make changes on the baseline scenario and observe the effect on the model.

6.8.1 When the rate of infection is increased

In this scenario, we enlarge the initial infection patch, as shown in Figure 6.3, to assess its impact on the model's behaviour and output. This includes testing the model's performance when this parameter is doubled.

The simulation area was set to 17×17, maintaining a CHV population of 100, while the initial infection patch was expanded from a radius of 3 to 6.

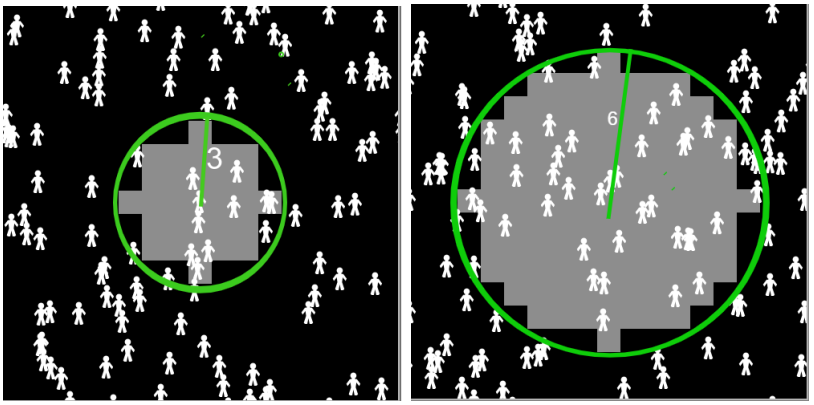

FIGURE 6.3: Size of patch representing initial infection: a green circle centred at the origin with a radius of 3 (left) was increased to 6 (right). The circle is then filled with square grids.

In practice, this model, serving as a proof of concept, does not aim to provide a realistic representation of a geographical area or the dynamics of infection. To illustrate, the patch in the model symbolizes a specific habitat of *M. ulcerans* bacteria, resembling an aquatic environment like a lake. The spatial units of grid squares correspond to the typical size of a lake, delineating an infectious patch.

It is assumed that individuals become infected when interacting with the environment where *M. ulcerans* bacteria reside, such as a lake. Although the exact route of infection from the environment is unknown, for the purpose of this model, it is assumed that any interaction of an individual with the environment leads to infection with a 100% probability.

To give realistic values of the incidence rate β, the size of the infected patch would need to be exceedingly small relative to the grid size. Additionally, achieving a more realistic population distribution across the area would require incorporating spatial movements based on actual data rather than at random.

We represent the case in subsection 6.8.1 as SR2 and SR2CHV2 indicating SR and CHV when the rate of infection is increased respectively. SR2 and SR2CHV2 are compared

with the base case scenario SR1 and SR1CHV1 and the results are illustrated in Figure 6.4.

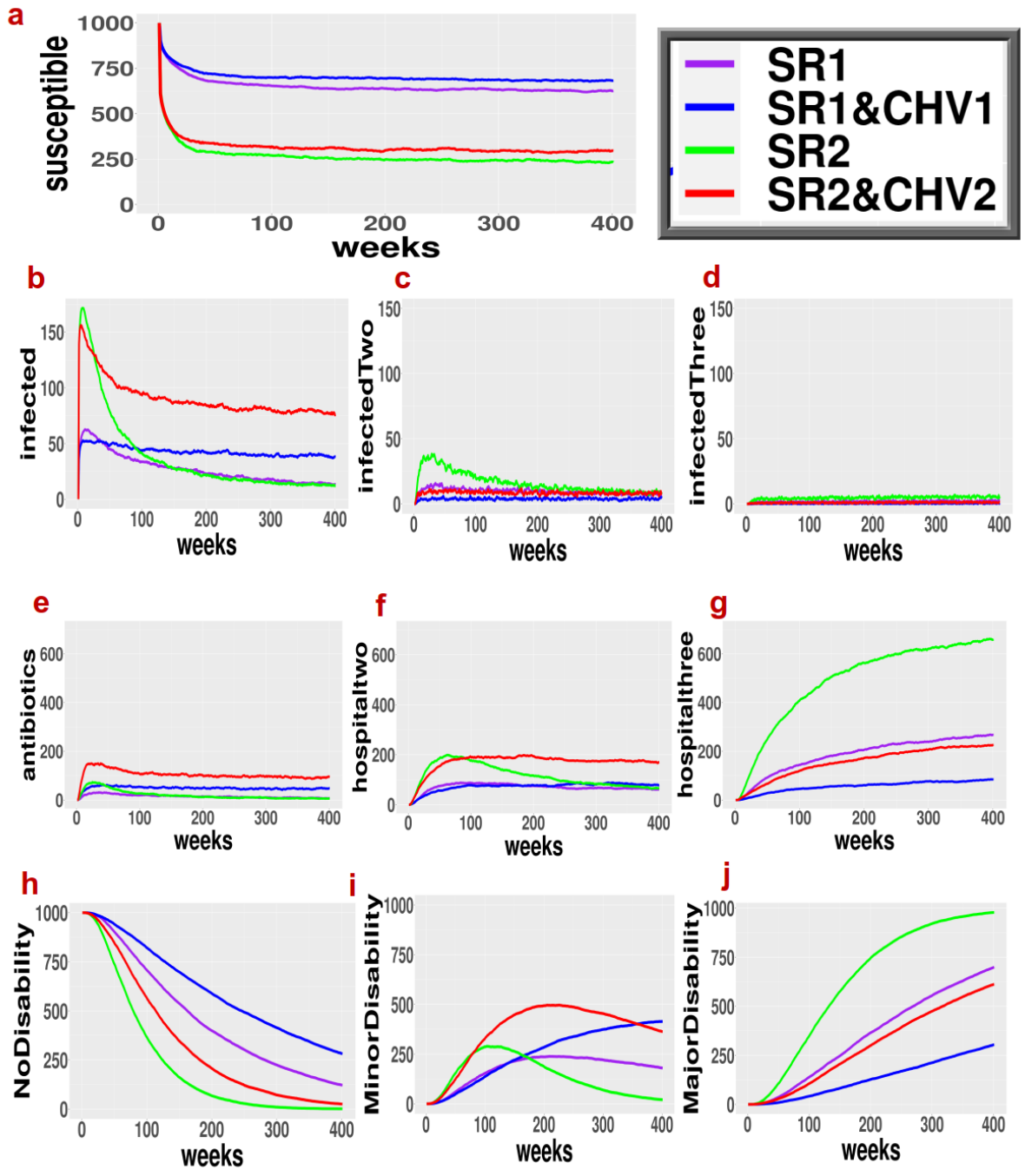

FIGURE 6.4: The size of the patch representing the environment where *M. ulcerans* bacteria resides is enlarged by increasing the radius of the patch from 3 to 6 square grids, symbolizing an increase in the probability of infection. These plots illustrate data as the average of 10 simulations from 10 model runs of the ABM. Individual plots for each run are indicated in Figures B.3 and B.4 in appendix B.

Fewer individuals progress to categories 2 and 3 and do not remain in the infected compartment for an extended period. This transition suggests a rapid transition to different categories. The limited cases in infectedTwo (c) and infectedThree (d) may be attributed to people experiencing symptoms and promptly seeking treatment. In scenarios SR2 and SR2CHV2, the initial surge in the infected population can be attributed to an increase in initial infection patch set at 6.

We observed the highest number of individuals on antibiotics (e) and Hospitaltwo (f) in scenario SR2CHV2. This observation could be due to the proactive identification and referral of cases by CHV. Furthermore, we noted a high number of Hospitalthree (g) patients in scenarios SR2 and SR1, where only self-referral occurs, and treatment initiation is delayed.

The entire population begins in a healthy state with no disabilities, and by the end of the simulation, most individuals have recovered with major disabilities at some point. The introduction of CHV interventions reveals that scenarios SR1CHV1 and SR2CHV2 have the highest numbers of individuals with minor disabilities. In the case of major disabilities, scenarios SR2 and SR1 have the highest numbers, likely due to delayed detection of BU patients, resulting in major disabilities. The presence of CHV interventions leads to a higher number of healthy individuals with no disabilities. The comparison results indicate that the scenario with an initial infection patch size of 6 and only self-referral results in the highest number of Hospitalthree (g) cases and major disabilities (j).

The substantial numbers of individuals recovering without disabilities and with minor disabilities in the SR1CHV1 scenario emphasize the positive impact of CHV referrals, enabling early diagnosis and treatment initiation. The scenario with an initial infection patch size of 3, along with SR and CHV referrals, yields the highest number of individuals recovering without disabilities and the lowest number with major disabilities which aligns with our expectations.

The introduction of CHV interventions, which identify symptomatic individuals early, plays a pivotal role in reducing major disabilities and offers more opportunities to control the disease. We recommend further exploration of the implications of reducing the infection site size and how it could affect the incidence of disabilities.

In real-world applications, expanding the initial infection patch size serves as a means to simulate worst-case scenarios, such as those with a high prevalence of BU cases. The findings presented in the figures are crucial for illuminating potential worst-case scenarios, can be used in understanding disease outbreaks, and gaining insights into widespread BU infections. This information could be invaluable for effective planning and making informed decisions for policy-makers.

6.8.2 Varying the number of CHVs

In this scenario, we investigate the impact of varying the number of CHV on the SITR populations in the simulation. We begin by reducing the number of CHVs from 100 to 80 and observe the resulting patterns. The initial population is set at 1000, the simulation area is 17×17, and the ratio of CHV-to-population is $80 : 1000$, indicating there are 8 CHVs for every 100 people.

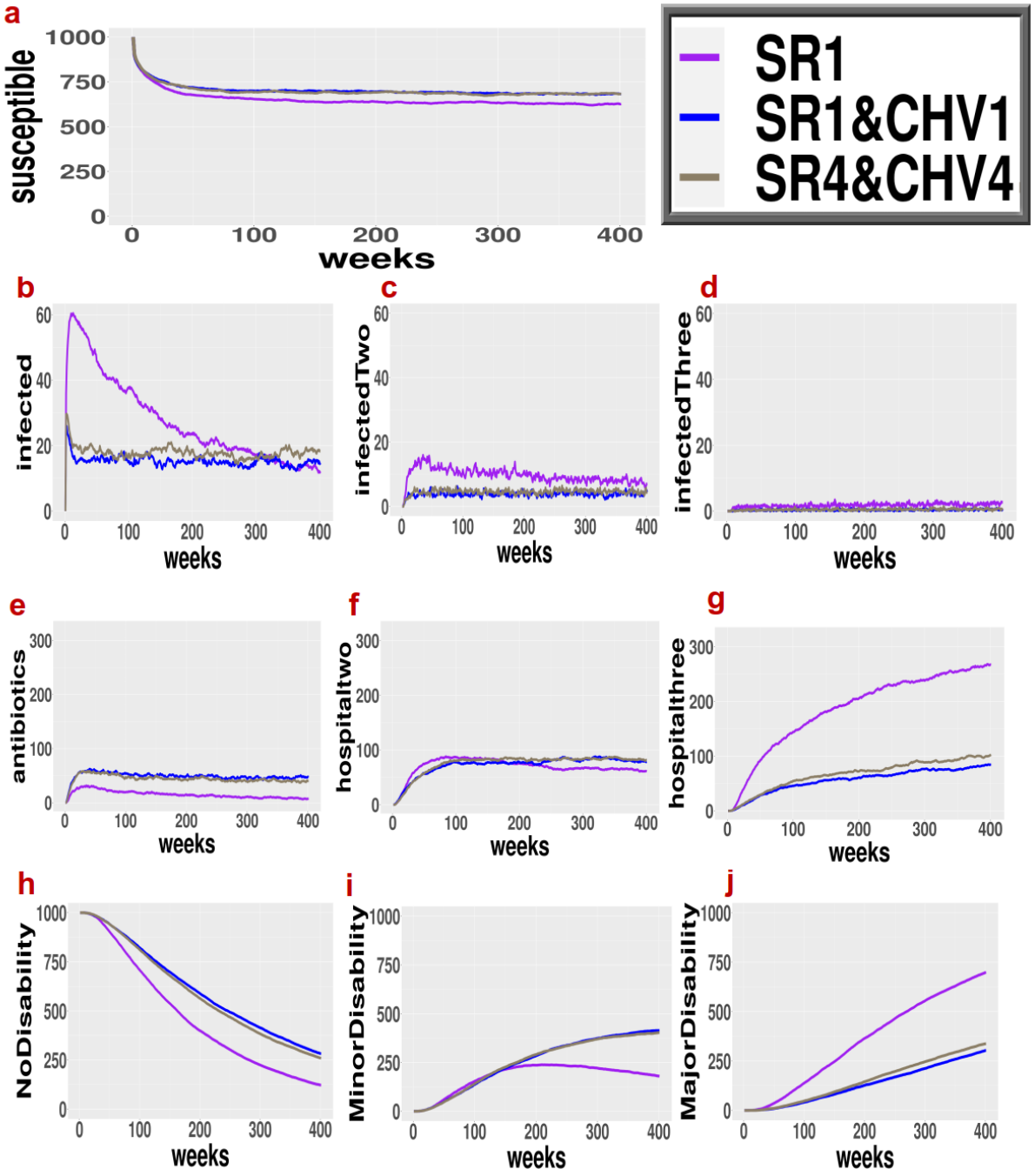

FIGURE 6.5: **When the number of CHV is decreased from** 100 **to** 80**.** (SR4 and SR4CHV4): comparison with the base case scenario (SR1 and SR1CHV1). The data illustrated is the average of 10 simulations from 10 model runs of the ABM. Individual plots for each run are indicated in **??** in appendix B.

In Figure 6.5, we noted that reducing the number of CHVs to 80 did not result in significant differences compared to the scenario with 100 CHVs, with outcomes falling between those observed with 100 CHVs and when only SR was in effect. Furthermore, it became apparent that the presence of a higher number of CHVs was associated with an

increased count of individuals recovering without disability, while concurrently decreasing the populations of patients recovering with minor and major disabilities.

Now, we investigate the impact of changing CHV numbers from 20, 40, 60, 80, to 100 on the mean number of people who recover without disability, with minor disability, and with major disability.

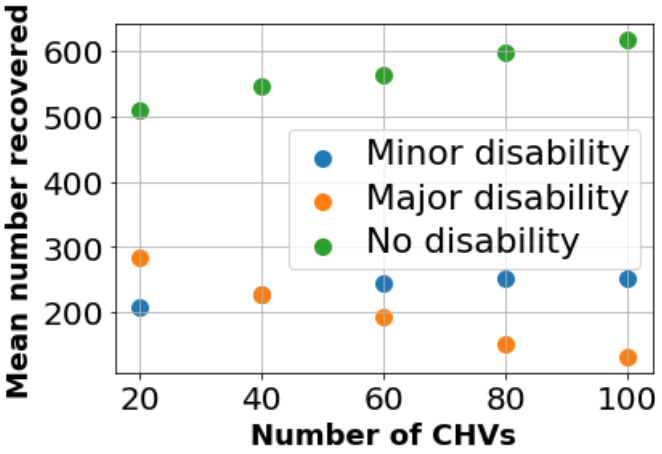

FIGURE 6.6: **Varying the number of CHV:** The mean number of people that recover with a major, minor and no disability between 300 and 400 weeks for different numbers of CHV.

In Figure 6.6, as the number of CHVs increases, we observe a corresponding increase in the number of individuals recovering without disability and a decrease in cases with minor and major disabilities. These findings align with our expectations, highlighting the crucial role of CHVs in reducing late-category cases and disabilities.

A recent study by Alo et al. (2022) emphasized the critical role of training CHVs in the rapid detection of BU cases and their subsequent referral to hospitals. Alo et al. (2022)'s research identified a significant increase in the number of cases detected and referred post-intervention, underscoring the effectiveness of CHVs in this regard. They concluded that integrating CHVs as an intervention, and further scaling up their training, could be pivotal in the rapid detection and referral of BU cases. Policy makers should take note of these findings and consider integrating and expanding the services of trained CHVs to bolster early detection.

6.8.3 When the area of simulation is increased

In this scenario, we increase the domain size (area of simulation) from (17×17) grids to (50×50) grids and keeping the step size the same at 1. We observe and analyse the resultant patterns of the SITR populations in the simulation.

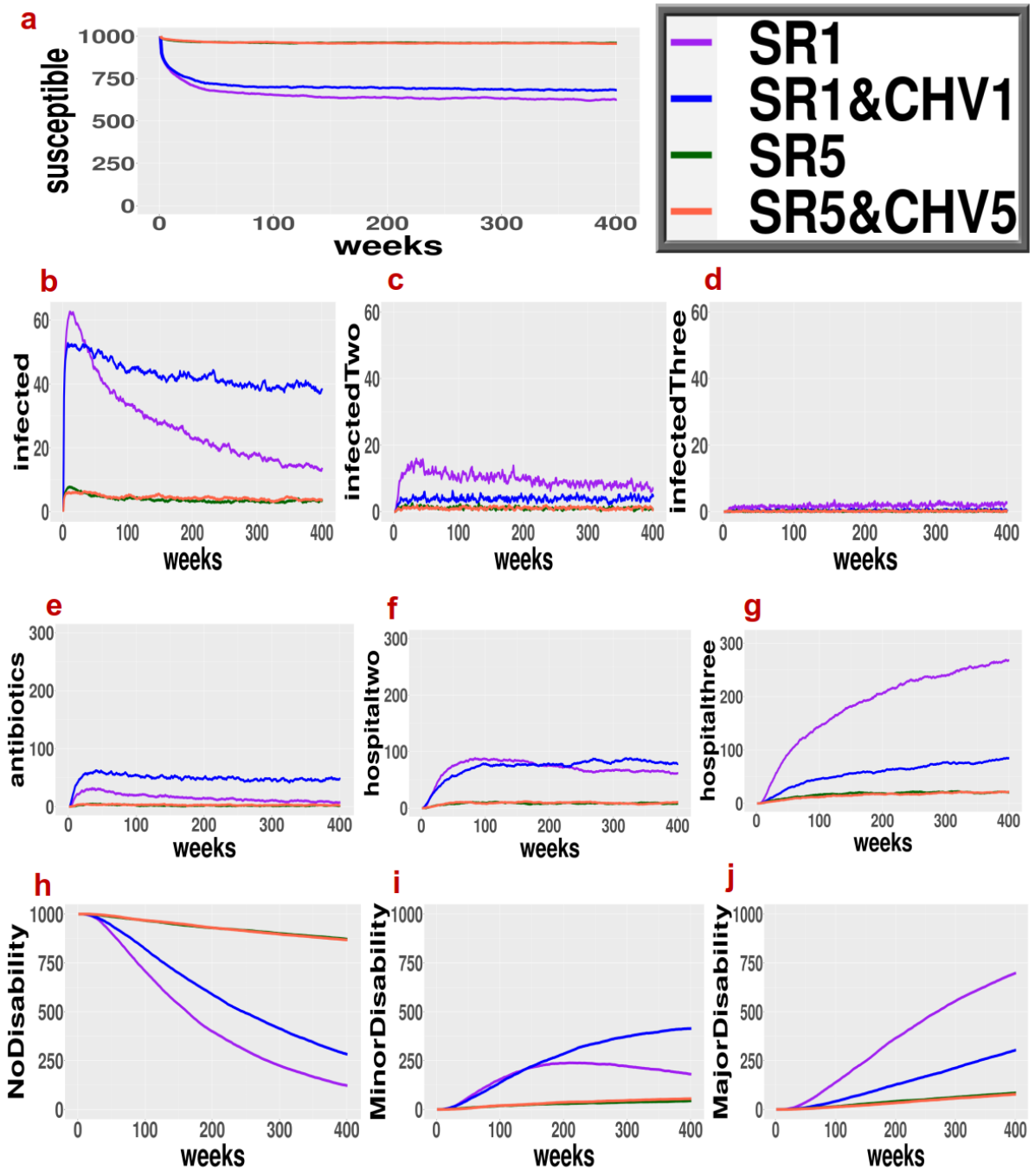

FIGURE 6.7: **When the area of simulation is increased from (17×17) grids to (50×50) grids** (SR5 and SR5CHV5): comparison with the base case scenario (SR1 and SR1CHV1). The data illustrated is the average of 10 simulations from 10 model runs of the ABM. Individual plots for each run are indicated in B.5 and B.6 in appendix B.

In Figure 6.7, when the area of simulation is increased, people are more spread out within it. People are less likely to move into the infectious patch and so less likely to become infected. In other words, a bigger area of simulation implies a lower probability of crossing over the infection region leading to reduced infections.

In contrast, when the step size is reduced from 1 to 0.5, and the domain size remained at a (17×17) grids, we observed agents moving at a slower pace in each time step, covering a smaller distance compared to the original step size of 1. The agents took a longer time to traverse the entire domain and this increased the computation time of the simulation. Reduction in the step distance impacts the spatial dynamics and movement behaviour of agents in the model.

In the future, we recommend exploring different combinations of domain sizes and stepping distances to better understand their interactions and effects on the simulation dynamics. This will address how the reduction in domain size affects the spatial resolution and granularity of the model and how the stepping distance influences the diffusion patterns and movement behaviour of agents.

6.9 Conclusion

In this chapter, we presented an agent-based model (ABM) that incorporated the interaction of BU patients with community health volunteers (CHV) in improving early diagnosis and treatment of BU. We illustrated the individual interactions of BU patients with CHV, compared and contrasted the effect of either self-referral (SR) independently or both SR and CHV. In addition, we observed BU disease progression within the infected and treated population over a certain period.

We explored possible outcomes when we varied parameters like the rate of infection, the initial population, area of simulation, the number of CHV and observed their effect on BU progression. We compared each of these scenarios with the base case scenario and tracked the patterns of infected and treated populations in a period of 400 weeks.

Our simulation results indicated the ABM with both SR and CHV had the highest number of patients on antibiotics treatment in all scenarios. This led to more people recovering with no disability and few individuals with minor and major disabilities. With only self referral, we observed an increasing number of late category cases leading to starting treatment late and consequently recovering with minor and major disabilities. Our results do not differ from what we expected: that is an introduction of CHV for active case finding of infected BU has a positive correlation with starting treatment early.

Results from our model shed light on the proportion of patients in each stage with or without CHV. This information is important in predicting disease progression when there is insufficient data on BU cases by category. This model allowed the representation of individual movements and interactions of populations over space.

6.9.1 Limitations

Limited information on CHV for BU, for example, the ratio of CHV to the area population was assumed and the absence of experimental data for model validation, posed

challenges. The lack of data on BU cases that self-referred hindered comprehensive model validation. Furthermore, our model's assumption of CHVs being 100% accurate at immediately detecting BU upon encountering an infected patient might not always hold true, especially considering that CHVs are in the process of clinical training and may not be fully trained.

Our CHV model considered three infection categories, wherein we merged the incubation period and category one. For improved model clarity, in the future, it may be beneficial to distinguish the incubation period and category one more explicitly.

We recommend collection of mobility data on movements of agents within a community, as this could enhance our model's ability to track spatial elements. Furthermore, conducting an updated review of the impact of CHV on BU would provide valuable insights for future modelling.

In addition, several design concepts of the ABM, such as emergence, adaptation, sensing, and learning, were not incorporated into our current model. Access to information that influences these elements would contribute to model improvement.

The model can be customised to model introduction of CHV in other neglected tropical diseases. This can be implemented by adjusting features of the infection, treatment and recovery processes of the disease being modelled.

This model serves as a proof of concept and if integrated with clinical and behavioural data, it has the potential to enhance parameter values for improved realism. With the incorporation of clinical and behavioural data, this model could be utilized as a public health tool enabling the analysis of diverse control programs, playing a crucial role in preventing late-stage BU cases.

Chapter 7

Conclusion

The main objective of this work was to develop mathematical models which describe and advise on the dynamics of Buruli ulcer disease. To tackle this, we focused on skin-cell death mechanisms, BU disease progression and treatment pathway, the cost-effectiveness of diagnostic tests and the role of community health volunteers (CHV) in referring BU patients while the disease is still early categories.

7.1 Synthesis

This section presents a succinct overview of each chapter of this thesis.

In the first part of the thesis, specifically in chapter chapter 3, we investigated the contribution of direct cytotoxicity and ischaemia in the skin cell death processes in BU disease. We developed a mathematical model that described the dynamics of ulcer formation, including mycolactone diffusion, *M.ulcerans* growth, decrease in cell densities and increase in fibrin deposition in the skin as time evolves. The novel aspect untangled by our model is the contribution of either ischaemia or direct cytotoxicity pathways in ulcer formation in BU. In addition, we analysed the speed of wound spread observed in BU.

Simulation results indicated that cell death happened earliest for system parameters corresponding to a higher mycolactone equilibrium concentration, and when both direct cytotoxicity and ischaemia operate simultaneously, and the latest with a lower mycolactone equilibrium value and direct cytotoxicity only. When analysed independently, skin cell death through ischaemia was more rapid than direct cytotoxicity. Additionally, we observed rapid wound enlargement when mycolactone diffused faster than *M.ulcerans*. In chapter 4, chapter 5 and chapter 6, we focused on modelling BU disease progression and treatment pathways.

In chapter 4, we developed an epidemiological model for the incidence, progression and treatment of BU. We briefly described the aetiology and epidemiology of BU as a neglected tropical disease and explored possible interventions for reducing the number of

late-category cases. We formulated a susceptible, infected, treated and recovered (SITR) model that mimicked the natural history of BU. Our simulation illustrated the pattern that the population susceptible to BU takes from infection to treatment and recovery. We used our model to predict the prevalence of BU in Ghana, the Democratic Republic of Congo (DRC), Benin and the Ivory Coast. DRC had the lowest prevalence of the order of 10^{-6}, and Ivory Coast had the highest prevalence of the order of 10^{-5}.

Results from the sensitivity analysis indicated that when the transfer rates from one infection category to another category were increased, the proportion of the population infected also increased. In addition, a high rate of starting treatment led to a significant decrease in the number of late-category BU cases. To encourage early diagnosis and treatment, we proposed interventions such as introducing a rapid diagnostic test (RDT) and community health volunteers (CHV). We discussed these interventions in detail in chapter 5 and chapter 6, respectively.

In chapter 5, we evaluated the cost-effectiveness of diagnosing BU with the proposed RDT compared to the standard test using Polymerase chain reaction (PCR) in Ghana. We calculated the extent of disability caused by delayed treatment of BU using disability-adjusted life years (DALY). Using a decision tree analysis model, we established the probabilities, costs and effects of adopting a RDT and a PCR.

The main result of this model was the incremental cost-effectiveness ratio (ICER) of $-\$272.73$ per additional DALY averted from using a RDT compared to a PCR. The probabilistic sensitivity analysis showed that most ICER pairs spread out in the south east quadrant, where the RDT is less costly and yields less DALYs.

In chapter 6, we examined the potential impact of introducing CHV in referring BU patients for diagnosis and treatment in the early categories of the disease. We employed an agent-based model (ABM) to analyse interactions between BU patients and CHV. We compared and contrasted the effect of either self-referral (SR) independently or both SR and CHV.

Simulation results showed that the ABM with both SR and CHV had fewer people that proceeded to late categories of BU and the highest number of patients on antibiotic treatment in all scenarios. This led to more people recovering with no disability and few individuals with minor and major disabilities. In the case of only self-referral, we observed an increasing number of late category cases leading to starting treatment late and consequently recovering with minor and major disabilities. The results in chapter 6 assert what we expected that is an introduction of CHV for active case-finding of infected BU has a positive impact on the early start of treatment.

7.2 Thesis contributions

Mathematical modelling offers an avenue for exploring complex biological systems. In this research, we constructed four novel mathematical models that focused on skin cell death processes in BU, BU progression and treatment pathway, the cost-effectiveness of diagnostic tests and the role of CHV in referring BU patients in early stages, respectively.

The model discussed in chapter 3 gives insights into the processes that lead to wound development as observed in BU. These results could help in the direction and current progress on BU treatment options such as surgery.

Chapter 4 provides a simple model for understanding the transitions of populations from infection to treatment and recovery after contracting BU. To the best of our knowledge, this is the first time that BU has been modelled in this way, where the compartments are divided to mimic the WHO classification of BU disease (WHO et al., 2012).

The modelling work in chapter 4 provides a foundation for building more extensive models for understanding BU disease. provided insight into the dynamics of BU progression and treatment.

The results of the work in chapter 5 and chapter 6 could aid decision-making on resource allocation of health facilities, for example, in terms of implementation of cost-friendly diagnostic tools for BU in Ghana or adopting CHV for BU diagnosis and treatment.

One of the WHO's research priorities towards BU disease control is the development of rapid diagnostic tests. Our work in chapter 5 is the first time, to the best of our knowledge, that the cost-effectiveness analysis of rapid tests for BU has been carried out. It provides crucial information on the affordability of the rapid tests for BU.

In addition, chapter 5 information on costs and effects adds to the bank of literature on cost-effectiveness analysis models, which could be adopted for other neglected diseases in the future.

The work in chapter 5 and chapter 6 could be instrumental in the planning to prevent disability which is a critical feature in recovered BU populations. Our results concur with WHO's recommendation for managing BU, in particular, reaffirming the need to evaluate the effectiveness of the new rapid diagnostic tests and the role of community involvement in the referral of BU-infected populations and BU disease management.

The mathematical frameworks described in this thesis contribute to the bank of knowledge for research on BU. Models on cell death mechanisms, CEA of the RDT for BU, and analysis of the impact of CHV in BU are an addition to knowledge on mathematical modelling for BU.

This work contributes to the literature on neglected tropical diseases and can help stimulate further work on such diseases.

7.3 Limitations

In chapter 3, we faced limitations in parameter estimation due to insufficient data. Some key parameters, such as the production rate of mycolactone (λ_m), the degradation rate of mycolactone (K_m) and the density-dependent bacterial death rate (K_u) were estimated based on assumptions. These assumptions, like the artificial system for bacterial growth, may deviate from real-world scenarios, potentially impacting the accuracy of parameter values.

In chapter 4, under parameter estimation, we made the simplifying assumption of uniform transfer rates from infection to treatment (γ) across all BU categories. This simplification was necessary due to limited data and literature, but in reality, treatment initiation is influenced by various factors like diagnosis, waiting times, healthcare accessibility, and infection severity, making this a limitation.

In chapter 5, we relied on data for 1998 for cost estimation (Amofah et al., 2002), despite the evolution of BU treatment costs and incidence. Limited literature and parameter values forced us to use estimates from other diseases or experimental work, which may not fully represent natural BU infections. Additionally, the data for cost-effectiveness analysis, including cost and disability-adjusted life years, was limited.

In chapter 6, for model simplicity, we combined incubation period and category 1 into a single state resulting into three infection categories. This simplification was a limitation, and future improvements could involve distinguishing the incubation period and category 1 more explicitly for better model clarity.

Furthermore, limited data on CHVs for BU, such as the assumed ratio of CHVs to the area population, posed challenges. The absence of experimental data for model validation and the assumption of CHVs being 100% accurate in detecting BU upon encountering an infected patient also need to be considered carefully, as CHVs are still in the process of clinical training and may not always be fully trained.

7.4 Future work

Future efforts should be directed towards sourcing data for model fitting, for example, a constant update of records on the number of BU patients in each compartment. There is limited data on the infected population from the WHO website. However, we found no comprehensive data on populations undergoing treatment and those who recovered.

There is also a need for updated data on costs for treatment of BU, disability-adjusted life years, records on CHV and the BU patients they have referred. In addition, a comprehensive estimation of unknown parameters for models in each chapter would improve the overall model outcomes. The availability of such data would be valuable in the validation and formulation of the model.

The models themselves could also be developed further to include more realistic detail. For example, we recommend including other types of skin cells in the formulation of the wound model and consideration of a realistic spatial arrangement of cells.

The work presented in these chapters elucidates the benefits of control strategies in minimising late-BU category cases. In the future, we could use mathematical models to experiment with the effect of combined interventions. For example, we could explore the effect of integrating strategies such as mass screening and treatment with mass community education on BU infections.

This research demonstrates the potential role of mathematical modelling in answering pertinent questions regarding Buruli ulcer disease. There is no doubt that mathematical modelling will continue to play a critical role as we adopt an integrated approach to managing neglected tropical skin diseases.

Appendix A

Chapter 5: calculation of costs and effects

A.1 Calculation of costs (c) and effects (e) at each node

$$
\begin{aligned}
e_1 &= p_{15}DALY_{2a} + p_{16}DALY_{2b}, & c_1 &= p_{15}(Cost_1 + Cost_{PCR}) + p_{16}(Cost_1 + Cost_{PCR}),\\
e_2 &= p_{17}DALY_3 + p_{18}DALY_4, & c_2 &= p_{17}(Cost_2 + Cost_{PCR}) + p_{18}(Cost_2 + Cost_{PCR}),\\
e_3 &= p_5DALY_x + p_6e_1 + p_7e_2, & c_3 &= p_5(Cost_x + Cost_{PCR}) + p_6c_1 + p_7c_2,\\
e_4 &= p_9DALY_1, & c_4 &= Cost_{PCR} + p_9Cost_2,\\
e_5 &= p_1e_3 + p_2e_4, & c_5 &= p_1c_3 + p_2c_4,\\
e_6 &= p_{19}DALY_{2a} + p_{20}DALY_{2b}, & c_6 &= (p_{19} + p_{20})(cost_1 + Cost_{RDT}),\\
e_7 &= p_{21}DALY_3 + p_{22}DALY_4, & c_7 &= (p_{21} + p_{22})(cost_2 + Cost_{RDT}),\\
e_8 &= p_{12}(DALY_x) + p_{11}e_7 + p_{10}e_6, & c_8 &= p_{12}(Cost_x + Cost_{RDT}) + p_{11}c_7 + p_{10}c_6,\\
e_9 &= p_{14}DALY_1, & c_9 &= p_{13}(Cost_{RDT}) + p_{14}(Cost_{RDT} + Cost_2),\\
e_{10} &= p_3e_8 + p_4e_9, & c_{10} &= p_3c_8 + p_4c_9.
\end{aligned}
$$

Outcome	**Costs**	**Effects**
Nodes-PCR		
Node 1	\$17.870	1.653
Node 2	\$2669.952	9.688
Node 3	\$2452.568	9.030
Node 4	\$86.043	0.193
Node 5	\$1500.752	5.475
Nodes-RDT		
Node 6	\$5.39	1.653
Node 7	\$2657.472	9.688
Node 8	\$2114.012	8.042
Node 9	\$382.033	1.005
Node 10	\$1311.760	4.782
Incremental cost or effect	−188.992	−0.692
ICER	\$272.734	\$272.734

TABLE A.1: A summary of the expected costs and effects at every node evaluated from the decision tree. We used these values to evaluate the ICER as (Cost of RDT - Cost of PCR)/(Effect of RDT - Effect of PCR).

$$\begin{aligned} \text{ICER} &= \frac{c_{10} - c_5}{e_{10} - e_5}, \\ &= \frac{105.2202 - 1344.422}{1.397417 - 9.768379}, \\ &= \$272.734 \text{ per DALY averted.} \end{aligned}$$

Appendix B

Chapter 6: ABM plots for the SITR

B.1 When the initial infection starts with 3 square grids

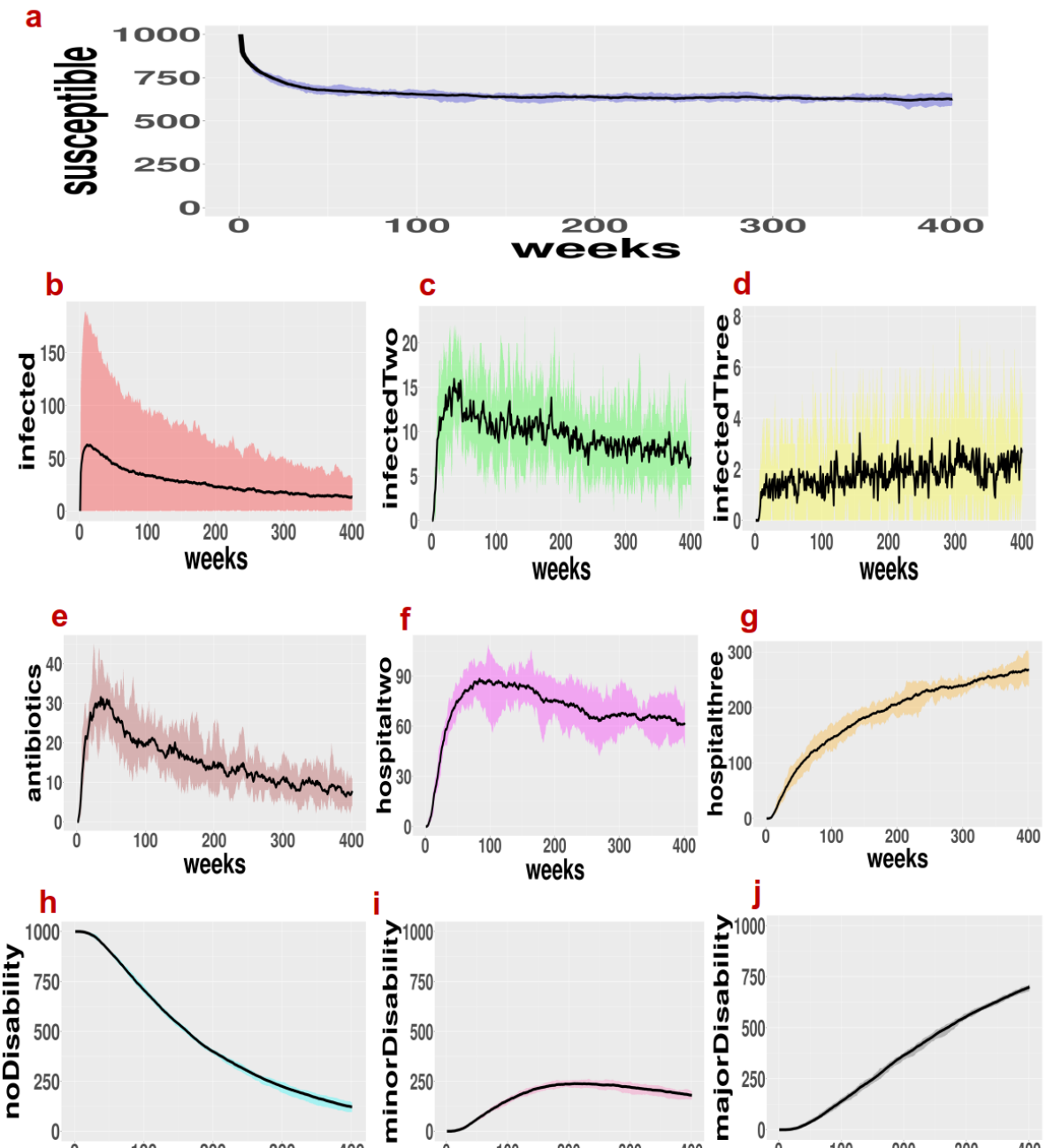

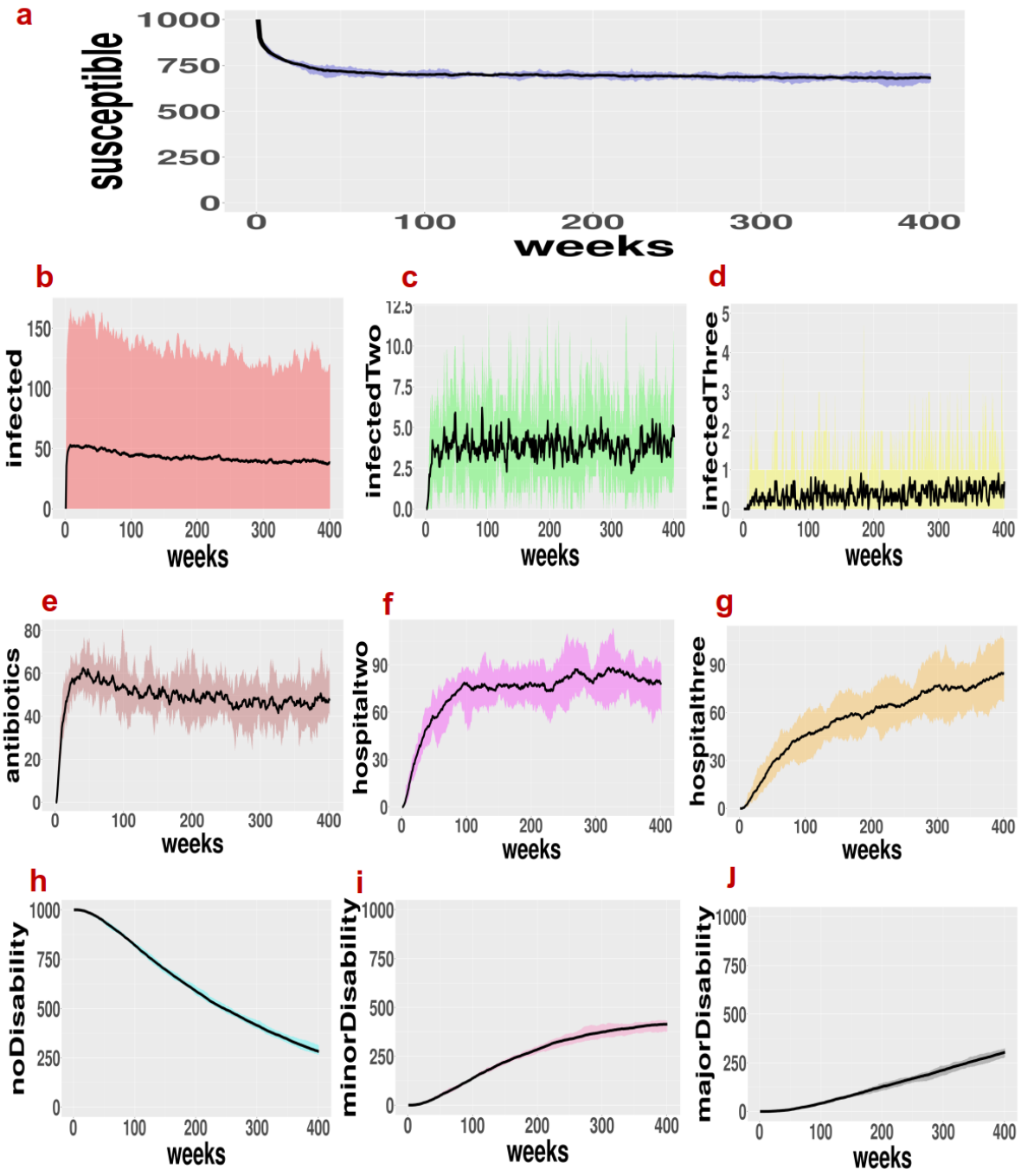

FIGURE B.2: **SR and CHV (SR1CHV1): When the size of the patch representing initial infection is set such that the radius of the circle is 3 square grids**

B.2 When the initial infection starts with 6 square grids

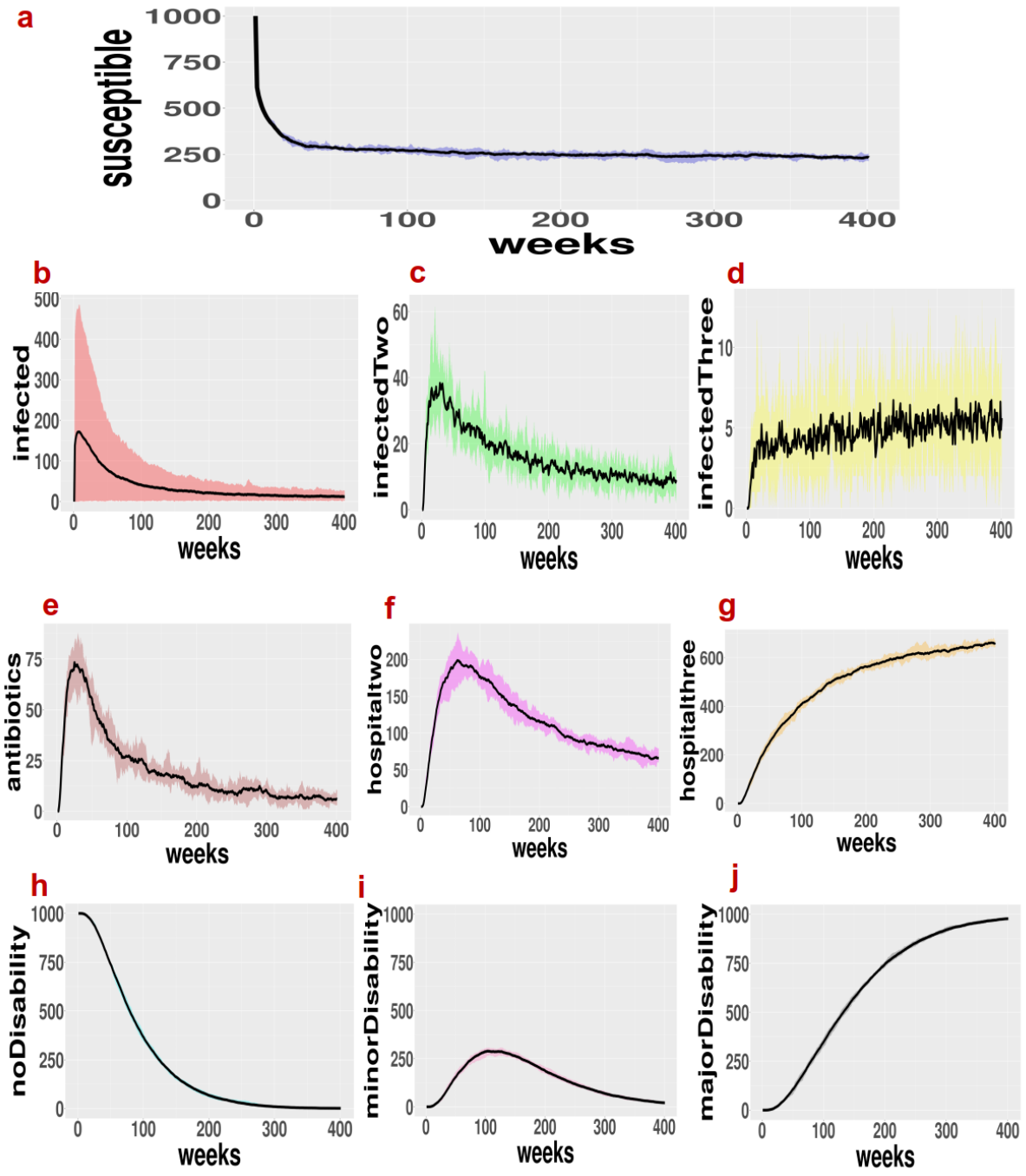

FIGURE B.3: **SR only (SR2): When the size of the patch representing initial infection is increased. The radius of the circle was increased from 3 to 6 square grids**

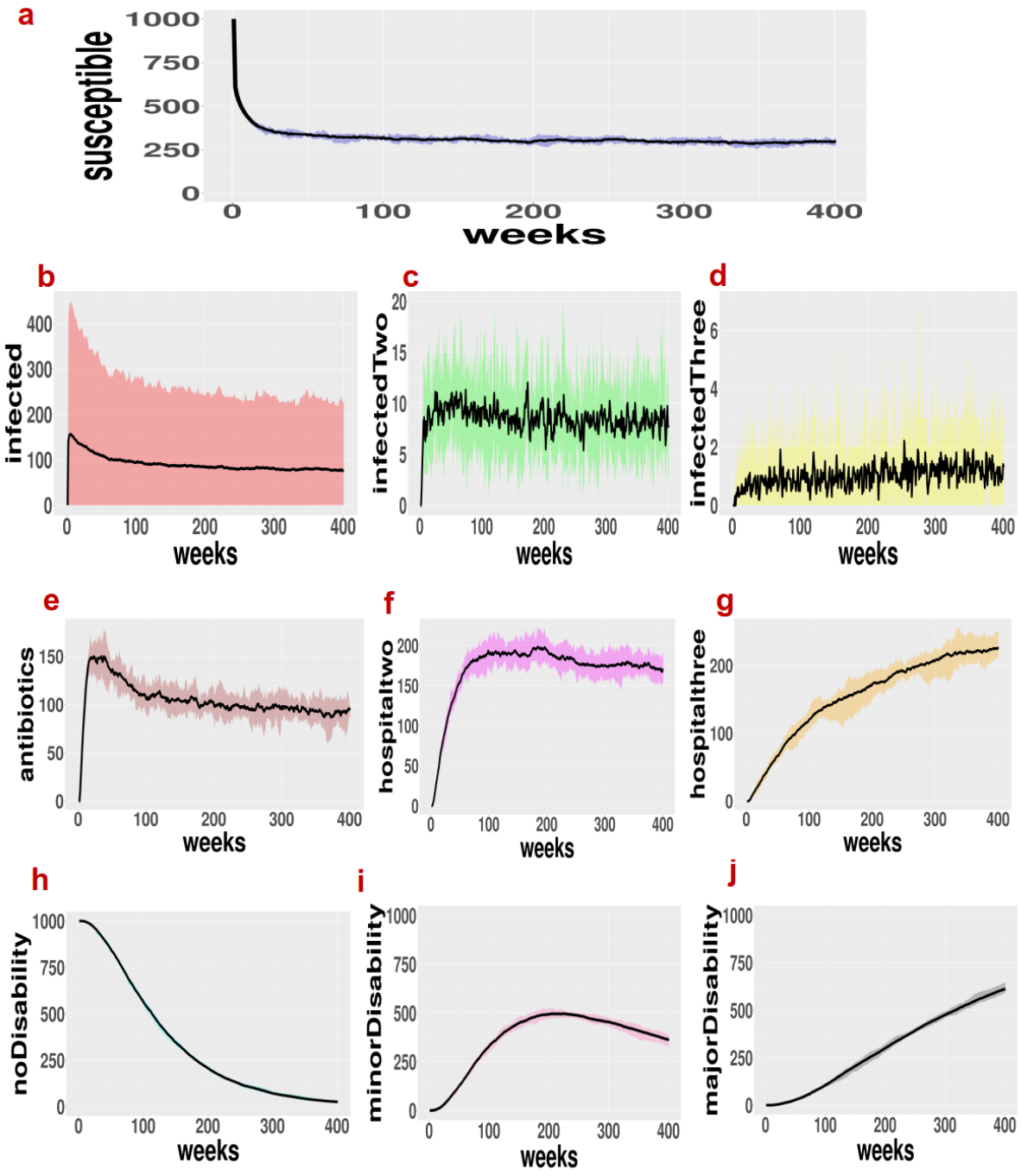

FIGURE B.4: **SR and CHV (SR2CHV2): When the size of the patch representing initial infection is increased. The radius of the circle was increased from 3 to 6 square grids**

B.3 When the area of simulation is increased

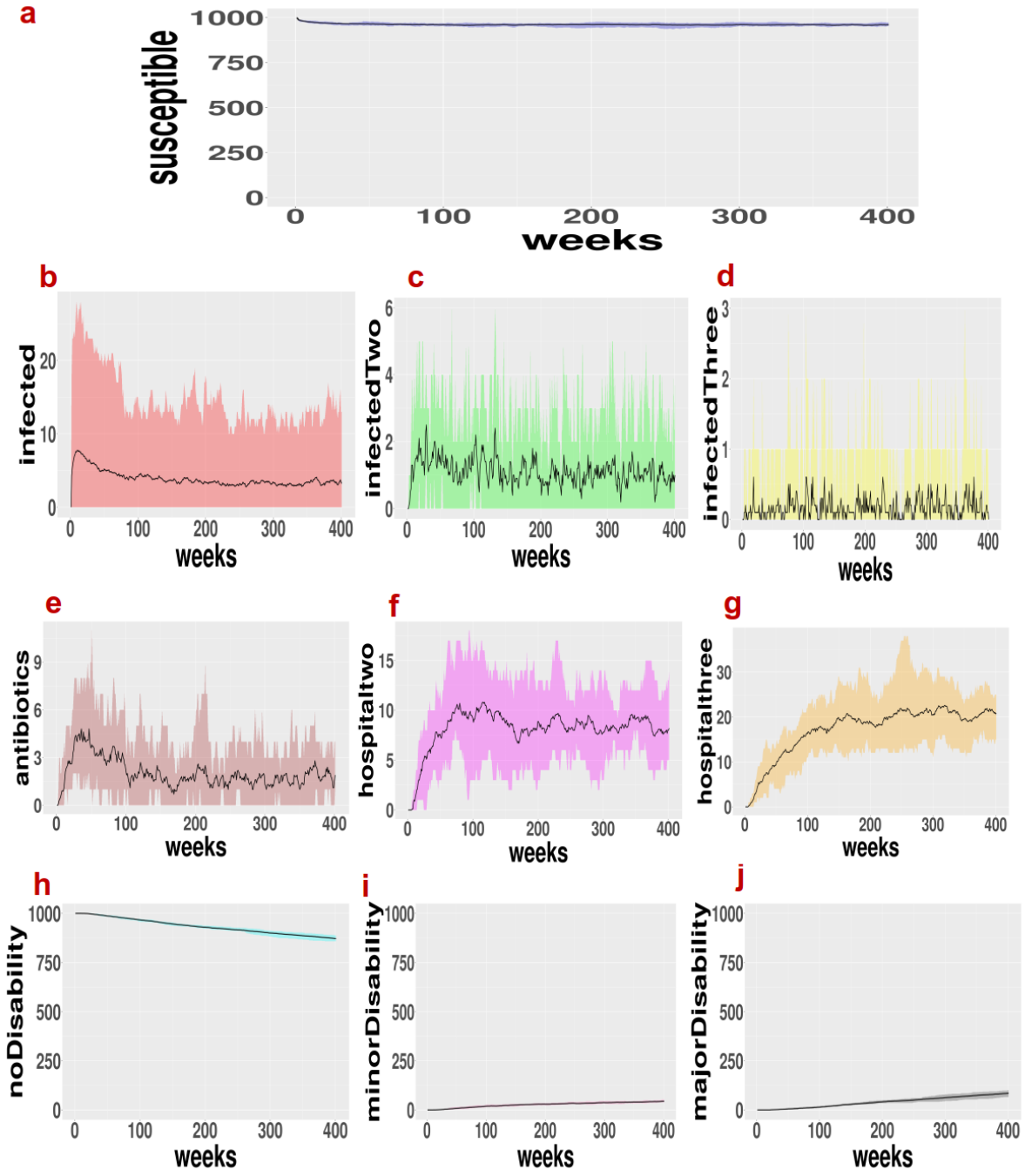

FIGURE B.5: **SR only (SR5): When the area of simulation is increased from 17×17 square grids to 50×50 square grids.**

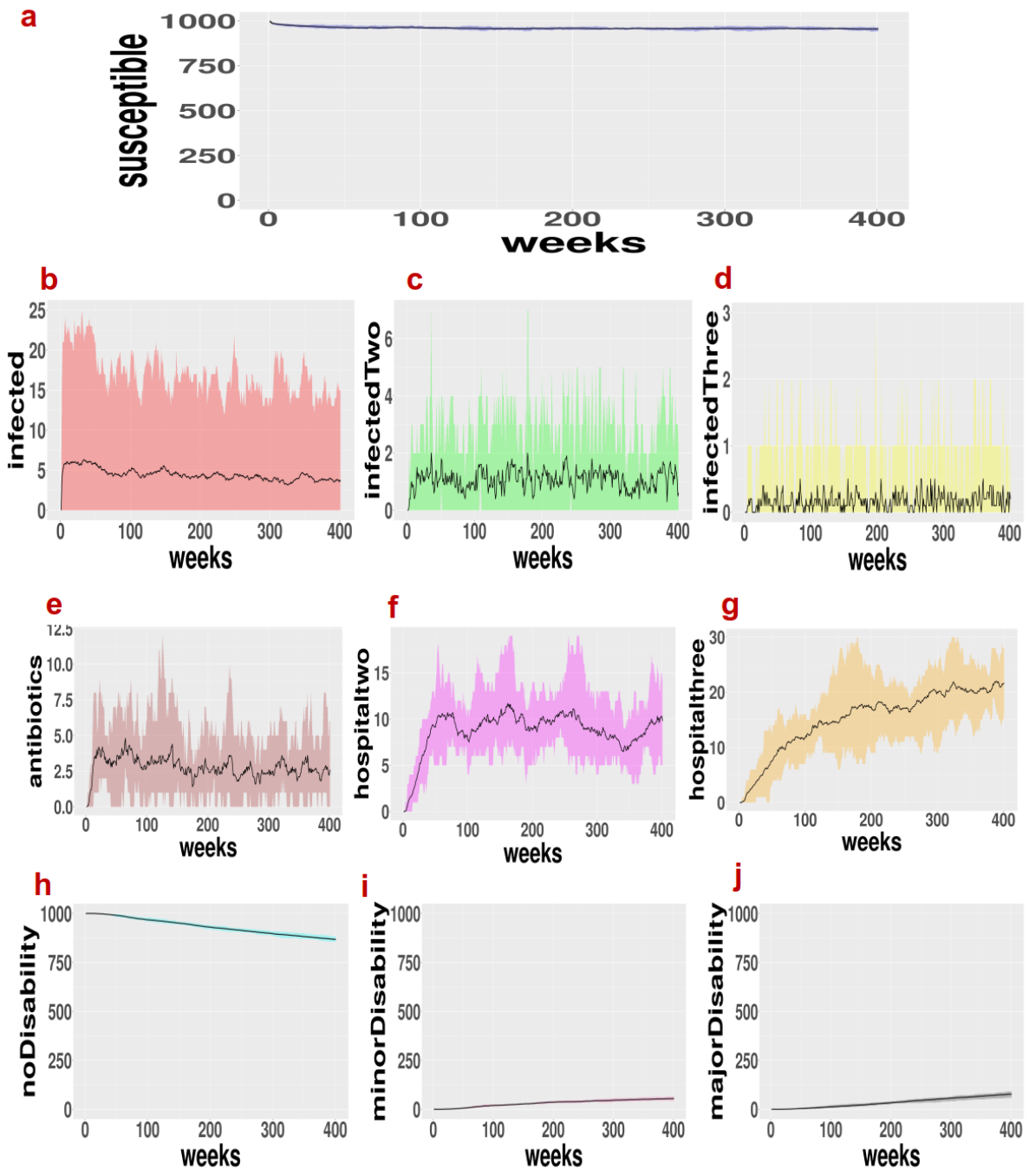

FIGURE B.6: **SR and CHV (SR5CHV5): When the area of simulation is increased from 17×17 square grids to 50×50 square grids.**

Appendix C

Codes used for the simulations

C.1 Python scripts for analysis for chapter 3

C.1.1 Code for *M.ulcerans* and mycolactone model

```
# Import necessary packages
import numpy as np
from scipy.integrate import odeint
import matplotlib.pyplot as plt
from mpl_toolkits.mplot3d import Axes3D, proj3d
import matplotlib.mlab as mlab
from matplotlib import rcParams

# Update the font size for the plot
rcParams.update({"font.size":15})

# Set the total population size N
N = 500

# Define various parameter values
Dm = 1.0*10**(-9)
Du = 5.0*10**(-8)
Km = 5.0*10**(-5)
lambdau = 4.011*10**(-6)
de = 6.6625*10**(-6)
dk = 2.6625*10**(-5)
ds = 6.6625*10**(-6)

# Parameters for transformations
lambdam = 1.0*10**(-8)

#Two Ku for ce and cs
#Ku = 1.337*10**(-1)# For ce = 4.0*10**(-9)
Ku = 5.348*10**(-3) # For cs = 1.25*10**(-7)
```

```
ce = 4.0*10**(-9)
cs = 1.25*10**(-7)
u1 = 1.0*10**(-6)

#Nondimensional transformations
To = (1/lambdau)
Xo = np.math.sqrt((Du/lambdau))
Uo = (lambdau/Ku)
Mo = (lambdam/Ku)
A = 0.01
B = 0.01
C1 = ce/Mo
C2 = cs/Mo
L = 30/Xo
deltae = (de/lambdau)
deltas = (ds/lambdau)
deltak = (dk/lambdau)
alpha  = (Dm/Du)
beta   = (Km/lambdau)
ne = 0.001
ns = 0.009
epsilon = u1/Uo

# Create a spatial grid
X, h = np.linspace(0, L, N, retstep=True)

# Define the model and equations
def model(es,t):
    ba = es[:N]
    My = es[N:2*N]
    ne = es[2*N:3*N]
    ns = es[3*N:]
    dbadt = np.zeros_like(ba)
    dMydt = np.zeros_like(My)
    dnedt = np.zeros_like(ne)
    dnsdt = np.zeros_like(ns)

    # Calculate finite differences
    D2ba = (ba[2:] + ba[:-2] - 2*ba[1:-1]) / h**2
    D2My = (My[2:] + My[:-2] - 2*My[1:-1]) / h**2

    # Define differential equations
    dbadt[1:-1] = ba[1:-1] + D2ba - ba[1:-1]**2
    dMydt[1:-1] = ba[1:-1] + alpha * D2My - beta * My[1:-1]
    A1 = np.heaviside((My-(C1)), 0)
    A2 = np.heaviside((My-(C2)), 0)
    dnedt = (-deltas * ne * A1 ) - (deltak * ne * A1)
    dnsdt = (-deltas * ns * A2 ) - (deltak * ns * A1)
    return np.hstack([dbadt, dMydt, dnedt, dnsdt])
```

```
# Set initial conditions
mu, sig =  L/2, 0.5
u0= epsilon*np.exp(-np.power((X - mu)/sig, 2.)/2)
ba0 = u0 *np.ones_like(X)
My0 = 0.0 *np.ones_like(X)
ne0 = 0.1 *np.ones(N)
ns0 = 0.9 *np.ones(N)
initi = np.hstack([ba0, My0, ne0, ns0])

# Stop the simulation before it reaches the wound edges
Nt = 37

# Define time and space grids
t = np.linspace(0, Nt, N)
x = np.linspace(0, L, N)

# Solve ODE using odeint
sols = odeint(model, initi, t, mxstep = 5000000)
usolution = Uo* (sols[:, :N])
msolution = Mo* (sols[:, N:2*N])
uso =  A* (sols[:, 2*N:3*N])
umso = B* (sols[:, 3*N:4*N])
tdim = (t*To)/(24*60*60)
xdim = (x*Xo)

#Plotting here
#Used to establish the times for the travelling wave legend
fig, ax = plt.subplots()
ax.set_xlabel('Time (Days)', fontsize=19, fontweight='bold')
ax.set_ylabel('Position of wound edge (cm)', fontsize=19, fontweight='
    bold')
fontsize = 14
for tick in ax.xaxis.get_major_ticks():
    tick.label1.set_fontsize(fontsize)
    tick.label1.set_fontweight('bold')
for tick in ax.yaxis.get_major_ticks():
    tick.label1.set_fontsize(fontsize)
    tick.label1.set_fontweight('bold')

for m in range(len(tdim)):
    plt.clf()
    plt.plot(xdim, usolution[m], linewidth=5.0)
    plt.rcParams["axes.labelweight"] = "bold"
    plt.xlabel('Distance(cm)', fontsize=20,  fontweight='bold')
    plt.ylabel('Endothelial Cell density (gcm$^{-3}$)', fontsize=20,
    fontweight='bold')
    plt.title('t = {0}'.format(tdim[m]), fontsize=20,  fontweight='bold')
    plt.savefig('Tw__t{0:03d}.png'.format(m))#Both DT &Isch at M2 10^{-7}
     save the plots

# Plotting travelling wave solution
```

```
# Create a plot to save multiple images
fig, ax = plt.subplots()
plt.plot(xdim, usolution[1], label='$t$ = 0 ', linewidth=4.0)
plt.plot(xdim, usolution[50], label='$t$ = 10.69 ',linewidth=4.0)
plt.plot(xdim, usolution[65], label='$t$ = 13.90 ',linewidth=4.0)
plt.plot(xdim, usolution[100], label='$t$ = 21.39 ', linewidth=3.0)
plt.plot(xdim, usolution[150], label='$t$ = 32.09 ', linewidth=3.0)
plt.plot(xdim, usolution[200], label='$t$ = 42.79 ', linewidth=3.0)
plt.plot(xdim, usolution[250], label='$t$ = 53.49 ',linewidth=3.0)
plt.plot(xdim, usolution[300], label='$t$ = 64.18 ',linewidth=3.0)
plt.plot(xdim, usolution[350], label='$t$ = 74.88 ',linewidth=3.0)
plt.plot(xdim, usolution[400], label='$t$ = 85.58 ',linewidth=3.0)
plt.plot(xdim, usolution[450], label='$t$ = 96.28 ',linewidth=3.0)
plt.plot(xdim, usolution[499], label='$t$ = 106.76 ',linewidth=3.0)
plt.rcParams["font.weight"] = "bold"
plt.rcParams["axes.labelweight"] = "bold"
plt.xlabel('Distance(x) in cm', fontsize=20,  fontweight='bold')
plt.ylabel('Bacteria Cell density \n in (gcm$^{-3}$)', fontsize=20,
    fontweight='bold')
plt.title('Travelling wave solution for \n bacteria at various times',
    rotation=0, fontsize=16,  fontweight='bold')
legend = ax.legend(loc='best', bbox_to_anchor=(1, 1.1), fontsize='smaller
    ', title="Time in days",)
legend.get_frame().set_facecolor('white')

# Plot 3D surface plots
SX, ST = np.meshgrid(xdim , tdim)
fig = plt.figure(figsize=(12, 6))
ax1 = fig.add_subplot(121, projection='3d')
W=ax1.plot_surface(SX, ST, usolution, cmap='jet', label='Model length')
ax1.ticklabel_format(style='sci',scilimits=(0.001,0),axis='z')
ax1.zaxis.major.formatter._useMathText = True
plt.margins(0.0)
plt.setp(ax1.get_xticklabels(), rotation='vertical', fontsize=14,
    fontweight='bold')
plt.setp(ax1.get_yticklabels(), rotation='60', fontsize=14, fontweight='
    bold')
plt.setp(ax1.get_zticklabels(), fontsize=14, fontweight='bold')

# First plot
ax1.tick_params(axis='x', pad=-6)
ax1.tick_params(axis='y', pad=-6)
ax1.xaxis.labelpad = 5
ax1.yaxis.labelpad = 5
ax1.zaxis.labelpad = 8
ax1.set_title('Bacteria cell density', fontsize=22,  fontweight='bold')
ax1.set_xlabel('Distance (cm)', fontsize=18,  fontweight='bold')
ax1.set_ylabel('Time (Days)', fontsize=18,  fontweight='bold')
ax1.set_zlabel('Bacteria (gml$^{-1}$)', fontsize=18,  fontweight='bold')
ax1.view_init(elev=14, azim=-124)
bbar=plt.colorbar(W,format='%.0e',shrink=0.5, pad=0.0001)
```

```
# Second plot
ax2 = fig.add_subplot(122, projection='3d')
Z=ax2.plot_surface(SX, ST, msolution, cmap='jet', label='Model')
ax2.ticklabel_format(style='sci',scilimits=(cs,0),axis='z')
ax2.zaxis.major.formatter._useMathText = True
plt.margins(0.0)
plt.setp(ax2.get_xticklabels(), rotation='vertical', fontsize=14,
    fontweight='bold')
plt.setp(ax2.get_yticklabels(), rotation='60', fontsize=14, fontweight='
    bold')
plt.setp(ax2.get_zticklabels(), fontsize=14, fontweight='bold')
ax2.tick_params(axis='x', pad=-6)
ax2.tick_params(axis='y', pad=-6)
ax2.xaxis.labelpad = 5
ax2.yaxis.labelpad = 5
ax2.zaxis.labelpad = 8
ax2.set_title('Mycolactone concentration', fontsize=22,  fontweight='bold
    ')
ax2.set_xlabel('Distance (cm)', fontsize=18,  fontweight='bold')
ax2.set_ylabel('Time (Days)', fontsize=18,  fontweight='bold')
ax2.set_zlabel('Mycolactone (gml$^{-1}$)', fontsize=15,  fontweight='bold
    ')
ax2.view_init(elev=14, azim=-124)
mbar=plt.colorbar(Z,format='%.0e',shrink=0.5, pad=0.0001)
plt.show()
```

LISTING C.1: Code for *M.ulcerans* and mycolactone model

C.1.2 Code for endothelial and stromal cell density

```
# Import necessary packages
import numpy as np
from scipy.integrate import odeint
import matplotlib.pyplot as plt
from mpl_toolkits.mplot3d import Axes3D, proj3d
import matplotlib.mlab as mlab
from matplotlib import rcParams

# Update the font size for the plot
rcParams.update({"font.size":15})

# Set the total population size N
N = 500

# Define various parameter values
Dm = 1.0*10**(-9)
Du = 5.0*10**(-8)
Km = 5.0*10**(-5)
lambdau = 4.011*10**(-6)
```

```
de = 6.6625*10**(-6)
dk = 2.6625*10**(-5)
ds = 6.6625*10**(-6)

# Parameters for transformations
lambdam = 1.0*10**(-8)
#Ku = 1.337*10**(-1) # For ce = 6.0*10**(-9)
Ku = 5.348*10**(-3)  # For cs = 1.5*10**(-7)
ce = 4.0*10**(-9)
cs = 1.25*10**(-7)
u1 = 1.0*10**(-6)

# Nondimensional transformations
To = (1/lambdau)
Xo = np.math.sqrt((Du/lambdau))
Uo = (lambdau/Ku)
Mo = (lambdam/Ku)
A = 0.01
B = 0.01
C1 = ce/Mo
C2 = cs/Mo
L = 30/Xo
deltae = (de/lambdau)
deltas = (ds/lambdau)
deltak = (dk/lambdau)
alpha = (Dm/Du)
beta = (Km/lambdau)
ne = 0.001 # Endothelial cell density
ns = 0.009 # Stromal cell density
epsilon = u1/Uo

# Create a spatial grid
X, h = np.linspace(0, L, N, retstep=True)

# Define the model and equations
def model(es,t):
    ba = es[:N]
    My = es[N:2*N]
    ne = es[2*N:3*N]
    ns = es[3*N:]
    dbadt = np.zeros_like(ba)
    dMydt = np.zeros_like(My)
    dnedt = np.zeros_like(ne)
    dnsdt = np.zeros_like(ns)

    # Central finite differences
    D2ba = (ba[2:] + ba[:-2] - 2*ba[1:-1]) / h**2
    D2My = (My[2:] + My[:-2] - 2*My[1:-1]) / h**2

    # Define differential equations
    dbadt[1:-1] = ba[1:-1] + D2ba - ba[1:-1]**2
```

```
    dMydt[1:-1] = ba[1:-1] + alpha * D2My - beta * My[1:-1]
    A1 = np.heaviside((My-(C1)), 0)#endothelial
    A2 = np.heaviside((My-(C2)), 0)#stromal
    dnedt = (-deltas * ne * A1 ) - (deltak * ne * A1) #All
    dnsdt = (-deltas * ns * A2 ) - (deltak * ns * A1) #All
    dnedt = (-deltas * ne * A1 ) # DT
    dnsdt = (-deltas * ns * A2 ) # DT
    dnedt = (-deltak * ne * A1 )#Isch only
    dnsdt = (-deltak * ns * A1 )#Isch only
    return np.hstack([dbadt, dMydt, dnedt, dnsdt])

# Set initial conditions
mu, sig =  L/2, 0.5
u0= epsilon*np.exp(-np.power((X - mu)/sig, 2.)/2)
ba0 = u0 *np.ones_like(X)
My0 = 0.0 *np.ones_like(X)
ne0 = 0.1 *np.ones(N)
ns0 = 0.9 *np.ones(N)
initi = np.hstack([ba0, My0, ne0, ns0])

# Stop the simulation before it reaches the wound edges
Nt = 37

# Define time and space grids
t = np.linspace(0, Nt, N) #Dimesionless time
x = np.linspace(0, L, N) #Dimesionless space

# Solve ODE using odeint
sols = odeint(model, initi, t, rtol = 10**(-1), mxstep = 500000)
usolution = Uo*(sols[:, :N])
msolution = Mo*(sols[:, N:2*N])
uso  = A* (sols[:, 2*N:3*N])
umso = B* (sols[:, 3*N:4*N])
tdim = (t*To)/(24*60*60)
xdim = (x*Xo)

# Plot 3D surface plots
SX, ST = np.meshgrid(xdim, tdim)
fig = plt.figure(figsize=(12, 6))

# First plot
ax1 = fig.add_subplot(121, projection='3d')
W1= ax1.plot_surface(SX, ST, uso, cmap='jet')
ax1.ticklabel_format(style='sci',scilimits=(0.001,0),axis='z')
ax1.zaxis.major.formatter._useMathText = True
plt.margins(0.0)
plt.setp(ax1.get_xticklabels(), rotation='vertical', fontsize=14,
    fontweight='bold')
plt.setp(ax1.get_yticklabels(), rotation='60', fontsize=14, fontweight='
    bold')
plt.setp(ax1.get_zticklabels(), fontsize=14, fontweight='bold')
```

```
ax1.tick_params(axis='x', pad=-6)
ax1.tick_params(axis='y', pad=-6)
ax1.xaxis.labelpad = 8
ax1.yaxis.labelpad = 5
ax1.zaxis.labelpad = 8
ax1.set_title('Endothelial cell death', fontsize=22,  fontweight='bold')
ax1.set_xlabel('Distance (cm)', fontsize=18,  fontweight='bold')
ax1.set_ylabel('Time (Days)', fontsize=18,  fontweight='bold')
ax1.set_zlabel('Endothelial density(gcm$^{-3}$)',  fontsize=14,
    fontweight='bold')
ax1.view_init(elev=14, azim=-124)
bbar=plt.colorbar(W1,format='%.0e',shrink=0.5, pad=0.0001)

# Second plot
ax2 = fig.add_subplot(122, projection='3d')
W2=ax2.plot_surface(SX, ST, umso, cmap='jet')
ax2.ticklabel_format(style='sci',scilimits=(0.009,0),axis='z')
ax2.zaxis.major.formatter._useMathText = True
plt.margins(0.0)
plt.setp(ax2.get_xticklabels(), rotation='vertical', fontsize=14,
    fontweight='bold')
plt.setp(ax2.get_yticklabels(), rotation='60', fontsize=14, fontweight='
    bold')
plt.setp(ax2.get_zticklabels(), fontsize=14, fontweight='bold')
ax2.tick_params(axis='x', pad=-6)
ax2.tick_params(axis='y', pad=-6)
ax2.xaxis.labelpad = 9
ax2.yaxis.labelpad = 5
ax2.zaxis.labelpad = 5
ax2.set_title('Stromal cell death', fontsize=22,  fontweight='bold')
ax2.set_xlabel('Distance (cm)', fontsize=18,  fontweight='bold')
ax2.set_ylabel('Time (Days)', fontsize=18,  fontweight='bold')
ax2.set_zlabel('Stromal density (gcm$^{-3}$)', fontsize=14, fontweight='
    bold')
ax2.view_init(elev=14, azim=-124)
bbar=plt.colorbar(W2,format='%.0e',shrink=0.5, pad=0.0001)

plt.tight_layout()

# Create a new figure, set labels for the x and y axes with specified
    font size and weight.
fig, ax = plt.subplots()
ax.set_xlabel('Time (Days)', fontsize=19, fontweight='bold')
ax.set_ylabel('Position of wound edge (cm)', fontsize=19, fontweight='
    bold')
fontsize = 14

# Customize tick labels for x & y axes.
for tick in ax.xaxis.get_major_ticks():
    tick.label1.set_fontsize(fontsize)
    tick.label1.set_fontweight('bold')
```

```
for tick in ax.yaxis.get_major_ticks():
    tick.label1.set_fontsize(fontsize)
    tick.label1.set_fontweight('bold')

# Loop through different time steps for creating and saving plots
for j in range(len(tdim)):
    plt.clf()
    plt.plot(xdim, uso[j], linewidth=5.0)
    plt.ticklabel_format(style='sci',scilimits=(0.001,0),axis='z')
    plt.rcParams["font.weight"] = "bold"
    plt.rcParams["axes.labelweight"] = "bold"
    plt.xlabel('Distance(cm)', fontsize=20,  fontweight='bold')
    plt.ylabel('Endothelial Cell density (gcm$^{-3}$)', fontsize=20,
    fontweight='bold')
    plt.title('t = {0}'.format(tdim[j]), fontsize=20,  fontweight='bold')

    # Save different versions of the same plot with varying file names.
    plt.savefig('QA__t{0:03d}.png'.format(j))#Both DT &Isch at  M1
    10^{-9}
    plt.savefig('QAm__t{0:03d}.png'.format(j))#Both DT &Isch at M2
    10^{-7}
    plt.savefig('QDTM1__t{0:03d}.png'.format(j))#DT M1 10^{-9}
    plt.savefig('QDTM2__t{0:03d}.png'.format(j))#DTM2 10^{-7}
    plt.savefig('QIsM1__t{0:03d}.png'.format(j))#Is m1 10^{-9}
    plt.savefig('QIsM2__t{0:03d}.png'.format(j))#Is m2 10^{-7}

# Create a new figure and axes for plotting the variation in density
fig, ax = plt.subplots()

# Plot the variation in density for M1 = 6*10**(-9)
plt.plot(xdim, uso[0], label='$t$ = 0 ', linewidth=3.0)
plt.plot(xdim, uso[57],label='$t$ = 12.19 ', linewidth=3.0)
plt.plot(xdim, uso[74], label='$t$ = 15.83 ', linewidth=3.0)
plt.plot(xdim, uso[100], label='$t$ = 21.39 ', linewidth=3.0)
plt.plot(xdim, uso[150], label='$t$ = 32.09 ', linewidth=3.0)
plt.plot(xdim, uso[200], label='$t$ = 42.79 ', linewidth=3.0)
plt.plot(xdim, uso[250], label='$t$ = 53.49 ', linewidth=3.0)
plt.plot(xdim, uso[300], label='$t$ = 64.18 ', linewidth=3.0)
plt.plot(xdim, uso[350], label='$t$ = 74.88 ', linewidth=3.0)
plt.plot(xdim, uso[400], label='$t$ = 85.58 ', linewidth=3.0)
plt.plot(xdim, uso[499], label='$t$ = 106.76 ', linewidth=3.0)

# Set labels and formatting for the plot
plt.ticklabel_format(style='sci',scilimits=(0.001,0),axis='z')
plt.rcParams["font.weight"] = "bold"
plt.rcParams["axes.labelweight"] = "bold"
plt.xlabel('Distance(cm)', fontsize=20,  fontweight='bold')
plt.ylabel('Endothelial Cell \n density (gcm$^{-3}$)', fontsize=20,
    fontweight='bold')
```

```
# Create a new figure and axes for plotting the variation in density for
    M2 = 1.5*10**(-7)
fig, ax = plt.subplots()

# Plot the variation in density for M2 = 1.5*10**(-7)
plt.plot(xdim, uso[0], label='$t$ = 0 ',linewidth=3.0)
plt.plot(xdim, uso[57],label='$t$ = 12.19 ', linewidth=3.0)
plt.plot(xdim, uso[74], label='$t$ = 15.83 ', linewidth=3.0)
plt.plot(xdim, uso[100],label='$t$ = 21.39 ', linewidth=3.0)
plt.plot(xdim, uso[150],label='$t$ = 32.09 ', linewidth=3.0)
plt.plot(xdim, uso[200],label='$t$ = 42.79 ', linewidth=3.0)
plt.plot(xdim, uso[250], label='$t$ = 53.49 ',linewidth=3.0)
plt.plot(xdim, uso[300], label='$t$ = 64.18 ',linewidth=3.0)
plt.plot(xdim, uso[350], label='$t$ = 74.88 ',linewidth=3.0)
plt.plot(xdim, uso[400], label='$t$ = 85.58 ',linewidth=3.0)
plt.plot(xdim, uso[499], label='$t$ = 106.76 ',linewidth=3.0)

# Set labels and formatting for the plot
plt.ticklabel_format(style='sci',scilimits=(0.001,0),axis='z')
plt.rcParams["font.weight"] = "bold"
plt.rcParams["axes.labelweight"] = "bold"
plt.xlabel('Distance(cm)', fontsize=20,  fontweight='bold')
plt.ylabel('Endothelial Cell \n density (gcm$^{-3}$)', fontsize=20,
    fontweight='bold')
```

LISTING C.2: Code for endothelial and stromal cell density

C.1.3 Code for the speed of the wound spread

```
# Import necessary packages
import numpy as np
from scipy.integrate import odeint
import matplotlib.pyplot as plt
from mpl_toolkits.mplot3d import Axes3D
import matplotlib.mlab as mlab
from matplotlib import rcParams

# Update the font size for the plot
rcParams.update({"font.size":15})

# Set the total population size N
N = 500

# Define various parameter values
Dm = 1.0*10**(-9)
Du = 5.0*10**(-8)
Km = 5.0*10**(-5)
lambdau = 4.011*10**(-6)
de = 6.6625*10**(-6)
dk = 2.6625*10**(-5)
ds = 6.6625*10**(-6)
```

```
# Parameters for transformations
lambdam = 1.0*10**(-8)
# Ku = 1.337*10**(-1)# For ce = 4.0*10**(-9)
Ku = 5.348*10**(-3) # For cs = 1.5*10**(-7)
ce = 4.0*10**(-9)
cs = 1.25*10**(-7)
u1 = 1.0*10**(-6)

# Nondimensional transformations
To = (1/lambdau)
Xo = np.math.sqrt((Du/lambdau))
Uo = (lambdau/Ku)
Mo = (lambdam/Ku)
A = 0.01
B = 0.01
C1 = ce/Mo
C2 = cs/Mo
L = 30/Xo
deltae = (de/lambdau)
deltas = (ds/lambdau)
deltak = (dk/lambdau)

# Different alpha values
alpha, beta = 0.0002, 12.46
alpha, beta = 0.02, 12.46
alpha, beta = 0.2, 12.46
alpha, beta = 2, 12.46
alpha, beta = 20, 12.46
alpha, beta = 200, 12.46
alpha, beta = 2000, 12.46

# Change beta values
alpha, beta = 0.02, 12.46
alpha, beta = 0.02, 1.246
alpha, beta = 0.02, 0.1246
alpha, beta = 0.02, 0.01246
alpha, beta = 0.02, 0.001246

ne = 0.001 # Endothelial cell density
ns = 0.009 # Stromal cell density
epsilon = u1/Uo

# Create a spatial grid
X, h = np.linspace(0, L, N, retstep=True)

# Define the model and equations
def model(es,t):
    ba = es[:N]
    My = es[N:2*N]
    ne = es[2*N:3*N]
```

```
    ns = es[3*N:]
    dbadt = np.zeros_like(ba)
    dMydt = np.zeros_like(My)
    dnedt = np.zeros_like(ne)
    dnsdt = np.zeros_like(ns)

    # Calculate finite differences
    D2ba = (ba[2:] + ba[:-2] - 2*ba[1:-1]) / h**2
    D2My = (My[2:] + My[:-2] - 2*My[1:-1]) / h**2

    # Define differential equations
    dbadt[1:-1] = ba[1:-1] + D2ba - ba[1:-1]**2
    dMydt[1:-1] = ba[1:-1] + alpha * D2My - beta * My[1:-1]

    A1 = np.heaviside((My-(C1)), 0) # Endothelial
    A2 = np.heaviside((My-(C2)), 0) # Stromal
    dnedt = (-deltas * ne * A1 ) - (deltak * ne * A1)
    dnsdt = (-deltas * ns * A2 ) - (deltak * ns * A1)
    return np.hstack([dbadt, dMydt, dnedt, dnsdt])

# Set initial conditions
mu, sig =  L/2, 0.5
u0= epsilon*np.exp(-np.power((X - mu)/sig, 2.)/2)
#initial conditions here
ba0 = u0 *np.ones_like(X)
My0 = 0.0 *np.ones_like(X)
ne0 = 0.1 *np.ones(N)
ns0 = 0.9 *np.ones(N)
initi = np.hstack([ba0, My0, ne0, ns0])

# Stop the simulation before it reaches the wound edges
Nt = 37

# Dimensionless time and space
t = np.linspace(0, Nt, N)
x = np.linspace(0, L, N)

# Solve ODE using odeint
sols = odeint(model, initi, t, rtol = 10**(-1), mxstep = 500000)#
usolution = Uo*(sols[:, :N])
msolution = Mo*(sols[:, N:2*N])
uso  = A* (sols[:, 2*N:3*N])
umso = B* (sols[:, 3*N:4*N])

# Calculate dimensionless time and space
tdim = (t*To)/(24*60*60)
xdim = (x*Xo)
SX, ST = np.meshgrid(xdim, tdim)

# Define a function to calculate the distance from the wound
def distwound():
```

```
    lst = []
    lst2 = []
    for line in uso:
        for k, elem in enumerate(line):
            if elem!= ne:
                lst.append(xdim[k])
                lst2.append(tdim[k])
                break
    return(lst, lst2)

# Distance and time for different alpha and beta combinations
D1, T1 = distwound()
D2, T2 = distwound()
D3, T3 = distwound()
D4, T4 = distwound()
D5, T5 = distwound()
D6, T6 = distwound()
D7, T7 = distwound()
D8, T8 = distwound()

# Plot distance vs. time for different alpha and beta combinations
plt.plot((tdim[(N-len(D1)):N]), (D1[:len(D1)]), label='$\\alpha$, $\\
    beta$ = 0.02, 12.46 ', linewidth=3.0)
plt.plot((tdim[(N-len(D2)):N]), (D2[:len(D2)]), label='$\\alpha$, $\\
    beta$ = 0.002, 12.46 ', linewidth=3.0)
plt.plot((tdim[(N-len(D3)):N]), (D3[:len(D3)]), label='$\\alpha$, $\\
    beta$ = 0.0002, 12.46 ', linewidth=3.0)
plt.plot((tdim[(N-len(D4)):N]), (D4[:len(D4)]), label='$\\alpha$, $\\
    beta$ = 0.2, 12.46 ', linewidth=3.0)
plt.plot((tdim[(N-len(D5)):N]), (D5[:len(D5)]), label='$\\alpha$, $\\
    beta$ = 2, 12.46 ', linewidth=3.0)
plt.plot((tdim[(N-len(D6)):N]), (D6[:len(D6)]), label='$\\alpha$, $\\
    beta$ = 20, 12.46 ', linewidth=3.0)
plt.plot((tdim[(N-len(D7)):N]), (D7[:len(D7)]), label='$\\alpha$, $\\
    beta$ = 200, 12.46 ', linewidth=3.0)
plt.plot((tdim[(N-len(D8)):N]), (D8[:len(D8)]), label='$\\alpha$, $\\
    beta$ = 2000, 12.46 ', linewidth=3.0)

plt.title('Distance against time when \n $\\alpha$ is varied and $\\beta
    =12.46$', fontsize=18,  fontweight='bold')
plt.ylabel('Distance (x value) \n corresponding to the \n fall of density
     (cm)',
           rotation=90, fontsize=18, fontweight='bold')
plt.xlabel('Time (Days)', fontsize=18, fontweight='bold')
legend = plt.legend(loc='best', bbox_to_anchor=(0.9, -0.2), fontsize='
    medium')
plt.grid()
plt.show()

# Calculate and store the slopes for the distance vs. time plots
slope1, intercept1 = np.polyfit((tdim[N-len(D1):N]),(D1[:len(D1)]),1)
```

```
slope2, intercept2 = np.polyfit((tdim[N-len(D2):N]),(D2[:len(D2)]),1)
slope3, intercept3 = np.polyfit((tdim[N-len(D3):N]),(D3[:len(D3)]),1)
slope4, intercept4 = np.polyfit((tdim[N-len(D4):N]),(D4[:len(D4)]),1)
slope5, intercept5 = np.polyfit((tdim[N-len(D5):N]),(D5[:len(D5)]),1)
slope6, intercept6 = np.polyfit((tdim[N-len(D6):N]),(D6[:len(D6)]),1)
slope7, intercept7 = np.polyfit((tdim[N-len(D7):N]),(D7[:len(D7)]),1)
slope8, intercept8 = np.polyfit((tdim[N-len(D8):N]),(D8[:len(D8)]),1)

AllSlopes = (slope1, slope2, slope3, slope4, slope5, slope6,slope7, slope
    8)
AllSlopes

# A's for the plot of when betas are changed, and alphas kept constant.
A1, T1 = distwound()
A2, T2 = distwound()
A3, T3 = distwound()
A4, T4 = distwound()
A5, T5 = distwound()
A6, T6 = distwound()
A7, T7 = distwound()
A8, T8 = distwound()


# Plot distance vs. time for different alpha values and varied beta
plt.plot((tdim[(N-len(A1)):N]), (A1[:len(A1)]), label='$\\alpha$, $\\
    beta$ = 0.02, 12.46 ', linewidth=3.0)
plt.plot((tdim[(N-len(A2)):N]), (A2[:len(A2)]), label='$\\alpha$, $\\
    beta$ = 0.02, 1.246 ', linewidth=3.0)
plt.plot((tdim[(N-len(A3)):N]), (A3[:len(A3)]), label='$\\alpha$, $\\
    beta$ = 0.02, 0.1246 ', linewidth=3.0)
plt.plot((tdim[(N-len(A4)):N]), (A4[:len(A4)]), label='$\\alpha$, $\\
    beta$ = 0.02, 0.01246 ', linewidth=3.0)
plt.plot((tdim[(N-len(A5)):N]), (A5[:len(A5)]), label='$\\alpha$, $\\
    beta$ = 0.02, 124.6 ', linewidth=3.0)
plt.plot((tdim[(N-len(A6)):N]), (A6[:len(A6)]), label='$\\alpha$, $\\
    beta$ = 0.02, 1246.0  ', linewidth=3.0)
plt.plot((tdim[(N-len(A7)):N]), (A7[:len(A7)]), label='$\\alpha$, $\\
    beta$ = 0.02, 12460 ', linewidth=3.0)
plt.plot((tdim[(N-len(A8)):N]), (A8[:len(A8)]), label='$\\alpha$, $\\
    beta$ = 0.02, 0.001246 ', linewidth=3.0)
#Plot here
plt.title('Distance against time when \n $\\alpha=0.02$ and $\\beta$ is
    varied', fontsize=18,  fontweight='bold')
plt.ylabel('Distance (x value) \n corresponding to the \n fall of density
     (cm)',
           rotation=90, fontsize=18, fontweight='bold')
plt.xlabel('Time (Days)', fontsize=18, fontweight='bold')
legend = plt.legend(loc='best', bbox_to_anchor=(0.9, -0.2), fontsize='
    medium')
plt.grid()
plt.show()
```

```
# Calculate and store the slopes for the distance vs. time plots
slope21, intercept21 = np.polyfit((tdim[N-len(A1):N]),(A1[:len(A1)]),1)
slope22, intercept22 = np.polyfit((tdim[N-len(A2):N]),(A2[:len(A2)]),1)
slope23, intercept23 = np.polyfit((tdim[N-len(A3):N]),(A3[:len(A3)]),1)
slope24, intercept24 = np.polyfit((tdim[N-len(A4):N]),(A4[:len(A4)]),1)
slope25, intercept25 = np.polyfit((tdim[N-len(A5):N]),(A5[:len(A5)]),1)
slope26, intercept26 = np.polyfit((tdim[N-len(A6):N]),(A6[:len(A6)]),1)
slope27, intercept27 = np.polyfit((tdim[N-len(A7):N]),(A7[:len(A7)]),1)
slope28, intercept28 = np.polyfit((tdim[N-len(A8):N]),(A8[:len(A8)]),1)
slopes2 = (slope21, slope22, slope23, slope24, slope25, slope28, slope26,
    slope27)
slopes2
```

Listing C.3: Code for the speed of the wound spread

C.2 Python scripts for analysis in chapter 4

C.2.1 Code for the SITR model

```
#I used small letters for the subscripts for ease of notation. ie for
    deltaa, I used deltaA, Tz for Td.

# Import necessary libraries
import numpy as np
from scipy.integrate import odeint
import matplotlib.pyplot as plt
from matplotlib import rcParams
# Update the font size for the plot
rcParams.update({"font.size":15})

# Set initial parameters and variables
N = 1

# Time points for the simulation
t = np.linspace(0, 400, 80)

# Infection rate
beta = 1.923 * 10**-7

# Transition rates within I
deltaA = 0.0769
deltaB = 0.25
deltaC = 0.166

#Recovery rates from T to S
lambdaB = 0.125
lambdaC = 0.033
lambdaD = 0.0192

#Transition rates (gamma) from I to T
```

```
gammaB = 0.25
gammaC = 0.25
gammaD = 0.25
# For re-runnining when delta = 0.11
# gammaB = gammaC = gammaD = 0.35

# Define the SIR model using differential equations
def sirmodel(E,t):
    S =  E[:N]
    Ia = E[N:2*N]
    Ib = E[2*N:3*N]
    Ic = E[3*N:4*N]
    Iz = E[4*N:5*N]
    Tb = E[5*N:6*N]
    Tc = E[6*N:7*N]
    Tz = E[7*N:8*N]

    # Define differential equations for each compartment
    dSdt = lambdaB * Tb + lambdaC * Tc + lambdaD * Tz - beta*S
    dIadt = beta*S - deltaA * Ia
    dIbdt = deltaA * Ia - Ib *(deltaB + gammaB)
    dIcdt = deltaB * Ib - Ic *(deltaC + gammaC)
    dIzdt = deltaC * Ic - gammaD * Iz
    dTbdt = gammaB * Ib - lambdaB *Tb
    dTcdt = gammaC * Ic - lambdaC *Tc
    dTzdt = gammaD * Iz - lambdaD *Tz
    return np.hstack([dSdt, dIadt, dIbdt, dIcdt, dIzdt, dTbdt, dTcdt,
    dTzdt])

# Set initial conditions
Ia0 = Ib0 = Ic0 = Iz0 = np.zeros(N)
Tb0 = Tc0 = Tz0 = np.zeros(N)
I0 = Ia0 + Ib0 + Ic0 + Iz0
T0 = Tb0 + Tc0 + Tz0
S0 = np.ones(N)
initi = np.hstack([S0, Ia0, Ib0, Ic0, Iz0, Tb0, Tc0, Tz0])

# Extract different compartments from the solutions
sols = odeint(sirmodel,initi,t)
Ssols = sols[:, :N]
Iasols = sols[:, N:2*N]
Ibsols = sols[:, 2*N:3*N]
Icsols = sols[:, 3*N:4*N]
Izsols = sols[:, 4*N:5*N]
Tbsols = sols[:, 5*N:6*N]
Tcsols = sols[:, 6*N:7*N]
Tzsols = sols[:, 7*N:]

# Calculate maximum and minimum values for plotting
Smax = (max(Ssols[:,1]))
Smin = (min(Ssols[:,1]))
```

```
Imax = max(max(Iasols[:,1]), max(Ibsols[:,1]), max(Icsols[:,1]), max(
    Izsols[:,1]))
Imin = min(min(Iasols[:,1]), min(Ibsols[:,1]), min(Icsols[:,1]), min(
    Izsols[:,1]))
Tmax = max(max(Tbsols[:,1]), max(Tcsols[:,1]), max(Tzsols[:,1]))
Tmin = min(min(Tbsols[:,1]), min(Tcsols[:,1]), min(Tzsols[:,1]))

# Create a plot
fig = plt.figure()
ax = fig.add_subplot(111, axisbelow=True)
ax.ticklabel_format(useOffset=False)

# Plot different compartments with labels
ax.plot(t, (Ssols[:,1]), 'black', lw=2.5, label='S')
ax.ticklabel_format(style='sci',scilimits=(Smax,Smin),axis='y')
#Infected
ax.ticklabel_format(style='sci',scilimits=(Imax,Imin),axis='y')
ax.plot(t, (Iasols[:,1])/1,'orange', lw=2.5, label='$I_{a}$')
ax.plot(t, (Ibsols[:,1])/1, 'blue', lw=2.5, label='$I_{b}$')
ax.plot(t, (Icsols[:,1])/1, 'red', lw=2.5, label='$I_{c}$')
ax.plot(t, (Izsols[:,1])/1, 'green', lw=2.5, label='$I_{d}$')
#Treated
ax.ticklabel_format(style='sci',scilimits=(Tmin,Tmax),axis='y')
ax.plot(t, (Tbsols[:,1])/1, 'yellow', lw=2.5, label='$T_{b}$')
ax.plot(t, (Tcsols[:,1])/1, 'greenyellow', lw=2.5, label='$T_{c}$')
ax.plot(t, (Tzsols[:,1])/1, 'purple', lw=2.5, label='$T_{d}$')


# Customize the plot with titles, labels, and legend
ax.set_title('Susceptible population', fontsize=22)
ax.set_title('Infected population', fontsize=22)
ax.set_title('Treated population', fontsize=22)
ax.set_xlabel('Time (Weeks)',  fontweight='bold')
ax.set_ylabel('Susceptible population (S)',fontweight='bold')
ax.set_ylabel('Infected proportion of \n  the total population',
    fontweight='bold')
ax.set_ylabel('Treated proportion of  \n the total population',
    fontweight='bold')
ax.grid(b=True, which='major', c='#bbbbbb', lw=1, ls='-')
legend = ax.legend()
legend = ax.legend(loc='lower right', bbox_to_anchor=(1.0, 0.8),shadow=
    True,
                   fontsize='large',fontweight='bold')
legend = ax.legend(loc='upper right', bbox_to_anchor=(1.35, 1.0),
                   shadow=True, fontsize='x-large')

# Show the plot
plt.show()
```

Listing C.4: Code for the SITR model

C.2.2 Code for the betas

```
# Import necessary packages
import numpy as np
from scipy.integrate import odeint
import matplotlib.pyplot as plt
from matplotlib import collections as matcoll
from matplotlib import rcParams
rcParams.update({"font.size": 15})

N = 1
t = np.linspace(0, 400, 80)

def sirmodel(E, t, beta, deltaA, deltaB, deltaC, lambdaB, lambdaC,
    lambdaD, gammaB, gammaC, gammaD):
    S = E[:N]
    Ia = E[N:2*N]
    Ib = E[2*N:3*N]
    Ic = E[3*N:4*N]
    Iz = E[4*N:5*N]
    Tb = E[5*N:6*N]
    Tc = E[6*N:7*N]
    Tz = E[7*N:8*N]

    dSdt = lambdaB * Tb + lambdaC * Tc + lambdaD * Tz - beta * S
    dIadt = beta * S - deltaA * Ia
    dIbdt = deltaA * Ia - Ib * (deltaB + gammaB)
    dIcdt = deltaB * Ib - Ic * (deltaC + gammaC)
    dIzdt = deltaC * Ic - gammaD * Iz
    dTbdt = gammaB * Ib - lambdaB * Tb
    dTcdt = gammaC * Ic - lambdaC * Tc
    dTzdt = gammaD * Iz - lambdaD * Tz

    return np.hstack([dSdt, dIadt, dIbdt, dIcdt, dIzdt, dTbdt, dTcdt,
    dTzdt])

Ia0 = Ib0 = Ic0 = Iz0 = np.zeros(N)
Tb0 = Tc0 = Tz0 = np.zeros(N)

I0 = Ia0 + Ib0 + Ic0 + Iz0
T0 = Tb0 + Tc0 + Tz0
S0 = np.ones(N)

initi = np.hstack([S0, Ia0, Ib0, Ic0, Iz0, Tb0, Tc0, Tz0])

beta = (3.0099 * 10**-8, 1.923 * 10**-7, 6.2798 * 10**-7, 8.0410 * 10**-7
    )
deltaA = 0.0769
deltaB = 0.25
deltaC = 0.166
```

```
lambdaB = 0.125
lambdaC = 0.033
lambdaD = 0.0192

gammaB = 0.25
gammaC = 0.25
gammaD = 0.25

TDD_t303 = []

for i in range(len(beta)):
    sols = odeint(sirmodel, initi, t, args=(beta[i], deltaA, deltaB,
    deltaC, lambdaB, lambdaC, lambdaD, gammaB, gammaC, gammaD))
    Ssols = sols[:, :N]
    Iasols = sols[:, N:2*N]
    Ibsols = sols[:, 2*N:3*N]
    Icsols = sols[:, 3*N:4*N]
    Izsols = sols[:, 4*N:5*N]
    Tbsols = sols[:, 5*N:6*N]
    Tcsols = sols[:, 6*N:7*N]
    Tzsols = sols[:, 7*N:]
    D1 = (Ibsols + Icsols + Izsols + Tbsols + Tcsols + Tzsols)
    TDD_t303.append(D1[:, 1][60])

x = beta
y = TDD_t303

lines = []
for i in range(len(x)):
    pair = [(x[i], 0), (x[i], y[i])]
    lines.append(pair)

linecoll = matcoll.LineCollection(lines)
fig = plt.figure()
ax = fig.add_subplot(111, axisbelow=True)
fig, ax = plt.subplots()
ax.add_collection(linecoll)
colours = ['red', 'blue', 'green', 'gold']
plt.scatter(x, y, s=100, c=colours)
xz = ('DRC', 'Ghana', 'Benin', 'Ivory Coast')
plt.xticks(x, xz, rotation=10, fontsize=14, fontweight='bold')
plt.ticklabel_format(axis="y", style="sci", scilimits=(0, 0))
plt.ylabel('Prevalence of BU', fontweight='bold')
plt.xlabel('Countries', fontsize=18, fontweight='bold')
plt.xlim(1e-9, 8.5e-7)
plt.ylim(5e-9, 2.5e-5)
plt.grid()
plt.show()
```

Listing C.5: Code for a range of betas

C.2.3 Code for the deltas

```
# Import necessary packages
import numpy as np
from scipy.integrate import odeint
import matplotlib.pyplot as plt
from matplotlib import rcParams

# Update the font size for the plot
rcParams.update({"font.size": 15})

N = 1
t = np.linspace(0, 400, 80)

def sirmodel(E, t, beta, deltaA, deltaB, deltaC, lambdaB, lambdaC,
    lambdaD, gammaB, gammaC, gammaD):
    S = E[0]
    Ia = E[1]
    Ib = E[2]
    Ic = E[3]
    Iz = E[4]
    Tb = E[5]
    Tc = E[6]
    Tz = E[7]

    dSdt = lambdaB * Tb + lambdaC * Tc + lambdaD * Tz - beta * S
    dIadt = beta * S - deltaA * Ia
    dIbdt = deltaA * Ia - Ib * (deltaB + gammaB)
    dIcdt = deltaB * Ib - Ic * (deltaC + gammaC)
    dIzdt = deltaC * Ic - gammaD * Iz
    dTbdt = gammaB * Ib - lambdaB * Tb
    dTcdt = gammaC * Ic - lambdaC * Tc
    dTzdt = gammaD * Iz - lambdaD * Tz

    return np.hstack([dSdt, dIadt, dIbdt, dIcdt, dIzdt, dTbdt, dTcdt,
    dTzdt])

Ia0 = Ib0 = Ic0 = Iz0 = 0
Tb0 = Tc0 = Tz0 = 0

I0 = Ia0 + Ib0 + Ic0 + Iz0
T0 = Tb0 + Tc0 + Tz0
S0 = 1
initi = np.hstack([S0, Ia0, Ib0, Ic0, Iz0, Tb0, Tc0, Tz0])

beta = 1.0 * 10**-5
deltaA = 0.0769
deltaB = deltaC = (0.05, 0.075, 0.1, 0.125, 0.15, 0.175, 0.2)

lambdaB = 0.125
```

```
lambdaC = 0.033
lambdaD = 0.0192

gammaB = 0.25
gammaC = 0.25
gammaD = 0.25

IRatio = (20.7/100000) * np.ones(len(deltaB))

TDDD_t303 = []

for i in range(len(deltaB)):
    sols = odeint(sirmodel, initi, t, args=(beta, deltaA, deltaB[i],
    deltaC[i], lambdaB, lambdaC, lambdaD, gammaB, gammaC, gammaD))
    Ssols = sols[:, 0]
    Iasols = sols[:, 1]
    Ibsols = sols[:, 2]
    Icsols = sols[:, 3]
    Izsols = sols[:, 4]
    Tbsols = sols[:, 5]
    Tcsols = sols[:, 6]
    Tzsols = sols[:, 7]

    D1 =  (Ibsols + Icsols + Izsols + Tbsols + Tcsols + Tzsols)
    TDDD_t303.append(D1[60])

fig = plt.figure()
ax = fig.add_subplot(111, axisbelow=True)

deltaB_values = ('0.05', '0.075', '0.1', '0.125', '0.15', '0.175', '0.2')
plt.plot(deltaB, TDDD_t303, marker="o", linewidth=3.0, linestyle="-",
    markersize=12, label=r'$\delta$', color='green')
plt.plot(deltaB, IRatio, linewidth=3.0, linestyle='dashed', label= r'$Z_\
    delta$', color='red')
plt.xticks(deltaB, deltaB_values)
plt.xticks(rotation=45)
plt.ticklabel_format(axis="y", style="sci", scilimits=(0, 0))
plt.ylabel('Proportion of the infected \n and treated population',
    fontweight='bold')
plt.xlabel(r'$\delta_b, \delta_c$ values', fontsize=18, fontweight='bold'
    )
legend = ax.legend()
legend = ax.legend(loc='upper left', bbox_to_anchor=(0, 1), shadow=True,
    fontsize='smaller')
plt.grid()
plt.show()
```

LISTING C.6: Code for the Deltas

C.2.4 Code for the gammas

```
# Import necessary packages
import numpy as np
from scipy.integrate import odeint
import matplotlib.pyplot as plt
from matplotlib import rcParams

# Update the font size for the plot
rcParams.update({"font.size": 15})

# Set the total population size N
N = 1
t = np.linspace(0, 400, 80)

# Define the SIR model equations
def sirmodel(E, t, beta, deltaA, deltaB, deltaC, lambdaB, lambdaC,
    lambdaD, gammaB, gammaC, gammaD):
    S = E[:N]
    Ia = E[N:2*N]
    Ib = E[2*N:3*N]
    Ic = E[3*N:4*N]
    Iz = E[4*N:5*N]
    Tb = E[5*N:6*N]
    Tc = E[6*N:7*N]
    Tz = E[7*N:8*N]

    dSdt = lambdaB * Tb + lambdaC * Tc + lambdaD * Tz - beta * S
    dIadt = beta * S - deltaA * Ia
    dIbdt = deltaA * Ia - Ib * (deltaB + gammaB)
    dIcdt = deltaB * Ib - Ic * (deltaC + gammaC)
    dIzdt = deltaC * Ic - gammaD * Iz
    dTbdt = gammaB * Ib - lambdaB * Tb
    dTcdt = gammaC * Ic - lambdaC * Tc
    dTzdt = gammaD * Iz - lambdaD * Tz

    return np.hstack([dSdt, dIadt, dIbdt, dIcdt, dIzdt, dTbdt, dTcdt,
    dTzdt])

# Initial conditions for compartments
Ia0 = Ib0 = Ic0 = Iz0 = np.zeros(N)
Tb0 = Tc0 = Tz0 = np.zeros(N)
I0 = Ia0 + Ib0 + Ic0 + Iz0
T0 = Tb0 + Tc0 + Tz0
S0 = np.ones(N)
initi = np.hstack([S0, Ia0, Ib0, Ic0, Iz0, Tb0, Tc0, Tz0])

# Define parameter values
beta = 1.923 * 10**-7
deltaA = 0.0769
deltaB = 0.25
```

```
deltaC = 0.166
lambdaB = 0.125
lambdaC = 0.033
lambdaD = 0.0192

gammaB = gammaC = gammaD = (0.20, 0.25, 0.30, 0.35, 0.40, 0.45, 0.5)
Ratio = (7/10) * np.ones(len(gammaD))

# Initialize a list to store results
TgAll_t303 = []

# Solve the SIR model for different gamma values
for i in range(len(gammaD)):
    sols = odeint(sirmodel, initi, t, args=(beta, deltaA, deltaB, deltaC,
     lambdaB, lambdaC, lambdaD, gammaB[i], gammaC[i], gammaD[i]))
    Ssols = sols[:, :N]
    Iasols = sols[:, N:2*N]
    Ibsols = sols[:, 2*N:3*N]
    Icsols = sols[:, 3*N:4*N]
    Izsols = sols[:, 4*N:5*N]
    Tbsols = sols[:, 5*N:6*N]
    Tcsols = sols[:, 6*N:7*N]
    Tzsols = sols[:, 7*N:]
    TD = (Icsols +Izsols)/Ibsols
    TgAll_t303.append(TD[60])

# Create the plot
fig = plt.figure()
ax = fig.add_subplot(111, axisbelow=True)
tggD = ('0.20', '0.25', '0.30', '0.35', '0.40', '0.45', '0.5')

plt.plot(gammaD, TgAll_t303, marker="o", linestyle='-', linewidth=3.0,
    markersize=12, label= r'$\gamma$')
plt.plot(gammaD, Ratio, linewidth=3.0, linestyle='dashed', label= r'$Z_\
    gamma$')
plt.xticks(gammaD, tggD)
plt.xticks(rotation=45)
plt.ticklabel_format(axis="y", style="sci", scilimits=(0, 0))
plt.ylabel('Ratio of the ulcerative to \n total BU lesion cases',
    fontweight='bold')
plt.xlabel(r'$\gamma$ values', fontsize=18, fontweight='bold')
legend = ax.legend()
legend = ax.legend(loc='upper right', bbox_to_anchor=(1.0, 1.0), shadow=
    True, fontsize='smaller')
plt.grid()
plt.show()
```

LISTING C.7: Code for the gammas

C.2.5 Code for γ_b

```
# Import necessary packages
import numpy as np
from scipy.integrate import odeint
import matplotlib.pyplot as plt
from matplotlib import rcParams

# Update the font size for the plot
rcParams.update({"font.size": 15})

# Set the total population size N
N = 1
t = np.linspace(0, 400, 80)

# Define the SIR model equations
def sirmodel(E, t, beta, deltaA, deltaB, deltaC, lambdaB, lambdaC,
    lambdaD, gammaB, gammaC, gammaD):
    # Define compartments
    S = E[0]
    Ia = E[1]
    Ib = E[2]
    Ic = E[3]
    Iz = E[4]
    Tb = E[5]
    Tc = E[6]
    Tz = E[7]

    # Define differential equations for each compartment
    dSdt = lambdaB * Tb + lambdaC * Tc + lambdaD * Tz - beta * S
    dIadt = beta * S - deltaA * Ia
    dIbdt = deltaA * Ia - Ib * (deltaB + gammaB)
    dIcdt = deltaB * Ib - Ic * (deltaC + gammaC)
    dIzdt = deltaC * Ic - gammaD * Iz
    dTbdt = gammaB * Ib - lambdaB * Tb
    dTcdt = gammaC * Ic - lambdaC * Tc
    dTzdt = gammaD * Iz - lambdaD * Tz
    return np.hstack([dSdt, dIadt, dIbdt, dIcdt, dIzdt, dTbdt, dTcdt,
    dTzdt])

# Initial conditions for compartments
Ia0 = Ib0 = Ic0 = Iz0 = 0
Tb0 = Tc0 = Tz0 = 0
I0 = Ia0 + Ib0 + Ic0 + Iz0
T0 = Tb0 + Tc0 + Tz0
S0 = 1
initi = np.hstack([S0, Ia0, Ib0, Ic0, Iz0, Tb0, Tc0, Tz0])

# Define various parameter values
beta = 1.923 * 10**-7
deltaA = 0.0769
```

```
deltaB = 0.25
deltaC = 0.166
lambdaB = 0.125
lambdaC = 0.033
lambdaD = 0.0192
gammaB = (0.05, 0.2, 0.35, 0.5, 0.65, 0.8, 0.95)
gammaC = 0.25
gammaD = 0.25

# Initialize a list to store results
TDDD_t303b = [ ]
TDDD_t303c = [ ]
TDDD_t303z = [ ]

# Solve the SIR model for different gammaB values
for i in range((len(gammaB))):
    sols = odeint(sirmodel, initi, t, args=(beta, deltaA, deltaB, deltaC,
     lambdaB, lambdaC, lambdaD, gammaB[i], gammaC, gammaD))
    Ssols = sols[:, 0]
    Iasols = sols[:, 1]
    Ibsols = sols[:, 2]
    Icsols = sols[:, 3]
    Izsols = sols[:, 4]
    Tbsols = sols[:, 5]
    Tcsols = sols[:, 6]
    Tzsols = sols[:, 7]
    TDDD_t303b.append(Ibsols[78])
    TDDD_t303c.append(Icsols[78])
    TDDD_t303z.append(Izsols[78])

# Create the plot
fig = plt.figure()
ax = fig.add_subplot(111, axisbelow=True)
tgDD = ('0.05', '0.2', '0.35', '0.5', '0.65', '0.8', '0.95')

plt.plot(gammaB, TDDD_t303b, marker="o", linewidth=3.0, linestyle="-",
    markersize=12, label= r'$I_{b}$')
plt.plot(gammaB, TDDD_t303c, marker="o", linewidth=3.0, linestyle="-",
    markersize=12, label= r'$I_{c}$')
plt.plot(gammaB, TDDD_t303z, marker="o", linewidth=3.0, linestyle="-",
    markersize=12, label= r'$I_{d}$')
plt.xticks(gammaB, tgDD)
plt.xticks(rotation=45)
plt.ticklabel_format(axis="y", style="sci", scilimits=(0, 0))
plt.ylabel('Proportion of the \n infected population', fontweight='bold')
plt.xlabel(r'$\gamma_b$ values', fontsize=18, fontweight='bold')
legend = ax.legend()
legend = ax.legend(loc='upper left', bbox_to_anchor=(0.8, 1), shadow=True
    , fontsize='smaller')
plt.grid()
plt.show()
```

LISTING C.8: Code for the γ_b

C.3 R scripts for chapter 5

C.3.1 Code for the probabilistic sensitivity analysis

```
# Set the scientific notation threshold
options(scipen = 999)
# Load required libraries
library(plyr)
library(ggplot2)
library(fitdistrplus)
library(mc2d)
library(scales)

# Set the number of simulations and willingness to pay
Num_Sim = 10000
WTP = 200
# Define a function to calculate probabilities
dTreeProbs <- function(sigma_p, sigma_r, omega_p, omega_r, beta_p, beta_r
    , alpha_1, alpha_2, treatment_completion, minor_disability) {
  p1 <- (omega_p*(alpha_1 + alpha_2)) + ((1 - sigma_p)*(1 - alpha_1 -
    alpha_2))
  p2 <- 1 - p1
  p3 <- (omega_r*(alpha_1 + alpha_2)) + ((1 - sigma_r)*(1 - alpha_1 -
    alpha_2))
  p4 <- 1 - p3
  p5 <- ((1 - sigma_p)*(1 - alpha_1 - alpha_2))/p1
  p6 <- (omega_p * alpha_1 * beta_p)/p1
  p7 <- 1 - p6 - p5
  p8 <- (sigma_p*(1 - alpha_1 - alpha_2))/p2
  p9 <- 1 - p8
  p10 <- omega_r * alpha_1 * beta_r / p3
  p12 <- ((1 - sigma_r)*(1 - alpha_1 - alpha_2))/p3
  p11 <- 1 - p10 - p12
  p13 <- (sigma_r*(1 - alpha_1 - alpha_2))/p4
  p14 <- 1 - p13
  p15 <- treatment_completion
  p16 <- 1 - p15
  p17 <- minor_disability
  p18 <- 1 - p17
  p19 <- treatment_completion
  p20 <- 1 - p19
  p21 <- minor_disability
  p22 <- 1 - p21
  probs <- c(p1, p2, p3, p4, p5, p6, p7, p8, p9, p10, p11, p12, p13, p14,
     p15, p16, p17, p18, p19, p20, p21, p22)
  return(probs)
```

```
}
# Set parameter values
sigma_p <- 1
sigma_r <- 1
omega_p <- 0.98
omega_r <- 0.88
beta_p <- 0.4
beta_r <- 1
alpha_1 <- 0.125
alpha_2 <- 0.485
treatment_completion <- 0.652
minor_disability <- 0.8

# Calculate probabilities
probs <- dTreeProbs(sigma_p, sigma_r, omega_p, omega_r, beta_p, beta_r,
    alpha_1, alpha_2, treatment_completion, minor_disability)

# Define DALY values
D1  = 6.364
D2a = 0
D2b = 4.752
D3  = 6.952
D4  = 20.636
Dx  = 0
dalys <- c(D1, D2a, D2b, D3, D4, Dx)

# Define cost values
Zr = 0.29
Zp = 12.77
Zx = 5.1
Z1 = 5.1
Z2 = 2415.62
Z3 = 3623.43
costs <- c(Zr, Zp, Zx, Z1, Z2, Z3)

# Define a function to calculate expected effects
dTreeEffects <- function(probs, dalys) {
  e1 <- probs[15]*dalys[2] +probs[16]*dalys[3]
  e2 <- probs[17]*dalys[4] + probs[18]*dalys[5]
  e3 <- probs[5]*dalys[6] + probs[6]*e1 + probs[7]*e2
  e4 <- probs[9]*dalys[1]
  e5 <- probs[1]*e3 + probs[2]*e4
  e6 <- probs[19]*dalys[2] + probs[20]*dalys[3]
  e7 <- probs[21]*dalys[4]+ probs[22]*dalys[5]
  e8 <- probs[12]*dalys[6] + probs[11]*e7 + probs[10]*e6
  e9 <- probs[14]*dalys[1]
  e10 <- probs[3]*e8 + probs[4]*e9
  expEffects <- c(e1, e2, e3, e4, e5, e6, e7, e8, e9, e10)
  return(expEffects)
}
```

```
expEffects <- dTreeEffects(probs, dalys)

# Define a function to calculate expected costs
dTreeCosts <- function(probs, costs){
  c1 <- costs[2] + costs[4]
  c2 <- probs[17]*(costs[5]+costs[2]) + probs[18]*(costs[6]+costs[2])
  c3 <- probs[5]*costs[3] + probs[6]*c1 + probs[7]*c2
  c4 <- costs[2] + probs[9]*costs[5]
  c5 <- probs[1]*c3 + probs[2]*c4
  c6 <- costs[1] + costs[4]
  c7 <- probs[21] * (costs[1] + costs[5]) + probs[22] * (costs[1] + costs
    [6])
  c8 <- probs[10] * c6 + probs[11] * c7 + probs[12] * (costs[1] + costs[3
    ])
  c9 <- costs[1] + probs[14] * costs[5]
  c10 <- probs[3] * c8 + probs[4] * c9
  expCosts <- c(c1, c2, c3, c4, c5, c6, c7, c8, c9, c10)
  return(expCosts)
}

expCosts = dTreeCosts(probs, costs)

# Calculate Incremental Cost-Effectiveness Ratio (ICER)
A = expCosts[10] - expCosts[5]
B = expEffects[10] - expEffects[5]
icer = A / B
icer

serial = c(seq(1,Num_Sim))
simdataX = as.data.frame(serial)

# Simulate data for sensitivity analysis
simdataX$sigma_p = runif(Num_Sim, min = 0.69, max = 1)
simdataX$sigma_r = runif(Num_Sim, min = 0.84, max = 1)
simdataX$omega_p = runif(Num_Sim, min = 0.91, max = 1)
simdataX$omega_r = runif(Num_Sim, min = 0.77, max = 0.95)
simdataX$beta_p = runif(Num_Sim, min = 0.3, max = 0.9)
simdataX$beta_r = runif(Num_Sim, min = 0.9, max = 1)
simdataX$alpha_1 = runif(Num_Sim, min = 0.1125, max = 0.1375)
simdataX$alpha_2 = runif(Num_Sim, min = 0.4365, max = 0.5335)
simdataX$treatment_completion = runif(Num_Sim, min = 0.46, max = 0.84)
simdataX$minor_disability = runif(Num_Sim, min = 0.72, max = 0.88)

simdataX$D1  = runif(Num_Sim, min = 6.1776, max = 7.5504)
simdataX$D2a = runif(Num_Sim, min = 0.000, max = 0.50)
simdataX$D2b = runif(Num_Sim, min = 4.2768, max = 5.2272)
simdataX$D3  = runif(Num_Sim, min = 6.2568, max = 7.6472)
simdataX$D4  = runif(Num_Sim, min = 18.5724, max = 22.6996)
simdataX$Dx  = runif(Num_Sim, min = 0, max = 0.5)

simdataX$Zr = runif(Num_Sim, min = 0.16, max = 0.58)
```

```
simdataX$Zp = runif(Num_Sim, min = 11.4929, max = 14.047)
simdataX$Zx = runif(Num_Sim, min = 0.57, max = 5.1)
simdataX$Z1 = runif(Num_Sim, min = 0.57, max = 5.1)
simdataX$Z2 = runif(Num_Sim, min = 2217.22, max = 2614.02)
simdataX$Z3 = runif(Num_Sim, min = 3325.83, max = 3921.03)

simdataX$A = numeric(Num_Sim)
simdataX$B = numeric(Num_Sim)
simdataX$ICER = numeric(Num_Sim)

for (i in 1:Num_Sim) {
  simDALYS <- c(simdataX$D1[i], simdataX$D2a[i], simdataX$D2b[i],
    simdataX$D3[i], simdataX$D4[i], simdataX$Dx[i])
  simCosts <- c(simdataX$Zr[i], simdataX$Zp[i], simdataX$Zx[i], simdataX$
    Z1[i], simdataX$Z2[i], simdataX$Z3[i])
  simProbs <- dTreeProbs(simdataX$sigma_p[i], simdataX$sigma_r[i],
    simdataX$omega_p[i], simdataX$omega_r[i], simdataX$beta_p[i], simdataX
    $beta_r[i], simdataX$alpha_1[i], simdataX$alpha_2[i], simdataX$
    treatment_completion[i], simdataX$minor_disability[i])
  expEffects <- dTreeEffects(simProbs, simDALYS)
  expCosts <- dTreeCosts(simProbs, simCosts)
  simdataX$A[i] <- expCosts[10] - expCosts[5]
  simdataX$B[i] <- expEffects[5] - expEffects[10]
  simdataX$ICER[i] <- simdataX$A[i]/simdataX$B[i]
}

# Write the simulation data to a CSV file
write.csv(simdataX, "simdataX.csv")

# Calculate Cost-Effectiveness (CE) and create a CE column
simdataX$model = WTP * simdataX$B
simdataX$model_true = simdataX$model - simdataX$A
simdataX$CE = ifelse(test = simdataX$model_true > 0, yes = 1, no = 0 )
simdataX$CE_col = ifelse(test = simdataX$CE == 0, yes = 2, no = 3 )
table(simdataX$CE_col )

# Create a scatter plot of Incremental DALY averted vs. Incremental costs
df <- data.frame(simdataX$B, simdataX$A)
h <- 0
v <- 0
plot1 <- ggplot(df, aes(x=simdataX$B, y=simdataX$A)) + geom_point()
Z = coef(lm(simdataX$A ~ simdataX$B))
plot1 + geom_hline(aes(yintercept=h)) + geom_vline(aes(xintercept=v)) +
  labs(x = "Incremental DALY averted", y = "Incremental costs") +
  scale_y_continuous(labels=dollar_format(prefix="$")) +
  geom_point(colour = "blue") + theme(text = element_text(size = 35))
```

LISTING C.9: Code for the probabilistic sensitivity analysis

C.4 NetLogo scripts for chapter 6

C.4.1 Code for SR and CHV

```
globals [
  sink-patches
]

breed [popns popn]
breed [chvs chv]

popns-own [
 ; Individual attributes
  noDisability?
  minorDisability?
  majorDisability?
  infected?
  infectedTwo?
  infectedThree?
  hospitaltwo?
  hospitalthree?
  antibiotics?
  susceptible?
  infection-length
  infection-lengthTwo
  antibiotic-time
  hospital-time-two
  hospital-time-three
  threshold-timeone
  threshold-timeTwo
  recovery-timeone
  recovery-timetwo
  recovery-timethree
  BU-symptoms
  infectiousness
  threshold-time
  self-refer-prob-category1
  self-refer-prob-category2
  self-refer-prob-category3
  nb-susceptible
  nb-infected
  nb-recovered
  nb-infectedTwo
  nb-infectedThree
  nb-antibiotics
  nb-hospitaltwo
  nb-hospitalthree
  nb-noDisability
  nb-minorDisability
  nb-majorDisability
]
```

```
to setup
  clear-all
  setup-patches
  setup-people
  reset-ticks
end

to setup-patches
  clear-all
  let sink-patch-radius Size-of-the-patch
  let sink-centre patch 0 0
  set sink-patches [patches in-radius sink-patch-radius] of sink-centre
  ask sink-patches [ set pcolor gray ]
end

; Set initial attributes for people
to setup-people
  create-popns initial-people
  [
    setxy random-xcor random-ycor
    set noDisability? true
    set minorDisability? false
    set majorDisability? false
    set hospitaltwo? false
    set hospitalthree? false
    set antibiotics? false
    set infected? false
    set infectedTwo? false
    set infectedThree? false
    set susceptible? true
    set shape "person"
    set color blue
    set infection-length 0
    set infection-lengthTwo 0
    set antibiotic-time 0
    set hospital-time-two 0
    set hospital-time-three 0
    set BU-symptoms random-exponential average-time-BU-symptoms
    set threshold-timeone random-exponential average-threshold-timeone
    set threshold-timeTwo random-exponential average-threshold-timetwo
    set recovery-timeone random-exponential average-recovery-timeone
    set recovery-timetwo random-exponential average-recovery-timetwo
    set recovery-timethree random-exponential average-recovery-timethree
    set threshold-time BU-symptoms + threshold-timeone
    set infectiousness average-infectiousness
    set self-refer-prob-category1 average-self-refer-prob-category1
    set self-refer-prob-category2 average-self-refer-prob-category2
    set self-refer-prob-category3 average-self-refer-prob-category3
  ]
```

```
  create-chvs initial-chv
  [
    setxy random-xcor random-ycor
    set shape "person"
    set color white
  ]
end

to assign-color
  if noDisability? [ set color cyan ]
  if minorDisability? [ set color pink ]
  if majorDisability? [ set color gray ]
  if antibiotics? [ set color brown ]
  if hospitaltwo? [ set color magenta ]
  if hospitalthree? [ set color orange ]
  if infected? [ set color red ]
  if infectedTwo? [ set color green ]
  if infectedThree? [ set color yellow ]
end

to go
  ask popns[ assign-color]
  ask popns[ infect_start]
  ask popns with [ infected? ]
    [  infect_two ]
  ask popns with [ infectedTwo? ]
    [  infect_three ]
  ask popns [self-referral]
  ask popns [meet-chvs]
  ask popns [recover]
  ask popns [move-time-on]
  ask turtles [move]
  ask popns [ clear-count ]
  tick
end

to move
  rt random-float 360
  fd 1
end
; Define a function to reset count variables
to clear-count
  set nb-susceptible initial-people
  set nb-infected 0
  set nb-infectedTwo 0
  set nb-infectedThree 0
  set nb-antibiotics 0
  set nb-hospitaltwo 0
  set nb-hospitalthree 0
  set nb-noDisability initial-people
  set nb-minorDisability 0
```

```
  set nb-majorDisability 0
end

; Handle the initial infection
to infect_start
  let healthy (popns-on sink-patches) with [ susceptible? ]
  ask healthy
    [
      set infected? true
      set susceptible? false
      set nb-infected (nb-infected + 1)
      set nb-susceptible (nb-susceptible - 1)
    ]
end

; Handle the first category of infection
to infect_two
  if infection-length > threshold-time
  [
    set infected? false
    set infectedTwo? true
    set nb-infectedTwo (nb-infectedTwo + 1)
    set nb-infected (nb-infected - 1)
  ]
end

; Handle the second category of infection
to infect_three
  if infection-lengthTwo > threshold-timeTwo
  [
    set infectedTwo? false
    set infectedThree? true
    set nb-infectedThree (nb-infectedThree + 1)
    set nb-infectedTwo (nb-infectedTwo - 1)
  ]
end

; Handle self-referral to treatment or hospitals
to self-referral
  if (infection-length > BU-symptoms)
  [
    if (infected? and random-float 100 < self-refer-prob-category1)
    [
      set antibiotics? true
      set infected? false
      set nb-antibiotics (nb-antibiotics + 1)
      set nb-infected (nb-infected - 1)
    ]

    if (infectedtwo? and random-float 100 < self-refer-prob-category2)
    [
```

```
      set hospitaltwo? true
      set infectedtwo? false
      set nb-hospitaltwo (nb-hospitaltwo + 1)
      set nb-infectedTwo (nb-infectedTwo - 1)
    ]

    if (infectedthree? and random-float 100 < self-refer-prob-category3)
    [
      set hospitalthree? true
      set infectedthree? false
      set nb-hospitalthree (nb-hospitalthree + 1)
      set nb-infectedThree (nb-infectedThree - 1)
    ]
  ]
end

; Handle interaction with CHVs
to meet-chvs
   if any? other chvs-here
    \textcolor{red}{[if infected? and (infection-length > BU-symptoms)}
         [set antibiotics? true
          set infected? false
          set nb-antibiotics (nb-antibiotics + 1)
          set nb-infected (nb-infected - 1)
          set infection-length 0 ]
    if infectedtwo?
         [set hospitaltwo? true
          set infectedtwo? false
          set nb-hospitaltwo (nb-hospitaltwo + 1)
          set nb-infectedTwo (nb-infectedTwo - 1)
          set infection-length 0
          set infection-lengthtwo 0 ]
    if infectedthree?
         [set hospitalthree? true
          set infectedthree? false
          set nb-hospitalthree (nb-hospitalthree + 1)
          set infection-length 0
          set infection-lengthtwo 0
          set nb-infectedThree (nb-infectedThree - 1) ]
    ]
end

; Handle recovery from antibiotics or hospitalization
to recover
  if antibiotics?
  [
    if antibiotic-time > recovery-timeone
     [
      set susceptible? true
      set nb-susceptible (nb-susceptible + 1)
      set antibiotics? false
```

```
    set nb-antibiotics (nb-antibiotics - 1)
    set antibiotic-time 0
    set threshold-timeone random-exponential average-threshold-timeone
    set threshold-timeTwo random-exponential average-threshold-timetwo
    set recovery-timeone random-exponential average-recovery-timeone
    set recovery-timetwo random-exponential average-recovery-timetwo
    set recovery-timethree random-exponential
  average-recovery-timethree
    set BU-symptoms random-exponential average-time-BU-symptoms
    set threshold-time BU-symptoms + threshold-timeone
  ]
]

if hospitaltwo?
[
  if hospital-time-two > recovery-timetwo
  [
    if not majordisability?
    [ set minorDisability? true ]
      set noDisability? false
      set nb-noDisability (nb-noDisability - 1)
      set susceptible? true
      set nb-susceptible (nb-susceptible + 1)
      set hospitaltwo? false
      set nb-hospitaltwo (nb-hospitaltwo - 1)
      set hospital-time-two 0
      set threshold-timeone random-exponential
  average-threshold-timeone
      set threshold-timeTwo random-exponential
  average-threshold-timetwo
      set recovery-timeone random-exponential average-recovery-timeone
      set recovery-timetwo random-exponential average-recovery-timetwo
      set recovery-timethree random-exponential
  average-recovery-timethree
      set BU-symptoms random-exponential average-time-BU-symptoms
      set threshold-time BU-symptoms + threshold-timeone
  ]
]

if hospitalthree?
[
  if hospital-time-three > recovery-timethree
   [
    set majorDisability? true
    set minorDisability? false
    set noDisability? false
    set nb-noDisability (nb-noDisability - 1)
    set susceptible? true
    set nb-susceptible (nb-susceptible + 1)
    set hospitalthree? false
    set nb-hospitalthree (nb-hospitalthree - 1)
```

```
      set hospital-time-three 0
      set threshold-timeone random-exponential average-threshold-timeone
      set threshold-timeTwo random-exponential average-threshold-timetwo
      set recovery-timeone random-exponential average-recovery-timeone
      set recovery-timetwo random-exponential average-recovery-timetwo
      set recovery-timethree random-exponential
    average-recovery-timethree
      set BU-symptoms random-exponential average-time-BU-symptoms
      set threshold-time BU-symptoms + threshold-timeone
    ]
  ]
end

to move-time-on
  if (infected? or infectedtwo? or infectedthree?) [set infection-length
    infection-length + 1 ]
  if infectedtwo? [set infection-lengthtwo infection-lengthtwo + 1 ]
  if antibiotics? [set antibiotic-time antibiotic-time + 1 ]
  if hospitaltwo? [set hospital-time-two hospital-time-two + 1 ]
  if hospitalthree? [set hospital-time-three hospital-time-three + 1]
end
```

LISTING C.10: Code for SR and CHV

C.4.2 Pseudo R scripts used for reading output data for the Figures in chapter 6

```
# Load necessary libraries
library(tidyverse)

# Remove all objects from the workspace
rm(list=ls())

# Load datasets for various scenarios
abm_dataq1 <- load_data("S1-spreadsheet.csv")  # SR default 1
abm_datac1 <- load_data("SC1-spreadsheet.csv")  # SR+CHV
abm_dataq2 <- load_data("S2-spreadsheet.csv")  # SR increase grey area 2
abm_datac2 <- load_data("SC2-spreadsheet.csv")  # SR+CHV increase grey
    area
abm_dataq3 <- load_data("S3-spreadsheet.csv")  # SR increase initial popn
abm_datac3 <- load_data("SC3-spreadsheet.csv")  # SR+CHV increase
    initial popn
abm_datac4 <- load_data("b80SC-spreadsheet.csv")  # SR+CHV increase CHV
abm_dataq5 <- load_data("S5-spreadsheet.csv")  # SR+CHV increase
    simulation area
abm_datac5 <- load_data("SC5-spreadsheet.csv")  # SR+CHV increase
    simulation area
abm_datac6 <- load_data("SC66-spreadsheet.csv")  # SR+CHV category 2&3

# Extract and rename columns
for each dataset:
```

```
    Rename columns by removing "count.popns.with..."
    Extract columns related to "infected" and create a "weeks" column
    Convert data from wide to long format
    Add a "Dataset" column to classify the dataset

# Combine dataframes for comparison
abm_df1 <- rbind(abm_data111, abm_datac111)  # SR1 and SR1&CHV1
abm_df12 <- rbind(abm_data111, abm_datac111, abm_data222, abm_datac222)
    # SR1, SR1&CHV1, SR2, SR2&CHV2
abm_df13 <- rbind(abm_data111, abm_datac111, abm_data333, abm_datac333)
    # SR1, SR1&CHV1, SR3, SR3&CHV3
abm_df14 <- rbind(abm_data111, abm_datac111, abm_datac444)  # SR1,
    SR1&CHV1, SR4&CHV4
abm_df15 <- rbind(abm_data111, abm_datac111, abm_data555, abm_datac555)
    # SR1, SR1&CHV1, SR5, SR5&CHV5
abm_df16 <- rbind(abm_data111, abm_datac111, abm_datac666)  # SR1,
    SR1&CHV1, SR6&CHV6

# Create plots for comparison
for each dataframe:
    Create a ggplot comparing "weeks" to "infected" for different
    datasets
    Customize colors and appearance
    Display the plot

# Show or save the plots
```

LISTING C.11: Pseudo R script used for reading output data for the Figures in chapter 6

Bibliography

Abass, K. M., Van Der Werf, T. S., Phillips, R. O., Sarfo, F. S., Abotsi, J., Mireku, S. O., Thompson, W. N., Asiedu, K., Stienstra, Y., and Klis, S.-A. (2015). Buruli ulcer control in a highly endemic district in Ghana: role of community-based surveillance volunteers. *The American Journal of Tropical Medicine and Hygiene*, 92(1):115–117.

Ablordey, A., Amissah, D. A., Aboagye, I. F., Hatano, B., Yamazaki, T., Sata, T., Ishikawa, K., and Katano, H. (2012). Detection of Mycobacterium ulcerans by the loop mediated isothermal amplification method. *PLoS Neglected Tropical Diseases*, 6(4):e1590.

Ackumey, M. M., Gyapong, M., Pappoe, M., Maclean, C. K., and Weiss, M. G. (2012). Socio-cultural determinants of timely and delayed treatment of Buruli ulcer: Implications for disease control. *Infectious Diseases of Poverty*, 1(1):1–13.

Ackumey, M. M., Kwakye-Maclean, C., Ampadu, E. O., De Savigny, D., and Weiss, M. G. (2011). Health services for Buruli ulcer control: lessons from a field study in Ghana. *PLoS Neglected Tropical Diseases*, 5(6):e1187.

Adu, E. J. and Ampadu, E. (2015). Mycobacterium ulcerans disease in the Middle Belt of Ghana: An 8-year review from six endemic districts. *International Journal of Mycobacteriology*, 4:10.

Agbenorku, P., Donwi, I. K., Kuadzi, P., and Saunderson, P. (2012). Buruli ulcer: treatment challenges at three centres in Ghana. *Journal of Tropical Medicine*, 2012.

Aidoo, A. Y. and Osei, B. (2007). Prevalence of aquatic insects and arsenic concentration determine the geographical distribution of Mycobacterium ulcerans infection. *Computational and Mathematical Methods in Medicine*, 8(4):235–244.

Alber, M. S., Kiskowski, M. A., Glazier, J. A., and Jiang, Y. (2003). On cellular automaton approaches to modeling biological cells. In *Mathematical systems theory in biology, communications, computation, and finance*, pages 1–39. Springer.

Alo, C., Okedo-Alex, I. N., Akamike, I. C., Agu, A. P., Okeke, I. M., Amuzie, C. I., and Alo, N. C. (2022). Utilising community volunteers can increase the detection and

referral of buruli ulcer cases in endemic communities in southeast, nigeria. *Tropical Diseases, Travel Medicine and Vaccines*, 8(1):24.

Amoakoh, H. B. and Aikins, M. (2013). Household cost of out-patient treatment of Buruli ulcer in Ghana: a case study of Obom in Ga South Municipality. *BMC Health Services Research*, 13(1):507.

Amofah, G., Bonsu, F., Tetteh, C., Okrah, J., Asamoa, K., Asiedu, K., and Addy, J. (2002). Buruli ulcer in Ghana: results of a national case search. *Emerging Infectious Diseases*, 8(2):167.

Apondi, R., Bunnell, R., Awor, A., Wamai, N., Bikaako-Kajura, W., Solberg, P., Stall, R. D., Coutinho, A., and Mermin, J. (2007). Home-based antiretroviral care is associated with positive social outcomes in a prospective cohort in Uganda. *JAIDS Journal of Acquired Immune Deficiency Syndromes*, 44(1):71–76.

Asiedu, K., Raviglione, M. C., Scherpbier, R., Organization, W. H., Initiative, G. B. U., et al. (2000). Buruli ulcer: Mycobacterium ulcerans infection. https://apps.who.int/iris/handle/10665/66164.

Asiedu, Kingsley and Etuaful, Samuel (1998). Socioeconomic implications of Buruli ulcer in Ghana: a three-year review. *The American Journal of Tropical Medicine and Hygiene*, 59(6):1015–1022.

Assan, B., Nyabadza, F., Landi, P., and Hui, C. (2017). Modeling the transmission of Buruli ulcer in fluctuating environments. *International Journal of Biomathematics*, 10(05):1750063.

Aydin, F., Sun, R., and Swanson, J. M. (2019). Mycolactone Toxin Membrane Permeation: Atomistic versus Coarse-Grained MARTINI Simulations. *Biophysical Journal*, 117(1):87–98.

Bank, T. W. (2022). Life expectancy at birth, total (years) for Sub-Saharan Africa. Technical report, The World Bank. Last accessed: 29 March 2022.

Barker, D. (1972). The distribution of Buruli disease in Uganda. *Transactions of the Royal Society of tropical Medicine and Hygiene*, 66(6):867–874.

Barogui, Y. T., Sopoh, G. E., Johnson, R. C., de Zeeuw, J., Dossou, A. D., Houezo, J. G., Chauty, A., Aguiar, J., Agossadou, D., Edorh, P. A., et al. (2014). Contribution of the community health volunteers in the control of Buruli ulcer in Bénin. *PLoS Neglected Tropical Diseases*, 8(10):e3200.

Baron, L., Paatero, A. O., Morel, J.-D., Impens, F., Guenin-Macé, L., Saint-Auret, S., Blanchard, N., Dillmann, R., Niang, F., Pellegrini, S., et al. (2016). Mycolactone subverts immunity by selectively blocking the Sec61 translocon. *Journal of Experimental Medicine*, 213(13):2885–2896.

Bath, D., Goodman, C., and Yeung, S. (2020). Modelling the cost-effectiveness of introducing subsidised malaria rapid diagnostic tests in the private retail sector in sub-Saharan Africa. *BMJ Global Health*, 5(5):e002138.

Behforouz, H. L., Farmer, P. E., and Mukherjee, J. S. (2004). From directly observed therapy to accompagnateurs: enhancing AIDS treatment outcomes in Haiti and in Boston. *Clinical Infectious Diseases*, 38(Supplement_5):S429–S436.

Bieri, R., Scherr, N., Ruf, M.-T., Dangy, J.-P., Gersbach, P., Gehringer, M., Altmann, K.-H., and Pluschke, G. (2017). The macrolide toxin mycolactone promotes Bim-dependent apoptosis in Buruli ulcer through inhibition of mTOR. *ACS Chemical Biology*, 12(5):1297–1307.

Bolz, M., Ruggli, N., Borel, N., Pluschke, G., and Ruf, M.-T. (2016). Local cellular immune responses and pathogenesis of Buruli ulcer lesions in the experimental Mycobacterium ulcerans pig infection model. *PLoS Neglected Tropical Diseases*, 10(4):e0004678.

Bonyah, E., Dontwi, I., and Nyabadza, F. (2014a). A theoretical model for the transmission dynamics of the Buruli ulcer with saturated treatment. *Computational and Mathematical Methods in Medicine*, 2014:14.

Bonyah, E., Dontwi, I., and Nyabadza, F. (2014b). Optimal control applied to the spread of buruli uclcer disease. *American Journal of Computational and Applied Mathematics*, 4(3):61–76.

Bonyah, E., Dontwi, I., Nyabadza, F., et al. (2014c). An age-structured model for the spread of Buruli Ulcer: Analysis and simulation in Ghana. *British Journal of Mathematics & Computer Science*, 4(16):2298.

Boyle, D. S., McNerney, R., Low, H. T., Leader, B. T., Pérez-Osorio, A. C., Meyer, J. C., O'Sullivan, D. M., Brooks, D. G., Piepenburg, O., and Forrest, M. S. (2014). Rapid detection of Mycobacterium tuberculosis by recombinase polymerase amplification. *PloS One*, 9(8):e103091.

Bratschi, M. W., Ruf, M.-T., Andreoli, A., Minyem, J. C., Kerber, S., Wantong, F. G., Pritchard, J., Chakwera, V., Beuret, C., Wittwer, M., et al. (2014). Mycobacterium ulcerans persistence at a village water source of Buruli ulcer patients. *PLoS Neglected Tropical Diseases*, 8(3):e2756.

Bretzel, G., Huber, K. L., Kobara, B., Beissner, M., Piten, E., Herbinger, K.-H., Wiedemann, F. X., Amekuse, K., Kere, A. B., Helfrich, K., et al. (2011). Laboratory confirmation of Buruli ulcer disease in Togo, 2007–2010. *PLoS Neglected Tropical Diseases*, 5(7).

Briggs, A., Sculpher, M., and Claxton, K. (2006). *Decision modelling for health economic evaluation*. Oup Oxford.

Cadapan, L., Arslanian, R., Carney, J., Zavala, S., Small, P., and Licari, P. (2001). Suspension cultivation of Mycobacterium ulcerans for the production of mycolactones. *FEMS Microbiology Letters*, 205(2):385–389.

Carter, A. M., Standeven, K. F., and Grant, P. J. (2013). Common genetic determinants of coagulation and fibrinolysis. *Emery and Rimoin's Essential Medical Genetics*, page 209.

Carter, S. B. (1967). Haptotaxis and the mechanism of cell motility. *Nature*, 213(5073):256–260.

Chaplain, M. A., Giles, S. M., Sleeman, B., and Jarvis, R. J. (1995). A mathematical analysis of a model for tumour angiogenesis. *Journal of Mathematical Biology*, 33(7):744–770.

checker, P. (2020). Rifampin (Rifadin) prices. https://www.pharmacychecker.com/. Last accessed: 1 September 2020.

Cherrington, A., Ayala, G. X., Elder, J. P., Arredondo, E. M., Fouad, M., and Scarinci, I. (2010). Recognizing the diverse roles of community health workers in the elimination of health disparities: from paid staff to volunteers. *Ethnicity & Disease*, 20(2):189.

Chu, Y.-M., Farhan, M., Khan, M. A., Alshahrani, M. Y., Muhammad, T., Islam, S., et al. (2021). Mathematical modeling and stability analysis of Buruli ulcer in Possum mammals. *Results in Physics*, 27:104471.

Chukwu, J. N., Meka, A. O., Nwafor, C. C., Oshi, D. C., Madichie, N. O., Ekeke, N., Anyim, M. C., Chukwuka, A., Obinna, M., Adegbesan, J., et al. (2017). Financial burden of health care for Buruli ulcer patients in Nigeria: the patients' perspective. *International Health*, 9(1):36–43.

Clift, E. (1998). IEC interventions for health: a 20 year retrospective on dichotomies and directions. *Journal of Health Communication*, 3(4):367–375.

Collinson, S., Frimpong, V. N., Agbavor, B., Montgomery, B., Oppong, M., Frimpong, M., Amoako, Y. A., Marks, M., and Phillips, R. O. (2020). Barriers to buruli ulcer treatment completion in the ashanti and central regions, ghana. *PLoS Neglected Tropical Diseases*, 14(5):e0008369.

Connor, D. H., Lunn, H., et al. (1966). Buruli ulceration. A clinicopathologic study of 38 Ugandans with Mycobacterium ulcerans ulceration. *Arch. Pathol.*, 81(3):183–99.

Counihan, H., Harvey, S. A., Sekeseke-Chinyama, M., Hamainza, B., Banda, R., Malambo, T., Masaninga, F., and Bell, D. (2012). Community health workers use malaria rapid diagnostic tests (RDTs) safely and accurately: results of a longitudinal study in Zambia. *The American Journal of Tropical Medicine and Hygiene*, 87(1):57.

Coutanceau, E., Decalf, J., Martino, A., Babon, A., Winter, N., Cole, S. T., Albert, M. L., and Demangel, C. (2007). Selective suppression of dendritic cell functions by Mycobacterium ulcerans toxin mycolactone. *Journal of Experimental Medicine*, 204(6):1395–1403.

Cowan, R., Athan, E., Friedman, N. D., Hughes, A. J., McDonald, A., Callan, P., Fyfe, J., and O'Brien, D. P. (2015). Mycobacterium ulcerans treatment–can antibiotic duration be reduced in selected patients? *PLoS Neglected Tropical Diseases*, 9(2):e0003503.

Davis, T. P., Wetzel, C., Avilan, E. H., de Mendoza Lopes, C., Chase, R. P., Winch, P. J., and Perry, H. B. (2013). Reducing child global undernutrition at scale in Sofala Province, Mozambique, using Care Group Volunteers to communicate health messages to mothers. *Global Health: Science and Practice*, 1(1):35–51.

De Rijk, B., Sewalt, L., and Doelman, A. (2016). Traveling wave solutions of reaction-diffusion equations in population dynamics. *Journal of Population Dynamics*, 1(34):1–34.

Debacker, M., Aguiar, J., Steunou, C., Zinsou, C., Meyers, W., Scott, J. T., Dramaix, M., and Portaels, F. (2004). Mycobacterium ulcerans disease: role of age and gender in incidence and morbidity. *Tropical Medicine & International Health*, 9(12):1297–1304.

Debacker, M., Portaels, F., Aguiar, J., Steunou, C., Zinsou, C., Meyers, W., and Dramaix, M. (2006). Risk factors for Buruli ulcer, Benin. *Emerging Infectious Diseases*, 12(9):1325.

Dega, H., Bentoucha, A., Robert, J., Jarlier, V., and Grosset, J. (2002). Bactericidal activity of rifampin-amikacin against Mycobacterium ulcerans in mice. *Antimicrobial Agents and Chemotherapy*, 46(10):3193–3196.

Dhungel, L., Benbow, M. E., and Jordan, H. R. (2021). Linking the Mycobacterium ulcerans environment to Buruli ulcer disease: Progress and challenges. *One Health*, 13:100311.

Dobos, K. M., Small, P. L., Deslauriers, M., Quinn, F. D., and King, C. H. (2001). Mycobacterium ulcerans cytotoxicity in an adipose cell model. *Infection and Immunity*, 69(11):7182–7186.

Drummond, C. and Butler, J. R. (2004). Mycobacterium ulcerans treatment costs, Australia. *Emerging Infectious Diseases*, 10(6):1038.

Duker, A. A., Carranza, E. J., and Hale, M. (2004). Spatial dependency of Buruli ulcer prevalence on arsenic-enriched domains in Amansie West District, Ghana: implications for arsenic mediation in Mycobacterium ulcerans infection. *International Journal of Health Geographics*, 3(1):19.

Eberlein, R. L. and Peterson, D. W. (1992). Understanding models with Vensim™. *European journal of Operational Research*, 59(1):216–219.

Eddyani, M., Vandelannoote, K., Meehan, C. J., Bhuju, S., Porter, J. L., Aguiar, J., Seemann, T., Jarek, M., Singh, M., Portaels, F., et al. (2015). A genomic approach to resolving relapse versus reinfection among four cases of Buruli ulcer. *PLoS Neglected Tropical Diseases*, 9(11):e0004158.

Ellen, D. E., Stienstra, Y., Teelken, M. A., Dijkstra, P. U., Van Der Graaf, W. T., and Van Der Werf, T. S. (2003). Assessment of functional limitations caused by Mycobacterium ulcerans infection: towards a Buruli ulcer functional limitation score. *Tropical Medicine & International Health*, 8(1):90–96.

En, J., Goto, M., Nakanaga, K., Higashi, M., Ishii, N., Saito, H., Yonezawa, S., Hamada, H., and Small, P. L. (2008). Mycolactone is responsible for the painlessness of mycobacterium ulcerans infection (buruli ulcer) in a murine study. *Infection and Immunity*, 76(5):2002–2007.

Esmon, C. T. (1995). Thrombomodulin as a model of molecular mechanisms that modulate protease specificity and function at the vessel surface. *The FASEB Journal*, 9(10):946–955.

Esmon, C. T., Esmon, N., and Harris, K. (1982). Complex formation between thrombin and thrombomodulin inhibits both thrombin-catalyzed fibrin formation and factor V activation. *Journal of Biological Chemistry*, 257(14):7944–7947.

Expatistan (2020). Price of Antibiotics in Accra. https://www.expatistan.com/price/antibiotics/accra. Last accessed: 1 June 2020.

Ezennia, I. J., Nduka, S. O., and Ekwunife, O. I. (2017). Cost benefit analysis of malaria rapid diagnostic test: the perspective of Nigerian community pharmacists. *Malaria Journal*, 16(1):7.

Folcik, V. A., An, G. C., and Orosz, C. G. (2007). The Basic Immune Simulator: an agent-based model to study the interactions between innate and adaptive immunity. *Theoretical Biology and Medical Modelling*, 4(1):1–18.

Frimpong, M., Ahor, H. S., Wahed, A. A. E., Agbavor, B., Sarpong, F. N., Laing, K., Wansbrough-Jones, M., and Phillips, R. O. (2019). Rapid detection of Mycobacterium ulcerans with isothermal recombinase polymerase amplification assay. *PLoS Neglected Tropical Diseases*, 13(2):e0007155.

Garchitorena, A., Ngonghala, C. N., Texier, G., Landier, J., Eyangoh, S., Bonds, M. H., Guégan, J.-F., and Roche, B. (2015). Environmental transmission of Mycobacterium ulcerans drives dynamics of Buruli ulcer in endemic regions of Cameroon. *Scientific Reports*, 5:18055.

GBoDC, N. (2017). Global Burden of Disease Study 2016 (GBD 2016) disability weights. *Seattle, Washington:(IHME) IfHMaE*.

George, K. M., Chatterjee, D., Gunawardana, G., Welty, D., Hayman, J., Lee, R., and Small, P. (1999). Mycolactone: a polyketide toxin from Mycobacterium ulcerans required for virulence. *Science*, 283(5403):854–857.

George, K. M., Pascopella, L., Welty, D. M., and Small, P. (2000). A Mycobacterium ulcerans toxin, mycolactone, causes apoptosis in guinea pig ulcers and tissue culture cells. *Infection and Immunity*, 68(2):877–883.

Gérard, S. F., Hall, B. S., Zaki, A. M., Corfield, K. A., Mayerhofer, P. U., Costa, C., Whelligan, D. K., Biggin, P. C., Simmonds, R. E., and Higgins, M. K. (2020). Structure of the inhibited state of the Sec translocon. *Molecular Cell*, 79(3):406–415.

Goto, M., Nakanaga, K., Aung, T., Hamada, T., Yamada, N., Nomoto, M., Kitajima, S., Ishii, N., Yonezawa, S., and Saito, H. (2006). Nerve damage in Mycobacterium ulcerans-infected mice: probable cause of painlessness in Buruli ulcer. *The American Journal of Pathology*, 168(3):805–811.

Grassly, N. C. and Fraser, C. (2008). Mathematical models of infectious disease transmission. *Nature Reviews Microbiology*, 6(6):477–487.

Grimm, V., Berger, U., Bastiansen, F., Eliassen, S., Ginot, V., Giske, J., Goss-Custard, J., Grand, T., Heinz, S. K., Huse, G., et al. (2006). A standard protocol for describing individual-based and agent-based models. *Ecological Modelling*, 198(1-2):115–126.

Grimm, V., Railsback, S. F., Vincenot, C. E., Berger, U., Gallagher, C., DeAngelis, D. L., Edmonds, B., Ge, J., Giske, J., Groeneveld, J., et al. (2020). The ODD protocol for describing agent-based and other simulation models: A second update to improve clarity, replication, and structural realism. *Journal of Artificial Societies and Social Simulation*, 23(2).

Hackl, J. and Dubernet, T. (2019). Epidemic spreading in urban areas using agent-based transportation models. *Future Internet*, 11(4):92.

Hall, B. S., Hill, K., McKenna, M., Ogbechi, J., High, S., Willis, A. E., and Simmonds, R. E. (2014). The pathogenic mechanism of the Mycobacterium ulcerans virulence factor, mycolactone, depends on blockade of protein translocation into the ER. *PLoS Pathogens*, 10(4):e1004061.

Hall, J. (2011). Effective community-based interventions to improve exclusive breast feeding at four to six months in low-and low–middle-income countries: a systematic review of randomised controlled trials. *Midwifery*, 27(4):497–502.

Hansen, K. S., Grieve, E., Mikhail, A., Mayan, I., Mohammed, N., Anwar, M., Baktash, S. H., Drake, T. L., Whitty, C. J., Rowland, M. W., et al. (2015). Cost-effectiveness

of malaria diagnosis using rapid diagnostic tests compared to microscopy or clinical symptoms alone in Afghanistan. *Malaria Journal*, 14(1):1–15.

Hansen, K. S., Ndyomugyenyi, R., Magnussen, P., Lal, S., and Clarke, S. E. (2017). Cost-effectiveness analysis of malaria rapid diagnostic tests for appropriate treatment of malaria at the community level in Uganda. *Health Policy and Planning*, 32(5):676–689.

Hollingsworth, T. D. (2009). Controlling infectious disease outbreaks: Lessons from mathematical modelling. *Journal of Public Health Policy*, 30(3):328–341.

Hong, H., Demangel, C., Pidot, S. J., Leadlay, P. F., and Stinear, T. (2008). Mycolactones: immunosuppressive and cytotoxic polyketides produced by aquatic mycobacteria. *Natural Product Reports*, 25(3):447–454.

Hsieh, L. T.-H., Dos Santos, S. J., Hall, B. S., Ogbechi, J., Loglo, A. D., Salguero, F. J., Ruf, M.-T., Pluschke, G., and Simmonds, R. E. (2022). Aberrant stromal tissue factor localisation and mycolactone-driven vascular dysfunction, exacerbated by IL-1β, are linked to fibrin formation in Buruli ulcer lesions. *PLoS Pathogens*, 18(1):e1010280.

Jacobsen, K. H. and Padgett, J. J. (2010). Risk factors for Mycobacterium ulcerans infection. *International Journal of Infectious Diseases*, 14(8):e677–e681.

Jamison, D. T., Breman, J. G., Measham, A. R., Alleyne, G., Claeson, M., Evans, D. B., Jha, P., Mills, A., and Musgrove, P. (2006). Cost-effective strategies for the excess burden of disease in developing countries. In *Priorities in Health*. The International Bank for Reconstruction and Development/The World Bank.

Johnson, P. D., Stinear, T., Pamela, L., Pluschke, G., Merritt, R. W., Portaels, F., Huygen, K., Hayman, J. A., and Asiedu, K. (2005). Buruli ulcer (M. ulcerans infection): new insights, new hope for disease control. *PLoS Medicine*, 2(4):e108.

Jones, E., Oliphant, T., and Peterson, P. (2014). SciPy: Open source scientific tools for Python.

Kanga, J., Kacou, D., Sangaré, A., Dabila, Y., Asse, N., and Djakeaux, S. (2003). Recurrence after surgical treatment of Buruli ulcer in Cote d'Ivoire. *Bulletin de la Societe de Pathologie Exotique (1990)*, 96(5):406–409.

Kim, Y.-C. (1996). Diffusivity of bacteria. *Korean Journal of Chemical Engineering*, 13(3):282–287.

Klis, S., Kingma, R., Tuah, W., Stienstra, Y., and van der Werf, T. S. (2014). Compliance with antimicrobial therapy for Buruli ulcer. *Antimicrobial Agents and Chemotherapy*, 58(10):6340–6340.

Kong, L., Wang, J., Han, W., and Cao, Z. (2016). Modeling heterogeneity in direct infectious disease transmission in a compartmental model. *International Journal of Environmental Research and Public Health*, 13(3):253.

Kpeli, G. S. and Yeboah-Manu, D. (2019). Secondary infection of Buruli ulcer lesions. *Buruli Ulcer: Mycobacterium ulcerans Disease. Cham*, pages 227–39.

Mabey, D., Peeling, R. W., Ustianowski, A., and Perkins, M. D. (2004). Diagnostics for the developing world. *Nature Reviews Microbiology*, 2(3):231–240.

Macal, C. M. (2016). Everything you need to know about agent-based modelling and simulation. *Journal of Simulation*, 10(2):144–156.

Macal, C. M. and North, M. J. (2005). Tutorial on agent-based modeling and simulation. In *Proceedings of the Winter Simulation Conference, 2005*, pages 14–pp. IEEE.

Maman, I., Tchacondo, T., Kere, A. B., Beissner, M., Badziklou, K., Tedihou, E., Nyaku, E., Amekuse, K., Wiedemann, F. X., Karou, D. S., et al. (2018). Molecular detection of Mycobacterium ulcerans in the environment and its relationship with Buruli ulcer occurrence in Zio and Yoto districts of maritime region in Togo. *PLoS Neglected Tropical Diseases*, 12(5):e0006455.

Maman, Issaka and Tchacondo, Tchadjobo and Kere, Abiba Banla and Piten, Ebekalisai and Beissner, Marcus and Kobara, Yiragnima and Kossi, Komlan and Badziklou, Kossi and Wiedemann, Franz Xaver and Amekuse, Komi and others (2018). Risk factors for Mycobacterium ulcerans infection (Buruli Ulcer) in Togo-a case-control study in Zio and Yoto districts of the maritime region. *BMC Infectious Diseases*, 18(1):1–11.

Marsollier, L., Brodin, P., Jackson, M., Korduláková, J., Tafelmeyer, P., Carbonnelle, E., Aubry, J., Milon, G., Legras, P., Saint André, J.-P., et al. (2007). Impact of Mycobacterium ulcerans biofilm on transmissibility to ecological niches and Buruli ulcer pathogenesis. *PLoS Pathogens*, 3(5):e62.

McKenna, M., Simmonds, R. E., and High, S. (2016). Mechanistic insights into the inhibition of Sec61-dependent co-and post-translational translocation by mycolactone. *Journal of Cell Science*, 129(7):1404–1415.

McKenna, M., Simmonds, R. E., and High, S. (2017). Mycolactone reveals the substrate-driven complexity of Sec61-dependent transmembrane protein biogenesis. *Journal of Cell Science*, 130(7):1307–1320.

Merritt, R. W., Walker, E. D., Small, P. L., Wallace, J. R., Johnson, P. D., Benbow, M. E., and Boakye, D. A. (2010). Ecology and transmission of Buruli ulcer disease: a systematic review. *PLoS Neglected Tropical Diseases*, 4(12):e911.

Modu, B., Polovina, N., and Konur, S. (2020). Agent-Based Modelling of Malaria Transmission Dynamics. *arXiv preprint arXiv:2004.06477*.

Momoh, A. A., Abdullahi, H. M., Abimbola, N. G., and Michael, A. I. (2021). Modeling, optimal control of intervention strategies and cost effectiveness analysis for buruli ulcer model. *Alexandria Engineering Journal*, 60(2):2245–2264.

NHIS (2020). National Health Insurance Scheme Medicines List. http://www.nhis.gov.gh/medlist.aspx. Last accessed: 2 August 2020.

Nienhuis, W. A., Stienstra, Y., Thompson, W. A., Awuah, P. C., Abass, K. M., Tuah, W., Awua-Boateng, N. Y., Ampadu, E. O., Siegmund, V., Schouten, J. P., et al. (2010). Antimicrobial treatment for early, limited Mycobacterium ulcerans infection: a randomised controlled trial. *The Lancet*, 375(9715):664–672.

Nyabadza, F. and Bonyah, E. (2015). On the transmission dynamics of Buruli ulcer in GHANA: Insights through a mathematical model. *BMC Research Notes*, 8(1):656.

Nyarko, P., Adikorley, I., Amoakoyirenkyi, P., and Dontwi, I. (2017). Mathematical Modeling and Numerical Simulation for Mycobacterium Ulcerans Tissue Invasion: A Macroscopic Model for the Buruli Ulcer Disease; The iier International Conference. *International Journal of Advances in Science, Engineering and Technology*, 4:41–48.

O'Brien, D. P., Callan, P., Friedman, N. D., Athan, E., Hughes, A., and McDonald, A. (2019). Mycobacterium ulcerans disease management in Australian patients: the re-emergence of surgery as an important treatment modality. *ANZ Journal of Surgery*, 89(6):653–658.

Ogbechi, J., Hall, B. S., Sbarrato, T., Taunton, J., Willis, A. E., Wek, R. C., and Simmonds, R. E. (2018). Inhibition of Sec61-dependent translocation by mycolactone uncouples the integrated stress response from ER stress, driving cytotoxicity via translational activation of ATF4. *Cell death & Disease*, 9(3):397.

Ogbechi, J., Ruf, M.-T., Hall, B. S., Bodman-Smith, K., Vogel, M., Wu, H.-L., Stainer, A., Esmon, C. T., Ahnström, J., Pluschke, G., et al. (2015). Mycolactone-dependent depletion of endothelial cell thrombomodulin is strongly associated with fibrin deposition in Buruli ulcer lesions. *PLoS Pathogens*, 11(7):e1005011.

Organization, W. H. et al. (2008). Task shifting: Global recommendations and guidelines. *Geneva: World Health Organization*, 1.

O'Brien, D. P., Wynne, J. W., Buultjens, A. H., Michalski, W. P., Stinear, T. P., Friedman, N. D., Hughes, A., and Athan, E. (2017). Exposure risk for infection and lack of human-to-human transmission of Mycobacterium ulcerans disease, Australia. *Emerging Infectious Diseases*, 23(5):837.

Pak, J., O'Brien, D. P., Quek, T., and Athan, E. (2012). Treatment costs of Mycobacterium ulcerans in the antibiotic era. *International Health*, 4(2):123–127.

Perry, H. B., Zulliger, R., and Rogers, M. M. (2014). Community health workers in low-, middle-, and high-income countries: an overview of their history, recent evolution, and current effectiveness. *Annual Review of Public Health*, 35:399–421.

Phillips, R., Horsfield, C., Kuijper, S., Lartey, A., Tetteh, I., Etuaful, S., Nyamekye, B., Awuah, P., Nyarko, K., Osei-Sarpong, F., et al. (2005). Sensitivity of PCR targeting the IS2404 insertion sequence of Mycobacterium ulcerans in an assay using punch biopsy specimens for diagnosis of Buruli ulcer. *Journal of Clinical Microbiology*, 43(8):3650–3656.

Phillips, R., Sarfo, F. S., Guenin-Macé, L., Decalf, J., Wansbrough-Jones, M., Albert, M. L., and Demangel, C. (2009). Immunosuppressive signature of cutaneous Mycobacterium ulcerans infection in the peripheral blood of patients with buruli ulcer disease. *The Journal of Infectious Diseases*, 200(11):1675–1684.

Pluschke, G. and Röltgen, K. (2019). *Buruli Ulcer*. Springer.

Portaels, F. (1989). Epidémiologie des ulcères à Mycobacterium ulcerans. *Ann Soc Belg Med Trop*, 69(2):91–103.

Portaels, F. (1995). Epidemiology of mycobacterial diseases. *Clinics in Dermatology*, 13(3):207–222.

Portaels, F., Johnson, P., Meyers, W. M., Organization, W. H., Initiative, G. B. U., et al. (2001). Buruli ulcer: diagnosis of Mycobacterium ulcerans disease: a manual for health care providers. Technical report.

Preziosi, L. (2003). *Cancer modelling and simulation*. CRC Press.

Prost, A., Colbourn, T., Seward, N., Azad, K., Coomarasamy, A., Copas, A., Houweling, T. A., Fottrell, E., Kuddus, A., Lewycka, S., et al. (2013). Women's groups practising participatory learning and action to improve maternal and newborn health in low-resource settings: a systematic review and meta-analysis. *The Lancet*, 381(9879):1736–1746.

Rikitake, Y. and Takai, Y. (2011). Directional cell migration: regulation by small G proteins, Nectin-like molecule-5, and afadin. *International Review of Cell and Molecular Biology*, 287:97–143.

Riley, S. (2007). Large-scale spatial-transmission models of infectious disease. *Science*, 316(5829):1298–1301.

Saito, M. K., Parry, C. M., and Yeung, S. (2018). Modelling the cost-effectiveness of a rapid diagnostic test (IgMFA) for uncomplicated typhoid fever in Cambodia. *PLoS Neglected Tropical Diseases*, 12(11):e0006961.

Sakyi, S. A., Aboagye, S. Y., Darko Otchere, I., and Yeboah-Manu, D. (2016). Clinical and laboratory diagnosis of Buruli ulcer disease: a systematic review. *Canadian Journal of Infectious Diseases and Medical Microbiology*, 2016.

Sarfo, F. S., Phillips, R., Wansbrough-Jones, M., and Simmonds, R. E. (2016). Recent advances: role of mycolactone in the pathogenesis and monitoring of Mycobacterium ulcerans infection/Buruli ulcer disease. *Cellular Microbiology*, 18(1):17–29.

Schugart, R. C., Friedman, A., Zhao, R., and Sen, C. K. (2008). Wound angiogenesis as a function of tissue oxygen tension: a mathematical model. *Proceedings of the National Academy of Sciences*, 105(7):2628–2633.

Service, G. S. et al. (2020). Population of Ghana by region. Technical report, Ghana Statistical Service. Last accessed: 28 April 2020.

Sherratt, J. A. and Murray, J. D. (1990). Models of epidermal wound healing. *Proceedings of the Royal Society of London. Series B: Biological Sciences*, 241(1300):29–36.

Shillcutt, S., Morel, C., Goodman, C., Coleman, P., Bell, D., Whitty, C. J., and Mills, A. (2008). Cost-effectiveness of malaria diagnostic methods in sub-Saharan Africa in an era of combination therapy. *Bulletin of the World Health Organization*, 86:101–110.

Shina, A. (2011). Burden of Buruli ulcer: how affected households in a Ghanaian district cope. *African Study Monographs*, 32(2):pp–43.

Singh, A., McBride, W. J. H., Govan, B., and Pearson, M. (2018). Potential animal reservoir of Mycobacterium ulcerans: a systematic review. *Tropical Medicine and Infectious Disease*, 3(2):56.

Smith, N. R., Trauer, J. M., Gambhir, M., Richards, J. S., Maude, R. J., Keith, J. M., and Flegg, J. A. (2018). Agent-based models of malaria transmission: a systematic review. *Malaria Journal*, 17(1):1–16.

Stienstra, Y., van der Graaf, W. T., Asamoa, K., and van der Werf, T. S. (2002). Beliefs and attitudes toward Buruli ulcer in Ghana. *The American Journal of Tropical Medicine and Hygiene*, 67(2):207–213.

Stinear, T., Ross, B. C., Davies, J. K., Marino, L., Robins-Browne, R. M., Oppedisano, F., Sievers, A., and Johnson, P. D. (1999). Identification and characterization of IS 2404 and IS 2606: two distinct repeated sequences for detection of Mycobacterium ulcerans by PCR. *Journal of Clinical Microbiology*, 37(4):1018–1023.

Stinear, T. P., Mve-Obiang, A., Small, P. L., Frigui, W., Pryor, M. J., Brosch, R., Jenkin, G. A., Johnson, P. D., Davies, J. K., Lee, R. E., et al. (2004). Giant plasmid-encoded polyketide synthases produce the macrolide toxin of Mycobacterium ulcerans. *Proceedings of the National Academy of Sciences*, 101(5):1345–1349.

Stock, J. B. and Baker, M. (2009). Chemotaxis. In *Encyclopedia of Microbiology*, pages 71–78. Elsevier Inc.

Taylor, C., Koyuk, H., Coyle, J., Waggoner, R., and Newman, K. (2007). An Agent-Based Model of Predator-Prey Relationships Between Transient Killer Whales and Other Marine Mammals.

Tisue, S. and Wilensky, U. (1999). Center for Connected Learning and Computer-Based Modeling Northwestern University, Evanston, Illinois. *NetLogo: A Simple Environment for Modeling Complexity, Citeseer*.

Trubiano, J. A., Lavender, C. J., Fyfe, J. A., Bittmann, S., and Johnson, P. D. (2013). The incubation period of Buruli ulcer (Mycobacterium ulcerans infection). *PLoS Neglected Tropical Diseases*, 7(10):e2463.

UBLS (2020). US Bureau of Labor Statistics (UBLS), CPI Inflation Calculator. https://www.bls.gov/data/inflation_calculator.htm. Last accessed: 12 August 2020.

UN (2022a). Benin total population (World Population Prospects 2022). https://worldpopulationreview.com/countries/benin-population. Last accessed: 01 September 2022.

UN (2022b). DR Congo total population (World Population Prospects 2022). https://worldpopulationreview.com/countries/dr-congo-population. Last accessed: 01 September 2022.

UN (2022c). Ivory Coast total population (World Population Prospects 2022). https://worldpopulationreview.com/countries/ivory-coast-population. Last accessed: 01 September 2022.

Van der Werf, T., van der Graaf, W. T., Groothuis, D., and Knell, A. (1989). Mycobacterium ulcerans infection in Ashanti region, Ghana. *Transactions of the Royal Society of Tropical Medicine and Hygiene*, 83(3):410–413.

van der Werf, T. S. (2018). Diagnostic tests for Buruli ulcer: clinical judgment revisited.

Van der Werf, T. S., Van der Graaf, W. T., Tappero, J. W., and Asiedu, K. (1999). Mycobacterium ulcerans infection. *The Lancet*, 354(9183):1013–1018.

Van Hinsbergh, V. W. (2012). Endothelium—role in regulation of coagulation and inflammation. In *Seminars in Immunopathology*, volume 34, pages 93–106. Springer.

Vouking, M. Z., Takougang, I., Mbam, L. M., Mbuagbaw, L., Tadenfok, C. N., and Tamo, C. V. (2014). The contribution of community health workers to the control of Buruli ulcer in the Ngoantet area, Cameroon. *Pan African Medical Journal*, 16(1).

Vouking, M. Z., Tamo, V. C., and Mbuagbaw, L. (2013). The impact of community health workers (CHWs) on Buruli ulcer in sub-Saharan Africa: a systematic review. *Pan African Medical Journal*, 15(1).

Walsh, D. S., Portaels, F., and Meyers, W. M. (2008). Buruli ulcer (Mycobacterium ulcerans infection). *Transactions of the Royal Society of Tropical Medicine and Hygiene*, 102(10):969–978.

Watanabe, M., Nakamura, H., Nabekura, R., Shinoda, N., Suzuki, E., and Saito, H. (2015). Protective effect of a dewaxed whole-cell vaccine against Mycobacterium ulcerans infection in mice. *Vaccine*, 33(19):2232–2239.

website, G. F. (2022a). Pooled Procurement Mechanism Reference Pricing: RDTs. https://www.theglobalfund.org/media/7564/psm_hivrdtreferencepricing_table_en.pdf. Last accessed: 28 March 2022.

website, G. F. (2022b). Price, quality, and market dynamics of malaria rapid diagnostic tests: analysis of Global Fund 2009–2018 data. *Malaria Journal*, 21(1):1–15.

WHO (2018). Buruli ulcer (Mycobacterium ulcerans infection). http://www.who.int/buruli/en/. Last accessed: 16 April 2018.

WHO (2019). Country data for Buruli ulcer. http://apps.who.int/neglecteddiseases/ntddata/buruli/buruli.html. Last accessed: 11 September 2019.

WHO (2022). Number of new reported cases of Buruli ulcer. https://www.who.int/data/gho/data/indicators/indicator-details/GHO/number-of-new-reported-cases-of-buruli-ulcer. Last accessed: 07 November 2022.

WHO et al. (2004). Provisional guidance on the role of specific antibiotics in the management of Mycobacterium ulcerans disease (Buruli ulcer). In *Provisional guidance on the role of specific antibiotics in the management of Mycobacterium ulcerans disease (Buruli ulcer)*, pages 33–33.

WHO et al. (2008). The global burden of disease 2004 update: disability weights for diseases and conditions.

WHO et al. (2012). Treatment of Mycobacterium ulcerans disease (Buruli ulcer): guidance for health workers. https://www.who.int/publications/i/item/9789241503402.

WHO et al. (2018). Report of a WHO–FIND meeting on diagnostics for Buruli ulcer: Geneva, 26–27 March 2018. Technical report, World Health Organization.

WHO et al. (2022). Target product profile for a rapid test for diagnosis of mycetoma at primary health-care level.

WHO, G. (2013). WHO methods and data sources for global burden of disease estimates 2000-2011. *Geneva: Department of Health Statistics and Information Systems*.

Wilensky, U. (1997). Netlogo segregation model (evanston, ill.: Center for connected learning and computer-based modeling, northwestern university).

Wilensky, U. (1999). NetLogo. Evanston, IL: Northwestern University. *Center for Connected Learning and Computer-Based Modeling. Retrieved from http://ccl. northwestern. edu/netlogo*.

Wollinka, O., Keeley, E., Burkhalter, B. R., and Bashir, N. (1997). Hearth nutrition model: Applications in Haiti, Viet Nam and Bangladesh. *Arlington, Va., USA: BASICS*.

Wouters, E., Van Damme, W., Van Loon, F., Van Rensburg, D., and Meulemans, H. (2009). Public-sector ART in the Free State Province, South Africa: community support as an important determinant of outcome. *Social science & Medicine*, 69(8):1177–1185.

Wynne, J. W., Stinear, T. P., Athan, E., Michalski, W. P., and O'Brien, D. P. (2018). Low incidence of recurrent buruli ulcers in treated australian patients living in an endemic region. *PLoS neglected tropical diseases*, 12(8):e0006724.

Yang, C. and Wilensky, U. (2011). Netlogo epidem basic model. *Center for Connected Learning and ComputerBased Modeling Northwestern University Evanston IL, pages Evanston, IL*.

Yeboah-Manu, D., Asante-Poku, A., Asan-Ampah, K., Ampadu, E. D. E., and Pluschke, G. (2011). Combining PCR with microscopy to reduce costs of laboratory diagnosis of Buruli ulcer. *The American Journal of Tropical Medicine and Hygiene*, 85(5):900–904.

Yotsu, R. R., Murase, C., Sugawara, M., Suzuki, K., Nakanaga, K., Ishii, N., and Asiedu, K. (2015). Revisiting buruli ulcer. *The Journal of Dermatology*, 42(11):1033–1041.

Zingue, D., Bouam, A., Tian, R. B., and Drancourt, M. (2018a). Buruli ulcer, a prototype for ecosystem-related infection, caused by Mycobacterium ulcerans. *Clinical Microbiology Reviews*, 31(1):e00045–17.

Zingue, D., Panda, A., and Drancourt, M. (2018b). A protocol for culturing environmental strains of the Buruli ulcer agent, Mycobacterium ulcerans. *Scientific Reports*, 8(1):1–12.

Zong, G., Hu, Z., O'keefe, S., Tranter, D., Iannotti, M. J., Baron, L., Hall, B., Corfield, K., Paatero, A. O., Henderson, M. J., et al. (2019). Ipomoeassin F binds Sec61α to inhibit protein translocation. *Journal of the American Chemical Society*, 141(21):8450–8461.